Universidad Internacional del Ecuador

Escuela de Ingeniería Mecánica Automotriz

Trabajo de Integración Curricular

Articulo Investigación para la obtención del Título de Ingeniera en Mecánica Automotriz

Diseño de un dispositivo para la identificación térmica en vehículos de transporte masivo.

Nicolas Francisco Gordon Bedon

Oscar Fabian Intriago García

Andrés Sebastián Pérez Aguirre

Director: Msc. Gorky G. Reyes C.

Quito, mayo 2021

CERTIFICACIÓN

Nosotros, Nicolas Francisco Gordon Bedon, Oscar Fabian Intriago García, Andrés Sebastián Pérez Aguirre, declaramos bajo juramento, que el trabajo aquí descrito es de nuestra autoría; que no ha sido presentado anteriormente para ningún grado o calificación profesional y que se ha consultado la bibliografía detallada.

Cedo mis derechos de propiedad intelectual a la Universidad Internacional del Ecuador, para que sea publicado y divulgado en internet, según lo establecido en la Ley de propiedad Intelectual, reglamento y leyes.

Nicolas Francisco Gordon Bedon

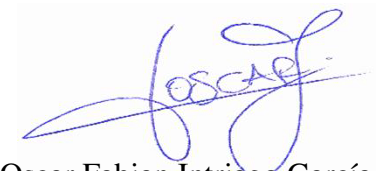

Oscar Fabian Intriago García

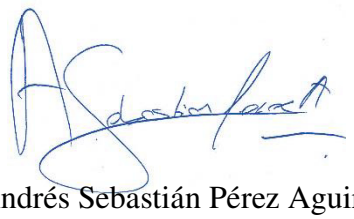

Andrés Sebastián Pérez Aguirre

Yo, Guillermo Gorky Reyes Campaña, certifico que conozco al autor del presente trabajo siendo el responsable exclusivo tanto de su originalidad y autenticidad, como de su contenido.

Guillermo Gorky Reyes Campaña

DEDICATORIA

Después de 5 años de una carrera de resistencia, en la cual pude palpar varios obstáculos que supieron revelar que la mecánica automotriz es mi vida y mi pasión; después de los más de 1825 días de esfuerzo y sacrificio compartido, quiero dedicar este trabajo de titulación a mi motor para vivir, a la luz que me da la fuerza para seguir adelante, a mi mami Naty que todos los días sacrifico todo de ella para brindarme la herencia más valiosa, el estudio; a mi papi Ani & a mi Mami Celi que me guiaron por un camino de bien, enseñándome que si tengo a Dios lo tengo todo y sobre todo que nací para triunfar puesto que poseo la inteligencia, la ciencia, el arte para conseguir todo lo que desee mi corazón; a primos, mis hermanos JuanDa & Dome, a mis tíos Ruthy & Byron, que siempre me brindaron su incondicional ayuda; a mi tío Gabo y su familia que me animaban a seguir; a mi papa Jogre & mami Fani, que a la distancia lo dieron todo para ser parte de este sueño; a mis amigos LBDLU que me motivaban y finalmente pero no menos importante a mi enamorada Nicole que estuvo a mi lado, brindándome su aliento y apoyo en este largo proceso.

- Nicolas Francisco Gordon Bedon

DEDICATORIA

El presente trabajo se lo dedico a mis padres, Oscar Intriago y Nelly García, por el infinito apoyo y amor brindado a lo largo de mi vida como estudiante y por ser siempre un buen ejemplo para su hijo ya que nunca dudaron de las capacidades que yo tenía. A ellos, quienes a lo largo de mi vida han sido un gran apoyo en todo momento, que a pesar de los errores que he cometido como adolescente ellos siempre han estado y estarán ahí para guiar mi camino tanto como un buen ser humano como un buen profesional. A mi hermana mayor, Katherine Intriago, de quien aprendí muchas cosas de ser un adulto y asumir responsabilidades, a mis hermanas menores, Diana Intriago y Daniela Intriago, a quienes siempre trato de ser un buen ejemplo para ellas, siempre tratando de ser un hermano mayor ejemplar ayudándolas en sus tareas, responsabilidades y estudios, a mis grupos de amigos con los que las locuras en los buenos y malos momentos nunca faltaron y su apoyo siempre estuvo ahí incondicionalmente, en especial a mi gran amigo de la infancia Anthony Araujo; también dedico este trabajo a mis familiares que me han apoyado todos estos años brindándome sus bendiciones y ánimos por cumplir tan anhelado sueño de todo estudiante que es el tener un título universitario.

-Oscar Fabian Intriago García

DEDICATORIA

Este proyecto se lo dedico con todo mi corazón a los grandes pilares y referentes que gracias a Dios los tengo junto a mí, mis padres Ramiro Y Jeanette, gracias infinitas por todo su apoyo diario, su bendición para cada paso y por siempre caminar de mi lado, cada uno de mis logros se los dedico a ustedes por enseñarme siempre que con esfuerzo y dedicación se puede alcanzar todos los objetivos de vida planteados, a pesar de las diferentes adversidades durante el camino, juntos lo logramos. A demás quiero dedicar a mis hermanos, Jose e Isabella, siempre confiaron en su hermano mayor y hoy les agradezco por todo su apoyo moral dedicando este proyecto para ustedes.

A mi abuela Marina, por ser mi ángel terrenal, por siempre ser una guía en mi vida espiritual y enseñarme que la fe lo puede todo.

Finalmente, este proyecto es para mi pareja Belén, gracias por el apoyo en cada una de las decisiones durante todo el trayecto, por la paciencia, la compresión y la voluntad de impulsarme a lograr este gran objetivo.

- Andrés Sebastián Pérez Aguirre

AGRADECIMIENTO

Primero quiero agradecer a Dios por brindarme la vida, por la familia tan maravillosa que tengo, por las bendiciones, por las dificultades y por la fuerza para seguir; quiero agradecer de forma especial a la Universidad Internacional del Ecuador, mi casa que permanecerá siempre en mi alama, puesto que supo darme la mano cuando más lo necesitaba. Gracias a mis amigos de promoción, Osqui, Sebas, Isaac, Stalin, Stephano, David, Kevin, Daniel, Jorge, Valentina y Emilio, que supieron ser apoyo en las buenas y en las malas y por ultimo gracias a los directores de orquesta, los profesionales que supieron nutrir mi conocimiento, gracias a los buenos y a los no tan buenos, porque de ellos aprendí lecciones que me ayudaran en varios ámbitos profesionales y personales; finalmente gracias a la gran comunidad UIDE con ellos se queda una gran parte de mi corazón.

- Nicolas Francisco Gordon Bedon

AGRADECIMIENTO

Mi más sincero agradecimiento a mis padres por permitirme realizar mis estudios en la Universidad Internacional Del Ecuador y por ese sacrificio dado por ellos hacia mí de brindarme un regalo tan preciado como lo es el estudio. Al Ingeniero Gorky Reyes, profesor y tutor de la Facultad de Ingeniería Automotriz (F.I.A.), por su importante apoyo para la realización y culminación exitosa del presente artículo. Así mismo, a todo el personal docente de la F.I.A. que han aportado de alguna manera en formarme como buen profesional. A mis compañeros, Nicolás Gordon B. y Sebastián Pérez A., con quienes hemos desarrollado este articulo y con quienes he compartido grandes experiencias a lo largo de la carrera, en los momentos buenos y también en los malos, agradecerles siempre por esa amistad y poder darme el lujo de llamarlos hermanos.

- Oscar Fabian Intriago García

AGRADECIMIENTO

Primeramente, quiero agradecer a Dios por haberme guiado durante todo este complejo trayecto de carrera universitaria. A mi prestigiosa institución UNIVERSIDAD INTERNACIONAL DEL ECUADOR por haberme aceptado ser parte de ella y abrirme sus puertas de sus diferentes instalaciones para estudiar una carrera que siempre la quise, así como también a los diferentes docentes que fueron parte de ella en especial a los señores Pedro Montoya, Ricardo Moreta, Armando Romero y Juan Carlos Rubio, gracias a sus conocimientos impartidos hicieron que tenga mucho más amor y entrega a la Ingeniería Automotriz. Agradezco infinitamente a mi tutor de tesis, Mgs. Gorky Reyes, por haberme brindado la oportunidad de guiarme durante todo el proyecto, siempre con su buen ánimo, responsabilidad, capacidad y conocimiento científico, un Dios le pague infinito por toda su entrega. Finalmente quiero agradecer a mis compañeros de tesis Nicolás y Oscar por ayudarme en el momento más complicado del proyecto, los llevo siempre en mi corazón.

- Andrés Sebastián Pérez Aguirre

ÍNDICE DE CONTENIDO

ÍNDICE DE TABLAS

ÍNDICE DE FIGURAS

ÍNDICE DE ECUACIONES

DISEÑO DE UN DISPOSITIVO PARA LA IDENTIFICACIÓN TÉRMICA EN VEHÍCULOS DE TRASPORTE MASIVO.

Ing. Gorky Reyes C MSc [1], Nicolas Gordon B.[2], Oscar Intriago G.[3], Sebastián Pérez A.[4]
[1] Ingeniería Automotriz -Universidad Internacional del Ecuador, gureyesca@uide.edu.ec,
[2] Ingeniería Automotriz -Universidad Internacional del Ecuador, nigordonbe@uide.edu.ec,
[3] Ingeniería Automotriz – Universidad Internacional del Ecuador, osintriagoga@uide.edu.ec,
[4] Ingeniería Automotriz – Universidad Internacional del Ecuador, anperezag@uide.edu.ec,

RESUMEN

La tecnología ha permitido el desarrollo de dispositivos termográficos, con la capacidad de realizar mediciones en varios cuerpos, y debido a la crisis sanitaria que atraviesa el mundo por el virus (SARS-Cov-2), este tipo de elementos se han convertido en herramientas necesarias para identificar posibles casos de contagio, puesto que la enfermedad descrita se ha manifestado como un trastorno de carácter sintomático, donde gracias a la recopilación de datos entre grupos de personas contagiadas, se ha logrado identificar que, con una prevalencia porcentual superior, el aumento del límite de temperatura es el trastorno con mayor incidencia. Por lo que en base a la necesidad de implementar medidas de bioseguridad para el público que se moviliza en el trasporte masivo, se diseñó un dispositivo con la capacidad de identificar el espectro térmico de las personas, que dependiendo de su esto de salud variara entre los 36 °C y 40 °C. Las pruebas de campo y la recopilación de datos revelaron que el dispositivo termográfico, capto la temperatura de una forma precisa y el sistema integrado en el dispositivo logro identificar la normo termia de un individuo con un margen de error reducido al centrar su medición en 3 lugares fijos, a una distancia de 0.50 metros. El análisis realizado después de obtener los resultados determinó que el dispositivo termográfico al variar su rango y sus puntos de medición cambia su comportamiento y refleja distintos valores, es decir que si no se consideran estas variables tendrá un margen de error considerable.

Palabras clave: Dispositivo termográfico, temperatura, puntos de medición, (SARS-CoV-2), espectro térmico.

ABSTRACT

Technology has allowed the development of thermographic devices, with the ability to perform measurements on various bodies, and due to the health crisis that the world is experiencing due to the virus (SARS-Cov-2), these types of elements have become tools. necessary to identify possible cases of contagion, since the disease described has manifested itself as a symptomatic disorder, where, thanks to the collection of data between groups of infected people, it has been possible to identify that, with a higher percentage prevalence, the increase temperature limit is the disorder with the highest incidence. Therefore, based on the need to implement biosafety measures for the public that is mobilized in mass transport, a device was designed with the ability to identify the thermal spectrum of people, which depending on their health this will vary between the 36 ° C and 40 ° C. Field tests and data collection revealed that the thermographic device captured the temperature accurately and the system integrated in the device was able to identify the normal thermic of an individual with a reduced margin of error by focusing its measurement in 3 places. fixed at 0.50 meters. The analysis carried out after obtaining the results determined that the thermographic device by varying its range and its measurement points changes its behavior and reflects different values, that is, if these variables are not considered, it will have a considerable margin of error.

Keywords: Thermographic device, temperature, measurement points, (SARS-CoV-2), thermal spectrum.

1. INTRODUCCIÓN

El 31 de diciembre del 2020 en el país de China se dan los primeros 26 brotes de una desconocida enfermedad, que por sus características y por su evolución, tenía mucha similitud con una tos común. Sin embargo, un paciente de los primeros 26 casos originados en un mercado de mariscos de la ciudad de Wuhan presentaba un diagnóstico de neumonía por etiología desconocida, lo que elevo las sospechas de un nuevo tipo de enfermedad en el paciente. Después de haber presenciado los primeros casos y las primeras muertes por esta enfermedad el 7 de enero del 2020, el centro chino para el control y prevención de enfermedades identificó un agente relacionado con síndromes reparatorios similares al (SARS) y en base a la similitud con el (SARS-CoV) descubierto en 2003, se lo denominó como (SARS-CoV-2). La identificación de este nuevo tipo de virus revelo varias características clínicas que afectaban al organismo de los contagiados. Entre los síntomas con mayor frecuencia en las personas se detectó neumonía, tos seca, fatiga, dolor en la garganta, malestar muscular y fiebre, pero cabe recalcar que los síntomas dependen del paciente ya que, también se logró comprobar que un grupo reducido de personas experimentaron otro tipo de síntomas como vomito, dolores de cabeza, diarrea, hemoptisis, disnea, producción de esputo y linfopenia [1, 2].
Después de los hechos expuestos hace meses en china, el mundo se ve afectado por este nuevo agente que se ha propagado por todas las naciones, puesto que el (SARS-Cov-2) también fue identificada como una enfermedad altamente contagiosa en humanos, ya que tiene la característica de permanecer suspendido en el aire a una distancia aproximada de 1,8 metros y además de esto se ha detectado que el virus se mantiene en superficies de diferentes materiales [3].
Lamentablemente existe un crecimiento exponencial de contagios, que ha obligado a los países a implementar nuevos protocolos de bioseguridad como una medida de prevención para identificar de posibles casos.
Con la finalidad de implementar una medida de bioseguridad para evitar contagios, el presente artículo se basó en el desarrollo de un dispositivo capaz de identificar la temperatura corporal de las personas que se movilizan en el transporte público de la ciudad de Quito-Ecuador. El desarrollo del tema parte en base a la problemática que se da por la afluencia de personas en el trasporte público sin el control de temperatura corporal, ya que uno de los síntomas con mayor frecuencia entre los posibles contagios por (SARS-CoV-2) es la fiebre, que se define como la elevación de la temperatura corporal fuera de un determinado rango. Obteniendo así la necesidad por desarrollar un dispositivo que permita realizar este tipo de mediciones bajo parámetros específicos dictados por síntomas corporales [4, 5].
Al elemento en mención, se lo ha definido como un equipo termográfico, mediante entrada visual, el cual facilite la medición de la temperatura corporal y se adapte para funcionar en los vehículos del transporte público de la ciudad de Quito, brindando apoyo ante la propagación del (SARS-CoV-2), identificando a las personas con temperatura elevada y recopilando información en tiempo real.
El monitoreo de la temperatura corporal se da gracias a la disponibilidad e interacción de elementos electrónicos y se lo interpreta como una necesidad para verificar el estado de salud de las personas, puesto que al implementar dispositivos que realicen este tipo de mediciones, se brinda el seguimiento necesario, para cuantificar variaciones en el cuerpo humano, que en escenarios específicos pueden significar afecciones a la salud, [6].
En la investigación de un equipo termográfico, capaz de obtener lecturas rápidas, precisas y eficientes de la temperatura corporal, es importante analizar la interacción de varios materiales como, sensores térmicos, pantallas de transmisión de imágenes, tarjetas programables que permitan proporcionar una

interfaz controlable, un panel exterior capaz de modificar el funcionamiento del dispositivo, elementos de alimentación hacia la batería y una carcasa interactiva protectora del sistema en general [7].

2. FUNDAMENTO TEÓRICO

Es de suma importancia comprender que el (SARS-CoV-2) se ha propagado por el planeta, de una forma agresiva, iniciando así una batalla diaria para implementar medidas de prevención y detección, con el claro objetivo de frenar la curva de contagios a nivel mundial, mientras se afinan todos los detalles de las vacunas y de su distribución. Esta lucha se basa en la implementación de elementos capaces de, revelar síntomas y de identificar la presencia del virus en las personas.

Entre la amplia gama de posibilidades se estableció alternativas amigables hacia las personas, debido a la evidencia de organismos vivos con la capacidad de desempeñar un papel fundamental en la detección de enfermedades infecciosas y parasitarias, así como el cáncer. Con respecto a otras enfermedades no infecciosas, varios estudios han sugerido que los perros pueden usarse como "perros de alerta" para pacientes diabéticos y epilépticos, para mejorar la calidad de vida del paciente. Los resultados de este estudio de prueba de concepto son un primer paso prometedor que proporciona alguna evidencia de que los perros pueden detectar muestras positivas de (SARS-CoV-2) recolectadas del sudor axilar de personas que muestran síntomas clínicos. Tras todas las pruebas realizadas durante las primeras semanas los perros tenían entre un 76% y 100% de precisión en la detección de (SARS-CoV-2). En los últimos meses, los investigadores han mejorado sus técnicas de entrenamiento para que los perros ahora, en promedio, puedan identificar a las personas con (SARS-CoV-2) con un margen del 95% de precisión, y en algunos casos un se manejan con un 97% [8].

2.1. Instrumentos médicos de medición

Debido a las dificultades provocadas por el (SARS-CoV-2), muchas de las personas se han visto en la necesidad de adquirir instrumentos médicos en sus hogares en caso de presentar síntomas referentes a la enfermedad, debido a que busca mantener un control del cuerpo en general.

Tabla 1 Instrumentos de medición (SARS-CoV-2)

Instrumentos médicos de medición	
Equipo	**Característica**
Estetoscopio	Se utiliza para escuchar los sonidos que se producen en el corazón y en los pulmones. Para identificar posibles problemas respiratorios se realizan diversas mediciones auditivas en diferentes partes de la caja torácica del paciente.
Oxímetro de pulso	Dispositivo pequeño que permite conocer el nivel de oxígeno presente en la sangre. Los niveles normales de oxígeno en la sangre que una persona deba poseer están considerados entre 75mmHg y 100mmHg.
Termómetro digital	Herramienta utilizada para verificar la temperatura de una persona en caso de que haya sospecha de fiebre. Se realizan mediciones en la frente, por lo general los rangos de mediciones que el dispositivo puede ofrecer se encuentran entre los 32°C y los 42,2°C.

Fuente: Elementos de medición medica [9, 10, 11]

Es de suma importancia que el análisis de datos obtenidos con estos instrumentos sea evaluado por un profesional de la salud, debido a que esta persona será la encargada de interpretar de una manera adecuada los diversos signos vitales obtenidos, gracias a su capacidad profesional para evaluar, diagnosticar y manejar diferentes patologías.

2.2. Temperatura corporal

El cuerpo humano se caracteriza por ser un sistema que se encarga de mantener su temperatura central constante, aproximadamente en los 37 °C por regulación fisiológica, que está controlada por el hipotálamo y que se asocia con el equilibrio entre el flujo sanguíneo y el metabolismo, de acuerdo con la teoría de la "*Eliminación de calor*" [12].

El cuerpo de las personas en general es capaz de obtener calor pasivamente de un ambiente cálido y activamente del metabolismo generador de energía, por lo que cuando se hace referencia a la teoría de la "*Eliminación de calor*", hablamos de que en el momento que un cuerpo empieza a subir su temperatura la piel se encarga de disipar el exceso de calor a través de la vasodilatación cutánea que, al desviar la sangre caliente desde el centro del sistema hacia la periferia, facilita la conducción pasiva, la convección y la radiación de calor hacia una ambiente más frio; y también podemos encontrar un proceso de secreción de sudor en la superficie, que tiene la finalidad de enfriar por evaporación incluso cuando la temperatura externa excede a la de la piel [13].

Tabla 2. Equilibrio de calor en el cuerpo humano

Equilibrio térmico		
Fase	**Temp (°C)**	**Características**
Hipertermia	>40	Degeneración celular, hemorragias locales y daño cerebral (permanente).
Febrícula	37.5 – 37.9	Sudoración, escalofríos y fatiga muscular.
Normo termia	36 – 37.2	Estado normal del cuerpo.
Hipotermia	<35	Arritmias, depresión de la funciones metabólicas y circulatorias, muerte cerebro.

Fuente: Temperatura y sus características [14].

La temperatura y su elevación sin control en el cuerpo humano se debe considerar como un signo de alerta, que en ciertas ocasiones se lo puede tratar con la eliminación de un ambiente caluroso, el reposo y la rehidratación. Pero cuando se presentan otro tipo de factor causante de dicha elevación como él (SARS-CoV-2), se puede presentar la hipertermia que se relaciona con el aumento de temperatura mayor a 37 °C, que desencadena una fase prodrómica, que se define como el agotamiento por calor, que puede progresar rápidamente a un golpe de calor. El golpe de calor se caracteriza por tener una temperatura mayor a los 40 °C, con varios signos y síntomas de disfunción en el sistema nervioso centrar, que puede progresar a una falla de órganos y en pocas ocasiones la muerte. Por esto es importante que si se llega presentar este tipo de escenario se maneje un proceso de enfriamiento inmediato, seguido de atención medica profesional [13].

Otra consideración por tomar en cuenta sobre el tema tratado previamente es la oscilación térmica entre las personas, debido a que su valor nominal cambia y se diferencia en función de la edad.

Tabla 3. Rangos de temperatura según la edad

Temperatura		
Grupo	**Edad**	**°C**
RN	Nacimiento- 6 semanas	38
Infante	7 semanas – 1 años	37.5 a 37.8
Lactante mayor	1-2 años	37.5 a 37.8
Preescolar	2-6 años	37.5 a 37.8
Escolar	6-13 años	37 a 37.5
Adolescente	13-16 años	37
Adulto	16 años y más	36.2 a 37.2

Fuente: Intervalos térmicos según la edad [15].

La elevación de temperatura se la considera como un factor a tomar en cuenta en la crisis

sanitaria producida por el (SARS-CoV-2), debido que es uno de los síntomas con mayor frecuencia entre las personas contagiadas por el virus. Varios estudios que se han realizo a nivel mundial revelan esta característica y como claro ejemplo sobre el tema, se analizó el estudio provisto por "*Cable News Network (CNN)*", que se basó en el la recopilación de datos de un grupo de 24,410 personas adultas, logrando así identificar que la febrícula y la hipertermia, son síntomas con un 78% de prevalencia entre las personas, a comparación de otros síntomas como, la tos, la fatiga, la perdida de olfato, la dificultad al respirar, entre otros más [16].

2.3. Dispositivos Electrónicos

En la actualidad los dispositivos electrónicos toman un papel fundamental en la vida de las personas, puesto que brindar una amplia gama de beneficios al desarrollar e implementar avances tecnológicos año tras año, por lo que el artículo enfatizó el desarrollo de un equipo termográfico electrónico, mediante entrada visual adaptable a la medición de la temperatura de las personas, puesto que este parámetro está estrechamente relacionado con las funciones del cuerpo y en general, se entiende que es posible realizan una evaluación rápida de la salud de un individuo.

2.4. Cámara termográfica

Se la define como un elemento capaz de obtener imágenes de la distribución de calor sobre una superficie, mediante la aplicación de principios referentes a la termografía infrarroja y a la utilización de la trasmisión de calor como una variable en relación con la temperatura sin la necesidad del contacto físico con el objeto o en este caso en específico, con la piel de las personas, puesto que brinda características especiales mediante la aplicación de ensayos no destructivos con capacidad de inspección al 100% [17].

Según la norma *"ISO 18434-1:2008",* la capacidad de un elemento termográfico de realizar ensayos no destructivos se relaciona hacia el diagnostico de máquinas bajo condiciones y parámetros establecidos, como guía para la detección de anomalías, que usualmente se presentan por fallas en alguna parte del sistema. Analizando así que una estructura con la capacidad para implementar este tipo de tecnología de monitoreo hacia las condiciones de funcionamiento del sistema provee una solución no agresiva en intervalos cortos de tiempo [18].

Si bien es cierto la norma específica que el diagnostico de análisis es dirigido hacia la maquinaria, en la actualidad las características de funcionamiento de un elemento termográfico no están ligadas únicamente a la premisa expuesta, por lo cual durante varios se han conducido proyectos con una amplia gama de aplicaciones para el cuerpo humano, que han demostrado que esta clase de sistemas tienen un alto grado de fiabilidad para ser utilizados en el ramo de la salud [19].

La cámara termográfica sin duda tiene una amplia versatilidad de funciones que se basan en la recopilación de datos y en el análisis de imágenes bajo diferentes tipos de funcionamiento, puesto que no trabajan bajo el mismo estándar visible de 400-700 nanómetros de las cámaras convencionales de luz, debido a que las cámaras infrarrojas son sensibles a longitudes de onda que oscilan aproximadamente entre 1 a 14µm [20]. Este tipo de características y el avance tecnológico en el dispositivo mencionado, permiten la obtención de imágenes en tiempo real, con una escala de colores que representan la distribución de la temperatura por diferentes lugares del cuerpo de una persona o en si de un objeto, puesto que todos los cuerpos emiten radiación infrarroja y se ven afectados por factores como la emisividad, la temperatura ambiente, la distancia del objeto, la humedad relativa y la temperatura atmosférica [17].

Los fundamentos con los que trabaja una cámara termográfica se basan en varios enunciados y leyes propuestas sobre radiación infrarroja. Por lo que, para comprender el funcionamiento de un dispositivo con la capacidad de captar este tipo de imágenes, se

enfatiza el análisis la *"ley de Stefan-Boltzmann"* que afirma que la energía de radiación emitida por todos los cuerpos es proporcional a la cuarta potencia de la temperatura superficial del objeto [21].

$$W = \sigma T^4 \qquad \text{[Ec 1]}$$

Donde los "W" se considera como la potencia emisiva superficial; "σ" se define como la constante de Stefan-Boltzmann de $(5{,}67\ x\ 10^{-8}\ W/cm^2k^4)$ y por último "T" de la temperatura.

Después de comprender una de las leyes fundamentales, será de suma importancia considerar que, el espectro visual que brinda las cámaras se da gracias a su captación de ondas para la lectura de imágenes infrarrojas y según *"La ley de Wien"* es la relación establecida entre la temperatura y la longitud de onda de un cuerpo. [21]

$$\lambda max = \frac{2897{,}6}{T}\ (\mu m * K) \qquad \text{[Ec 2]}$$

Donde se considerará que la longitud de onda *"λ"* es igual a relación obtenida entre la constante propuesta por *"Wien"* de 2897,6 µm * K y la temperatura *"T"*. Es así como La ley de *"Wien"* interpreta una clara consecuencia, que se la define como los intervalos de térmicos de un cuerpo negro, bajo la clara premisa que especifica, mientras mayor sea la temperatura irradiada de dicho cuerpo menor será la longitud de onda y, por el contrario, mientras menor sea la temperatura mayor será la longitud de la onda [22].

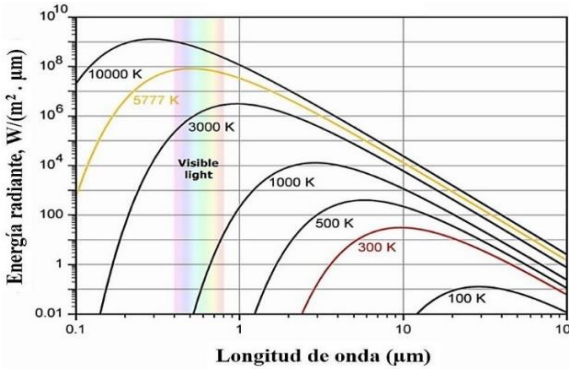

Figura. 1 Longitud de Onda vs Energía Radiada.
Fuente. Densidad espectral [22].

2.4.1. Parámetros para la medición

Es importante comprender que la capacidad de obtener imágenes en tiempo real de los equipos termográficos se debe a la naturaleza de los cuerpos para irradiar su energía en función de su temperatura, como lo proclama e identifica la relación de *"la ley de Kirchhoff"*.

$$\alpha = \mathcal{E} \qquad \text{[Ec 3]}$$

Afirmando así que todos los cuerpos son capaces de emitir "Ɛ" su propia energía radiante y absorber "α" la misma cantidad de energía proveniente de elementos externos [23].

$$\mathcal{E} + \tau + \rho = 1 \qquad \text{[Ec 4]}$$

Siendo así que "τ" es la radiación trasmitida que atraviesa al cuerpo sin afectarlo; "ρ" es la radiación reflejada y "Ɛ" es la radiación saliente de un cuerpo, que sumada con las anteriores equivalen a "1" y se definen como radiación incidente de un cuerpo ideal. Sin embargo, en la realidad no todos los organismos son "cuerpos negros", es decir que no todos emiten el 100% de su energía, mientras igualan a 0 su capacidad de trasmitir y reflejar energía radiante, sino todo lo contrario, puesto que los cuerpos varían su opacidad y limitan su capacidad de trasmitir energía infrarroja [21].

$$\tau = 0 \ \rightarrow \ \mathcal{E} + \rho = 1 \qquad \text{[Ec 5]}$$

Donde la suma de la radiación saliente "Ɛ" y la radiación reflejada "ρ", se la conoce como el 100% de la energía infrarroja saliente.

3. MATERIALES Y METODOS

3.1. Método

Para la elaboración del proyecto se emplearon dos métodos, primero el deductivo y segundo el inductivo, donde el primero se caracteriza por extraer una conclusión referente a una premisa establecida en base a una serie de

proposiciones interpretadas como aseveraciones que fueron utilizadas como fundamentos para el segundo método; donde se aplicó el estudio realizado de forma general, en relación a los hechos recopilados como conclusiones universales, fundamentos y leyes [24, 25]. Es así como la investigación se enfocó en el análisis termográfico del cuerpo humano, debido a su capacidad para recibir, producir y emanar energía, referente a la frecuencia de ondas infrarrojas irradiadas, que varían su espectro ante la intermitencia térmica de una baja y alta temperatura, que será medida en un rango espectral que oscila entre las 8 y 14 µm a una tasa de imagen proyectada sobre los 8.7 Hz, mediante la comparación cuantitativa, referente a múltiples parámetros que interviene en la medición como un método de evaluación; que en este caso se lo atribuye al diseño de un equipo termográfico, mediante entrada visual, con la capacidad de cuantificar y procesar un valor total, dentro de un determinado ecosistema [26].

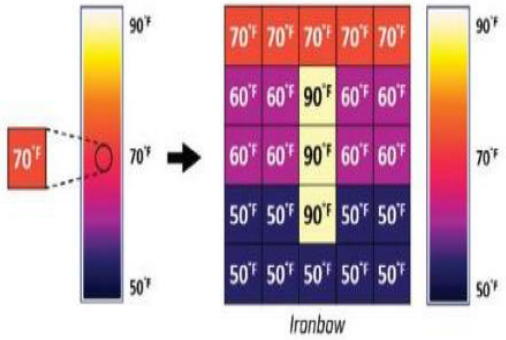

Figura. 2 Intermitencia térmica a baja y alta.
Fuente. Cámara térmica [27, 28].

3.2. Materiales

3.2.1. Frecuencia de onda

El equipo termográfico, mediante entrada visual se caracteriza por ser un sistema que trabaja en conjunto con la implementación de un software y el desarrollo de un hardware que, gracias a la interacción de varios materiales, corrigen y compensan señales, con el claro objetivo de obtener un resultado de la energía registrada al 100% [29].

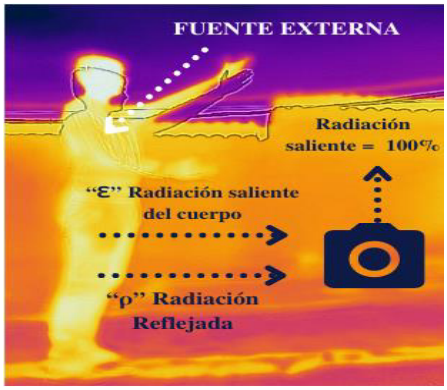

Figura. 3 Flujo de energía para medición termográfica.
Fuente. Cámara termográfica [30].

3.2.2. Cámara

En la actualidad la amplia gama de materiales y dispositivos electrónicos han permitido desarrollar equipos con la capacidad de ser implementados en diferentes campos, es por esto que con la finalidad de crear un equipo termográfico que se acople a la necesidad del proyecto, se realizó una comparación entre 3 cámaras termográficas y sus características.

Tabla 4. Comparación entre cámaras termográficas

Cámaras termográficas			
Características	**Seek Thermal Compact Pro**	**Fluke Tis60+**	**Flir One Pro**
Precisión	±3°C	±2°C	±3°C
Frecuencia de refresco	<9Hz	9- 30 Hz	8.7Hz
HFOV / VFOV	32°	34,1°/25,6°	55°/43° ±1°
Resolución térmica	320 x 240	320 x 240	160 x 120
Sensibilidad térmica NETD	<70mK	45mK	70mK
Banda espectral	7,5–14 µm	7,5–14 µm	8 – 14 µm
Resolución visual	76,800px	76,800px	1,555,200 px
Puntos de medición	2	3	3

Fuente. Empresas fabricantes [30, 31, 32]

Después de comparar las características expuestas, la cámara escogida como referencia para el desarrollo del equipo fue la FLIR®,

puesto que se acopla como un dispositivo termográfico con la habilidad de captar y realizar mediciones de imágenes infrarrojas en tiempo real, junto a varias características de diversos mecanismos sincronizaos entre sí. Lo que ha permitido entender que la construcción del elemento diseñado debe fundamentarse en base en la unión de partes como, instrumentos de imagen óptica infrarroja, interfases de proyección, programas de control termográfico y puertos periféricos, que trabajan en conjunto con la finalidad de obtener un valor determinado [30].

3.2.3. Instrumento de imagen óptica infrarroja

El instrumento encargado de la captación de imágenes parte del hardware constituido por la cámara termográfica IR, que tiene como principal característica la implementación del sistema MSX con 2 cámaras; la primera capaz de captar ondas infrarrojas y la segunda responsable de visualizar imágenes VGA, con la finalidad de obtener una imagen IR con detalles de mayor resolución [33].

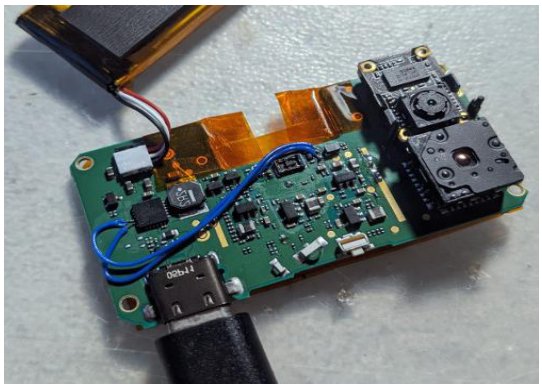

Figura. 4 Sistema MSX de 2 cámaras.
Fuente. Autores.

Los lentes ópticos detalladas previamente tienen la capacidad de realizar mediciones en base al procesamiento de algoritmos con fórmulas establecidas por leyes sobre la radiación infrarroja, para así ser utilizado como base en la medición de la variación térmica de varias personas, debido a que ofrece una amplia gama de características mostradas en la tabla 5.

Tabla 5. Principales características de funcionamiento

Rama	**Característica**
Precisión	±3°C o ±5%, porcentaje típico diferencial entre el ambiente y la escena térmica.
Rango dinámico	-20°C a 400°C
Distancia mínima de enfoque	Térmica 15cm / MSX 30cm
Frecuencia de refrescó	8.7 Hz
HFOV / VFOV	55° ±1° / 43° ±1°
Resolución térmica	160 x 120
Sensibilidad térmica NETD	70 mK
Banda espectral	8 – 14 µm, en un píxel de 12 µm
Resolución visual	Lente de 1440 x 1080
Puntos de medición	3 a la par

Fuente. Apliter Termografía [30, 33].

Las características del elemento y su funcionamiento en conjunto se rigen al cumplimiento de normas y certificaciones, creadas por organismos internacionales que proporcionan una o varias granatitas sobre la actividad a realizar en los diferentes entornos existentes, como se pueden observar en la tabla 6.

Tabla 6. Normativas y certificaciones.

Normativas y certificaciones	
Tipo	**Aplicación**
RoHS	Reducción de sustancias peligrosas en dispositivos eléctricos y electrónicos [34].
Ce / FCC	Comprobación del funcionamiento adecuado, bajo medidas establecidas en América y Europa [35].
Directiva 2014/30/EU	Compatibilidad electromagnética de los dispositivos [36].
Estándar EN 61000-3-2:2014	Límites para las emisiones de corriente armónica, según “EMC” (compatibilidad electromagnética) [37].
Estándar EN 61000-3-3:2013	Límites de cambio y fluctuación para sistemas de bajo voltaje, para “EMC” (compatibilidad electromagnética) [38].

Estándar EN 55032:2012	Requisitos de emisión de los equipos de multimedia según, "EMC" (compatibilidad electromagnética) [39].
Estándar EN 55022	Información técnica para realizar pruebas en base métodos de medición [39, 40].

Fuente. Organismos internacionales [34 - 40].

3.2.4. Puertos periféricos

El dispositivo termográfico en el proceso previo a la obtención de datos, se proyecta como un elemento que tiene la necesidad y la capacidad de relacionarse con otros instrumentos electrónicos como teléfonos, pantallas y computadoras, para exhibir imágenes con valores térmicos; es por esto que se consideró como prioridad establecer la conexión hacia la interfase por medio de cables macho / hembra USB 2.0 y USB tipo "c" en varios puertos, con el propósito de permitir la trasmisión de energía y datos por largos periodos de tiempo [41].

Figura. 5 cables de conexión.
Fuente. Autores.

4. RESULTADOS Y DISCUSIÓN

4.1. Procedimiento

El equipo termográfico, mediante entrada visual, se basa en la aplicación de varios procesos referentes al cumplimiento de parámetros establecidos por la integración de materiales, que se conjugan con el propósito de medir la temperatura de una forma precisa y objetiva para lograr identificar valores admisibles o inadmisibles, según las consideraciones del sector de la salud, en referencia a la crisis sanitaria provocada por el (SARS-CoV-2). Definiendo así que el procedimiento para la obtención de datos se basó en el análisis y la modificación de los parámetros del software para procesar la información proveniente del hardware, dentro del espacio protegido por una carcasa, que se adaptó hacia el entorno en donde se realizaron las pruebas de campo.

4.1.1. Software

El software es la herramienta que se encarga del control del elemento termográfico y se identifica como el conjunto de operaciones programadas en un determinado lenguaje, que permite realizar mediciones, tomar capturas y calibrar el dispositivo. Es así como el funcionamiento de la cámara termográfica se basó en la implementación del lenguaje de programación de tipo intermedio, que se caracteriza por compilar códigos fuente elaborados dentro de un programa informático, para poder ejecutarlos en varios dispositivos o en una máquina virtual. Por lo que para lograr diseñar y modificar parámetros, se utilizó el programa informático "MATLAB Resources", que se caracteriza por emparentar, alterar y facilitar la interacción entre el software y hardware [42].

```
defineCRT_SECURE_NO_WARNINGS_UIDE_SCA
N_CAM1#

#include "mex.h"_ RANGE _ VRBL//4S
#include "tc.file/tc.file.h"_
DSCT//0.5_1_1.5
#include <typeinfo> _ MOD // ENT_END
//01

//mex FlirMovieReaderMex.cpp -
I%FILESDKDIR%include -
L%FILESDKDIR%bin/x64/Release -ltc.lib
-ltc.file.lib -ltc.reduce.lib

//matlab data mashalling helper
functions
template<typenamekind>structmxClassFr
omType;
```

Figura. 6 Funciones para clasificación de datos.
Fuente. Autores.

4.1.1.1. Aplicación de control

Al referirnos a un sistema que se maneja por un software con lenguaje de programación es

importante comprender que se necesita de una aplicación que cumpla con las funciones e interprete los comandos del dispositivo, es por esto que con la ayuda del soporte brindado por FLIR® hacia el equipo termográfico y su sistema óptico, se utilizó la aplicación térmica desarrollada por la casa fabricante, debido a su capacidad para compartir similitudes en procesos informáticos, referentes a las funciones requeridas por proyecto.

4.1.2. Hardware

La composición del hardware se basa en la unión de los materiales detallados previamente dentro de un armazón, que funcionara como coraza y aloja puertos de múltiples entradas, para conectar, trasmitir datos y alimentar de energía al elemento, con la intención de que el proceso se desarrolle de la forma deseada. Es así como funcionamiento en conjunto se lo representa bajo la sucesión de pasos puntuales, con un determinado orden, como se lo puede observar en la Figura 7.

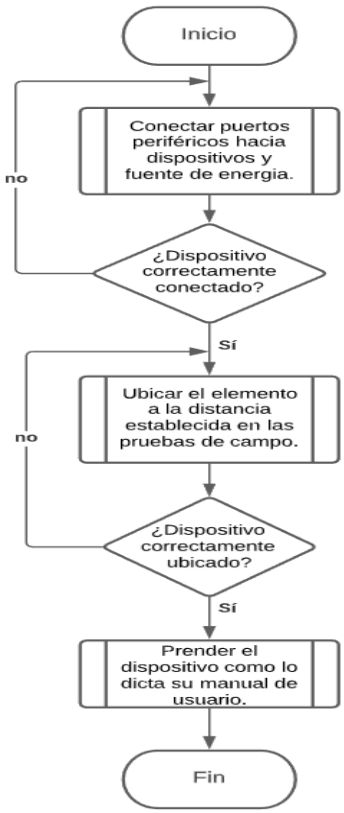

Figura. 7 Diagrama de conexión, ubicación e inicio hardware.
Fuente. Autores.

4.2. Software y hardware

La principal característica del sistema en general es la unión de elementos e información programada que funcionan en conjunto, bajo un determinado flujo de recopilación, recepción, análisis, comparación e interpretación de datos, para entregar y mostrar resultados térmicos precisos.

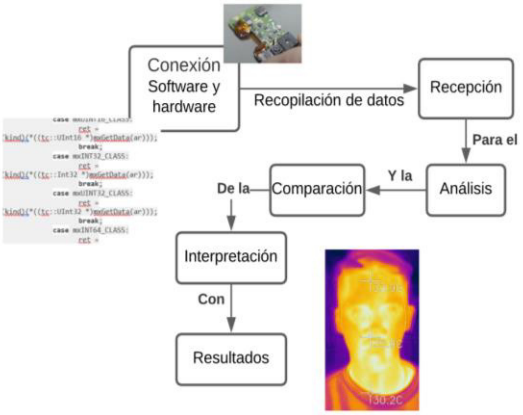

Figura. 8 Funcionamiento software y hardware.
Fuente. Autores.

4.3. Recopilación de datos

El dispositivo termográfico se define como un instrumento capaz realizar mediciones y entregar una serie de datos que revelan la temperatura de un individuo en relación con factores externos, por lo que, para garantizar el funcionamiento del elemento dentro del entorno escogido, se realizaron una serie de pruebas que permitieron analizar la efectividad de la cámara termográfica en relación con un termómetro infrarrojo de medición térmica.

Figura. 9 Termómetro infrarrojo LyfTrack.
Fuente. Autores.

El termómetro infrarrojo Lyftrack fue implementado en el análisis del presente estudio, debido a su capacidad para realizar ensayos no destructivos a distancia, debido a que basa su funcionamiento en un sensor infrarrojo que interactúa con otros componentes y registra la temperatura del cuerpo de una persona bajo normativas aceptadas por varios entes internacionales, como se puede observar en la tabla [43].

Tabla 7. Características de funcionamiento

Rama	**Característica**
Modelo	IR 988
Rango del display	34.8 °C – 42.5 °C
Distancia mínima de enfoque	Térmica 15cm / MSX 30cm
Precisión	0.1 °C/°F
Distancia de medición	3 – 5 Cm
Memoria interna	32 unidades
Error admisible	±0.2°C
Estabilización	20s
Certificaciones	FCC, FDA, VRohs & CE

Fuente. LyfTrack [43].

4.4. Comparativa de datos

La comparación de datos se define como un segmento capaz de observar el comportamiento del dispositivo, en un entorno influenciado por factores externos de diferente índole, es por esto que para desarrollarlo se instauro un proceso de medición térmica infrarroja que abarca variables como, la distancia, la temperatura ambiente, la sensación térmica, la distancia entre participantes, el lugar de medición, los puntos de medición y el horario en el que se registran los datos, con la finalidad de contrastar información y conocer la exactitud con la que es capaz de trabajar dispositivo termográfico diseñado.

4.4.1. Primera etapa

La medición grupal fue considerada como la primera etapa para comparar datos, debido a la capacidad del dispositivo termográfico para medir varios puntos en tiempo real.

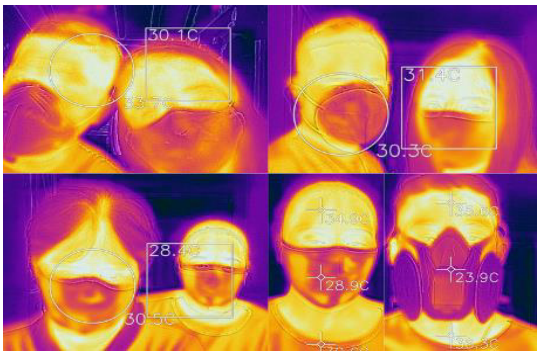

Figura. 10 Medición grupal.
Fuente. Autores.

Sin embargo, por las características del software para ajustar valores conforme el entorno y sobre todo por el riesgo de contagio grupal, se optó por descartar mediciones de este tipo. Además, no se realizó una comparación de datos con el termómetro infrarrojo LyfTrack debido a que el instrumento solo permite medir individualmente a las personas.

Con el objetivo de comprender que el dispositivo no está optimizado para obtener mediciones precisas en la presencia de varios individuos, se definieron parejas y se analizaron valores térmicos a 0.5m, 1m, 1.5m y 2 metros de distancia.

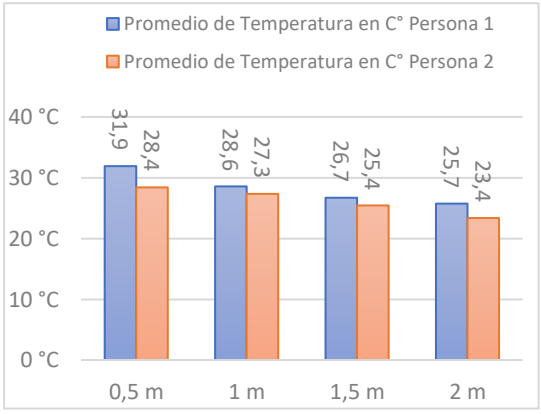

Figura. 11 Datos en pareja de la primera etapa.
Fuente. Autores.

4.4.2. Segunda etapa

Para la segunda etapa de recopilación y comparación de datos térmicos, se instauro un

proceso de medición con el dispositivo termográfico diseñado y con el termómetro infrarrojo LyTrack, a diferentes longitudes, que partían desde los 3 cm hasta 29 cm, con intervalos de 2 centímetros entre cada punto de medición.

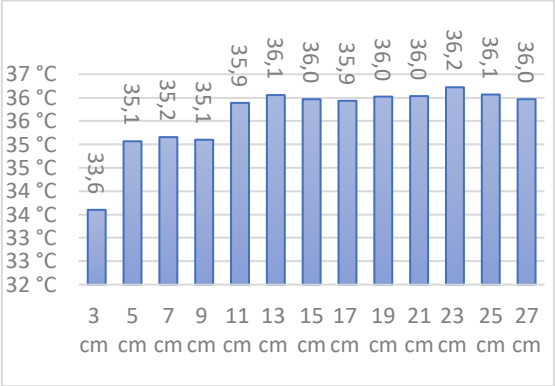

Figura. 12 Datos dispositivo termográfico diseñado.
Fuente. Autores.

La figura 12 indica que el dispositivo termográfico diseñado en distancias cortas tiende a emitir datos térmicos de forma ascendente y con grandes intervalos.

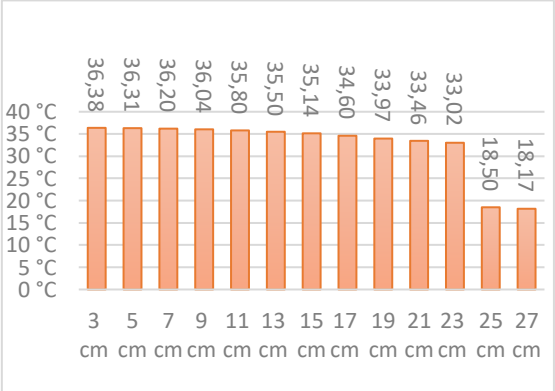

Figura. 13 Datos termómetro infrarrojo LyTrack.
Fuente. Autores.

La figura 13 muestra que el termómetro infrarrojo LyfTrack emite valores de forma descendente y su precisión aumenta cuando menor es la distancia.

En la comparativa de datos también se tomó en cuenta la temperatura del ambiente en diferentes horarios, para contemplar si la variación de la misma resulta en un incremento o una disminución en los valores arrojados por los instrumentos de medición. Donde las columnas ubicadas en el lado izquierdo hacen referencia al termómetro infrarrojo LyTrack y las columnas ubicadas en la derecha son del dispositivo termográfico diseñado.

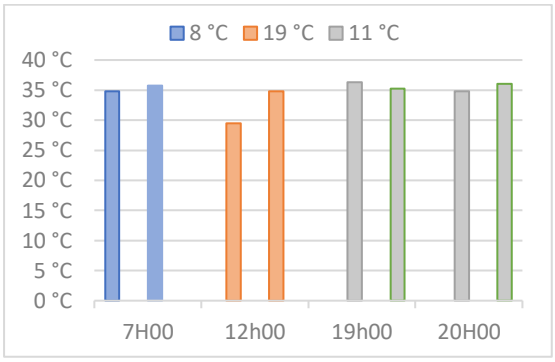

Figura. 14 Relación térmica Hora / Temperatura ambiente.
Fuente. Autores.

Después de realizar las pruebas de campo, se logró definir que el punto adecuado para medir la temperatura con el termómetro infrarrojo LyfTrack se encuentra en la frente a 3 centímetro del individuo; mientras que el dispositivo termográfico diseñado a esta distancia entrega valores imprecisos.

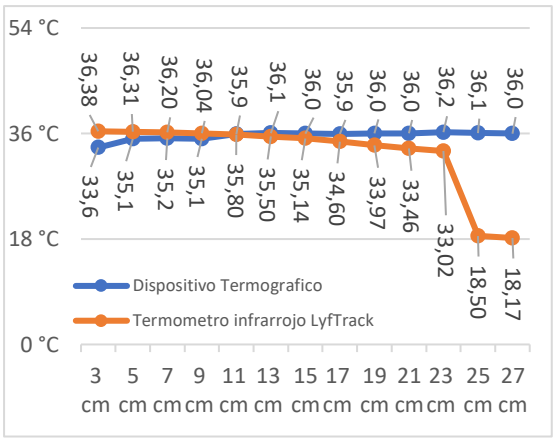

Figura. 15 Comparación entre dispositivos.
Fuente. Autores.

Además de lo mencionado previamente, fue posible constatar que el termómetro infrarrojo LyfTrack realiza mediciones precisas a cortas distancias. Por el contario el dispositivo termográfico diseñado, demostró que estos rangos no son favorables debido a la variación e intermitencia térmica captada.

4.4.3. Tercera etapa

La recolección de información en la tercera etapa se basó en ubicar el dispositivo termográfico diseñado en un lugar fijo, con tres puntos de medición constantes a 0.50m, 1m, 1.5m y 2 metros de longitud, con el propósito de lograr identificar la distancia adecuada, para conseguir mediciones precisas de la temperatura corporal de las personas.

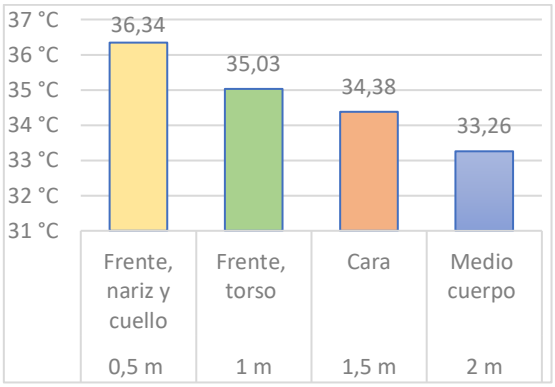

Figura. 16 Relación ubicación, distancia y temperatura.
Fuente. Autores.

Gracias a las mediciones realizadas en un grupo de 14 personas se logo identificar que la distancia adecuada para medir la temperatura de las personas es 0.50 metros, puesto que los valores se mantienen constantes y varían de 0.1 °C a 0.2 °C, como se puede observar en la imagen 17.

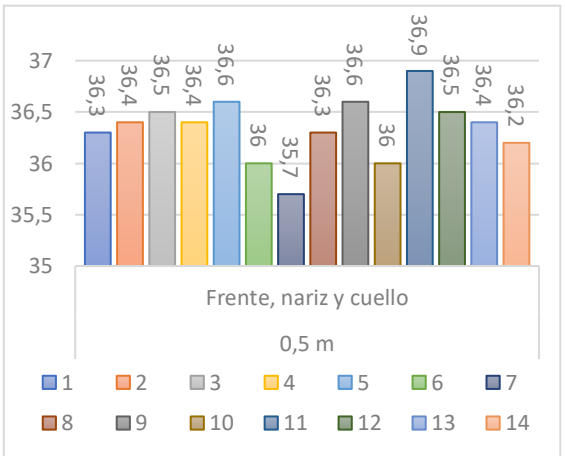

Figura. 17 Distancia referencial adecuada dispositivo termográfico diseñado.
Fuente. Autores.

Para demostrar que el dispositivo termográfico diseñado tiene la capacidad de identificar la temperatura de las personas de una forma precisa, se realizaron mediciones a la distancia adecuada de 0,03 metros del termómetro infrarrojo LyfTrack y se cortejaron con los datos capturados a la distancia adecuada del dispositivo termográfico diseñado.

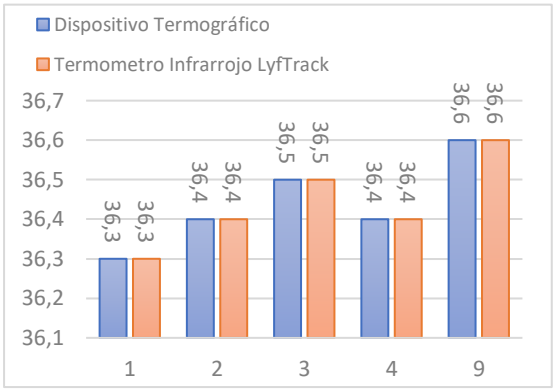

Figura. 18 Primer contraste entre dispositivos.
Fuente. Autores.

El primer contraste realizado entre los dispositivos permitió observar que 5 de las mediciones no tiene variaciones, es decir que el dispositivo se muestra como un instrumento que trabaja con un rango de error de ±0.0°C.

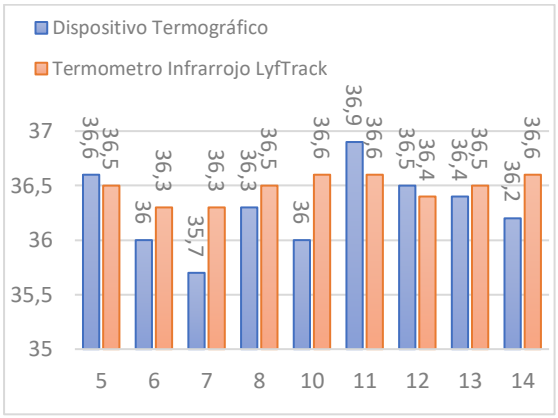

Figura. 19 Segundo contraste entre dispositivos.
Fuente. Autores.

Mientras que para el segundo contraste se observó que en 9 de las mediciones existieron fluctuaciones que se extendieron hasta un máximo de diferencia de 0.6 °C. Revelando que el dispositivo termográfico, mediante entrada visual se muestra como un instrumento capaz trabaja con un rango de error que no

excede los ±0.6°C grados de diferencia con relación a otros instrumentos, como el detallado previamente.

5. CONCLUSIONES

Un dispositivo termográfico que realiza mediciones en tiempo real a varios puntos del espectro térmico de un individuo interpreta leyes algorítmicas destinadas a revelar la temperatura mediante procesos realizados por un software y un hardware, ya que así, las partes implementadas establecen canales de comunicación y permiten recopilar datos de una forma precisa.

La cámara termográfica desarrollada tiene la capacidad para realizar mediciones a varias distancias, por lo que para interpretar y analizar la información entregada es necesario capturar datos en diferentes etapas.

El dispositivo termográfico y sus valores medidos tienen a cambiar, por lo que, se realizaron mediciones en 3 etapas; la primera etapa destinada a la medición grupal, revelo que el instrumento tiene la capacidad capturar y elaborar un promedio del cuadro captado, en relación al ambiente que lo rodea, sin embargo el valor de un punto en específico tiene un margen de error de ±10°C; la segunda etapa demostró que el elemento tiene la capacidad de medir puntos específicos a cortas distancias, pero su valor es inestable e impreciso con un margen de ±3°C a comparación con otro instrumento; en la tercera etapa se utilizaron más puntos y rangos para medir la temperatura, lo que relevo que a una distancia adecuada el instrumento es preciso en sus mediciones, debido a que tiene un margen de error de ±0.6°C, en relación con otro instrumento.

La distancia adecuada para realizar mediciones con el dispositivo termográfico fue de suma importancia, puesto que al contrastar los datos con otro instrumento termográfico, se logró identificar que en el 36% de los participantes, el margen de error es de ±0.0°C y en el 64% los de los participantes, el margen de error es de ±0.6°C, es decir que en el 100% de las muestras registradas, existe un margen de error que no supera el ±1°C, lo que demuestra que el instrumento es un artefacto capaz de realizar mediciones precisas. Es por esto que la identificación de condiciones para el funcionamiento óptimo del dispositivo tiene gran relevancia, puesto que revela su capacidad operativa en diversos ambientes.

6. REFERENCIAS

[1] V. Suárez, M. Suarez Qezada, S. Oros Ruiz y E. Ronquillo De Jesús, «Epidemiology of COVID-19 in Mexico: From the 27th of February to the 30th of April 2020,» *Elsevier España,* vol. 220, nº 5, pp. 463-471, 2020.

[2] C. Huang, Y. Wang, X. Li, L. Ren, J. Zhao, Y. Hu, L. Zhang, G. Fan, J. Xu, X. Gu, Z. Cheng, T. Yu, J. Xia, Y. Wei, W. Wu, X. Xie, W. Yin, H. Li, M. Liu, Y. Xiao, H. Gao, L. Guo, J. Xie, G. Wang, R. Jiang, Z. Gao, Q. Jin, J. Wangt y B. Caot, «Epidemiological and clinical characteristics of 99 cases of 2019 novel coronavirus pneumonia in Wuhan, China: a descriptive study,» *Elsevier Ltd,* vol. 395, nº S0140-6736(20)30183-5, pp. 507-513, 2020.

[3] M. Adnan Shereen, S. Khan, A. Kazmi, N. Bashir y R. Siddique, «COVID-19 infection: Origin, transmission, and characteristics of human coronaviruses,» *Journal of Advanced Research,* vol. 24, nº 2090-1232, pp. 91-98, 2020.

[4] N. Lovell, I. Carey, S. N. Etkind, I. J. Higginson y P. Edmonds, «Characteristics, Symptom Management, and Outcomes of 101 Patients With COVID-19 Referred for Hospital,» *Journal of Pain and Symptom Management,* pp. 77-81, 01 07 2020.

[5] Y. Wu, W. Jing, J. Liu, Q. Ma, J. Yuan, Y. Wang, M. Du y M. Liu, «Effects of temperature and humidity on the daily new cases and new deaths of COVID-19 in 166 countries,» *ELSEIVER Science of the Total Environment,* vol. 729, nº 139051, pp. 1-7, 2020.

[6] D.-S. Kim, T.-H. Hwang, J. Yong Song, S. Hwa Park, J. Park, E.-S. Yoo, N.-K. Lee y J.-S. Park, «Design and fabrication of smart band module for measurement of temperature and GSR (galvanic skin response) from human body,» *ELSEVIER,* vol. 168, nº 10.1016, pp. 1577-1580, 2016.

[7] F. Nieto del Amor y A. J. Pérez Jiménez, «Diseño de cámara térmica IR de bajo coste basada en microcontrolador.,» de *Diseño de cámara térmica IR de bajo coste basada en microcontrolador.*, Valencia, Ecuela técnica superior ingenieros industriales Valencia, 2017, pp. 1-23.

[8] D. Grandjean, R. Sarkis, C. Lecoq-Julien, A. Benard, V. Roger y E. Levesque, «¿Puede el perro de detección alertar sobre personas positivas a COVID-19 olfateando muestras de sudor axilar? Un estudio de prueba de concepto,» *Nadine Ravel, Universite de Lyon,* nº 10.1371, pp. 1-19, 2020.

[9] Medicina Humana, «Universidad Privada Telesup,» Universidad Privada Telesup, 02 02 2018. [En línea]. Available: https://utelesup.edu.pe/blog-medicina/estetoscopio-el-instrumento-necesario-para-el-primer-diagnostico-en-medicina-humana/. [Último acceso: 09 01 2021].

[10] M. Reis, «TUASAÚDE,» TUASAÚDE, 02 12 2020. [En línea]. Available: https://www.tuasaude.com/es/tipos-de-termometro/. [Último acceso: 04 01 2021].

[11] T. Parker, «¿Qué es un oxímetro de pulso?¿De verdad necesito uno en casa?,» *The New York Times,* 29 04 2020.

[12] W. Han-Ning, J. Li-Ping, X. Bin , Z. Si, Y. Lan, H. Yan-Mei, L. Dao-Guang, L. Wei, S. Xin-Nan , Z. Xiao-Xi y Z. Hai-Lu, «Characteristic patterns of normal meridian acupoint temperature,» *Journal of the Chinese Medical Association,* vol. 80, nº Issue 7, pp. 419-426, 2017.

[13] M. L. Williams K, «Global warming, heat-related illnesses, and the dermatologist,» *International Journal of Women's Dermatology,* vol. l, nº 2352-6475, pp. 70-84, 2020.

[14] Universidad de Guanajuato, Contenidos didácticos Licenciatura de Enfermeria Y Obstetricia , «Blog UGTO MX,» 15 02 2018. [En línea]. Available: https://blogs.ugto.mx/enfermeriaenlinea/unidad-didactica-5-cuidados-de-enfermeria-a-personas-con-problemas-de-termoregulacion/. [Último acceso: 17 01 2021].

[15] U.T.F. Alicante, «https://www.utfalicante.com/,» Unión de Trabajadores de Farmacias (U.T.F.) , 18 05 2017. [En línea]. Available: https://www.utfalicante.com/blog/tabla-de-signos-vitales-por-edad-44.html. [Último acceso: 14 01 2021].

[16] N. Leung, «Cable News Network CNN,» A Warner Media Company, 03 01 2021. [En línea]. Available: https://edition.cnn.com/search?size=10&q=Common%20symptoms%20of%20Covid-19&type=article. [Último acceso: 15 01 2021].

[17] M. Cañada Soriano y R. Royo Pastor, «Termografia,» de *Termografía Infrarroja. Nivel II*, Madrid, Fundación Confemetal, 2016, pp. 1-671.

[18] ISO - The International Organization for Standardization, «Condition monitoring and diagnostics of machines Thermography - Part1: General Procedures,» *International Standard,* vol. 01, nº ISO 18434-1, pp. 1-32, 2008.

[19] H. Maldonado, R. Bayareh, I. A. Torres, A. Vera, J. Gutiéttez y L. Lejia, «Automatic detection of risk zones in diabetic foot soles by processingthermographic images taken in an uncontrolled environment,» *Infrared Physics & Technology,* vol. 105, nº 103187, pp. 1-21, 2020.

[20] International Union of Railways - UIC, «UIC.org RAILsiliencia,» 07 2020. [En línea]. Available: https://uic.org/IMG/pdf/uic_covid_task force_thermal_cameras_espanol.pdf. [Último acceso: 18 01 2021].

[21] E. O. Peña Rodríguez y L. Y. Neita Duarte, «Temperatura Y Calor,» de *Principios Básicos de la Termografia Infrarroja y su Utilización como técnica para mantenimiento predictivo*, Floridablanca, Universidad Pontificia Bolivariana - Facultad de IngenierÍa Electrónica, 2011, pp. 56-221.

[22] I. Mártil, «Público,» 27 05 2016. [En línea]. Available: https://blogs.publico.es/ignacio-martil/2016/05/27/la-invisible-y-muy-real-radiacion-infrarroja/. [Último acceso: 23 05 2021].

[23] J. M. Ruiz Echeverri y J. M. Meza Arenas, Fundamentos para una metodología para el diagnóstico cuantitativo de la función lagrimal humana utilizando termografía Infra-Roja., Pereira: Universidad Tecnológica de Pereira - Departamento de Física, grupo de Electrofisiología, 2018.

[24] R. Hernández Sampieri, «Metodología de la investigación Sexta edición,» de *Metodología de la investigación Sexta edición*, Mexico, McGRAW-HILL Interamericana Editores, S.A. DE C.V., 2014, p. 634.

[25] A. Díaz Barriga López y O. Pulido Torres, «Sites Funadamentos de la investigación,» Instituto Tecnológico de Tijuana, 2019. [En línea]. Available: https://sites.google.com/site/fundamentosdelainvestigacion1a/unidad-2-la-investigacion-como-un-proceso-de-construccion-social/2-3-tipos-de-metodos-inductivo-deductivo-analitico-sintetico-comparativo-dialectico-entre-otros. [Último acceso: 25 01 2021].

[26] A. Mariño Mur, Caracterización Térmica de un conjunto de edificaciones del Pirineo Oscense Mediante Termografia Infrarroja, Valéncia: Universidad Politécnica de Valéncia, Escuela Técnica Superior Ingeniería de Edificación, 2012.

[27] Zoo Med University, «Training Zoo Med University,» Zoo Med University, 2021. [En línea]. Available: https://training.zoomed.com/associate-lighting/. [Último acceso: 03 02 2021].

[28] Camara Termica, «CamaraTermica.Info,» CamaraTermica.Info, 01 02 2021. [En línea]. Available: https://www.camaratermica.info/camara-termica-de-caza-nocturna/. [Último acceso: 03 02 2021].

[29] R. Pascual Arribas, «Captura y procesamiento de imágenes de una cámara térmica,» de *Captura y procesamiento de imágenes de una cámara térmica*, Madrid, Universidad Politécnica de Madrid - Escuela Técnica Superior de Ingenieros Informáticos., 2016, pp. 13-19.

[30] FLIR Systems, Inc©, «FLIR,» FLIR.com, 2020. [En línea]. Available: https://www.flir.com/products/flir-one-pro/. [Último acceso: 25 01 2021].

[31] Seek Thermal© , «Thermal.com,» 2020. [En línea]. Available: https://www.thermal.com/uploads/1/0/1/3/101388544/compactpro-sellsheet-usav1.pdf. [Último acceso: 15 02 2021].

[32] Fluke Corporation©, «Fluke.com,» 2021. [En línea]. Available: https://www.fluke.com/es-ec/producto/camaras-termicas/tis60plus. [Último acceso: 15 02 2021].

[33] FLIR Systems, Inc., «Apliter Termografia,» 11 04 2019. [En línea]. Available: https://apliter.com/wp-content/uploads/2019/09/FLIR-FLIR-ONE-PRO-C%C3%A1mara-termogr%C3%A1fica-para-smartphone-Ficha-t%C3%A9cnica.pdf. [Último acceso: 29 01 2021].

[34] AsIAP, «Asociación de Informáticos del Uruguay,» 2003. [En línea]. Available: http://www.asiap.org/AsIAP/index.php/raee/300-articulos/3004-que-es-el-rohs-y-por-que-es-importante. [Último acceso: 01 02 2021].

[35] Nativ Or , «CEO 360 Compliance,» [En línea]. Available: https://contact.telit.com/hubfs/Events/IoT%20Roadshow/2019/Minneapolis/Minneapolis%20Presentations/Telit_Technical_Workshop_2019_FCC_and_

CE_Wireless_Certification_Nativ_Or.pdf. [Último acceso: 01 02 2021].

[36] Diario Oficial de la Unión Europea, «Directiva 2014/30/UE del Parlamento Europeo y del Consejo,» *Diario Oficial de la Unión Europea,* vol. 30, nº L 96/79, pp. 1-28, 2014.

[37] EPSMA, «PFC Harmonic Current Emissions – Guide to EN61000-3-2:2014,» *European Power Supplies Manufacturers' Association ,* vol. 2, nº 3-2, pp. 1-19, 2018.

[38] IEC, «Electromagnetic compatibility (EMC) Limits – Limitation of voltage changes, voltage fluctuations and flicker in public low-voltage supply systems, for equipment with rated current ≤ 16 A per phase and not subject to conditional connection,» *International Electrotechnical Commission,* vol. 3, nº 3-3, pp. 1-24, 2013.

[39] ETSI, «Electromagnetic compatibility and Radio spectrum Matters (ERM); Impact of CENELEC EN 55032 on ETSI EMC Standards,» *European Telecommunications Standards Institute,* vol. 1.1.1, nº 1, pp. 1-12, 2015.

[40] ISL , «International Standards Laboratory,» 02 08 2017. [En línea]. Available: https://www.winstar.com.tw/uploads/files/f5c8e0a6d0e2e68dcf6f8347d1845011.pdf. [Último acceso: 01 02 2021].

[41] IDUS Technology, «Pinterest,» 09 10 2016. [En línea]. Available: https://www.pinterest.es/pin/583356957961688828/. [Último acceso: 10 03 2021].

[42] MATLAB Resource FLIR, «Face-Detection-and-Tracking-Sample-Code.zip,» FLIR, 14 02 2016. [En línea]. Available: https://flir.app.box.com/s/o1t1safir7o2soqj2vnv4vy7e1qnmz9a. [Último acceso: 03 03 2021].

[43] LYFTRACK©, «https://lyftrack.com/,» LYFTRACK©, 2020. [En línea]. Available: https://lyftrack.com/. [Último acceso: 21 03 2021].

[44] Centers for Disease Control and Prevention, «Centers for Disease Control and Prevention,» National Center for Immunization and Respiratory Diseases (NCIRD), 13 05 2020. [En línea]. Available: https://www.cdc.gov/coronavirus/2019-ncov/symptoms-testing/symptoms.html. [Último acceso: 10 07 2020].

[45] T. Al-Kadi, Z. AL-Tuwaijri y A. AL-Omran, «Arduino Wi-Fi Network Analyzer,» *Procedia Computer Science,* vol. 21, nº 522-529, pp. 1-8, 2013.

[46] M. Pérez Pérez, F. Martínez Pérez, H. Reyes Pacheco y M. Hernández Hernández, «Aplicación de la Termografía en la inspección y el diagnóstico de paredes de generadores de vapor bkz-340-140/29m,» *Revista Ciencias Técnicas Agropecuarias,* vol. 23, nº 4, pp. 3-7, 2014.

[47] Diario Oficial de la Unión Europea, «Directiva 2014/65/UE del Parlamento Europeo y del Consejo,» *Diario Oficial de la Unión Europea,* vol. 65, nº L173/349, pp. 1-30, 2014.

7. ANEXOS

INTRODUCCIÓN

ANEXO 1. V. Suárez, M. Suarez Qezada, S. Oros Ruiz y E. Ronquillo De Jesús, «Epidemiology of COVID-19 in Mexico: From the 27th of February to the 30th of April 2020,» *Elsevier España,* vol. 220, nº 5, pp. 463-471, 2020.

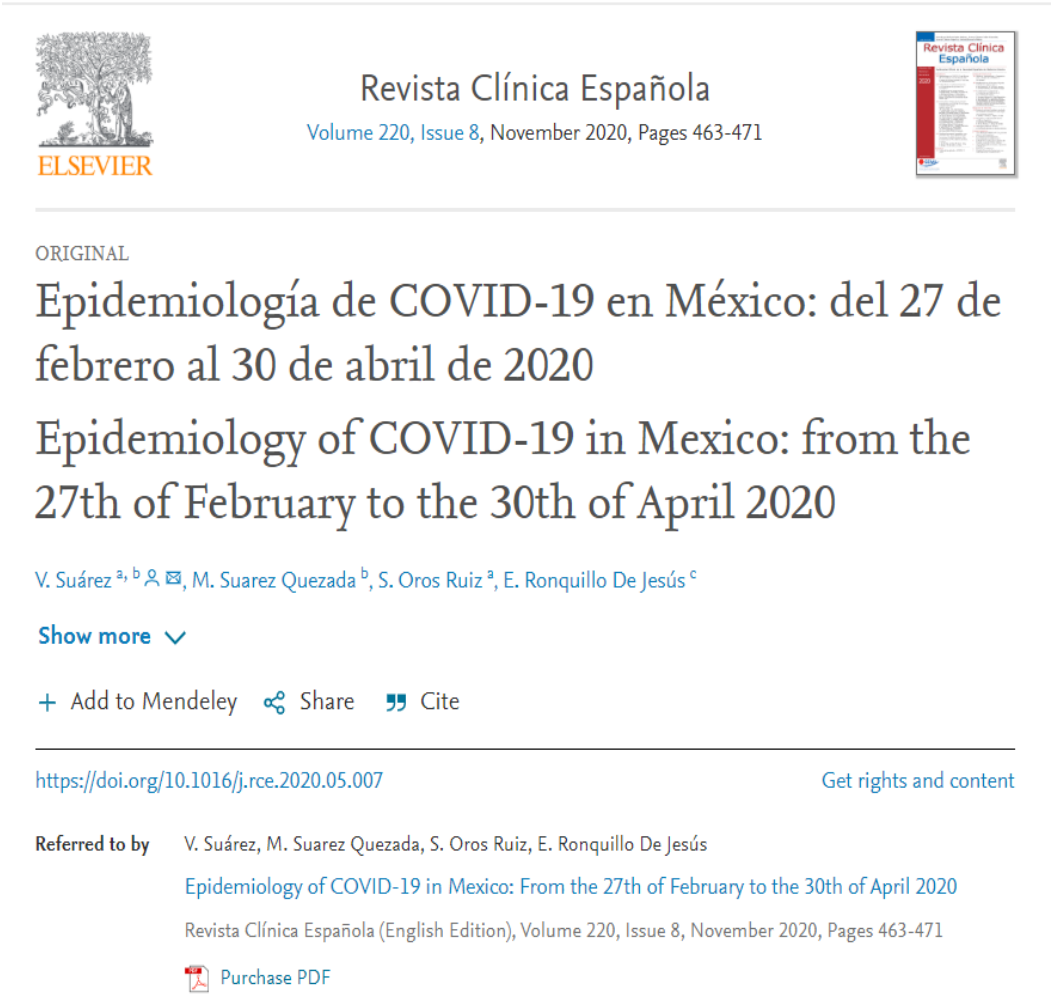

ELSEVIER

Revista Clínica Española
Volume 220, Issue 8, November 2020, Pages 463-471

ORIGINAL

Epidemiología de COVID-19 en México: del 27 de febrero al 30 de abril de 2020

Epidemiology of COVID-19 in Mexico: from the 27th of February to the 30th of April 2020

V. Suárez [a, b], M. Suarez Quezada [b], S. Oros Ruiz [a], E. Ronquillo De Jesús [c]

Show more

+ Add to Mendeley Share Cite

https://doi.org/10.1016/j.rce.2020.05.007

Get rights and content

Referred to by V. Suárez, M. Suarez Quezada, S. Oros Ruiz, E. Ronquillo De Jesús
Epidemiology of COVID-19 in Mexico: From the 27th of February to the 30th of April 2020
Revista Clínica Española (English Edition), Volume 220, Issue 8, November 2020, Pages 463-471

Purchase PDF

Resumen

Antecedentes

El primer caso de COVID-19 se detectó en México el 27 de febrero de 2020. El 30 de abril, 64 días después de este primer diagnóstico, el número de pacientes aumentó exponencialmente, alcanzando un total de 19.224 casos confirmados y 1.859 (9,67%) fallecidos. En respuesta a este brote global, resumimos el estado actual del conocimiento sobre COVID-19 en México.

Métodos

Los datos se obtuvieron del sitio web oficial del Ministerio de Salud en México. El período analizado fue entre el 27 de febrero y el 30 de abril de 2020. Los casos se confirmaron mediante RT-PCR en tiempo real y se analizaron los datos epidemiológicos, demográficos y clínicos.

Resultados

La mayoría de los casos de COVID-19 se ubicaron en la Ciudad de México. La edad promedio de los pacientes fue de 46 años. De los 12.656 casos confirmados, el mayor número de infectados ocurre en el rango de edad entre 30 y 59 años (65,85%), y hubo una mayor incidencia en hombres (58,18%) que en mujeres (41,82%). Los pacientes fallecidos tenían una o múltiples comorbilidades, principalmente hipertensión (45,53%), diabetes (39,39%) y obesidad (30,4%). En los primeros 64 días de epidemia,

China había reportado 80.304 casos con una tasa de mortalidad del 3,66%.

Conclusiones

Nuestros resultados indican la transmisión temprana de COVID-19 en México. La epidemiología descriptiva muestra las similitudes entre los casos de COVID-19 de México y China. En el mismo período de la curva epidémica, observamos en México una reducción en el número de casos confirmados de COVID-19 y una mayor tasa de mortalidad en comparación con China.

Abstract

Background

The first case of COVID-19 detected in Mexico was on the 27th of February 2020. On the 30th of April, 64 days after this first diagnosis, the number of patients had increased exponentially, reaching 19 224 confirmed cases and 1859 (9.67%) deaths. In response to this global outbreak, we summarize the current state of our understanding regarding COVID-19 in Mexico.

Methods

We obtained the data from the official website of the Ministry of Health in Mexico. The study period was between the 27th of February and the 30th of April 2020. The cases were confirmed using real-time reverse transcription-polymerase chain reaction, and we analysed epidemiological, demographic and clinical data.

Results

In Mexico, most cases of COVID-19 were located in Mexico City. The mean age of the patients was 46 years. Of the 12 656 confirmed cases, most infected individuals were between the ages of 30 and 59 years (65.85%), and there was a higher incidence rate in men (58.18%) than in women (41.82%). The patients who died had one or more comorbidities, mainly hypertension (45.53%), diabetes (39.39%) and obesity (30.4%). In the first 64 days of the epidemic, China had reported 80 304 cases with a mortality rate of 3.66%.

Conclusions

Our results indicate an early transmission of COVID-19 in Mexico. The descriptive epidemiology shows similarities between the cases of COVID-19 in Mexico and those in China. In the same period of the epidemic curve, we observed a reduction in the number of confirmed cases of COVID-19 in Mexico and a higher mortality rate compared with that of China.

ANEXO 2. C. Huang, Y. Wang, X. Li, L. Ren, J. Zhao, Y. Hu, L. Zhang, G. Fan, J. Xu, X. Gu, Z. Cheng, T. Yu, J. Xia, Y. Wei, W. Wu, X. Xie, W. Yin, H. Li, M. Liu, Y. Xiao, H. Gao, L. Guo, J. Xie, G. Wang, R. Jiang, Z. Gao, Q. Jin, J. Wangt y B. Caot, «Epidemiological and clinical characteristics of 99 cases of 2019 novel coronavirus pneumonia in Wuhan, China: a descriptive study,» *Elsevier Ltd,* vol. 395, nº S0140-6736(20)30183-5, pp. 507-513, 2020.

Epidemiological and clinical characteristics of 99 cases of 2019 novel coronavirus pneumonia in Wuhan, China: a descriptive study

Nanshan Chen, Min Zhou*, Xuan Dong*, Jieming Qu*, Fengyun Gong, Yang Han, Yang Qiu, Jingli Wang, Ying Liu, Yuan Wei, Jia'an Xia, Ting Yu, Xinxin Zhang, Li Zhang*

Summary

Background In December, 2019, a pneumonia associated with the 2019 novel coronavirus (2019-nCoV) emerged in Wuhan, China. We aimed to further clarify the epidemiological and clinical characteristics of 2019-nCoV pneumonia.

Methods In this retrospective, single-centre study, we included all confirmed cases of 2019-nCoV in Wuhan Jinyintan Hospital from Jan 1 to Jan 20, 2020. Cases were confirmed by real-time RT-PCR and were analysed for epidemiological, demographic, clinical, and radiological features and laboratory data. Outcomes were followed up until Jan 25, 2020.

Findings Of the 99 patients with 2019-nCoV pneumonia, 49 (49%) had a history of exposure to the Huanan seafood market. The average age of the patients was 55·5 years (SD 13·1), including 67 men and 32 women. 2019-nCoV was detected in all patients by real-time RT-PCR. 50 (51%) patients had chronic diseases. Patients had clinical manifestations of fever (82 [83%] patients), cough (81 [82%] patients), shortness of breath (31 [31%] patients), muscle ache (11 [11%] patients), confusion (nine [9%] patients), headache (eight [8%] patients), sore throat (five [5%] patients), rhinorrhoea (four [4%] patients), chest pain (two [2%] patients), diarrhoea (two [2%] patients), and nausea and vomiting (one [1%] patient). According to imaging examination, 74 (75%) patients showed bilateral pneumonia, 14 (14%) patients showed multiple mottling and ground-glass opacity, and one (1%) patient had pneumothorax. 17 (17%) patients developed acute respiratory distress syndrome and, among them, 11 (11%) patients worsened in a short period of time and died of multiple organ failure.

Interpretation The 2019-nCoV infection was of clustering onset, is more likely to affect older males with comorbidities, and can result in severe and even fatal respiratory diseases such as acute respiratory distress syndrome. In general, characteristics of patients who died were in line with the MuLBSTA score, an early warning model for predicting mortality in viral pneumonia. Further investigation is needed to explore the applicability of the MuLBSTA score in predicting the risk of mortality in 2019-nCoV infection.

Funding National Key R&D Program of China.

Lancet 2020; 395: 507–13

Published Online January 29, 2020 https://doi.org/10.1016/S0140-6736(20)30211-7

*Contributed equally

Tuberculosis and Respiratory Department (Prof N Chen MD, X Dong PhD, Y Wei MD, J Xia MD, T Yu MD, Prof L Zhang MD), **Infection Disease Department** (F Gong MD, J Wang MD), **Science and Education Department** (Y Han PhD), **and The Office of Drug Clinical Trial Institution** (Y Liu MD), **Wuhan Jinyintan Hospital, Wuhan, China; Department of Respiratory and Critical Care Medicine, Ruijin Hospital** (Prof M Zhou MD, Prof J Qu MD), **Institute of Respiratory Diseases** (Prof M Zhou, Prof J Qu), **Research Laboratory of Clinical Virology, Ruijin Hospital and Ruijin Hospital North** (Prof X Zhang MD), **and Clinical Research Center, Ruijin Hospital North** (Prof X Zhang), **Shanghai Jiaotong University School of Medicine, Shanghai, China; and State Key Laboratory of Virology, Wuhan Institute of Virology, Center for Biosafety Mega-Science, Chinese Academy of Sciences, Wuhan, China** (Prof Y Qiu PhD, Y Han)

Correspondence to: Prof Li Zhang, Tuberculosis and Respiratory Department, Wuhan Jinyintan Hospital, Dongxihu District, Wuhan 430023, China **zhangli080806@163.com**

or

Prof Xinxin Zhang, Research Laboratory of Clinical Virology, Ruijin Hospital and Ruijin Hospital North, Shanghai Jiaotong University School of Medicine, Shanghai 200025, China **zhangxx@shsmu.edu.cn**

Introduction

Since Dec 8, 2019, several cases of pneumonia of unknown aetiology have been reported in Wuhan, Hubei province, China.[1–3] Most patients worked at or lived around the local Huanan seafood wholesale market, where live animals were also on sale. In the early stages of this pneumonia, severe acute respiratory infection symptoms occurred, with some patients rapidly developing acute respiratory distress syndrome (ARDS), acute respiratory failure, and other serious complications. On Jan 7, a novel coronavirus was identified by the Chinese Center for Disease Control and Prevention (CDC) from the throat swab sample of a patient, and was subsequently named 2019-nCoV by WHO.[4]

Coronaviruses can cause multiple system infections in various animals and mainly respiratory tract infections in humans, such as severe acute respiratory syndrome (SARS) and Middle East respiratory syndrome (MERS).[5–7] Most patients have mild symptoms and good prognosis. So far, a few patients with 2019-nCoV have developed severe pneumonia, pulmonary oedema, ARDS, or multiple organ failure and have died. All costs of 2019-nCoV treatment are covered by medical insurance in China.

At present, information regarding the epidemiology and clinical features of pneumonia caused by 2019-nCoV is scarce.[1–3] In this study, we did a comprehensive exploration of the epidemiology and clinical features of 99 patients with confirmed 2019-nCoV pneumonia admitted to Jinyintan Hospital, Wuhan, which admitted the first patients with 2019-nCoV to be reported on.

Methods

Study design and participants

For this retrospective, single-centre study, we recruited patients from Jan 1 to Jan 20, 2020, at Jinyintan Hospital in Wuhan, China. Jinyintan Hospital is a hospital for adults (ie, aged ≥14 years) specialising in infectious diseases. According to the arrangements put in place by

Research in context

Evidence before this study

We searched PubMed on Jan 25, 2020, for articles that describe the epidemiological and clinical characteristics of the 2019 novel coronavirus (2019-nCoV) in Wuhan, China, using the search terms "novel coronavirus" and "pneumonia" with no language or time restrictions. Previously published research discussed the epidemiological and clinical characteristics of severe acute respiratory syndrome coronavirus or Middle East respiratory syndrome coronavirus, and primary study for the evolution of the novel coronavirus from Wuhan. The only report of clinical features of patients infected with 2019-nCoV was published on Jan 24, 2020, with 41 cases included.

Added value of this study

We have obtained data on 99 patients in Wuhan, China, to further explore the epidemiology and clinical features of 2019-nCoV. This study is, to our knowledge, the largest case series to date of 2019-nCoV infections, with 99 patients who were transferred to Jinyintan Hospital from other hospitals all over Wuhan, and provides further information on the demographic, clinical, epidemiological, and laboratory features of patients. It presents the latest status of 2019-nCoV infection in China and is an extended investigation of the previous report, with 58 extra cases and more details on combined bacterial and fungal infections. In all patients admitted with medical comorbidities of 2019-nCoV, a wide range of clinical manifestations can be seen and are associated with substantial outcomes.

Implications of all the available evidence

The 2019-nCoV infection was of clustering onset, is more likely to affect older men with comorbidities, and could result in severe and even fatal respiratory diseases such as acute respiratory distress syndrome. Early identification and timely treatment of critical cases of 2019-nCoV are important. Effective life support and active treatment of complications should be provided to effectively reduce the severity of patients' conditions and prevent the spread of this new coronavirus in China and worldwide.

the Chinese Government, adult patients were admitted centrally to the hospital from the whole of Wuhan without selectivity. All patients at Jinyintan Hospital who were diagnosed as having 2019-nCoV pneumonia according to WHO interim guidance were enrolled in this study.[4] All the data of included cases have been shared with WHO. The study was approved by Jinyintan Hospital Ethics Committee and written informed consent was obtained from patients involved before enrolment when data were collected retrospectively.

Procedures

We obtained epidemiological, demographic, clinical, laboratory, management, and outcome data from patients' medical records. Clinical outcomes were followed up to Jan 25, 2020. If data were missing from the records or clarification was needed, we obtained data by direct communication with attending doctors and other health-care providers. All data were checked by two physicians (XD and YQ).

Laboratory confirmation of 2019-nCoV was done in four different institutions: the Chinese CDC, the Chinese Academy of Medical Science, Academy of Military Medical Sciences, and Wuhan Institute of Virology, Chinese Academy of Sciences. Throat-swab specimens from the upper respiratory tract that were obtained from all patients at admission were maintained in viral-transport medium. 2019-nCoV was confirmed by real-time RT-PCR using the same protocol described previously.[3] RT-PCR detection reagents were provided by the four institutions. Other respiratory viruses including influenza A virus (H1N1, H3N2, H7N9), influenza B virus, respiratory syncytial virus, parainfluenza virus, adenovirus, SARS coronavirus (SARS-CoV), and MERS coronavirus (MERS-CoV) were also examined with real-time RT-PCR

Sputum or endotracheal aspirates were obtained at admission for identification of possible causative bacteria or fungi. Additionally, all patients were given chest x-rays or chest CT.

Outcomes

We describe epidemiological data (ie, short-term [occasional visits] and long-term [worked at or lived near] exposure to Huanan seafood market); demographics; signs and symptoms on admission; comorbidity; laboratory results; co-infection with other respiratory pathogens; chest radiography and CT findings; treatment received for 2019-nCoV; and clinical outcomes.

Statistical analysis

We present continuous measurements as mean (SD) if they are normally distributed or median (IQR) if they are not, and categorical variables as count (%). For laboratory results, we also assessed whether the measurements were outside the normal range. We used SPSS (version 26.0) for all analyses.

Role of the funding source

The funder of the study had no role in study design, data collection, data analysis, data interpretation, or writing of the report. The corresponding authors had full access to all the data in the study and had final responsibility for the decision to submit for publication.

Results

99 patients with 2019-nCoV were included in this study, two of whom were husband and wife. In total, 49 (49%)

patients were clustered and had a history of exposure to the Huanan seafood market. Among them, there were 47 patients with long-term exposure history, most of whom were salesmen or market managers, and two patients with short-term exposure history, who were shoppers. None of the patients were medical staff. Most patients were men, with a mean age of 55·5 years (SD 13·1; table 1). 50 (51%) patients had chronic diseases, including cardiovascular and cerebrovascular diseases, endocrine system disease, digestive system disease, respiratory system disease, malignant tumour, and nervous system disease (table 1).

On admission, most patients had fever or cough and a third of patients had shortness of breath (table 2). Other symptoms included muscle ache, headache, confusion, chest pain, and diarrhoea (table 2). Many patients presented with organ function damage, including 17 (17%) with ARDS, eight (8%) with acute respiratory injury, three (3%) with acute renal injury, four (4%) with septic shock, and one (1%) with ventilator-associated pneumonia (table 2).

On admission, leucocytes were below the normal range in nine (9%) patients and above the normal range in 24 (24%) patients (table 3). 38 (38%) patients had neutrophils above the normal range. Lymphocytes and haemoglobin were below the normal range in many

	Patients (n=99)
Age, years	
Mean (SD)	55·5 (13·1)
Range	21–82
≤39	10 (10%)
40–49	22 (22%)
50–59	30 (30%)
60–69	22 (22%)
≥70	15 (15%)
Sex	
Female	32 (32%)
Male	67 (68%)
Occupation	
Agricultural worker	2 (2%)
Self-employed	63 (64%)
Employee	15 (15%)
Retired	19 (19%)
Exposure to Huanan seafood market*	49 (49%)
Long-term exposure history	47 (47%)
Short-term exposure history	2 (2%)
Chronic medical illness	50 (51%)
Cardiovascular and cerebrovascular diseases	40 (40%)
Digestive system disease	11 (11%)
Endocrine system disease†	13 (13%)
Malignant tumour	1 (1%)
Nervous system disease	1 (1%)
Respiratory system disease	1 (1%)
Admission to intensive care unit	23 (23%)
Clinical outcome	
Remained in hospital	57 (58%)
Discharged	31 (31%)
Died	11 (11%)

Data are n (%) unless specified otherwise. 2019-nCoV=2019 novel coronavirus. *Long-term exposure is having worked at or lived in or around Huanan seafood market, whereas short-term exposure is having been to Huanan seafood market occasionally. †12 were diabetic.

Table 1: **Demographics, baseline characteristics, and clinical outcomes of 99 patients admitted to Wuhan Jinyintan Hospital (Jan 1–20, 2020) with 2019-nCoV pneumonia**

	Patients (n=99)
Signs and symptoms at admission	
Fever	82 (83%)
Cough	81 (82%)
Shortness of breath	31 (31%)
Muscle ache	11 (11%)
Confusion	9 (9%)
Headache	8 (8%)
Sore throat	5 (5%)
Rhinorrhoea	4 (4%)
Chest pain	2 (2%)
Diarrhoea	2 (2%)
Nausea and vomiting	1 (1%)
More than one sign or symptom	89 (90%)
Fever, cough, and shortness of breath	15 (15%)
Comorbid conditions	
Any	33 (33%)
ARDS	17 (17%)
Acute renal injury	3 (3%)
Acute respiratory injury	8 (8%)
Septic shock	4 (4%)
Ventilator-associated pneumonia	1 (1%)
Chest x-ray and CT findings	
Unilateral pneumonia	25 (25%)
Bilateral pneumonia	74 (75%)
Multiple mottling and ground-glass opacity	14 (14%)
Treatment	
Oxygen therapy	75 (76%)
Mechanical ventilation	
Non-invasive (ie, face mask)	13 (13%)
Invasive	4 (4%)
CRRT	9 (9%)
ECMO	3 (3%)
Antibiotic treatment	70 (71%)
Antifungal treatment	15 (15%)
Antiviral treatment	75 (76%)
Glucocorticoids	19 (19%)
Intravenous immunoglobulin therapy	27 (27%)

2019-nCoV=2019 novel coronavirus. ARDS=acute respiratory distress syndrome. ECMO=extracorporeal membrane oxygenation. CRRT=continuous renal replacement therapy.

Table 2: **Clinical characteristics and treatment of patients with 2019-nCoV pneumonia**

	Patients (n=99)
Blood routine	
Leucocytes (×10⁹ per L; normal range 3·5–9·5)	7·5 (3·6)
Increased	24 (24%)
Decreased	9 (9%)
Neutrophils (×10⁹ per L; normal range 1·8–6·3)	5·0 (3·3–8·1)
Increased	38 (38%)
Lymphocytes (×10⁹ per L; normal range 1·1–3·2)	0·9 (0·5)
Decreased	35 (35%)
Platelets (×10⁹ per L; normal range 125·0–350·0)	213·5 (79·1)
Increased	4 (4%)
Decreased	12 (12%)
Haemoglobin (g/L; normal range 130·0–175·0)	129·8 (14·8)
Decreased	50 (51%)
Coagulation function	
Activated partial thromboplastin time (s; normal range 21·0–37·0)	27·3 (10·2)
Increased	6 (6%)
Decreased	16 (16%)
Prothrombin time (s; normal range 10·5–13·5)	11·3 (1·9)
Increased	5 (5%)
Decreased	30 (30%)
D-dimer (μg/L; normal range 0·0–1·5)	0·9 (0·5–2·8)
Increased	36 (36%)
Blood biochemistry	
Albumin (g/L; normal range 40·0–55·0)	31·6 (4·0)
Decreased	97 (98%)
Alanine aminotransferase (U/L; normal range 9·0–50·0)	39·0 (22·0–53·0)
Increased	28 (28%)
Aspartate aminotransferase (U/L; normal range 15·0–40·0)	34·0 (26·0–48·0)
Increased	35 (35%)
Total bilirubin (μmol/L; normal range 0·0–21·0)	15·1 (7·3)
Increased	18 (18%)
Blood urea nitrogen (mmol/L; normal range 3·6–9·5)	5·9 (2·6)
Increased	6 (6%)
Decreased	17 (17%)
Serum creatinine (μmol/L; normal range 57·0–111·0)	75·6 (25·0)
Increased	3 (3%)
Decreased	21 (21%)
Creatine kinase (U/L; normal range 50·0–310·0)	85·0 (51·0–184·0)
Increased	13 (13%)
Decreased	23 (23%)
Lactate dehydrogenase (U/L; normal range 120·0–250·0)	336·0 (260·0–447·0)
Increased	75 (76%)
Myoglobin (ng/mL; normal range 0·0–146·9)	49·5 (32·2–99·8)
Increased	15 (15%)
Glucose (mmol/L; normal range 3·9–6·1)	7·4 (3·4)
Increased	51 (52%)
Decreased	1 (1%)

(Table 3 continues in next column)

	Patients (n=99)
(Continued from previous column)	
Infection-related biomarkers	
Procalcitonin (ng/mL; normal range 0·0–5·0)	0·5 (1·1)
Increased	6 (6%)
Interleukin-6 (pg/mL; normal range 0·0–7·0)	7·9 (6·1–10·6)
Increased	51 (52%)
Erythrocyte sedimentation rate (mm/h; normal range 0·0–15·0)	49·9 (23·4)
Increased	84 (85%)
Serum ferritin (ng/mL; normal range 21·0–274·7)	808·7 (490·7)
Increased	62 (63%)
C-reactive protein (mg/L; normal range 0·0–5·0)*	51·4 (41·8)
Increased	63/73 (86%)
Co-infection	
Other viruses	0
Bacteria	1 (1%)
Fungus	4 (4%)

Data are n (%), n/N (%), mean (SD), and median (IQR). Increased means over the upper limit of the normal range and decreased means below the lower limit of the normal range. 2019-nCoV=2019 novel coronavirus. *Data available for 73 patients.

Table 3: Laboratory results of patients with 2019-nCoV pneumonia

patients (table 3). Platelets were below the normal range in 12 (12%) patients and above the normal range in four (4%). 43 patients had differing degrees of liver function abnormality, with alanine aminotransferase (ALT) or aspartate aminotransferase (AST) above the normal range (table 3); one patient had severe liver function damage (ALT 7590 U/L, AST 1445 U/L). Most patients had abnormal myocardial zymogram, which showed the elevation of creatine kinase in 13 (13%) patients and the elevation of lactate dehydrogenase in 75 (76%) patients, one of whom also showed abnormal creatine kinase (6280 U/L) and lactate dehydrogenase (20740 U/L). Seven (7%) patients had different degrees of renal function damage, with elevated blood urea nitrogen or serum creatinine. Regarding the infection index, procalcitonin was above the normal range in six (6%) patients. Most patients had serum ferritin above the normal range (table 3). 73 patients were tested for C-reactive protein, most of whom had levels above the normal range (table 3).

All patients were tested for nine respiratory pathogens and the nucleic acid of influenza viruses A and B. Bacteria and fungi culture were done at the same time. We did not find other respiratory viruses in any of the patients. *Acinetobacter baumannii*, *Klebsiella pneumoniae*, and *Aspergillus flavus* were all cultured in one patient. *A baumannii* turned out to be highly resistant to antibiotics. One case of fungal infection was diagnosed as *Candida glabrata* and three cases of fungal infection were diagnosed as *Candida albicans*.

According to chest x-ray and CT, 74 (75%) patients showed bilateral pneumonia (75%) with just 25 (25%)

patients showing unilateral pneumonia (table 2). 14 (14%) patients showed multiple mottling and ground-glass opacity (table 2; figure). Additionally, pneumothorax occurred in one (1%) patient.

All patients were treated in isolation. 75 (76%) patients received antiviral treatment, including oseltamivir (75 mg every 12 h, orally), ganciclovir (0·25 g every 12 h, intravenously), and lopinavir and ritonavir tablets (500 mg twice daily, orally). The duration of antiviral treatment was 3–14 days (median 3 days [IQR 3–6]).

Most patients were given antibiotic treatment (table 2); 25 (25%) patients were treated with a single antibiotic and 45 (45%) patients were given combination therapy. The antibiotics used generally covered common pathogens and some atypical pathogens; when secondary bacterial infection occurred, medication was administered according to the results of bacterial culture and drug sensitivity. The antibiotics used were cephalosporins, quinolones, carbapenems, tigecycline against methicillin-resistant *Staphylococcus aureus*, linezolid, and antifungal drugs. The duration of antibiotic treatment was 3–17 days (median 5 days [IQR 3–7]). 19 (19%) patients were also treated with methylprednisolone sodium succinate, methylprednisolone, and dexamethasone for 3–15 days (median 5 [3–7]).

13 patients used non-invasive ventilator mechanical ventilation for 4–22 days (median 9 days [IQR 7–19]). Four patients used an invasive ventilator to assist ventilation for 3–20 days (median 17 [12–19]). The ventilator adopted P-SIMV mode, the inhaled oxygen concentration was 35–100%, and the positive end-expiratory pressure was 6–12 cm H_2O. All four patients were still using ventilators at data cutoff. Moreover, nine (9%) patients received continuous blood purification due to renal failure and three (3%) patients were treated with extracorporeal membrane oxygenation (ECMO; table 2).

By the end of Jan 25, 31 (31%) patients had been discharged and 11 (11%) patients had died; all other patients were still in hospital (table 1). The first two deaths were a 61-year-old man (patient 1) and a 69-year-old man (patient 2). They had no previous chronic underlying disease but had a long history of smoking. Patient 1 was transferred to Jinyintan Hospital and diagnosed with severe pneumonia and ARDS. He was immediately admitted to the intensive care unit (ICU) and given an intubated ventilator-assisted breathing therapy. Later, the patient, having developed severe respiratory failure, heart failure, and sepsis, experienced a sudden cardiac arrest on the 11th day of admission and was declared dead. Patient 2 had severe pneumonia and ARDS after admission. The patient was transferred to the ICU and given ventilator-assisted breathing, and received anti-infection and ECMO treatment after admission. The patient's hypoxaemia remained unresolved. On the ninth day of admission, the patient died of severe pneumonia, septic shock, and respiratory failure. The intervals

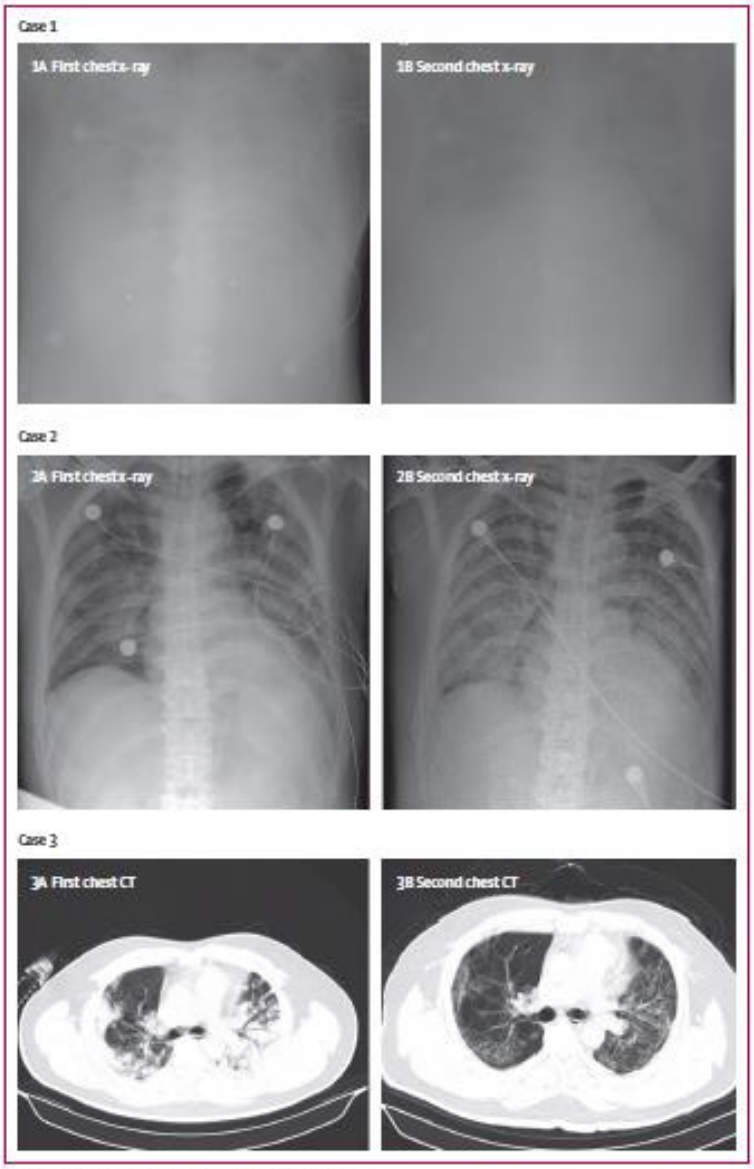

Figure: Chest x-rays and chest CTs of three patients
Case 1: chest x-ray was obtained on Jan 1 (1A). The brightness of both lungs was diffusely decreased, showing a large area of patchy shadow with uneven density. Tracheal intubation was seen in the trachea and the heart shadow outline was not clear. The catheter shadow was seen from the right axilla to the mediastinum. Bilateral diaphragmatic surface and costal diaphragmatic angle were not clear, and chest x-ray on Jan 2 showed worse status (1B). Case 2: chest x-ray obtained on Jan 6 (2A). The brightness of both lungs was decreased and multiple patchy shadows were observed; edges were blurred, and large ground-glass opacity and condensation shadows were mainly on the lower right lobe. Tracheal intubation could be seen in the trachea. Heart shadow roughly presents in the normal range. On the left side, the diaphragmatic surface is not clearly displayed. The right side of the diaphragmatic surface was light and smooth and rib phrenic angle was less sharp. Chest x-ray on Jan 10 showed worse status (2B). Case 3: chest CT obtained on Jan 1 (3A) showed mass shadows of high density in both lungs. Bright bronchogram is seen in the lung tissue area of the lesion, which is also called bronchoinflation sign. Chest CT on Jan 15 showed improved status (3B).

between the onset of symptoms and the use of ventilator-assisted breathing in the two patients were 3 days and 10 days, respectively. The course of the disease and lung lesions progressed rapidly in both patients, with both developing multiple organ failure in a short time. The deaths of these two patients were consistent with the MuLBSTA score, an early warning model for predicting mortality in viral pneumonia.[8]

Of the remaining nine patients who died, eight patients had lymphopenia, seven had bilateral pneumonia, five were older than 60 years, three had hypertension, and one was a heavy smoker.

Discussion

This is an extended descriptive study on the epidemiology and clinical characteristics of the 2019-nCoV, including data on 99 patients who were transferred to Jinyintan Hospital from other hospitals across Wuhan. It presents the latest status of the 2019-nCoV infection in China and adds details on combined bacterial and fungal infections.

Human coronavirus is one of the main pathogens of respiratory infection. The two highly pathogenic viruses, SARS-CoV and MERS-CoV, cause severe respiratory syndrome in humans and four other human coronaviruses (HCoV-OC43, HCoV-229E, HCoV-NL63, HCoV-HKU1) induce mild upper respiratory disease. The major SARS-CoV outbreak involving 8422 patients occurred during 2002–03 and spread to 29 countries globally.[9,10] MERS-CoV emerged in Middle Eastern countries in 2012 but was imported into China.[11,12] The sequence of 2019-nCoV is relatively different from the six other coronavirus subtypes but can be classified as betacoronavirus. SARS-CoV and MERS-CoV can be transmitted directly to humans from civets and dromedary camels, respectively, and both viruses originate in bats, but the origin of 2019-nCoV needs further investigation.[13–15] 2019-nCoV also has enveloped virions that measure approximately 50–200 nm in diameter with a single positive-sense RNA genome.[16] Club-shaped glycoprotein spikes in the envelope give the virus a crown-like or coronal appearance. Transmission rates are unknown for 2019-nCoV; however, there is evidence of human-to-human transmission. None of the 99 patients we examined were medical staff, but 15 medical workers have been reported with 2019-nCoV infection, 14 of whom are assumed to have been infected by the same patient.[17] The mortality of SARS-CoV has been reported as more than 10% and MERS-CoV at more than 35%.[5,18] At data cutoff for this study, mortality of the 99 included patients infected by 2019-nCoV was 11%, resembling that in a previous study.[1] However, additional deaths might occur in those still hospitalised.

We observed a greater number of men than women in the 99 cases of 2019-nCoV infection. MERS-CoV and SARS-CoV have also been found to infect more males than females.[19,20] The reduced susceptibility of females to viral infections could be attributed to the protection from X chromosome and sex hormones, which play an important role in innate and adaptive immunity.[21] Additionally, about half of patients infected by 2019-nCoV had chronic underlying diseases, mainly cardiovascular and cerebrovascular diseases and diabetes; this is similar to MERS-CoV.[19] Our results suggest that 2019-nCoV is more likely to infect older adult males with chronic comorbidities as a result of the weaker immune functions of these patients.[19–22]

Some patients, especially severely ill ones, had co-infections of bacteria and fungi. Common bacterial cultures of patients with secondary infections included *A baumannii*, *K pneumoniae*, *A flavus*, *C glabrata*, and *C albicans*.[8] The high drug resistance rate of *A baumannii* can cause difficulties with anti-infective treatment, leading to higher possibility of developing septic shock.[23] For severe mixed infections, in addition to the virulence factors of pathogens, the host's immune status is also one of the important factors. Old age, obesity, and presence of comorbidity might be associated with increased mortality.[24] When populations with low immune function, such as older people, diabetics, people with HIV infection, people with long-term use of immunosuppressive agents, and pregnant women, are infected with 2019-nCoV, prompt administration of antibiotics to prevent infection and strengthening of immune support treatment might reduce complications and mortality.

In terms of laboratory tests, the absolute value of lymphocytes in most patients was reduced. This result suggests that 2019-nCoV might mainly act on lymphocytes, especially T lymphocytes, as does SARS-CoV. Virus particles spread through the respiratory mucosa and infect other cells, induce a cytokine storm in the body, generate a series of immune responses, and cause changes in peripheral white blood cells and immune cells such as lymphocytes. Some patients progressed rapidly with ARDS and septic shock, which was eventually followed by multiple organ failure. Therefore, early identification and timely treatment of critical cases is of crucial importance. Use of intravenous immunoglobulin is recommended to enhance the ability of anti-infection for severely ill patients and steroids (methylprednisolone 1–2 mg/kg per day) are recommended for patients with ARDS, for as short a duration of treatment as possible. Some studies suggest that a substantial decrease in the total number of lymphocytes indicates that coronavirus consumes many immune cells and inhibits the body's cellular immune function. Damage to T lymphocytes might be an important factor leading to exacerbations of patients.[25] The low absolute value of lymphocytes could be used as a reference index in the diagnosis of new coronavirus infections in the clinic.

In general, the characteristics of patients who died were in line with the early warning model for predicting mortality in viral pneumonia in our previous study: the MuLBSTA score.[8] The MuLBSTA score system contains six indexes, which are multilobular infiltration, lymphopenia, bacterial

co-infection, smoking history, hypertension, and age. Further investigation is needed to explore the applicability of the MuLBSTA score in predicting the risk of mortality in 2019-nCoV infection.

This study has several limitations. First, only 99 patients with confirmed 2019-nCoV were included; suspected but undiagnosed cases were ruled out in the analyses. It would be better to include as many patients as possible in Wuhan, in other cities in China, and even in other countries to get a more comprehensive understanding of 2019-nCoV. Second, more detailed patient information, particularly regarding clinical outcomes, was unavailable at the time of analysis; however, the data in this study permit an early assessment of the epidemiological and clinical characteristics of 2019-nCoV pneumonia in Wuhan, China.

In conclusion, the infection of 2019-nCoV was of clustering onset, is more likely to infect older men with comorbidities, and can result in severe and even fatal respiratory diseases such as ARDS.

Contributors

NC, XD, FG, YH, YQ, JW, YL, YW, JX, TY, and LZ collected the epidemiological and clinical data and processed statistical data. NC and MZ drafted the manuscript. JQ and XZ revised the final manuscript. XZ is responsible for summarising all data related to the virus. LZ is responsible for summarising all epidemiological and clinical data.

Declaration of interests

We declare no competing interests.

Acknowledgments

This study was funded by the National Key R&D Program of China (number 2017YFC1309700). We thank all patients involved in the study.

References

1 Liu H, Stratton CW, Tang YW. Outbreak of pneumonia of unknown etiology in Wuhan China: the mystery and the miracle. *J Med Virol* 2020; published online Jan 16. DOI:10.1002/jmv.25678.

2 Hui DS, I Azhar E, Madani TA, et al. The continuing 2019-nCoV epidemic threat of novel coronaviruses to global health - the latest 2019 novel coronavirus outbreak in Wuhan, China. *Int J Infect Dis* 2020; 91: 264–66.

3 Huang C, Wang Y, Li X, et al. Clinical features of patients infected with 2019 novel coronavirus in Wuhan, China. *Lancet* 2020; published online Jan 24. https://doi.org/10.1016/S0140-6736(20)30183-5.

4 WHO. Clinical management of severe acute respiratory infection when Novel coronavirus (nCoV) infection is suspected: interim guidance. Jan 11, 2020. https://www.who.int/internal-publications-detail/clinical-management-of-severe-acute-respiratory-infection-when-novel-coronavirus-(ncov)-infection-is-suspected (accessed Jan 20, 2020).

5 Yin Y, Wunderink RG. MERS, SARS and other coronaviruses as causes of pneumonia. *Respirology* 2018; 23: 130–37.

6 Drosten C, Günther S, Preiser W, et al. Identification of a novel coronavirus in patients with severe acute respiratory syndrome. *N Engl J Med* 2003; 348: 1967–76.

7 Zaki AM, van Boheemen S, Bestebroer TM, Osterhaus AD, Fouchier RA. Isolation of a novel coronavirus from a man with pneumonia in Saudi Arabia. *N Engl J Med* 2012; 367: 1814–20.

8 Guo L, Wei D, Zhang X, et al. Clinical features predicting mortality risk in patients with viral pneumonia: the MuLBSTA score. *Front Microbiol* 2019; 10: 2752.

9 Hu B, Zeng LP, Yang XL, et al. Discovery of a rich gene pool of bat SARS-related coronaviruses provides new insights into the origin of SARS coronavirus. *PLoS Pathog* 2017; 13: e1006698.

10 Song HD, Tu CC, Zhang GW, et al. Cross-host evolution of severe acute respiratory syndrome coronavirus in palm civet and human. *Proc Natl Acad Sci USA* 2005; 102: 2430–35.

11 Haagmans BL, Al Dhahiry SH, Reusken CB, et al. Middle East respiratory syndrome coronavirus in dromedary camels: an outbreak investigation. *Lancet Infect Dis* 2014; 14: 140–45.

12 Azhar EI, El-Kafrawy SA, Farraj SA, et al. Evidence for camel-to-human transmission of MERS coronavirus. *N Engl J Med* 2014; 370: 2499–505.

13 Tao Y, Shi M, Chommanard C, et al. Surveillance of bat coronaviruses in Kenya identifies relatives of human coronaviruses NL63 and 229E and their recombination history. *J Virol* 2017; 91: e01953–16.

14 Cui J, Li F, Shi ZL. Origin and evolution of pathogenic coronaviruses. *Nat Rev Microbiol* 2019; 17: 181–92.

15 Zhou P, Fan H, Lan T, et al. Fatal swine acute diarrhoea syndrome caused by an HKU2-related coronavirus of bat origin. *Nature* 2018; 556: 255–58.

16 Xu XT, Chen P, Wang JF, et al. Evolution of the novel coronavirus from the ongoing Wuhan outbreak and modeling of its spike protein for the risk of human transmission. *Sci China Life Sci* 2020; published online Jan 21. DOI:10.1007/s11427-020-1637-5.

17 Chinese Academy of Sciences. Wuhan coronavirus has strong ability to infect humans. Press release. Jan 21, 2020. https://view.inews.qq.com/w2/20200121A0M08X00?tbkn=F&strategy=&openid=o04IBALMr1yGDxbWNOPoDM1IfG-s&uid=&refer=wx_hot (accessed Jan 29, 2020).

18 Song Z, Xu Y, Bao L, et al. From SARS to MERS, thrusting coronaviruses into the spotlight. *Viruses* 2019; 11: 59.

19 Badawi A, Ryoo SG. Prevalence of comorbidities in the Middle East respiratory syndrome coronavirus (MERS-CoV): a systematic review and meta-analysis. *Int J Infect Dis* 2016; 49: 129–33.

20 Channappanavar R, Fett C, Mack M, Ten Eyck PP, Meyerholz DK, Perlman S. Sex-based differences in susceptibility to severe acute respiratory syndrome coronavirus infection. *J Immunol* 2017; 198: 4046–53.

21 Jaillon S, Berthenet K, Garlanda C. Sexual dimorphism in innate immunity. *Clin Rev Allergy Immunol* 2019; 56: 308–21.

22 Dryden M, Baguneid M, Eckmann C, et al. Pathophysiology and burden of infection in patients with diabetes mellitus and peripheral vascular disease: focus on skin and soft-tissue infections. *Clin Microbiol Infect* 2015; 21 (suppl 2): S27–32.

23 Gao HN, Lu HZ, Cao B, et al. Clinical findings in 111 cases of influenza A (H7N9) virus infection. *N Engl J Med* 2013; 368: 2277–85.

24 Wang XF, Shi GC, Wan HY, et al. Clinical features of three avian influenza H7N9 virus-infected patients in Shanghai. *Clin Respir J* 2014; 8: 410–16.

25 Liu WJ, Zhao M, Liu K, et al. T-cell immunity of SARS-CoV: implications for vaccine development against MERS-CoV. *Antiviral Res* 2017; 137: 82–92.

ANEXO 3. M. Adnan Shereen, S. Khan, A. Kazmi, N. Bashir y R. Siddique, «COVID-19 infection: Origin, transmission, and characteristics of human coronaviruses,» *Journal of Advanced Research,* vol. 24, nº 2090-1232, pp. 91-98, 2020.

Contents lists available at ScienceDirect

Journal of Advanced Research

journal homepage: www.elsevier.com/locate/jare

COVID-19 infection: Emergence, transmission, and characteristics of human coronaviruses

Muhammad Adnan Shereen [b,1], Suliman Khan [a,1,*], Abeer Kazmi [c], Nadia Bashir [b], Rabeea Siddique [a]

[a] The Department of Cerebrovascular Diseases, The Second Affiliated Hospital of Zhengzhou University, Zhengzhou, PR China
[b] State Key Laboratory of Virology, College of Life Sciences, Wuhan University, Wuhan, PR China
[c] College of Life Sciences, Wuhan University, Wuhan, PR China

GRAPHICAL ABSTRACT

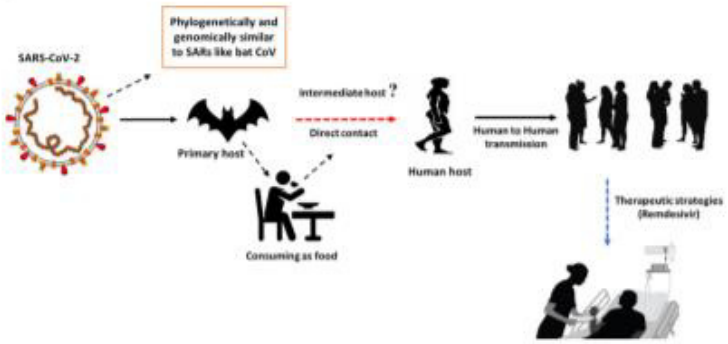

ARTICLE INFO

Article history:
Received 15 March 2020
Accepted 15 March 2020
Available online 16 March 2020

Keywords:
Coronaviruses
COVID-19
Transmission
Outbreak
Spread

ABSTRACT

The coronavirus disease 19 (COVID-19) is a highly transmittable and pathogenic viral infection caused by severe acute respiratory syndrome coronavirus 2 (SARS-CoV-2), which caused global pandemic that led to a dramatic loss of human life worldwide. Genomic analysis revealed that SARS-CoV-2 is phylogenetically related to severe acute respiratory syndrome-like (SARS-like) bat viruses, therefore bats could be the possible primary reservoir. The intermediate source of origin and transfer to humans is not known, however, the rapid human to human transfer has been confirmed widely. There is no clinically approved antiviral drug or vaccine available to be used against COVID-19. However, few broad-spectrum antiviral drugs have been evaluated against COVID-19 in clinical trials, resulted in clinical recovery. In the current review, we summarize and comparatively analyze the emergence and pathogenicity of COVID-19 infection and previous human coronaviruses including severe ascute respiratory syndrome coronavirus (SARS-CoV) and middle east respiratory syndrome coronavirus (MERS-CoV). We also discuss the approaches for developing effective vaccines and therapeutic combinations to cope with this viral outbreak.

Introduction

Coronaviruses belong to the Coronaviridae family in the Nidovirales order. Corona represents crown-like spikes on the outer surface of the virus; thus, it was named as a coronavirus.

Peer review under responsibility of Cairo University.
* Corresponding author.
E-mail address: suliman.khan18@mails.ucas.ac.cn (S. Khan).
[1] Contributed equally (M.A.S and S.K).

https://doi.org/10.1016/j.jare.2020.03.005
2090-1232/

Coronaviruses are minute in size (65–125 nm in diameter) and contain a single-stranded RNA as a nucleic material, size ranging from 26 to 32kbs in length (Fig. 1). The subgroups of coronaviruses family are alpha (α), beta (β), gamma (γ) and delta (δ) coronavirus. The severe acute respiratory syndrome coronavirus (SARS-CoV), H5N1 influenza A, H1N1 2009 and Middle East respiratory syndrome coronavirus (MERS-CoV) cause acute lung injury (ALI) and acute respiratory distress syndrome (ARDS) which leads to pulmonary failure and result in fatality. These viruses were thought to infect only animals until the world witnessed a severe acute respiratory syndrome (SARS) outbreak caused by SARS-CoV, 2002 in Guangdong, China [1]. Only a decade later, another pathogenic coronavirus, known as Middle East respiratory syndrome coronavirus (MERS-CoV) caused an endemic in Middle Eastern countries [2].

Recently at the end of 2019, Wuhan an emerging business hub of China experienced an outbreak of a novel coronavirus that killed more than eighteen hundred and infected over seventy thousand individuals within the first fifty days of the epidemic. This virus was reported to be a member of the β group of coronaviruses. The novel virus was named as 2019 novel coronavirus (2019-nCov) by the Chinese researchers. The International Committee on Taxonomy of Viruses (ICTV) named the virus as SARS-CoV-2 and the disease as COVID-19 [3–5]. In the history, SRAS-CoV (2003) infected 8098 individuals with mortality rate of 9%, across 26 contries in the world, on the other hand, novel corona virus (2019) infected 120,000 induviduals with mortality rate of 2.9%, across 109 countries, till date of this writing. It shows that the transmission rate of SARS-CoV-2 is higher than SRAS-CoV and the reason could be genetic recombination event at S protein in the RBD region of SARS-CoV-2 may have enhanced its transmission ability. In this review article, we discuss the transmission of human coronaviruses briefly. We further discuss the associated infectiousness and biological features of SARS and MERS with a special focus on COVID-19.

Comparative analysis of emergence and spreading of coronaviruses

In 2003, the Chinese population was infected with a virus causing Severe Acute Respiratory Syndrome (SARS) in Guangdong province. The virus was confirmed as a member of the Beta-coronavirus subgroup and was named SARS-CoV [6,7]. The infected patients exhibited pneumonia symptoms with a diffused alveolar injury which lead to acute respiratory distress syndrome (ARDS). SARS initially emerged in Guangdong, China and then spread rapidly around the globe with more than 8000 infected persons and 776 deceases. A decade later in 2012, a couple of Saudi Arabian nationals were diagnosed to be infected with another coronavirus. The detected virus was confirmed as a member of coronaviruses and named as the Middle East Respiratory Syndrome Coronavirus (MERS-CoV). The World health organization reported that MERS-coronavirus infected more than 2428 individuals and 838 deaths [8]. MERS-CoV is a member beta-coronavirus subgroup and phylogenetically diverse from other human-CoV. The infection of MERS-CoV initiates from a mild upper respiratory injury while progression leads to severe respiratory disease. Similar to SARS-coronavirus, patients infected with MERS-coronavirus suffer pneumonia, followed by ARDS and renal failure [9].

Recently, by the end of 2019, WHO was informed by the Chinese government about several cases of pneumonia with unfamiliar etiology. Although scientists suspected that Hunan seafood market in Wuhan helped the virus spread, however, it was not where the outbreak first emerged [10]. On 12 January 2020, the National Health Commission of China released further details about the epidemic, suggested viral pneumonia [10]. From the sequence-based analysis of isolates from the patients, the virus was identified as a novel coronavirus. Moreover, the genetic sequence was also provided for the diagnosis of viral infection. Initially, it was suggested that the patients infected with Wuhan coronavirus induced pneumonia in China may have visited the seafood market where live animals were sold or may have used infected animals or birds as a source of food. However, further investigations revealed that some individuals contracted the infection even with no record of visiting the seafood market. These observations indicated a human to the human spreading capability of this virus, which was subsequently reported in more than 100 countries in the world. The human to the human spreading of the virus occurs due to close contact with an infected person, exposed to coughing, sneezing, respiratory droplets or aerosols. These aerosols can penetrate the human body (lungs) via inhalation through the nose or mouth (Fig. 2) [11–14].

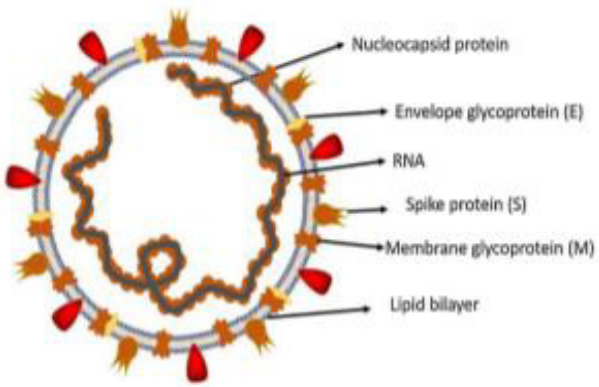

Fig. 1. Structure of respiratory syndrome causing human coronavirus.

Primary reservoirs and hosts of coronaviruses

The source of origination and transmission are important to be determined in order to develop preventive strategies to contain the infection. In the case of SARS-CoV, the researchers initially focused on raccoon dogs and palm civets as a key reservoir of infection. However, only the samples isolated from the civets at the food market showed positive results for viral RNA detection, suggesting that the civet palm might be secondary hosts [15]. In 2001 the samples were isolated from the healthy persons of Hongkong and the molecular assessment showed 2.5% frequency rate of antibodies against SARS-coronavirus. These indications suggested that SARS-coronavirus may be circulating in humans before causing the outbreak in 2003 [16]. Later on, Rhinolophus bats were also found to have anti-SARS-CoV antibodies suggesting the bats as a source of viral replication [17]. The Middle East respiratory syndrome (MERS) coronavirus first emerged in 2012 in Saudi Arabia [9]. MERS-coronavirus also pertains to beta-coronavirus and having camels as a zoonotic source or primary host [18]. In a recent study, MERS-coronavirus was also detected in Pipistrellus and Perimyotis bats [19], proffering that bats are the key host and transmitting medium of the virus [20,21]. Initially, a group of researchers suggested snakes be the possible host, however, after genomic similarity findings of novel coronavirus with SARS-like bat viruses supported the statement that not snakes but only bats could be the key reservoirs (Table 1) [22,23]. Further analysis of homologous recombination revealed that receptor binding spike glycoprotein of novel coronavirus is developed from a SARS-CoV (CoVZXC21 or CoVZC45) and a yet unknown Beta-CoV [24]. Nonetheless, to

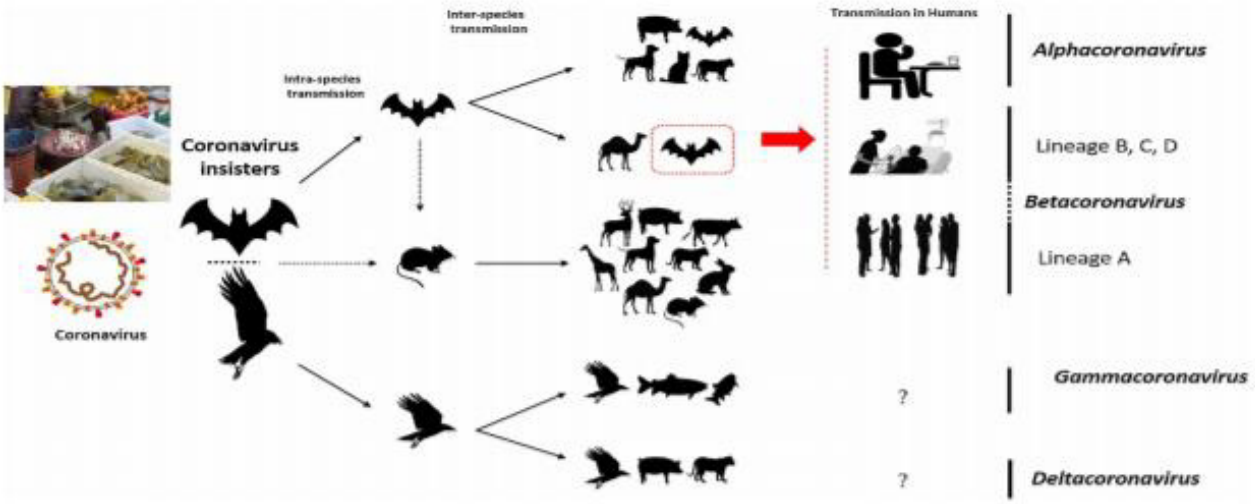

Fig. 2. The key reservoirs and mode of transmission of coronaviruses (suspected reservoirs of SARS-CoV-2 are red encircled); only α and β coronaviruses have the ability to infect humans, the consumption of infected animal as a source of food is the major cause of animal to human transmission of the virus and due to close contact with an infected person, the virus is further transmitted to healthy persons. Dotted black arrow shows the possibility of viral transfer from bat whereas the solid black arrow represent the confirmed transfer.

Table 1
Comparative analysis of biological features of SARS-CoV and SARS-CoV-2.

Features	SARS-CoV	SARS-CoV-2	Reference
Emergence date	November 2002	December 2019	[37,79–81]
Area of emergence	Guangdong, China	Wuhan, China	
Date of fully controlled	July 2003	Not controlled yet	
Key hosts	Bat, palm civets and Raccon dogs	Bat	[22,82,83]
Number of countries infected	26	109	[84]
Entry receptor in humans	ACE2 receptor	ACE2 receptor	[22,55,85]
Sign and symptoms	fever, malaise, myalgia, headache, diarrhoea, shivering, cough and shortness of breath	Cough, fever and shortness of breath	[12,23,85]
Disease caused	SARS, ARDS	SARS, COVID-19	[85,86]
Total infected patients	8098	123882	[84]
Total recovered patients	7322	67051	
Total died patients	776 (9.6% mortality rate)	4473 (3.61% mortality rate)	

eradicate the virus, more work is required to be done in the aspects of the identification of the intermediate zoonotic source that caused the transmission of the virus to humans.

Key features and entry mechanism of human coronaviruses

All coronaviruses contain specific genes in ORF1 downstream regions that encode proteins for viral replication, nucleocapsid and spikes formation [25]. The glycoprotein spikes on the outer surface of coronaviruses are responsible for the attachment and entry of the virus to host cells (Fig. 1). The receptor-binding domain (RBD) is loosely attached among virus, therefore, the virus may infect multiple hosts [26,27]. Other coronaviruses mostly recognize aminopeptidases or carbohydrates as a key receptor for entry to human cells while SARS-CoV and MERS-CoV recognize exopeptidases [2]. The entry mechanism of a coronavirus depends upon cellular proteases which include, human airway trypsin-like protease (HAT), cathepsins and transmembrane protease serine 2 (TMPRSS2) that split the spike protein and establish further penetration changes [28,29]. MERS-coronavirus employs dipeptidyl peptidase 4 (DPP4), while HCoV-NL63 and SARS-coronavirus require angiotensin-converting enzyme 2 (ACE2) as a key receptor [2,26].

SARS-CoV-2 possesses the typical coronavirus structure with spike protein and also expressed other polyproteins, nucleoproteins, and membrane proteins, such as RNA polymerase, 3-chymotrypsin-like protease, papain-like protease, helicase, glycoprotein, and accessory proteins [30,31]. The spike protein of SARS-CoV-2 contains a 3-D structure in the RBD region to maintain the van der Waals forces [32]. The 394 glutamine residue in the RBD region of SARS-CoV-2 is recognized by the critical lysine 31 residue on the human ACE2 receptor [33]. The entire mechanism of pathogenicity of SARS-CoV-2, from attachment to replication is well mentioned in Fig. 3.

Genomic variations in SARS-CoV-2

The genome of the SARS-CoV-2 has been reported over 80% identical to the previous human coronavirus (SARS-like bat CoV) [34]. The Structural proteins are encoded by the four structural genes, including spike (S), envelope (E), membrane (M) and nucleocapsid (N) genes. The *orf1ab* is the largest gene in SARS-CoV-2 which encodes the pp1ab protein and 15 nsps. The *orf1a* gene encodes for pp1a protein which also contains 10 nsps [34–36]. According to the evolutionary tree, SARS-CoV-2 lies close to the group of SARS-coronaviruses [37,38] (Fig. 5). Recent studies have indicated notable variations in SARS-CoV and SARS-CoV-2 such as the absence of 8a protein and fluctuation in the number of amino acids in 8b and 3c protein in SARS-CoV-2 [34] (Fig. 4). It is also reported that Spike glycoprotein of the Wuhan coronavirus

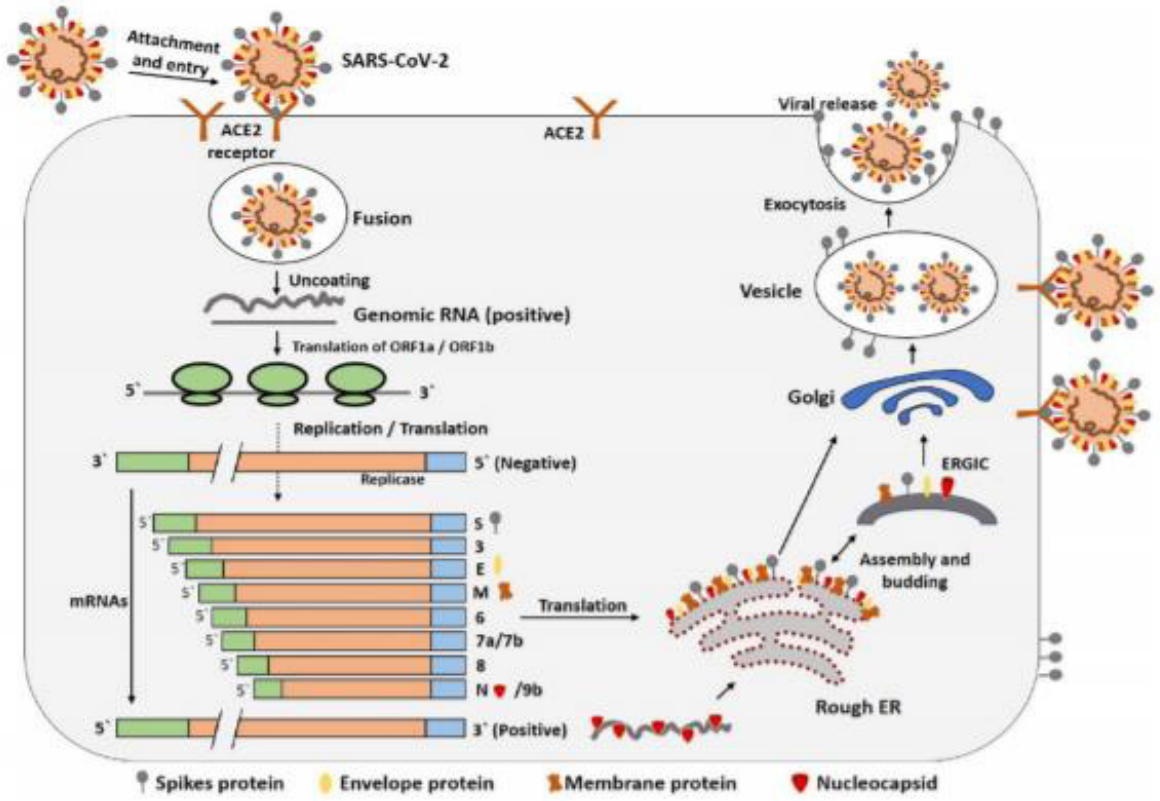

Fig. 3. The life cycle of SARS-CoV-2 in host cells; begins its life cycle when S protein binds to the cellular receptor ACE2. After receptor binding, the conformation change in the S protein facilitates viral envelope fusion with the cell membrane through the endosomal pathway. Then SARS-CoV-2 releases RNA into the host cell. Genome RNA is translated into viral replicase polyproteins pp1a and 1ab, which are then cleaved into small products by viral proteinases. The polymerase produces a series of subgenomic mRNAs by discontinuous transcription and finally translated into relevant viral proteins. Viral proteins and genome RNA are subsequently assembled into virions in the ER and Golgi and then transported via vesicles and released out of the cell. ACE2, angiotensin-converting enzyme 2; ER, endoplasmic reticulum; ERGIC, ER–Golgi intermediate compartment.

is modified via homologous recombination. The spike glycoprotein of SARS-CoV-2 is the mixture of bat SARS-CoV and a not known Beta-CoV [38]. In a fluorescent study, it was confirmed that the SARS-CoV-2 also uses the same ACE2 (angiotensin-converting enzyme 2) cell receptor and mechanism for the entry to host cell which is previously used by the SARS-CoV [39,40]. The single N501T mutation in SARS-CoV-2's Spike protein may have significantly enhanced its binding affinity for ACE2 [33].

The major obstacle in research progress

Animal models play a vital role to uncover the mechanisms of viral pathogenicity from the entrance to the transmission and designing therapeutic strategies. Previously, to examine the replication of SARS-CoV, various animal models were used which showed the symptoms of severe infection [43]. In contrast to SARS-CoV, no MERS-CoV pathogenesis was observed in small animals. Mice are not vulnerable to infection by MERS-coronavirus due to the non-compatibility of the DPP4 receptor [44]. As the entire genome of the 2019-novel coronavirus is more than 80% similar to the previous human SARS-like bat CoV, previously used animal models for SARS-CoV can be utilized to study the infectious pathogenicity of SARS-CoV-2. The human ACE2 cell receptor is recognized by both SARS and Novel coronaviruses. Conclusively, TALEN or CRISPR-mediated genetically modified hamsters or other small animals can be utilized for the study of the pathogenicity of novel coronaviruses. SARS-CoV has been reported to replicate and cause severe disease in Rats (F344), where the sequence analysis revealed a mutation at spike glycoprotein [45]. Thus, it could be another suitable option to develop spike glycoprotein targeting therapeutics against novel coronaviruses. Recently, mice models and clinical isolates were used to develop any therapeutic strategy against SARS-CoV-2 induced COVID-19 [46,47]. In a similar study, artificial intelligence prediction was used to investigate the inhibitory role of the drug against SARS-CoV-2 [48]. SARS-CoV-2 infected patients were also used to conduct randomized clinical trials [46,49,50]. It is now important that the scientists worldwide collaborate the design a suitable model and investigate the in vivo mechanisms associated with pathogenesis of SARS-CoV-2.

Potential therapeutic strategies against COVID-19

Initially, interferons-α nebulization, broad-spectrum antibiotics, and anti-viral drugs were used to reduce the viral load [49,51,52], however, only remdesivir has shown promising impact against the virus [53]. Remdesivir only and in combination with chloroquine or interferon beta significantly blocked the SARS-CoV-2 replication and patients were declared as clinically recovered [46,50,52]. Various other anti-virals are currently being evaluated against infection. Nafamostat, Nitazoxanide, Ribavirin, Penciclovir, Favipiravir, Ritonavir, AAK1, Baricitinib, and Arbidol exhibited moderate results when tested against infection in patients and *in-vitro* clinical isolates [46,48,50,52]. Several other combinations, such as combining the antiviral or antibiotics with traditional Chinese medicines were also evaluated against SARS-CoV-2 induced infection in humans and mice [46]. Recently in Shanghai, doctors isolated the blood plasma from clinically recovered patients of COVID-19 and injected it in the infected patients

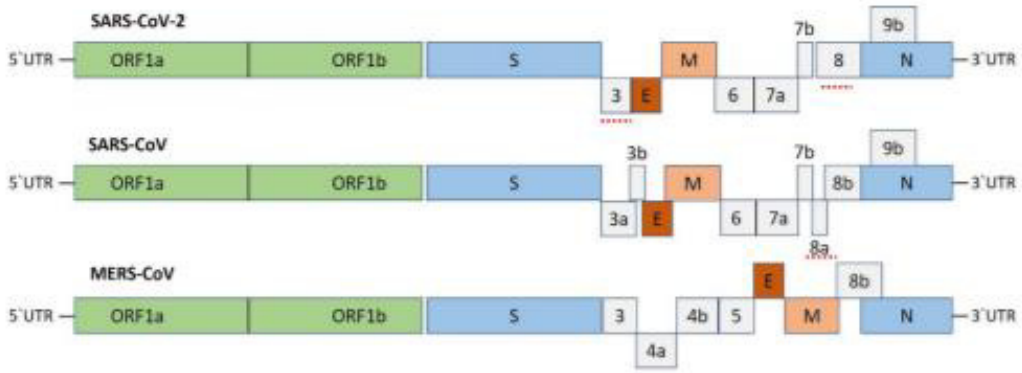

Fig. 4. Betacoronaviruses genome organization; The Betacoronavirus for human (SARS-CoV-2, SARS-CoV and MERS-CoV) genome comprises of the 5′-untranslated region (5′-UTR), open reading frame (orf) 1a/b (green box) encoding non-structural proteins (nsp) for replication, structural proteins including spike (blue box), envelop (maroon box), membrane (pink box), and nucleocapsid (cyan box) proteins, accessory proteins (light gray boxes) such as orf 3, 6, 7a, 7b, 8 and 9b in the SARS-CoV-2 genome, and the 3′-untranslated region (3′-UTR). The doted underlined in red are the protein which shows key variation between SARS-CoV-2 and SARS-CoV. The length of nsps and orfs are not drawn in scale.

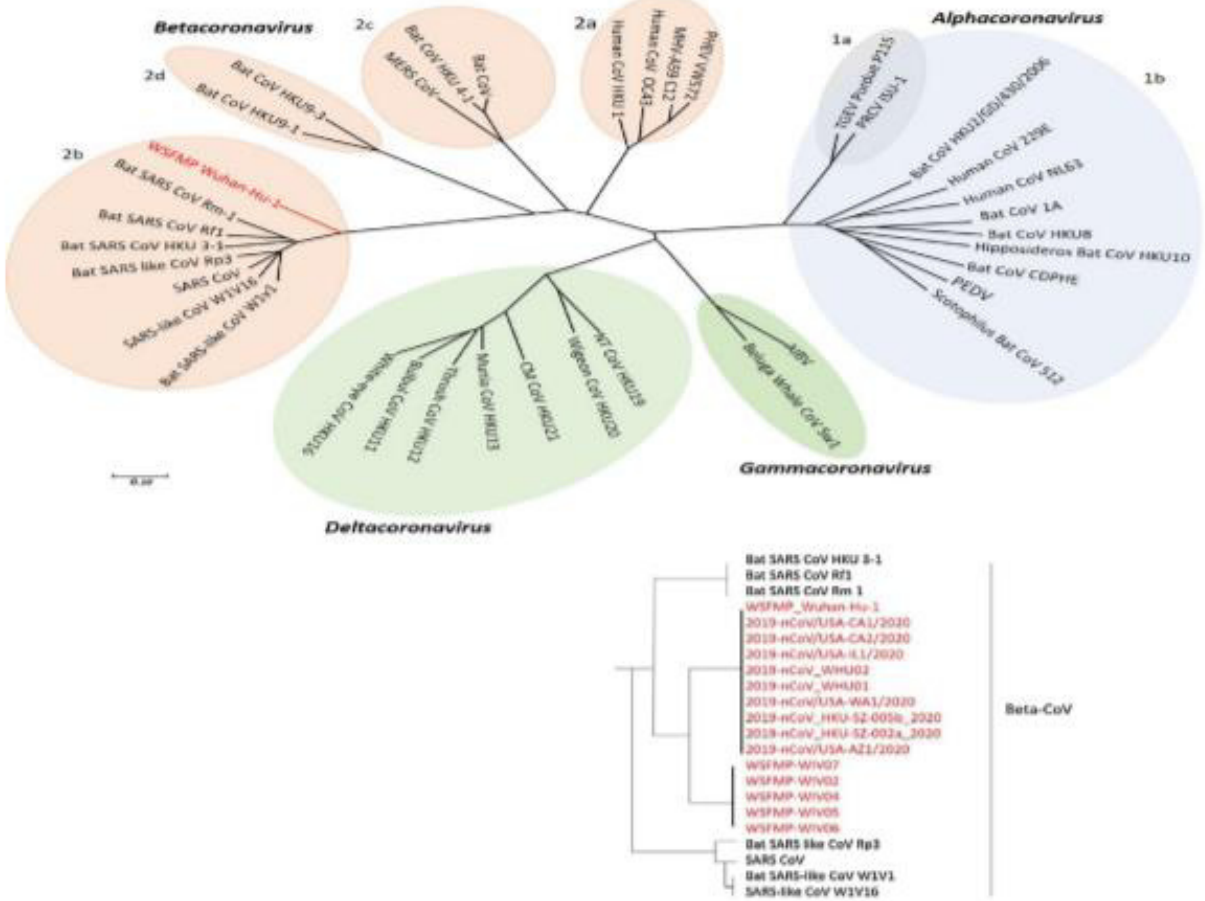

Fig. 5. Phylogenetic tree of coronaviruses (content in red is the latest addition of newly emerged SARS-CoV-2 and WSFMP Wuhan-Hu-1 is used as a reference in the tree); The phylogenetic tree showing the relationship of Wuhan-Hu-1 (denoted as red) to selected coronavirus is based on nucleotide sequences of the complete genome. The viruses are grouped into four genera (prototype shown): Alphacoronavirus (sky blue), Betacoronavirus (pink), Gammacoronavirus (green) and Deltacoronavirus (light blue). Subgroup clusters are labeled as 1a and 1b for the Alphacoronavirus and 2a, 2b, 2c, and 2d for the Betacoronavirus. This tree is based on the published trees of Coronavirinae [3,41] and reconstructed with sequences of the complete RNA- dependent RNA polymerase- coding region of the representative novel coronaviruses (maximum likelihood method using MEGA 7.2 software). severe acute respiratory syndrome coronavirus (SARS- CoV); SARS- related coronavirus (SARSr- CoV); the Middle East respiratory syndrome coronavirus (MERS- CoV); porcine enteric diarrhea virus (PEDV); Wuhan seafood market pneumonia (Wuhan-Hu-1). Bat CoV RaTG13 Showed high sequence identity to SARS-CoV-2 [42].

who showed positive results with rapid recovery [54]. In a recent study, it was identified that monoclonal antibody (CR3022) binds - with the spike RBD of SARS-CoV-2. This is likely due to the antibody's epitope not overlapping with the divergent ACE2 receptor-binding motif. CR3022 has the potential to be developed as a therapeutic candidate, alone or in combination with other neutralizing antibodies for the prevention and treatment of - COVID-19 infection [55].

Vaccines for SARS-CoV-2

There is no available vaccine against COVID-19, while previous vaccines or strategies used to develop a vaccine against SARS-CoV can be effective. Recombinant protein from the Urbani (AY278741) strain of SARS-CoV was administered to mice and hamsters, resulted in the production of neutralizing antibodies and protection against SARS-CoV [56,57]. The DNA fragment, inactivated whole virus or live-vectored strain of SARS-CoV (AY278741), significantly reduced the viral infection in various animal models [58–63]. Different other strains of SARS-CoV were also used to produce inactivated or live-vectored vaccines which efficiently reduced the viral load in animal models. These strains include, Tor2 (AY274119) [64,65], Utah (AY714217) [66], FRA (AY310120) [59], HKU-39849 (AY278491) [57,67], BJ01 (AY278488) [68,69], NS1 (AY508724) [70], ZJ01 (AY297028) [70], GD01 (AY278489) [69] and GZ50 (AY304495) [71]. However, there are few vaccines in the pipeline against SARS-CoV-2. The mRNA based vaccine prepared by the US National Institute of Allergy and Infectious Diseases against SARS-CoV-2 is under phase 1 trial [72]. INO-4800-DNA based vaccine will be soon available for human testing [73]. Chinese Centre for Disease Control and Prevention (CDC) working on the development of an inactivated virus vaccine [74,75]. Soon mRNA based vaccine's sample (prepared by Stermirna Therapeutics) will be available [76]. GeoVax-BravoVax is working to develop a Modified Vaccina Ankara (MVA) based vaccine [77]. While Clover Biopharmaceuticals is developing a recombinant 2019-nCoV S protein subunit-trimer based vaccine [78].

Although research teams all over the world are working to investigate the key features, pathogenesis and treatment options, it is deemed necessary to focus on competitive therapeutic options and cross-resistance of other vaccines. For instance, there is a possibility that vaccines for other diseases such as rubella or measles can create cross-resistance for SARS-CoV-2. This statement of cross-resistance is based on the observations that children in china were found less vulnerable to infection as compared to the elder population, while children are being largely vaccinated for measles in China.

Conclusion and perspective

Scientists are still investigating the emergence and origination of SARS-CoV-2. Moreover, its zoonotic source of transmission to humans has not been confirmed yet, however, sequence-based analysis suggested bats as the key reservoir. DNA recombination was found to be involved at spike glycoprotein which assorted SARS-CoV (CoVZXC21 or CoVZC45) with the RBD of another Beta CoV, thus could be the reason for cross-species transmission and rapid infection. According to phylogenetic trees, SARS-CoV is closer to SARS-like bat CoVs. Until now, no promising clinical treatments or prevention strategies have been developed against human coronaviruses. However, the researchers are working to develop efficient therapeutic strategies to cope with the novel coronaviruses. Various broad-spectrum antivirals previously used against influenza, SARS and MERS coronaviruses have been evaluated either alone or in combinations to treat COVID-19 patients, mice models, and clinical isolates. Remdesivir, Lopinavir, Ritonavir, and Oseltamivir significantly blocked the COVID-19 infection in infected patients. It can be cocluded that the homologus recombination event at the S protein of RBD region enhanced the transmission ability of the virus. While the decision of bring back the nationals from infected area by various countries and poor screening of passengers, become the leading cause of spreading virus in others countries.

Most importantly, human coronaviruses targeting vaccines and antiviral drugs should be designed that could be used against the current as well as future epidemics. There are many companies working for the development of effective SARS-CoV-2 vaccines, such as Moderna Therapeutics, Inovio Pharmaceuticals, Novavax, Vir Biotechnology, Stermirna Therapeutics, Johnson & Johnson, VIDO-InterVac, GeoVax-BravoVax, Clover Biopharmaceuticals, CureVac, and Codagenix. But there is a need for rapid human and animal-based trails as these vaccines still require 3–10 months for commercialization. There must be a complete ban on utilizing wild animals and birds as a source of food. Beside the development of most efficient drug, a strategy to rapidly diagnose SARS-CoV-2 in suspected patient is also required. The signs and symptoms of SARS-CoV-2 induced COVID-19 are a bit similar to influenza and seasonal allergies (pollen allergies). Person suffering from influenza or seasonal allergy may also exhibit temprature which can be detected by thermo-scanners, hence the person will become suspected. Therefore, an accurate and rapid diagnostic kit or meter for detection of SARS-CoV-2 in suspected patients is required, as the PCR based testing is expensive and time consuming. It is appreciable that the Chinese health workers have efficiently controlled the outbreak in china and limited the mortality rate to less than 3% only. The therapeutic strategies used by Chinese healthcare authorities, should also be followed by other countries.

Acknowledgments

The authors acknowledge the Postdoctoral grant from The Second Affiliated Hospital of Zhengzhou University (for S.K).

Author contribution

Suliman Khan: Conceptualization, investigation, data curation, writing- original draft preparation, reviewing and editing, and supervision. Muhammad Adnan Shereen: Writing-original draft Abber Kazmi, Nadia Bashir and Rabeea Siddique: writing- original draft.

Declaration of Competing Interest

The authors of this manuscript declare no conflict of interest.

References

[1] Zhong N, Zheng B, Li Y, Poon L, Xie Z, Chan K, et al. Epidemiology and cause of severe acute respiratory syndrome (SARS) in Guangdong, People's Republic of China, in February, 2003. The Lancet 2003;362(9393):1353–8.
[2] Wang N, Shi X, Jiang L, Zhang S, Wang D, Tong P, et al. Structure of MERS-CoV spike receptor-binding domain complexed with human receptor DPP4. Cell Res 2013;23(8):986.
[3] Cui J, Li F, Shi Z-L. Origin and evolution of pathogenic coronaviruses. Nat Rev Microbiol 2019;17(3):181–92.
[4] Lai C-C, Shih T-P, Ko W-C, Tang H-J, Hsueh P-R. Severe acute respiratory syndrome coronavirus 2 (SARS-CoV-2) and corona virus disease-2019 (COVID-19): the epidemic and the challenges. Int J Antimicrob Agents 2020;105924.
[5] Organization WH. Laboratory testing for coronavirus disease 2019 (COVID-19) in suspected human cases: interim guidance, 2 March 2020. World Health Organization, 2020.
[6] Peiris J, Guan Y, Yuen K. Severe acute respiratory syndrome. Nat Med 2004;10(12):S88–97.
[7] Pyrc K, Berkhout B, Van Der Hoek L. Identification of new human coronaviruses. Expert Review of Anti-infective Therapy 2007;5(2):245–53.
[8] Rahman A, Sarkar A. Risk factors for fatal middle east respiratory syndrome coronavirus infections in Saudi Arabia: analysis of the WHO Line List, 2013-2018. Am J Public Health 2019;109(9):1288–93.
[9] Memish ZA, Zumla AI, Al-Hakeem RF, Al-Rabeeah AA, Stephens GM. Family cluster of Middle East respiratory syndrome coronavirus infections. N Engl J Med 2013;368(26):2487–94.
[10] Wang C, Horby PW, Hayden FG, Gao GF. A novel coronavirus outbreak of global health concern. The Lancet 2020.
[11] Phan LT, Nguyen TV, Luong QC, Nguyen TV, Nguyen HT, Le HQ, et al. Importation and human-to-human transmission of a novel coronavirus in Vietnam. N Engl J Med 2020.

ANEXO 4. N. Lovell, I. Carey, S. N. Etkind, I. J. Higginson y P. Edmonds, «Characteristics, Symptom Management, and Outcomes of 101 Patients With COVID-19 Referred for Hospital,» Journal of Pain and Symptom Management, pp. 77-81, 01 07 2020.

COVID-19 Articles Fast Tracked Articles

Characteristics, Symptom Management, and Outcomes of 101 Patients With COVID-19 Referred for Hospital Palliative Care

Natasha Lovell, MBChB, BSc, MRCP, Matthew Maddocks, BSc, MCSP, PhD, Simon N. Etkind, MB, BChir, BA, MRCP, DTMH, Katie Taylor, BA (Hons)Oxon, MSc, MBBS, MRCP, Irene Carey, MB, BCh, BAO, MSc, FRCP, Vandana Vora, MBBS, FRCP, Lynne Marsh, BM, MSc, MRCP, Irene J. Higginson, BMedSci, BMBS, PhD, FMedSci, FRCP, FFPHM, Wendy Prentice, MBBS, MA, FRCP, Polly Edmonds, MBBS, FRCP, and Katherine E. Sleeman, BSc, MBBS, FRCP, PhD

King's College Hospital NHS Foundation Trust, London, UK (N.L., M.M., S.N.E., L.M., I.J.H., W.P., P.E., K.E.S.); King's College London (N.L., I.J.H., K.E.S.), Cicely Saunders Institute, London, UK; and Guy's and St Thomas' NHS Foundation Trust, London, UK (S.N.E., K.T., I.C., V.V.)

Abstract

Hospital palliative care is an essential part of the COVID-19 response but data are lacking. We identified symptom burden, management, response to treatment, and outcomes for a case series of 101 inpatients with confirmed COVID-19 referred to hospital palliative care. Patients (64 men, median [interquartile range (IQR)] age 82 [72–89] years, Elixhauser Comorbidity Index 6 [2–10], Australian-modified Karnofsky Performance Status 20 [10–20]) were most frequently referred for end-of-life care or symptom control. Median [IQR] days from hospital admission to referral was 4 [1–12] days. Most prevalent symptoms (n) were breathlessness (67), agitation (43), drowsiness (36), pain (23), and delirium (24). Fifty-eight patients were prescribed a subcutaneous infusion. Frequently used medicines (median [range] dose/24 hours) were opioids (morphine, 10 [5–30] mg; fentanyl, 100 [100–200] mcg; alfentanil, 500 [150–1000] mcg) and midazolam (10 [5–20] mg). Infusions were assessed as at least partially effective for 40/58 patients, while 13 patients died before review. Patients spent a median [IQR] of 2 [1–4] days under the palliative care team, who made 3 [2–5] contacts across patient, family, and clinicians. At March 30, 2020, 75 patients had died; 13 been discharged back to team, home, or hospice; and 13 continued to receive inpatient palliative care. Palliative care is an essential component to the COVID-19 response, and teams must rapidly adapt with new ways of working. Breathlessness and agitation are common but respond well to opioids and benzodiazepines. Availability of subcutaneous infusion pumps is essential. An international minimum data set for palliative care would accelerate finding answers to new questions as the COVID-19 pandemic develops. J Pain Symptom Manage 2020;60:e77–e81. © *2020 American Academy of Hospice and Palliative Medicine. Published by Elsevier Inc. All rights reserved.*

Key Words

COVID-19, coronavirus, palliative care, symptom management, hospice, end of life

Key Message

In this first case series of 101 patients with COVID-19 referred to palliative care, input was brief; most patients died in less than three days. The most common symptoms were breathlessness and agitation, controlled in most cases using relatively small doses of opioid and benzodiazepine, delivered by subcutaneous infusion. To meet the rapidly growing need for palliative care, services must adapt. Training and guidance for nonspecialists will help ensure symptoms are addressed promptly.

Introduction

People diagnosed with COVID-19 have an estimated mortality of 1%–3%, with those with multimorbidity most at risk of dying.[1] Estimates vary widely, but

Address correspondence to: Katherine E. Sleeman, BSc, MBBS, FRCP, PhD, King's College London, Cicely Saunders Institute, Bessemer Road, London SE5 9PJ, UK. E-mail: Katherine.Sleeman@kcl.ac.uk

Accepted for publication: April 6, 2020.

0885-3924/$ - see front matter
https://doi.org/10.1016/j.jpainsymman.2020.04.015

COVID-19 could directly cause up to 510,000 deaths in the U.K. and 2.2 million in the U.S.[2] Although the clinical characteristics of COVID-19 patients have been described, the focus has been on risk factors for ICU admission and death.[3] Data are lacking on the palliative care needs of people with COVID-19, including symptom burden and response to treatment, to help inform service planning for palliative care and hospice services in the U.K. and elsewhere. Here we describe the symptom burden, management, response to treatment, and outcomes for patients with COVID-19 referred to the palliative care teams in two large NHS hospital trusts in London, U.K.

Method

Design and Setting

This is a case series of 101 inpatients with confirmed COVID-19 infection, referred to the hospital palliative care teams at two large acute NHS Hospital Trusts in London, U.K. The two trusts comprise four hospitals and include a Highly Communicable Infectious Disease Unit. They serve populations who, during March 2020, had among the highest prevalence of COVID-19 in the U.K.

Data Collection and Analysis

Data were extracted from medical and nursing case notes by clinician-researchers (N. L., P. E., K. T., J. B., and S. E.). Variables included the following: baseline demographic and clinical characteristics; referral ward; comorbidities categorized by the Elixhauser Index[4]; clinician-assessed palliative care phase of illness (stable, unstable, deteriorating, and dying or deceased) based on care needs and suitability of the current care plan[5]; and Australia-modified Karnofsky Performance Status.[6] Symptoms were identified from standardized palliative care notes. Symptom control medicines with doses were extracted from drug charts, and clinical impressions of effectiveness were determined based on documentation at follow-up (e.g., improved breathing, agitation, comfort). Descriptive analyses were performed using SPSS (V.24, Armonk, NY). Comparisons between groups were expressed as medians and interquartile ranges (IQRs) due to the data distribution.

Results

For full demographic and other details, see Table 1. Between March 4 and March 26, 2020, 101 patients with COVID-19 were referred to palliative care, most frequently for end-of-life care or symptom control. Referrals rapidly increased from the first ($n = 2$) to the fourth week ($n = 51$). Sixty-four patients were men; the median age was 82 [72–89]. The Elixhauser Comorbidity Index was 6 [2–10]; the most common comorbidities were hypertension (54), diabetes (36), and dementia (31). Seventy-six patients had been admitted with COVID-19 and 25 were existing inpatients who developed COVID-19; median [IQR] days from admission to referral were 2 [1–6] and 16 [7–30] for these groups, respectively. At the time of referral, most patients ($n = 95$) were receiving ward-based care, with six on high-dependency or intensive care units (ICUs).

Table 1

Demographic and Clinical Characteristics, Palliative Care Contacts, and Outcomes of 101 Hospital Inpatients With COVID-19 Referred to Palliative Care

Characteristic	Median [IQR] or *n*
Age, yrs	82 [72–89]
Sex, male:female	64:37
Elixhauser Comorbidity Index	6 [2–10]
Comorbidities	
Hypertension	54
Diabetes	36
Dementia	31
Advanced/metastatic cancer	25
Chronic pulmonary disease	22
Renal failure	21
Congestive heart failure	18
Stroke/neurological disorder	12
Peripheral vascular disorder	4
Liver disease	2
AKPS	20 [10–20]
Missing	15
Level of care	
Ward-based care	95
High dependency unit	5
Intensive care unit	1
Reason(s) for referral to palliative care	
End-of-life care	70
Symptom control	41
Care planning	4
Psychological support	1
Phase of illness	
Dying	63
Unstable	24
Deteriorating	7
Stable	1
Missing	6
Days of palliative care involvement	2 [1–4]
Palliative care contacts	3 [2–5]
Contacts by recipient	
Patient	2 [1–3]
Family	1 [0–1]
Hospital staff	2 [1–4]
Contacts by type	
In person	3 [1–4]
Telephone	1 [0–1]
Outcome	
Death	75
Discharged	13
Back to team	10
Home	2
To hospice	1
Remains under palliative inpatient care	13

AKPS = Australia-modified Karnofsky Performance Status; IQR = interquartile range.
Data are median [IQR] or *n*.

Table 2
Symptoms, Drugs Prescribed, and Drug Effectiveness in 101 Hospital Inpatients With COVID-19 Referred to Specialist Palliative Care

Symptoms at Time of Referral	$N = 101$
Breathlessness	67
Agitation	43
Drowsiness	36
Pain	23
Delirium	24
Secretions	11
Fatigue	9
Fever	9
Cough	4
Other symptoms[a]	12
Symptom relieving drugs given by subcutaneous infusion	58
Morphine + midazolam	23
Morphine + midazolam + glycopyrronium	8
Morphine alone	4
Morphine + haloperidol	1
Morphine + midazolam + haloperidol	1
Fentanyl + midazolam	9
Fentanyl + midazolam + glycopyrronium	3
Alfentanil alone	2
Alfentanil + midazolam	4
Alfentanil + cyclizine	1
Alfentanil + midazolam + haloperidol	1
Midazolam alone	1
Median (range) dose/24 hours	
Morphine (mg)	10 (5–30)
Fentanyl (microgram)	100 (100–200)
Alfentanil (microgram)	500 (150–1000)
Midazolam (mg)	10 (5–20)
Glycopyrronium (microgram)	1200 (600–2400)
Haloperidol (mg)	2 (1–2)
Cyclizine (mg)	50
Clinical impression of effectiveness[b]	
Yes	40
Unclear (patient died before follow-up)	13
No	5

[a]Diarrhea (3), reduced oral intake (3), anxiety (2), seizures, ascites, incontinence, dysuria (1 each).
[b]Based on follow-up documentation, for example, improved breathing, agitation, comfort.

For full details of symptoms, drugs prescribed, and outcomes, see Table 2. The most prevalent symptoms were breathlessness, agitation, drowsiness, and pain. Twenty-four patients had symptoms of delirium. Ninety-six patients were prescribed "as needed" medication for symptom relief, and 58 patients were prescribed a subcutaneous infusion for symptom relief. Of the 37 patients who were prescribed morphine by subcutaneous infusion, the median final dose was 10 mg/24 hours. Fifty infusions contained midazolam, median final dose 10 mg/24 hours. The infusion was assessed as at least partially effective for 40/58 patients, while 13 patients died before effectiveness could be reviewed.

Patients spent a median [IQR] of 2 [1–4] days under the palliative care team and received 3 [2–5] contacts. As of March 30, 2020, patients had died (75), been discharged (13), or continued to receive palliative care input (13).

Discussion

We provide the first report of characteristics, symptom management, and outcomes of patients with COVID-19 referred for hospital palliative care. The main symptom experienced by these patients was breathlessness, similar to that found earlier in the disease trajectory.[7] In addition, we find patients near the end of life commonly experience agitation, while cough is infrequent. Time spent under the palliative care team was brief (median time 2 days), and symptom control with subcutaneous infusion was achieved in most cases using relatively small doses of opioid and benzodiazepine. Seventy-four percent of patients died.

Many services are currently facing dramatic increases in the number of people severely affected by COVID-19. In this series, the number of patients with COVID-19 referred for palliative care each week increased from 2 to 51 over four weeks. This is likely to necessitate changes in ways of working for palliative care teams such as an increase in remote patient assessment.

A proactive approach to symptom recognition, assessment, management, and escalation for people with COVID-19 is likely to be helpful.[8] Providing brief and accessible ward-base teaching on managing breathlessness and agitation, with a low threshold for prescribing anticipatory medicines for those with prognostic uncertainty, can ensure symptoms are addressed promptly.[9] Encouragingly, our data indicate that patients' symptoms can be managed using opioids and benzodiazepines at low doses. Subcutaneous infusions were frequently used to achieve symptom control. It is essential that adequate stocks of equipment are available to provide symptom control medication for those affected by COVID-19, both in inpatient and community settings.

Agitation was common among our patients. A high level of psychological distress may result from rapid deterioration and be exacerbated by isolation due to visitor restrictions. Ways to mitigate against this include use of technology such as tablet computers to communicate with carers and friends, though this may not be practical for people near the end of life. Chaplaincy, social work, and psychology teams' support are valuable.[9]

The demographic characteristics of patients in this case series, predominantly older men with comorbidities, reflect global data on COVID-19 mortality risk.[3] Hypertension and diabetes, the most frequent comorbidities in our patients, were risk factors for poor outcomes in a study of Chinese patients with COVID-19.[10] A small proportion of patients in our case series were referred to palliative care for reasons other than COVID-19 but subsequently diagnosed as COVID-19 positive. It is important to acknowledge that their

palliative care needs include both COVID-19 and non–COVID-19-related problems. In addition, there are likely to be knock-on impacts on non–COVID-19 patients resulting from the escalation in referrals, many of whom will receive less palliative care input as a result.

We included only patients referred to palliative care, and we have no information about the palliative care needs of other inpatients with COVID-19. We had few referrals from ICUs. Around 50% of patients with COVID-19 who are admitted to ICUs subsequently die and they are likely to have high palliative needs.[11,12] Information about symptoms was identified from the free-text notes, and we did not collect data on symptom severity. We report only on inpatient hospital patients and did not include community or inpatient palliative care units/hospices. The assessment of response to medication was subjective, and as the length of palliative care involvement was relatively short, there was not always sufficient time to assess effectiveness. Finally, this is an early case series and patterns are likely to change as the pandemic progresses.

Conclusion

Patients severely affected by COVID-19 frequently experience symptoms and distress, and palliative care is an essential part of the response to this pandemic. Urgent research is needed to understand more about symptom prevalence and management, and how best to deliver palliative care to those dying in ICU and community settings. An international minimum data set for COVID-19 patients receiving palliative care would accelerate finding answers to these questions.

Disclosures and Acknowledgments

The authors have no conflicts of interest to declare. All authors are members of the King's Health Partners Palliative Care Clinical Academic Group. The authors are grateful to other members of this group including Shaheen Khan, Teresa Beynon, Nick Gough, Rachel Burman, Sabrina Bajwah, Ruth Ting, and Richard Towers for supporting this work. The authors thank Jennifer Brooke for supporting data collection, and Andrew Wilcock for helpful comments on an early draft. The authors acknowledge the intense efforts of their colleagues at this time, including those within the palliative care teams and the Highly Communicable Infectious Disease Unit at Guy's and St Thomas NHS Foundation Trust.

This research did not receive any specific grant from funding agencies in the public, commercial, or not-for-profit sectors. K. E. S. is funded by a National Institute of Health Research (NIHR) Clinician Scientist Fellowship (CS-2015-15-005), M. M. is funded by an NIHR Career Development Fellowship (CDF-2017-10-009), I. J. H. is an NIHR Senior Investigator Emeritus. I. J. H. and M. M. are supported by the NIHR Applied Research Collaboration South London (NIHR ARC South London) at King's College Hospital NHS Foundation Trust. I. J. H. leads the Palliative and End of Life Care theme of the NIHR ARC South London and co-leads the national theme. S. N. E. and N. L. are previous Cicely Saunders International PhD training fellows. The views expressed are those of the authors and not necessarily those of the NHS, the NIHR, the Department of Health and Social Care, or the funding charities.

Ethical approval: The work was registered as a service evaluation with the King's College London and Guy's and St Thomas' NHS Foundation Trust Clinical Effectiveness Teams (registration numbers: PC043, PC044, and 10774).

References

1. Wu Z, McGoogan JM. Characteristics of and important lessons from the coronavirus disease 2019 (COVID-19) outbreak in China: summary of a report of 72314 cases from the Chinese center for disease control and prevention. JAMA 2020;323:1239–1242.

2. Ferguson NM, Laydon D, Nedjati-Gilani G, et al. Impact of non-pharmaceutical interventions (NPIs) to reduce COVID-19 mortality and healthcare demand. Report, Imperial College London. Available at: https://www.imperial.ac.uk/media/imperial-college/medicine/sph/ide/gida-fellowships/Imperial-College-COVID19-NPI-modelling-16-03-2020.pdf. Accessed May 1, 2020.

3. Chen N, Zhou M, Dong X, et al. Epidemiological and clinical characteristics of 99 cases of 2019 novel coronavirus pneumonia in Wuhan, China: a descriptive study. Lancet 2020;395:507–513.

4. van Walraven C, Austin PC, Jennings A, et al. A modification of the Elixhauser comorbidity measures into a point system for hospital death using administrative data. Med Care 2009;47:626–633.

5. Eagar K, Green J, Gordon R. An Australian casemix classification for palliative care: technical development and results. Palliat Med 2004;18:217–226.

6. Abernethy AP, Shelby-James T, Fazekas BS, et al. The Australia-modified Karnofsky Performance Status (AKPS) scale: a revised scale for contemporary palliative care clinical practice [ISRCTN81117481]. BMC Palliat Care 2005;4:7.

7. Yang X, Yu Y, Xu J, et al. Clinical course and outcomes of critically ill patients with SARS-CoV-2 pneumonia in Wuhan, China: a single-centered, retrospective, observational study. Lancet Respir Med 2020. https://doi.org/10.1016/s2213-2600(20)30079-5.

8. Bajwah S, Wilcock A, Towers R, et al. Managing the supportive care needs of those affected by COVID-19. Eur Respir J 2020;55:2000815.

ANEXO 5. Y. Wu, W. Jing, J. Liu, Q. Ma, J. Yuan, Y. Wang, M. Du y M. Liu, «Effects of temperature and humidity on the daily new cases and new deaths of COVID-19 in 166 countries,» *ELSEIVER Science of the Total Environment,* vol. 729, nº 139051, pp. 1-7, 2020.

Science of the Total Environment 729 (2020) 139051

Contents lists available at ScienceDirect

Science of the Total Environment

journal homepage: www.elsevier.com/locate/scitotenv

Effects of temperature and humidity on the daily new cases and new deaths of COVID-19 in 166 countries

Yu Wu [1], Wenzhan Jing [1], Jue Liu, Qiuyue Ma, Jie Yuan, Yaping Wang, Min Du, Min Liu *

Department of Epidemiology and Biostatics, School of Public Health, Peking University, No.38, Xueyuan Road, Haidian District, Beijing 100191, China

HIGHLIGHTS

- First study to explore the effects of temperature and humidity on the daily new cases and deaths of COVID-19 worldwide.
- We used log-linear GAM to analyze the effects.
- We considered the lag effects and the cumulative effects of weather conditions.
- Temperature and relative humidity were both negatively related to the daily new cases and daily new deaths of COVID-19

GRAPHICAL ABSTRACT

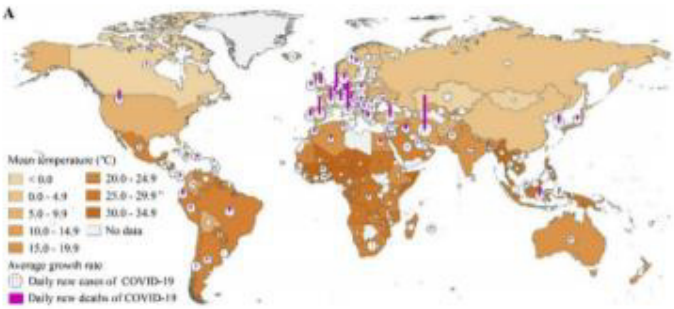

ARTICLE INFO

Article history:
Received 17 April 2020
Received in revised form 25 April 2020
Accepted 26 April 2020
Available online 28 April 2020

Editor: Jianmin Chen

Keywords:
COVID-19
Temperature
Relative humidity

ABSTRACT

The coronavirus disease 2019 (COVID-19) pandemic is the defining global health crisis of our time and the greatest challenge facing the world. Meteorological parameters are reportedly crucial factors affecting respiratory infectious disease epidemics; however, the effect of meteorological parameters on COVID-19 remains controversial. This study investigated the effects of temperature and relative humidity on daily new cases and daily new deaths of COVID-19, which has useful implications for policymakers and the public. Daily data on meteorological conditions, new cases and new deaths of COVID-19 were collected for 166 countries (excluding China) as of March 27, 2020. Log-linear generalized additive model was used to analyze the effects of temperature and relative humidity on daily new cases and daily new deaths of COVID-19, with potential confounders controlled for, including wind speed, median age of the national population, Global Health Security Index, Human Development Index and population density. Our findings revealed that temperature and relative humidity were both negatively related to daily new cases and deaths. A 1 °C increase in temperature was associated with a 3.08% (95% CI: 1.53%, 4.63%) reduction in daily new cases and a 1.19% (95% CI: 0.44%, 1.95%) reduction in daily new deaths, whereas a 1% increase in relative humidity was associated with a 0.85% (95% CI: 0.51%, 1.19%) reduction in daily new cases and a 0.51% (95% CI: 0.34%, 0.67%) reduction in daily new deaths. The results remained robust when different lag structures and the sensitivity analysis were used. These findings provide preliminary evidence that the COVID-19 pandemic may be partially suppressed with temperature and humidity increases. However, active measures must be taken to control the source of infection, block transmission and prevent further spread of COVID-19.

* Corresponding author.
E-mail address: liumin@bjmu.edu.cn (M. Liu).
[1] Contributed equally.

https://doi.org/10.1016/j.scitotenv.2020.139051

1. Introduction

In December 2019, several cases of a novel coronavirus disease (COVID-19) were reported in Wuhan, China (Guan et al., 2020), which is caused by severe acute respiratory syndrome coronavirus 2 (SARS-CoV-2) (Gorbalenya et al., 2020). The majority of individuals with coronavirus experience mild to moderate respiratory illness and recover without specific treatment (World Health Organization, 2020a). However, the elderly and people with underlying medical problems are at a higher risk of sever prognosis (World Health Organization, 2020a; National Health Commission and State Administration of Traditional Chinese Medicine, 2020). A model-based analysis estimated that the case fatality ratio in China was 1.38%, and up to 13.4% in individuals aged 80 years or older (Verity et al., 2020). On March 11, 2020, the World Health Organization (WHO) categorized COVID-19 as a pandemic, because the number of cases increased drastically outside China (World Health Organization, 2020b). As of April 10, 2020, there have been almost 1.5 million confirmed cases in 184 countries/regions, and over 92,000 deaths worldwide (World Health Organization, 2020c; Johns Hopkins University, 2020).

Research has reported that seasonal cyclicity is a ubiquitous feature of acute infectious diseases, which is also commonly observed in respiratory viral diseases (Martinez, 2018). For instance, influenza outbreaks occur every winter in temperate regions (Shaman et al., 2010). An epidemiological model in the United States indicated that absolute humidity affected the seasonality of influenza incidence (Shaman et al., 2010). Moreover, severe acute respiratory syndrome (SARS) broke out in China in mid-November 2002, and had almost entirely resolved by July 2003 (Tan et al., 2005; Ma et al., 2020). A study in China that was based on case studies in Hong Kong, Guangzhou, Beijing, and Taiyuan indicated that the outbreaks of SARS were significantly associated with variations in temperature (Tan et al., 2005).

Emerging laboratory and epidemiological data suggest that environmental conditions may affect the current COVID-19 pandemic (Jon Brassey et al., 2020). A published laboratory study by Chin et al. (2020) reported that SARS-CoV-2 was highly stable at 4 °C but sensitive to heat. The virus survival time was shortened to 5 min as the incubation temperature increased to 70 °C. Epidemiological studies have explored the relationship between COVID-19 and meteorological parameters; however, findings are controversial (Ma et al., 2020; Xie and Zhu, 2020; Yao et al., 2020). A study by Xie and Zhu (2020) reported that a 1 °C rise was associated with a 4.861% increase in the daily confirmed cases of COVID-19, when mean temperature (lag 0–14) was below 3 °C. A study by Ma et al. (2020) reported a positive association between daily deaths of COVID-19 and diurnal temperature range, and a negative association for relative humidity. However, a study by Yao et al. (2020) reported that COVID-19 transmission did not exhibit an association with temperature in Chinese cities.

COVID-19 continues to spread globally, and a second wave of COVID-19 appears probable (Leung et al., 2020; Price et al. 2019) thus, the effect of meteorological parameters on the spread of COVID-19 should be explored to help predict the development over the coming months, although numerous factors may affect the progression of the COVID-19 pandemic. Therefore, this study explored the effects of temperature and humidity on the daily new cases and deaths of COVID-19 in 166 countries using a generalized additive model (GAM), to provide useful implications for policymakers and the public.

2. Methods

2.1. Data collection

Data of COVID-19 cases were collected in 166 countries (excluding China) as of March 27, 2020 for analysis. Data, including daily new cases and daily new deaths, were collected from the WHO daily COVID-19 situation reports (https://www.who.int/emergencies/diseases/novel-coronavirus-2019/situation-reports).

The monitoring stations nearest to each country's capital were used. Daily meteorological data, including daily average temperature, average dew point, and average wind speed, were obtained from the National Oceanic and Atmospheric Administration Center (https://www.ncei.noaa.gov/access/search/data-search/global-summary-of-the-day).

2.2. Calculation of relative humidity

Relative humidity is the ratio of the actual water vapor pressure to the saturation water vapor pressure at the prevailing temperature, calculated using the following equation:

$$Relative\ humidity = \frac{E}{E_w} \times 100\%$$

where E (hPa) donates the vapor pressure of air at temperature t(°C). E_w (hPa) donates the saturated vapor pressure of the pure horizontal liquid surface at dry bulb temperature t (°C). The dew point is the temperature at which air must be cooled to become saturated with water vapor. The actual vapor pressure E can be calculated using the dew point temperature and the saturated vapor pressure can be calculated from the actual temperature using the Magnus formula for saturation water vapor pressure (Chen, 1997; Steven et al., 2020):

$$E = E_0 \times e^{\frac{At}{B+t}}$$

where E_0 denotes saturation vapor pressure at a reference temperature T_0 (273.15 K) which equals 6.11 mb. A is a constant of 17.43 and B is a constant of 240.73. t (°C) is the actual temperature or dew point.

2.3. Control variables

Five variables were included in the model as potential confounders: wind speed (https://www.ncei.noaa.gov/access/search/data-search/global-summary-of-the-day), median age of the national population (https://ourworldindata.org/age-structure2019), Global Health Security Index (GHSI, https://www.ghsindex.org/wp-content/uploads/2020/04/2019-Global-Health-Security-Index.pdf), Human Development Index (HDI, http://hdr.undp.org/sites/default/files/hdr2019.pdf) and population density (https://worldpopulationreview.com/countries/countries-by-density/). Wind is a crucial factor in the transmission of respiratory infectious diseases and it may modulate the dynamics of various vectors and pathogens (Ellwanger and Chies, 2018). Median age of the national population is an indicator of population aging; the incidence of severe cases is higher in countries with higher levels of population aging (Verity et al., 2020). GHSI is the first comprehensive assessment of global health security capabilities to be employed in 195 countries; the 2019 GHSI report scored (out of 100) the country-level capacity for "early detection and reporting for epidemics of potential concern." HDI is a summary measure of average achievement in three key dimensions of human development: a long and healthy life, being knowledgeable and have a decent standard of living. Population density is expressed as the number of people per square mile of land area; a high population density can promote the spread of epidemics (Khairat et al., 2020).

2.4. Statistical methods

In the present study, 166 countries with confirmed cases as of March 27, 2020 were included. Descriptive analyses were performed for all the data. A log-linear GAM was used to analyze the associations between meteorological factors (temperature and relative humidity) and daily new cases and daily new deaths of COVID-19 (Samet et al., 2000).

First, the basic models were constructed, including meteorological factors (temperature and relative humidity). Second, the variables were controlled to adjust for regional variation, including wind speed, median age of the population, GHSI, and country. Third, the day-of-week and the penalized smoothing spline functions were incorporated to control the time trend and cycle. The core GAM equation was as follows:

$$log(Y_t) = \alpha + \beta X_t + Wind + Country + Median.Age + GHSI + DOW + s(Time, df)$$

where t is the day of the observation. Considering that the number of daily new cases or daily new deaths in some countries is 0, Y_t is the number of daily new cases or daily new deaths on day t plus one. α is the intercept; β is the regression coefficient; X_t is the weather variables on day t; *Wind* is the wind speed; *Country* is a categorical variable for country; *Median.Age* is the median age of each countries' population; *GHSI* is the Global Health Security Index; *DOW* is a categorical variable indicating the date of the week; *s( )* refers to the smoother, which is based on the penalized smoothing spline; *Time* is the date of the observation; *df* is the degree of freedom.

The lag effects of weather conditions on daily new cases and daily new deaths of COVID-19 were then considered using single lag days (lag 0, 1, 2, 3). The cumulative effects of average exposure over multiple days were then assessed using additional analyses (lag 01, 02, 03) to control for the possible misalignment of a single lag day exposure.

All analyses were performed using R software (version 3.6.0) with the "mgcv" package (version 1.8–28). The results were expressed as percentage changes and 95% confidence intervals (CIs) in daily new cases and daily new deaths of COVID-19 associated with a 1 unit increase in weather variables. All tests were two-sided, and a value $P < 0.05$ was considered statistically significant.

2.5. Sensitivity analysis

Two other variables were included in the sensitivity analysis: HDI and population density. Because of the inconsistent outbreak time of COVID-19 in different countries, the transmission mechanism and transmission rate of COVID-19 may differ. Therefore, countries that first reported case relatively early and countries with more cases were selected to fit the core model to determine the stability of results.

3. Results

3.1. Description analysis

A total of 509,164 cumulative confirmed cases and 23,335 deaths had been documented globally as of March 27, 2020. Italy, the United States and Spain were the three countries with the most cases of COVID-19 outside of China. Moreover, Italy, Spain and Iran had the most deaths of COVID-19 outside of China. The average temperatures ranged from −5.28 to 34.30 °C, and the average relative humidity ranged from 11.39% to 88.42% (Fig. 1).

3.2. Effects of temperature and humidity on daily new cases and daily new deaths of COVID-19

After controlling the effects of potential confounders, temperature and relative humidity were both negatively related to the daily new cases and daily new deaths. A 1 °C increase in temperature was associated with a 3.08% (95% CI: 1.53%, 4.63%) reduction in daily new cases and a 1.19% (95% CI: 0.44%, 1.95%) reduction in daily new deaths. A 1% increase in relative humidity was associated with a 0.85% (95% CI: 0.51%, 1.19%) reduction in daily new cases and a 0.51% (95% CI: 0.34%, 0.67%) reduction in daily new deaths. Different lag structures also indicated that temperature and relative humidity were negatively correlated with daily new cases and daily new deaths (Fig. 2). The strongest cumulative effects were observed at lag 03, with a 1 °C increase in temperature being associated with a 5.94% and 2.30% reduction in daily new cases and daily new deaths, respectively, a 1% increase in relative humidity being associated with a 1.23% and 0.88% reduction in daily new cases and daily new deaths, respectively.

3.3. Sensitivity analysis

Two indicators of HDI and population density were adjusted based on the core model. The results revealed that a 1 °C increase in temperature was associated with a 2.85% reduction in daily new cases and no association with daily new deaths. A 1% increase in relative humidity was associated with a 0.87% reduction in daily new cases and a 0.46% reduction in daily new deaths (Table 1).

The cumulative number of cases and the outbreak time of COVID-19 exhibited a large variation between countries; thus the transmission mode and rate of COVID-19 differ between countries. We selected countries that reported their first case over 10 days before data collection and countries with over 100 cumulative cases to fit the core model. Among countries with over 10 days since the first reported case, a 1 °C increase in temperature was associated with a 3.05% and 1.22% reduction in daily new cases and daily new deaths, respectively, and a 1% increase in relative humidity was associated with a 0.87% and 0.51% reduction in daily new cases and daily new deaths, respectively. In countries with over 100 cumulative cases, a 1 °C increase in temperature was associated with a 2.82% and 1.25% reduction in daily new cases and daily new deaths, respectively; a 1% increase in relative humidity was associated with a 0.86% and 0.53% reduction in daily new cases and daily new deaths, respectively. The results of the comparisons of these datasets with the total data were not significant. These results demonstrate a robust effect of temperature and relative humidity on daily new cases and new deaths of COVID-19 (Table 2).

4. Discussion

The COVID-19 pandemic is the defining global health crisis of our time and the greatest challenge facing the world (United Nations Development Programme, 2020). Our findings revealed that temperature and humidity were inversely correlated with daily new cases and deaths of COVID-19. For every 1 °C increase in temperature, daily new cases of COVID-19 reduced by 3.08% (95% CI: 1.53%, 4.63%) and daily new deaths reduced by 1.19% (95% CI: 0.44%, 1.95%); for every 1% increase in humidity, daily new cases of COVID-19 reduced by 0.85% (95% CI: 0.51%, 1.19%), and daily new deaths reduced by 0.51% (95% CI: 0.34%, 0.67%), according to analyses of 166 countries. After adjusting for potential factors and lag days, the negative relationships remained robust. Furthermore, we hypothesized that the effects of temperature and humidity on daily cases and deaths of COVID-19 may not be evident in countries where the community transmission of COVID-19 had not occurred because the proportion of imported cases was high. Therefore, countries where the time of onset was fewer than 10 days prior, or countries with fewer than 100 cumulative confirmed cases were excluded in the sensitivity analysis. The model-fitting results remained stable.

Few studies have investigated the association of temperature and humidity with COVID-19 incidence and death rates. A preprint study, which investigated the total confirmed cases in 429 cities globally from January 20 to February 4, 2020 indicated that the cumulative number of confirmed cases reduced by 0.86 for every 1 °C increase in the minimum temperature of higher-temperature cities (Wang et al., 2020). Another preprint study by Bannister-Tyrrell et al. (2020) reported that as of February 29, 2020, average temperature increases of 1 °C were negatively correlated with the predicted number of cases worldwide (excluding Hubei Province). Furthermore, a study reported that relative humidity was inversely related to daily deaths of COVID-19 ($r = -0.32$), with the largest reduction in lag 3 [−11.41% (95% CI:

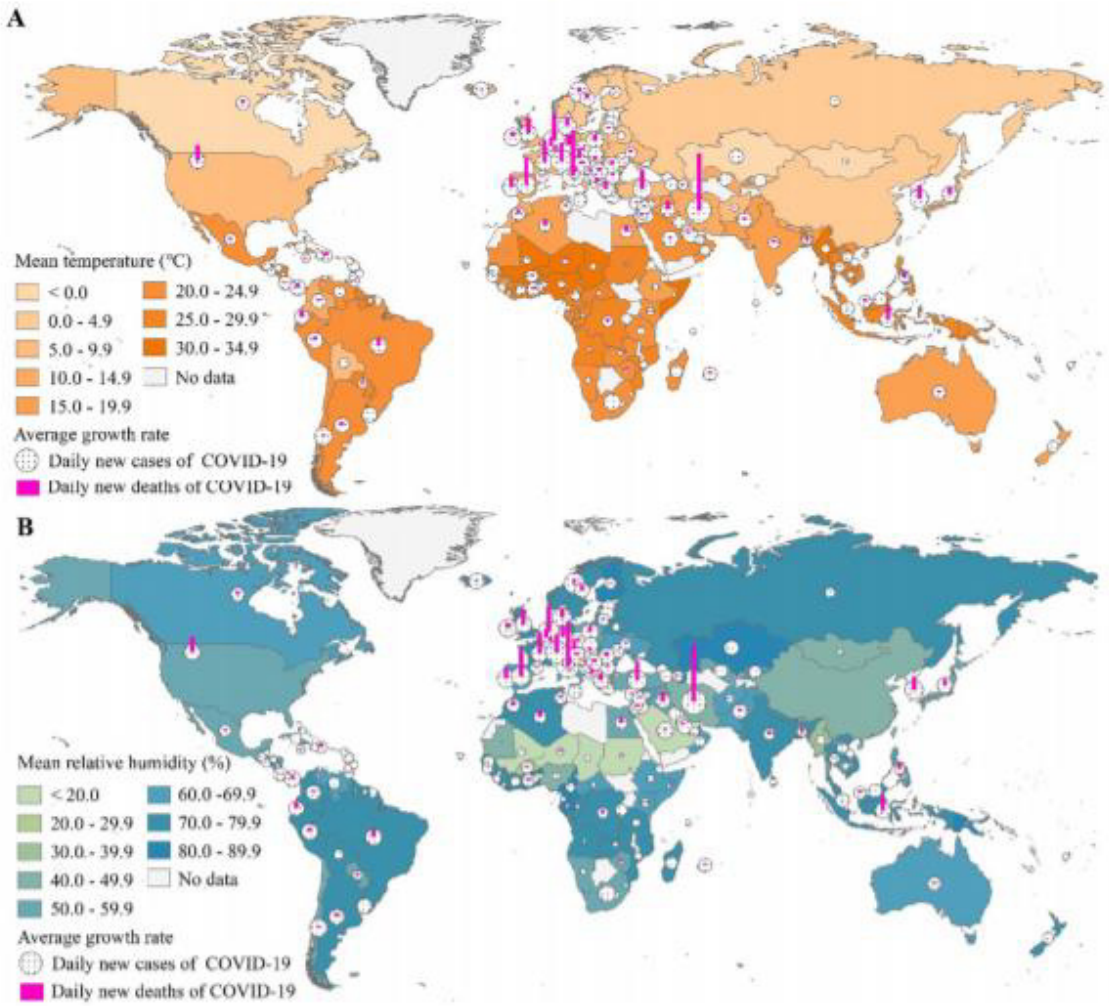

Fig. 1. As of March 27th 2020, distribution of (A) mean temperature and (B) mean relative humidity with the average growth rate of daily new cases and daily new deaths of COVID-19 worldwide. Note: Mean temperature (°C) was the sum of the daily average temperature divided by the number of observed days. Mean relative humidity (%) was the sum of the daily average relative humidity divided by the number of observed days. Average growth rate was the average of the natural logarithm of the number of daily new cases or daily new deaths.

−19.68%, −2.29%)] (Ma et al., 2020). These results accord with our findings.

Other studies have reported conflicting results. A study in 122 cities in China demonstrated that when the mean temperature (lag 0–14) was below 3 °C, the daily confirmed cases of COVID-19 increased by 4.861% (95% CI: 3.209, 6.513%) for every 1 °C rise in temperature (Xie and Zhu, 2020). However, no correlations were observed when the mean temperature was above 3 °C. Another study investigated the daily deaths of COVID-19 in Wuhan, China, from January 20 to February 29, 2020, which revealed that diurnal temperature ranges were positively correlated with daily COVID-19 deaths ($r = 0.44$) (Ma et al., 2020). However, these results were not stable, because the temperature was related to the reduction in COVID-19 deaths in lag 3 [−7.50% (95% CI: −10.99%, −3.88%)] and lag 5. These studies did not report the same trends as our study, which may be because of the different characteristics of the participants and different models. The conflicting study was only conducted in China and the temperature range was limited, whereas our study analyzed several countries.

There are several possible explanations for our findings. Firstly, studies have reported that SARS-CoV-2 is sensitive to high temperature and humidity (Chin et al., 2020; van Doremalen et al., 2020; Chan et al., 2011; Sun et al., 2020; Ma et al., 2020; Wu et al., 2020; Xie and Zhu, 2020; Yao et al., 2020). A laboratory study by Chin et al. (2020) demonstrated a 0.7 log-unit reduction after 14 days of incubation in the virus transport medium at 4 °C (final concentration – 6.8 log-unit of 50% tissue culture infectious dose per mL); over 3 log-unit reduction after 7 days of incubation at 22 °C, and no virus detected at 14 days; over 3 log-unit reduction after 1 day of incubation at 37 °C, and no detection afterward. Moreover, a study by van Doremalen et al. (2020) demonstrated that under experimental conditions, the stability of SARS-CoV-2 was similar to that of SARS-CoV. Chan et al. (2011) reported that at temperatures of 22–25 °C and relative humidity of 40%–50%, dried SARS-CoV could survive for over 5 days on smooth surfaces. However, the viability of SARS-CoV reduced rapidly when the temperature or relative humidity increased. Therefore, SARS-CoV-2 may be less stable in high-temperature and high-humidity environments. Second, the moisture in the exhaled bioaerosols evaporates rapidly in low relative humidity, forming droplet nuclei that remain in the air for longer, thereby increasing the likelihood of pathogen transmission (Lowen et al., 2007; Tellier, 2006). Third, the cold weather in winter hinders humans' innate immunity. Cold temperatures cause reduced blood supply and thus reduce the provision of immune cells to the nasal mucosa (Sun et al., 2020). Moreover, low humidity reduces the airway cilia cells' ability to remove virus particles, secrete mucus, and repair airway

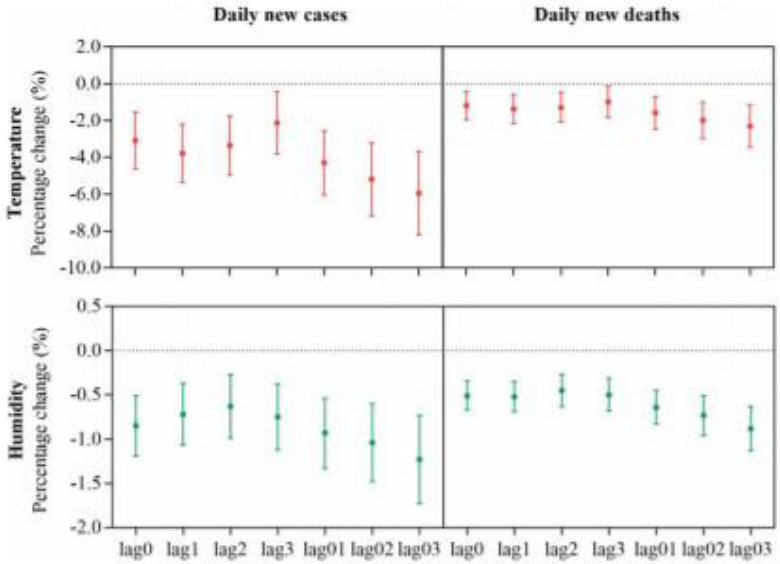

Fig. 2. Effects of temperature and relative humidity on daily new cases and daily new deaths of COVID-19 in different lag structures.

cells, thus exposing the host to the virus (Sun et al., 2020; Lowen et al., 2007). During viral infections, cells release signal proteins to alert neighboring cells of the danger of virus invasion. However, this innate immune defense system is compromised in low-humidity environments (Sun et al., 2020; Kudo et al., 2019). Therefore, the human body is at a higher risk of infection by viruses in low-temperature and low-humidity environments.

Most respiratory viruses exhibit a seasonal trend of infection, such as the influenza virus, SARS-CoV. In 2019, a study by Price et al. (2019) demonstrated that the respiratory syncytial virus and influenza A virus exhibited obvious seasonality, peaking in November–December and December–January, respectively. In 2010, Gaunt et al. (2010) analyzed samples from 11,661 patients with respiratory tract infection from Edinburgh Hospital. This study reported that three types of coronavirus (HCoV-HKU1, HCoV-NL63 and HCoV-OC43) had significant winter seasonality, mainly causing infection between December and April, which is similar to the transmission pattern of influenza (Gaunt et al., 2010). In 2005, Lin et al. (2006) analyzed the potential effect of environmental factors on the SARS epidemic in Hong Kong. The results revealed that temperature was significantly correlated with the spread of SARS after adjustment for several factors, including various interventions, the number of medical staffs infected, the number of patients in intensive care units. The risk of increased daily incidence of SARS in lower temperatures was 18.18-fold (95% CI: 5.6, 8.8) higher than that in higher temperatures (Lin et al., 2006). These studies indicate that SARS-CoV-2 may have a similar seasonal trend to other respiratory viruses, and high temperature may inhibit its spread.

The COVID-19 pandemic is currently displaying an even more adverse trend. The future growth trend of COVID-19 has attracted considerable attention as the northern hemisphere enters summer. Our results suggest that the growth rate of COVID-19 may slow with an increase in temperature and humidity. However, COVID-19 is in a stage of high infectivity and rapid transmission. The latest study estimated that the basic reproduction number (R0) of COVID-19 was approximately 5.7 (95% CI: 3.8–8.9) (Steven et al., 2020). Furthermore, confirmed cases of COVID-19 have been reported in the African equatorial and Amazon rainforest regions (Brazilian Health Agency, 2020); therefore, the effect of temperature and humidity on COVID-19 transmission is not sufficient to fully inhibit the pandemic. Countries must take active measures to control the first pandemic and prevent a second wave of COVID-19 (Leung et al., 2020).

The advantages of this study are as follows. First, all countries in which COVID-19 cases had been reported, as of March 27, 2020, were included in our study; thus the results reflect the global COVID-19 situation. Second, this study was a time series analysis, which eliminated the long-term trend of the COVID-19 epidemic, and daily meteorological data were used to accurately reflect the effect of temperature and humidity on the daily new cases and daily new deaths of COVID-19. Third, this study further included variables that reflected economic level, medical conditions, population aging, and population density to reduce confounding bias.

However, several limitations must be considered. First, the dates of reporting from the WHO daily COVID-19 situation reports were used instead of the date of onset in our study, which may engender bias because the time interval varied depending on the medical conditions, policy formulation and diagnostic criteria of each country. Second, the number of confirmed cases was inevitably underestimated, especially in low-income regions, because of the low detection coverage of COVID-19. Third, the effects of policies and measures on COVID-19 transmission were not assessed in our study; however, certain measures, such as quarantine, may affect the prevalence of infectious diseases. Finally, ecological fallacies may have arisen as a result of using

Table 1
Estimated changes with 95% confidence intervals in daily new cases and daily new deaths percentage change (%) associated with each 1 unit increase in temperature and relative humidity, after controlling the HDI and population density.

Variables	Daily new cases				Daily new deaths			
	β	95%CI		P	β	95%CI		P
Temperature (°C)	−2.85%	−4.40%	−1.31%	<0.01	−0.65%	−1.40%	0.099%	0.089
Relative humidity (%)	−0.87%	−1.22%	−0.53%	<0.01	−0.46%	−0.63%	−0.29%	<0.01

Table 2
Estimated changes with 95% confidence intervals in daily new cases and daily new deaths percentage change (%) associated with each 1 unit increase in temperature and relative humidity among countries with over 10 days since the first reported case and countries with over 100 cumulative cases.

Countries	Variables	Daily new cases				Daily new deaths			
		β	95%CI		P	β	95%CI		P
Over 10 days since the first reported case	Temperature (°C)	−3.05%	−4.63%	−1.47%	<0.01	−1.22%	−2.00%	−0.45%	<0.01
	Relative humidity (%)	−0.87%	−1.21%	−0.52%	<0.01	−0.51%	−0.68%	−0.34%	<0.01
Over 100 cumulative cases	Temperature (°C)	−2.82%	−4.60%	−1.03%	<0.01	−1.25%	−2.16%	−0.34%	<0.01
	Relative humidity (%)	−0.86%	−1.25%	−0.47%	<0.01	−0.53%	−0.73%	−0.33%	<0.01

the temperature and humidity of the capitals to reflect the national mean temperature and humidity, and using outdoor exposure as a proxy for personal exposure.

5. Conclusions

These findings provide preliminary evidence that the COVID-19 pandemic may be partially suppressed with temperature and humidity increases. However, active measures must be taken to control the source of infection, block transmission and prevent further spread of COVID-19.

Abbreviations

COVID-19
Corona Virus Disease 2019
SARS-CoV-2
severe acute respiratory syndrome coronavirus 2
WHO World Health Organization
GAM generalized additive model
GHSI Global Health Security Index
HDI Human Development Index
CIs confidence intervals

Ethical approval and consent to participate

Not applicable.

Availability of supporting data

The datasets used and/or analyzed during the current study are available from the websites.

Funding

This work was supported by National Key Research and Development Program of China [grant number 2020YFC0846300] and The National Natural Science Foundation of China [grant number 71934002].

CRediT authorship contribution statement

Yu Wu: Writing - original draft, Methodology, Software, Data curation.**Wenzhan Jing:**Writing - review & editing, Visualization.**Jue Liu:**Writing - review & editing, Supervision, Methodology.**Qiuyue Ma:** Data curation, Methodology, Validation.**Jie Yuan:**Data curation, Investigation.**Yaping Wang:**Data curation, Investigation.**Min Du:**Data curation, Investigation.**Min Liu:**Conceptualization, Funding acquisition, Project administration, Supervision.

Declaration of competing interest

The authors declare that they have no known competing financial interests or personal relationships that could have appeared to influence the work reported in this paper.

Acknowledgements

We are very grateful to Wei Li for guiding the use of the software.

References

Bannister-Tyrrell, M., Meyer, A., Faverjon, C., Cameron, A., 2020. Preliminary evidence that higher temperatures are associated with lower incidence of COVID-19, for cases reported globally up to 29th February 2020. medRxiv https://doi.org/10.1101/2020.03.18.20036731 2020.2003.2018.20036731.

Brazilian Health Agency, 2020. Falecimento de indígena Kokama por coronavírus. https://www.saude.gov.br/noticias/agencia-saude/46713-falecimento-de-indigena-kokama-por-coronavirus, Accessed date: 14 April 2020.

Chan, K.H., Peiris, J.S.M., Lam, S.Y., Poon, L.L.M., Yuen, K.Y., Seto, W.H., 2011. The effects of temperature and relative humidity on the viability of the SARS coronavirus. Advances in virology 2011, 734690. https://doi.org/10.1155/2011/734690.

Chen, Q., 1997. Correction, derivation and application of saturated water vapor pressure empirical formula. Meteorological,Hydrological and Marine Instruments (4), 12–22.

Chin, A.W.H., Chu, J.T.S., Perera, M.R.A., Hui, K.P.Y., Yen, H., Chan, M.C.W., Peiris, M., Poon, L.L.M., 2020. Stability of SARS-CoV-2 in different environmental conditions. The Lancet Microbe https://doi.org/10.1016/S2666-5247(20)30003-3.

United Nations Development Programme, 2020. COVID-19 pandemicHumanity needs leadership andsolidarity to defeat the coronavirus. https://www.undp.org/content/undp/en/home/coronavirus.html.

van Doremalen, N., Bushmaker, T., Morris, D.H., Holbrook, M.G., Gamble, A., Williamson, B.N., Tamin, A., Harcourt, J.L., Thornburg, N.J., Gerber, S.I., Lloyd-Smith, J.O., de Wit, E., Munster, V.J., 2020. Aerosol and surface stability of SARS-CoV-2 as compared with SARS-CoV-1. N. Engl. J. Med. https://doi.org/10.1056/NEJMc2004973.

Ellwanger, J.H., Chies, J.A.B., 2018. Wind: a neglected factor in the spread of infectious diseases. The Lancet Planetary Health 2 (11), e475. https://doi.org/10.1016/S2542-5196(18)30238-9.

Gaunt, E.R., Hardie, A., Claas, E.C., Simmonds, P., Templeton, K.E., 2010. Epidemiology and clinical presentations of the four human coronaviruses 229E, HKU1, NL63, and OC43 detected over 3 years using a novel multiplex real-time PCR method. J. Clin. Microbiol. 48 (8), 2940–2947. https://doi.org/10.1128/jcm.00636-10.

Gorbalenya, A.E., Baker, S.C., Baric, R.S., de Groot, R.J., Drosten, C., Gulyaeva, A.A., Haagmans, B.L., Lauber, C., Leontovich, A.M., Neuman, B.W., Penzar, D., Perlman, S., Poon, L.L.M., Samborskiy, D., Sidorov, I.A., Sola, I., Ziebuhr, J., 2020. Severe acute respiratory syndrome-related coronavirus: the species and its viruses – a statement of the Coronavirus Study Group. BioRxiv https://doi.org/10.1101/2020.02.07.937862 2020.2002.2007.937862.

Guan, W.J., Ni, Z.Y., Hu, Y., Liang, W.H., Ou, C.Q., He, J.X., Liu, L., Shan, H., Lei, C.L., Hui, D.S.C., Du, B., Li, L.J., Zeng, G., Yuen, K.Y., Chen, R.C., Tang, C.L., Wang, T., Chen, P.Y., Xiang, J., Li, S.Y., Wang, J.L., Liang, Z.J., Peng, Y.X., Wei, L., Liu, Y., Hu, Y.H., Peng, P., Wang, J.M., Liu, J.Y., Chen, Z., Li, G., Zheng, Z.J., Qiu, S.Q., Luo, J., Ye, C.J., Zhu, S.Y., Zhong, N.S., 2020. Clinical characteristics of coronavirus disease 2019 in China. N. Engl. J. Med. https://doi.org/10.1056/NEJMoa2002032.

Johns Hopkins University, 2020. Coronavirus Resource Center. https://coronavirus.jhu.edu/map.html, Accessed date: 14 April 2020.

Jon Brassey, C.H., Mahtani, Kamal R., Jeffrey, K.A., 2020. Do weather conditions influence the transmission of the coronavirus (SARS-CoV-2)?. Retrieved from. https://www.cebm.net/covid-19/do-weather-conditions-influence-the-transmission-of-the-coronavirus-sars-cov-2/

Khairat, S., Meng, C., Edson, B., Gianforcaro, R., 2020. Interpreting COVID-19 and Virtual Care Trends: Cohort Study. JMIR Public Health Surveill. 6 (2), e18811. https://doi.org/10.2196/18811.

Kudo, E., Song, E., Yockey, L.J., Rakib, T., Wong, P.W., Homer, R.J., Iwasaki, A., 2019. Low ambient humidity impairs barrier function and innate resistance against influenza infection. Proc. Natl. Acad. Sci. U. S. A. 116 (22), 10905–10910. https://doi.org/10.1073/pnas.1902840116.

Leung, K., Wu, J.T., Liu, D., Leung, G.M., 2020. First-wave COVID-19 transmissibility and severity in China outside Hubei after control measures, and second-wave scenario planning: a modelling impact assessment. Lancet https://doi.org/10.1016/S0140-6736(20)30746-7.

Lin, K., Yee-Tak Fong, D., Zhu, B., Karlberg, J., 2006. Environmental factors on the SARS epidemic: air temperature, passage of time and multiplicative effect of hospital infection. Epidemiol. Infect. 134 (2), 223–230. https://doi.org/10.1017/S0950268805005054.

ANEXO 6. D.-S. Kim, T.-H. Hwang, J. Yong Song, S. Hwa Park, J. Park, E.-S. Yoo, N.-K. Lee y J.-S. Park, «Design and fabrication of smart band module for measurement of temperature and GSR (galvanic skin response) from human body,» *ELSEVIER,* vol. 168, nº 10.1016, pp. 1577-1580, 2016.

ELSEVIER

Available online at www.sciencedirect.com

ScienceDirect

Procedia Engineering 168 (2016) 1577 – 1580

Procedia Engineering

www.elsevier.com/locate/procedia

30th Eurosensors Conference, EUROSENSORS 2016

Design and fabrication of smart band module for measurement of temperature and GSR (galvanic skin response) from human body

Dong-Sun Kim[a], Tae-Ho Hwang[a], Jae Yong Song[b], Sun Hwa Park[b], Jeanho Park[c], Eui-Sang Yoo[c], Nak-Kyu Lee[c], Joon-Shik Park[a,*]

[a]*Korea Electronics Technology Institute (KETI), 25 Saenari-ro, Bundang, Seongnam, Kyunggi, 13509, Rep. of Korea*
[b]*Korea Research institute of Standards and Science (KRISS),267 Gajeong-ro, Yuseong, Daejeon, 34113, Rep. of Korea*
[c]*Korea Institute of Industrial Technology(KITECH), 143, Hanggaul-ro, Sangnok, Ansan, Kyunggi, 15588, Rep. of Korea*

Abstract

In order to monitor health usually, the wearable type smart band module to measure the physiological signals from human body was designed, fabricated and characterized. Smart band module largely consisted of two parts, one was flexible sensors module and the other one was signal processing and communication module. And then two modules were interconnected with Cu wires. Finally, flexible temperature sensor of the fabricated smart band module was tested at the surfaces of ice pack, desk, and hot plate with temperature in the range of 4.5 ~ 74.1 ℃ including skin temperature around 30 ~ 33 ℃. And GSR data were measured at the skin with high sensitivity and normal atmosphere to compare. Measured data from sensors were signally processed and transmitted using via Bluetooth 4.0 wireless network, so we could display successfully those data using software on the lab-top computer. In the near future, conductive yarns will be used for the interconnections instead of general Cu wires and we are going to measure the emotion change from physiological signals from human body during usual life.

Peer-review under responsibility of the organizing committee of the 30th Eurosensors Conference

Keywords: Smart; band; module; flexible; temperature; GSR; sensor; human body

* Corresponding author. Tel.: +82-31-789-7278, fax.:+82-31-789-7279
E-mail address: jspark@keti.re.kr

Peer-review under responsibility of the organizing committee of the 30th Eurosensors Conference
doi:10.1016/j.proeng.2016.11.464

1. Introduction

R. W. Picard group suggested the idea of affective wearable computer and issued the necessity of wearable devices for long-term physiological signal measurement from human body [1]. Diverse monitoring technologies of indicating bio-signals have been widely developed with an increasing interest in self-healthcare. Among them, skin temperature and GSR (galvanic skin response) are the most basic parameters for bio-signals. Skin temperature sensor measures the relative change of temperature from human body. GSR sensor measures the real-time skin conductance which is related to the sweat gland activity depending on emotional response and environmental condition [2, 3].

In this study, the wearable type smart band module to measure the physiological signals such as temperature and GSR from human body was designed, fabricated and characterized. We have fabricated the flexible temperature sensor and GSR nanosensor. The flexible sensors mounted on FPCB (flexible printed circuit board) could be easily attached to the curved skin surface and integrated into multifunctional devices.

2. Design and fabrication of smart band module

Designed smart band module largely consisted of two parts, one was flexible sensors module and the other one was signal processing module. Flexible sensors module includes flexible temperature sensor and flexible GSR nanosensor. Signal process and communication module had signal readout, amplification, and signal transmission, and so on.

Flexible temperature sensor was fabricated using patterned Pt thin film on polyimide film. The thickness, initial resistance at 0 ℃ (R_0), and temperature coefficient of resistance (TCR) of patterned Pt thin film were 1.0 ㎛, 1330 ohm, and around 3000 ppm, respectively.

Flexible GSR nanosensor is composed of Ag nanowires embedded in polymer matrix, as shown in the schematic image of Fig.1. It is highly flexible due to the ultra-thin film, approximately 5 ~ 10 ㎛ in thickness. The Ag nanowires has a Ag/Au core-shell structure as sensing tips which are contacted to skin surface and measure skin conductance. The nanosensor is electrically conductive in the thickness direction and insulating in the in-plane direction as the Ag nanowires are vertically aligned within the polymer matrix. The anisotropic conductive configuration enables the sensor to be easily adapted to the curved skin surface for various active movement. The two electrodes of GSR nanosensor are placed on the bottom of Ag nanowires and connected to a smart band module. The detailed procedure of fabricating the anisotropic conductive sensor can be found in the previous report [4].

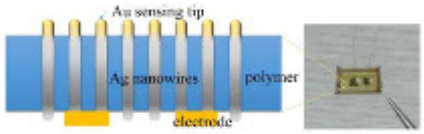

Fig. 1. Schematic image and optical image of flexible GSR sensor

Figure 2 shows the fabricated smart band module based on FPBC. The left-hand side is signal process and communication module and the right-hand side is flexible sensors module including flexible temperature sensor and flexible GSR nanosensor.

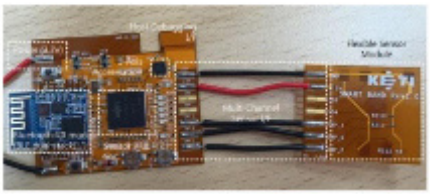

Fig. 2. Fabricated smart band module based on FPBC: (left-hand side) signal process and communication module and (right-hand side) flexible sensors module

3. Measurement of temperature and GSR within fabricated smart band module

3.1. Measurement system

Figure 3 shows the configuration of testing flexible sensor modules. The module powered by an AA battery pack gathers data from three ADC channels, and sends them to a host lap-top computer via Bluetooth 4.0 wireless network. On the host lap-top computer, a Python application monitors and plots any changes on the gathered sensor data in real-time basis. The application also saves and analysis the data. The test has conducted as touching the sensors on a 74.1 °C hot plate and 4.5 °C ice pack. Flexible GSR nanosensor has tested by touching it with a finger, which makes the sensor measuring moisture of skin on the contacts.

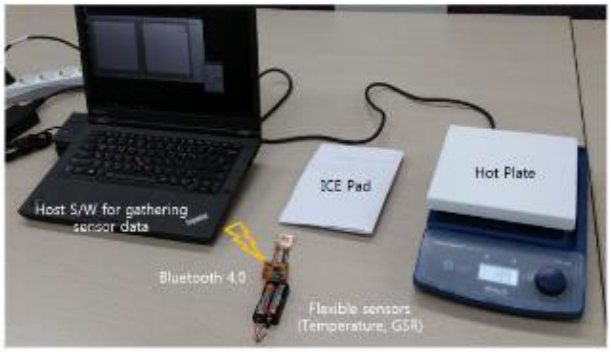

Fig. 3. Test system for flexible temperature and GSR nanosensors of smart band module

3.2. Measurement of temperature using flexible temperature sensor within smart band module

Figure 4 shows the measured data regarding resistance vs temperature using smart band module with flexible temperature sensor. In this figure, the lowest peak means the lowest temperature (4.5 ℃) due to the surface of ice pack. The highest peak means the highest temperature (74.1 ℃) due to the surface of hot plate. And the first, middle, and final points were same as the temperature of atmosphere (24.5 ℃).

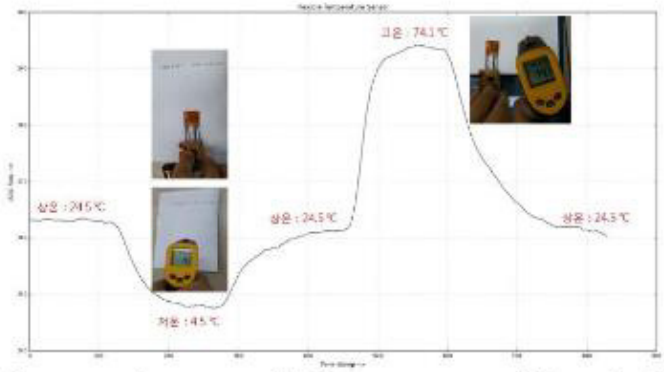

Fig. 4. Measurement of temperatures of flexible temperature sensor within smart band module

3.3. Measurement of GSR using flexible GSR nanosensor within smart band module

The flexible GSR nanosensor equipped into a smart band module shows a sensitive reaction with time of skin

conductance, as shown in Fig.5. The normalized signal of skin conductance increases with the attachment of finger skin and sharply decreases when the finger skin is removed. The sensitivity of flexible GSR was is around 9. The detection of skin conductances is repeatable without any hysterisis. Thus, the GSR nanosensor is supposed to be suitable for evaluating the emotional condition as a healthcare purpose.

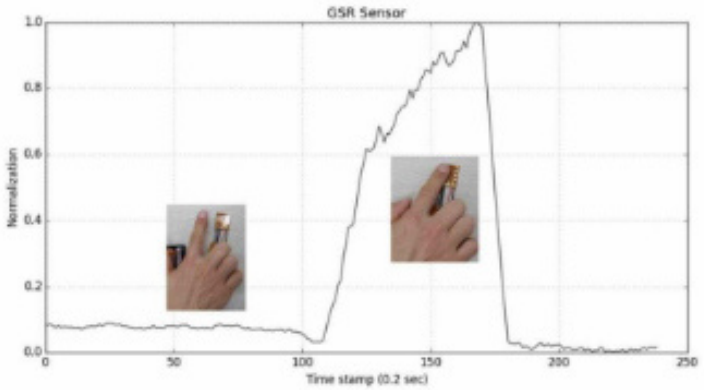

Fig. 5. Variation of skin conductance with the finger skin attached on flexible GSR nanosensor within smart band module

4. Conclusions

We have successfully fabricated the wearable type smart band module include flexible sensors module and signal and communication module to measure the physiological signals from human body. Using flexible sensors within smart band module, temperatures in the range of 4.5 ~ 74.1 ℃ including skin temperature around 30 ~ 33 ℃ by flexible temperature sensor were measured and skin conductance was measured with high sensitivity by flexible GSR nanosensor. In the near future, conductive yarns will be used for the interconnections instead of general wires and we are going to try to measure the emotion change from physiological signals from human body during usual life.

Acknowledgements

We would like to acknowledge the financial support from the R&D Convergence Program of MSIP (Ministry of Science, ICT and Future Planning) and NST (National Research Council of Science & Technology) of Republic of Korea (Grant CAP-13-1-KITECH).

References

[1] R.W. Picard and J.Healey, Affective Wearables, IEEE (1997) 90-97.
[2] R.W. Picard, J.Scheirer, The Galvactivator: A glove that senses and communicates skin conductivity, Proceedings 9th Int. Conf. on HCI (2001).
[3] S. R. Vrana. Emotional modulation of skin conductance and eye blink responses to startle probe. Psychophysiology, 32 (1995) 351-357.
[4] S.H. Park, H.S. Shin, Y.H. Kim, H.M. Park, J.Y. Song, Template-free filamentary growth of silver nanowires: application to anisotropic conductive transparent flexible electrodes, Nanoscale, 5 (2013), 1864-1869.

ANEXO 7. F. Nieto del Amor y A. J. Pérez Jiménez, «Diseño de cámara térmica IR de bajo coste basada en microcontrolador.,» de *Diseño de cámara térmica IR de bajo coste basada en microcontrolador.*, Valencia, Ecuela técnica superior ingenieros industriales Valencia, 2017, pp. 1-23.

UNIVERSITAT POLITÈCNICA DE VALÈNCIA

ESCUELA TÉCNICA SUPERIOR INGENIEROS INDUSTRIALES VALENCIA

TRABAJO FIN DE GRADO EN INGENIERÍA EN TECNOLOGÍAS INDUSTRIALES

DISEÑO DE CÁMARA TÉRMICA IR DE BAJO COSTE BASADA EN MICROCONTROLADOR.

AUTOR: FÉLIX NIETO DEL AMOR

TUTOR: ALBERTO JOSÉ PÉREZ JIMÉNEZ

Curso Académico: 2017-18

1. Introducción.

1.1. Objetivos.

El principal objetivo de este Trabajo Final de Grado es el desarrollo de una cámara térmica, la cual permita identificar focos de calor dentro de un rango térmico, permitiendo además conocer sobre que temperaturas se encuentra la zona analizada.

Para llevarlo a cabo, se van a plantear una serie de objetivos a cumplir, los cuales, tras alcanzarlos, culminaran con el desarrollo del proyecto y por tanto del objetivo principal. Estos objetivos serán:

- Interconectar por medio de software las distintas partes de hardware que se integran en el proyecto.
- Necesidad de dotar al modelo propuesto de un sistema de alimentación autónoma de energía.
- Dar soporte mecánico al conjunto de componentes del sistema, con el fin de lograr un sistema integrado.

Se plantea la opción de ser un proyecto competitivo como alternativa a nivel de mercado, puesto que otras opciones dentro de este sector pueden llegar a suponer elevados costes.

A nivel personal, mediante este proyecto se han conseguido desarrollar destrezas importantes en el ámbito de la ingeniería, tales como programación de software, integración de sistemas, sistemas energéticos o modelaje 3D a la vez que se ha obtenido una herramienta que puede resultar útil en campos donde se requiera la inspección y análisis de áreas donde se desprenda o se pierda calor, como puede ser el de instalaciones con aislamiento térmico.

1.2. Antecedentes.

Este proyecto surge para plantear una alternativa económica en los campos donde se requiera la detección y análisis de focos calientes o fríos en superficies.

Actualmente, como alternativa a la detección gráfica de estas áreas existen termómetros laser, los cuales permiten conocer con precisión la temperatura del área a la que estemos apuntando con el puntero. Sin embargo, para superficies donde existe gran cantidad de zonas calientes, resulta dificultoso la detección de la zona crítica.

De este modo, la cámara térmica resulta una alternativa a este sistema, proporcionando desde una pantalla cual será el foco crítico, sin necesidad de analizar el área punto por punto.

2. Conceptos básicos.

En este apartado se van a describir aquellos conceptos básicos, los cuales, mirados con la profundidad necesaria, proporcionan al lector de ésta el conocimiento para entender el desarrollo e implementación de las diferentes partes del proyecto. De esta forma no será objetivo de este capitulo desarrollar aspectos que carezcan de importancia para el posterior desarrollo del proyecto.

Puesto que el proyecto abarca el desarrollo de una cámara térmica, éste trata el desarrollo del software necesario, integración del hardware y alimentación energética autónoma, se dividirá esta introducción atendiendo a un orden funcional.

2.1. Sobre hardware y software.

Se introducirá a la placa Arduino Mega 2650 Rev3, TFT Touch Shield, y su entorno de desarrollo.

2.1.1. Arduino Mega 2650 Rev3 (1).

Arduino Mega es una placa de desarrollo de código abierto que incorpora una serie de entradas y salidas, analógicas y digitales, la cuales mediante su procesador Atmega2560 permite el desarrollo de sistemas embebidos, mediante un entorno de desarrollo basado en C++.

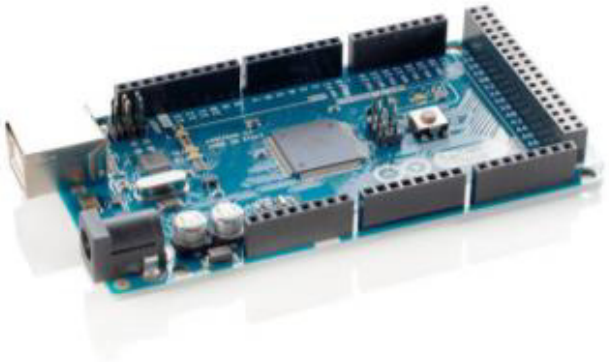

Ilustración 1. Arduino Mega 2650 Rev3.

Algunas de sus características se describen a continuación:

Alimentación (2): la tarjeta permite ser alimentada de varias formas. Mediante un conector macho (Power Jack) a una tensión de 7 a 20 V, aunque es aconsejable que sea entre 9 y 12 V para evitar inestabilidades o sobre calentamientos, o mediante una entrada USB, la cual proporciona un voltaje de entrada de 5V. Además, también permite la alimentación mediante los pines los pines de la propia tarjeta, conectando al pin VIn y aun GRN una tensión de entre 6 y 12 V, o por otro lado conectado a un pin de 5V y GRN una tensión de 5V. En cualquier caso, solo la entrada Power Jack nos

proporciona protección contra polaridad inversa y sobrecorriente, el pin Vin nos proporciona la misma protección que el Power Jack salvo contra polaridad inversa, mientras que la alimentación directa por pines de 5V y GRN (tierra) debe de ser totalmente regulada a 5V, esta tensión debe de ser estable ya que alimenta directamente los componentes de la placa Arduino, tampoco ofrece protección contra polaridad inversa.

Capacidad (3): este modelo de Arduino nos proporciona unas prestaciones altas en comparación con otros modelos de la misma entidad. Así se adjunta la siguiente tabla a modo comparativo e informativo.

Caracteristica de Arduino	UNO	Mega 2560	Leonardo	DUE
Memoria de programa (Flash)	32 Kb	256 Kb	32 Kb	512 Kb
Memoria de datos (SRAM)	2 Kb	8 Kb	2.5 Kb	96 Kb
Memoria auxiliar (EEPROM)	1 Kb	4 Kb	1 Kb	0 Kb

Tabla 1. Comparativa de Arduino.

La memoria flash nos proporcionará almacenamiento para el código de programa. La memoria SRAM es un tipo de memoria RAM en el que se almacenaran las variables dinámicas de nuestro programa. La memoria EEPROM es un tipo de almacenamiento estático, su uso en este tipo de placas se basa en el almacenamiento de constantes durante el tipo de ejecución del programa, que no queremos que se pierdan al cortar la alimentación.

Procesador: el procesador de la tarjeta Arduino Mega es el microcontrolador ATmega2560, el cual su reloj interno proporciona una velocidad de procesado de 16MHz. Dispone de 6 temporizadores, TimerX (donde X se numera del 0 al 5), necesarios para la sincronización en la comunicación con periféricos y para rutinas internas de procesamiento de datos.

En cuanto a los pines de entrada y salida, describiremos aquellos que son de interés para nuestro proyecto:

- **SPI (4):** es un estándar de comunicaciones para conectar la placa con el periférico. Como su nombre indica (*Serial Peripheral Interface)* es basado en un sistema de comunicación serial. Los pines que implementan esta función son 50, 51, 52 y 53.
- **I2C (5):** soporte para el protocolo de comunicaciones I2C (TWI) usando la librería Wire. En la tarjeta Arduino vienen integrados en los pines 20 (SDA) y 21 (SCL).

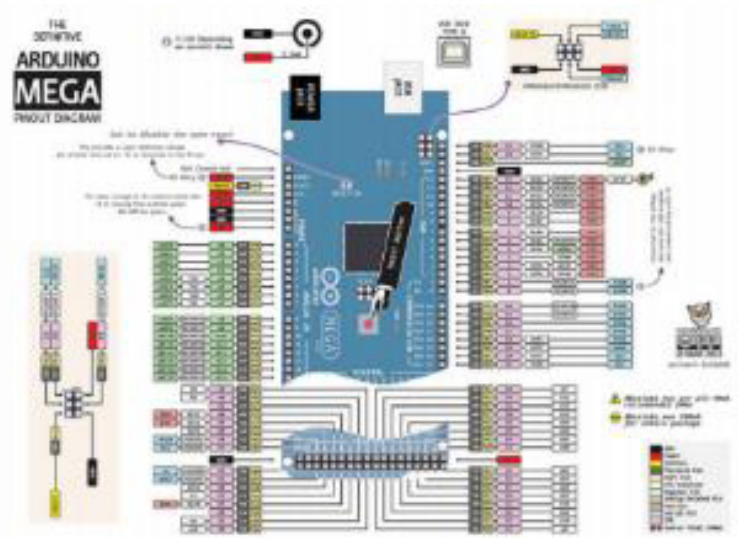

Ilustración 2. Esquema Arduino Mega.

2.1.2. TFT Touch Shield (6).

Se trata de una pantalla táctil la cual permite la comunicación con la placa Arduino, haciendo de soporte para la interfaz de usuario. Su resolución es de 320 x 240 pixeles, proporcionando unas dimensiones de 57.6mm*43.3mm, 2.8''. Su formato de color es de 65K RGB, con una interfaz de comunicación de un byte de datos en paralelo. Esto quiere decir que para transferir un color referido a un pixel necesitará 2 bytes, esto es $2^{16} = 65536$, lo cual se traduce en los anteriores 65K de colores posibles. El controlador de nuestra placa es el LGDP4535. Se debe de tener en cuenta que este nos permite la actualización selectiva de pixeles en la pantalla, esto es, no deberemos de actualizar todos los pixeles de la pantalla para mostrar simplemente una ventana, podremos lanzar directamente esa ventana actualizando solo los pixeles que en ella intervienen.

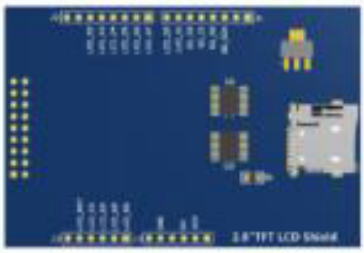

Ilustración 3. Esquema TFT Touch Shield.

Ahora se avanza al montaje de la cámara térmica con la placa Arduino.

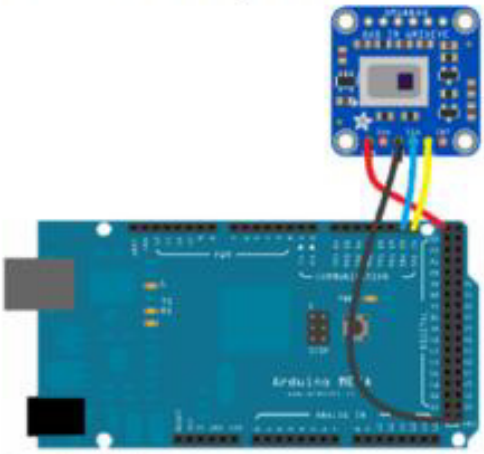

Ilustración 11. Montaje cámara Arduina

La comunicación se hace mediante un bus I2C, la alimentación mediante la entrada de 5V de tensión (cable rojo) y la tierra común (cable marrón).

3.2. Desarrollo del software.

Este apartado, en primer lugar, se centrará en el tratamiento y manipulación de los datos obtenidos por la cámara para, posteriormente, mostrarlos por la pantalla, de forma que el usuario pueda obtener una representación, lo más intuitivamente posible, de lo que se muestra por pantalla, a través de una interfaz atractiva para el mismo.

Además, se abordará el desarrollo de diferentes utilidades con el fin de mejorar las prestaciones que la cámara en sí puede aportar al usuario.

Así, se va a proceder de forma secuencial con el desarrollo de lo planteado.

3.2.1. Comunicación cámara-pantalla.

Para comenzar, pantalla y cámara no se conectan directamente, entre ellos es necesario que intervenga un mediador, en este caso la placa Arduino, que se encarga, a partir de los datos obtenidos por la cámara, procesarlos, y mandarlos a la pantalla, para mostrar al usuario una representación de lo que la cámara está captando.

FUNDAMENTACIÓN TEÓRICO

ANEXO 8. D. Grandjean, R. Sarkis, C. Lecoq-Julien, A. Benard, V. Roger y E. Levesque, «¿Puede el perro de detección alertar sobre personas positivas a COVID-19 olfateando muestras de sudor axilar? Un estudio de prueba de concepto,» *Nadine Ravel, Universite de Lyon,* nº 10.1371, pp. 1-19, 2020.

PLOS ONE

RESEARCH ARTICLE

Can the detection dog alert on COVID-19 positive persons by sniffing axillary sweat samples? A proof-of-concept study

Dominique Grandjean[1☯*], Riad Sarkis[2☯], Clothilde Lecoq-Julien[1☯], Aymeric Benard[3☯], Vinciane Roger[1‡], Eric Levesque[4‡], Eric Bernes-Luciani[3‡], Bruno Maestracci[3], Pascal Morvan[5‡], Eric Gully[6‡], David Berceau-Falancourt[7‡], Pierre Haufstater[8], Gregory Herin[9], Joaquin Cabrera[1‡], Quentin Muzzin[1‡], Capucine Gallet[1‡], Hélène Bacqué[1], Jean-Marie Broc[10], Leo Thomas[10], Anthony Lichaa[2], Georges Moujaes[2], Michele Saliba[2], Aurore Kuhn[10], Mathilde Galey[10], Benoit Berthail[10], Lucien Lapeyre[4], Anthoni Capelli[5‡], Steevens Renault[5‡], Karim Bachir[5‡], Anthony Kovinger[5‡], Eric Comas[6], Aymeric Stainmesse[6‡], Erwan Etienne[6‡], Sébastien Voeltzel[6‡], Sofiane Mansouri[6‡], Marlène Berceau-Falancourt[11‡], Aimé Dami[3], Lary Charlet[6], Eric Ruau[6], Mario Issa[2], Carine Grenet[12], Christophe Billy[13], Jean-Pierre Tourtier[4☯], Loïc Desquilbet[1☯]

1 Ecole Nationale Vétérinaire d'Alfort, Université Paris Est, Maisons-Alfort, France, **2** Université Franco-Libanaise St Joseph, Faculté de Médecine, Beirout, Lebanon, **3** Service d'Incendie et de Secours de Corse du Sud, Ajaccio, France, **4** Centre Hospitalo-Universitaire Henri-Mondor, Université Paris Est-Créteil, Maisons-Alfort, France, **5** DiagNose, Neuvy, France, **6** Service Départemental d'Incendie et de Secours de Seine et Marne, Melun, France, **7** Compagnie Cynophile de la Préfecture de Police, Paris, France, **8** Hôpital Universitaire Pitié-Salpêtrière, Paris, France, **9** Biodesive SAS, Strasbourg, France, **10** Hôpital d'Instruction des Armées Bégin, Saint-Mandé, France, **11** Cynopro Dectection Dogs, Paris, France, **12** Grand Hôpital de l'Est Francilien, Jossigny, France, **13** Centre Hospitalier François Quesnay, Mantes-la-Jolie, France

☯ These authors contributed equally to this work.
‡ These authors also contributed equally to this work.
* dominique.grandjean@vet-alfort.fr

OPEN ACCESS

Citation: Grandjean D, Sarkis R, Lecoq-Julien C, Benard A, Roger V, Levesque E, et al. (2020) Can the detection dog alert on COVID-19 positive persons by sniffing axillary sweat samples? A proof-of-concept study. PLoS ONE 15(12): e0243122. https://doi.org/10.1371/journal.pone.0243122

Editor: Nadine Ravel, Universite de Lyon, FRANCE

Received: June 27, 2020

Accepted: November 14, 2020

Published: December 10, 2020

Peer Review History: PLOS recognizes the benefits of transparency in the peer review process; therefore, we enable the publication of all of the content of peer review and author responses alongside final, published articles. The editorial history of this article is available here: https://doi.org/10.1371/journal.pone.0243122

Data Availability Statement: Data are provided as Supporting information file.

Funding: DiagNose, Cynopro Detection Dogs volunteered their dogs to participate to the study

Abstract

The aim of this proof-of-concept study was to evaluate if trained dogs could discriminate between sweat samples from symptomatic COVID-19 positive individuals (SARS-CoV-2 PCR positive) and those from asymptomatic COVID-19 negative individuals. The study was conducted at 2 sites (Paris, France, and Beirut, Lebanon), followed the same training and testing protocols, and involved six detection dogs (three explosive detection dogs, one search and rescue dog, and two colon cancer detection dogs). A total of 177 individuals were recruited for the study (95 symptomatic COVID-19 positive and 82 asymptomatic COVID-19 negative individuals) from five hospitals, and one underarm sweat sample per individual was collected. The dog training sessions lasted between one and three weeks. Once trained, the dog had to mark the COVID-19 positive sample randomly placed behind one of three or four olfactory cones (the other cones contained at least one COVID-19 negative sample and between zero and two mocks). During the testing session, a COVID-19 positive sample could be used up to a maximum of three times for one dog. The dog and its handler were both blinded to the COVID-positive sample location. The success rate per dog (i.e., the number of correct indications divided by the number of trials) ranged from 76% to 100%. The lower bound of the 95% confidence interval of the estimated success rate was most of the time higher than the success rate obtained by chance after removing the number

Participation à

l'étude de recherche Covid19

Objet : Dépistage précoce d'une contamination de l'Homme au coronavirus SARS-Cov2 par détection olfactive canine des composés organiques volatils liés à ce virus.

I- Participants

Hôpital..... / Ecole Nationale vétérinaire d'Alfort

II- Introduction

La détection olfactive précoce de maladies chroniques prolifératives (cancers) ou dégénératives (Parkinson) par des chiens dûment formés se développe rapidement de par le monde (France : projets NOSAÏS et KDOG). Les recherches antérieures ont confirmé la présence de VOC (Volatile Organic Compound) spécifiques engendrées par l'infection virale chez les personnes infectées, tout comme c'est le cas pour certaines maladies virales des bovins maintenant détectées par des chiens aux Etats Unis (Par exemple, maladie des muqueuses).

L'objectif de ce travail de recherche est d'augmenter nos moyens de dépistage facile et rapide, ce qui sera précieux à l'avenir. Et c'est en acceptant aujourd'hui de vous faire prélever, que vous participerai de façon active à ce projet de santé mondiale ! Nous insistons sur le mot mondial, car si nous réussissons, la méthodologie sera diffusée dans le monde entier.

Important : L'ensemble des résultats des tests demeureront codés et anonymes.

Le devenir de vos prélèvements ?

Perspectives :

La réussite de cette approche pourrait permettre de faire un pré-dépistage d'un grand nombre de personnes visant à ne tester de manière classique que les personnes positives à ce pré-test (gain de tests et de temps).

La validation de ce test pourrait présenter un grand intérêt lors de la procédure de déconfinement et en l'occasion de possibles vagues épidémiques futures.

Nom, prénom et signature du patient consentant, précédé de « lu et approuvé » : En Date du : / /

Fig 1. Individual informed consent form.

https://doi.org/10.1371/journal.pone.0243122.g001

brand) for COVID-19 positive and negative samples. Coolers were cleaned and disinfected with a 10% aqueous acetone solution after each use. All samples were then stored in the same place at the two sites (but positives and negatives were not mixed) at constant temperature (+18˚C for Alfort site and +6˚C for Beirut site) and humidity (45%).

Fig 2. Underarm sampling.

https://doi.org/10.1371/journal.pone.0243122.g002

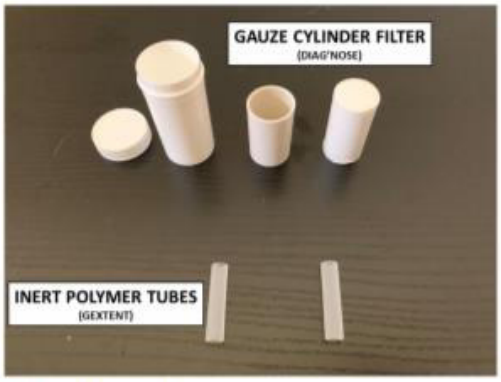

Fig 3. Sampling materials.

https://doi.org/10.1371/journal.pone.0243122.g003

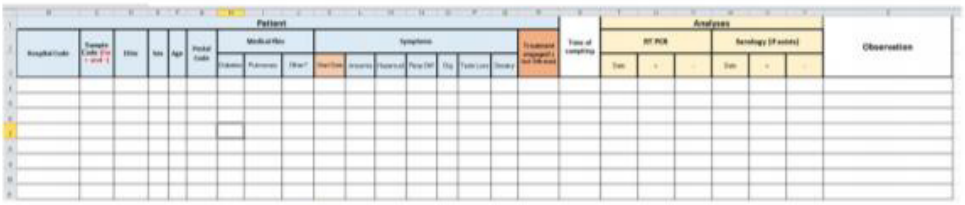

Fig 4. Anonymous form for each coded sample.

https://doi.org/10.1371/journal.pone.0243122.g004

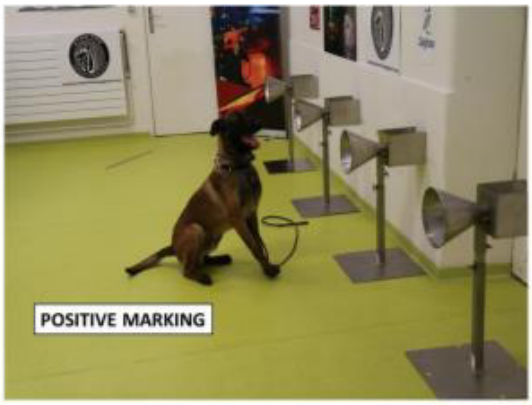

Fig 7. A dog marking a cone on a 4-cone lineup.

https://doi.org/10.1371/journal.pone.0243122.g007

and negative samples in the line-up was randomly assigned by a dedicated website (http://www.randomization.com/), and was blinded to the dog and its handler. During the testing session, the data recorder knew the COVID-19 positive sample location but there was no visual contact between the data recorder and either the dog or the dog handler. Once the samples were placed behind the cones, the dog entered the room with its handler who asked the dog to sniff each cone in the line-up. Since the dog had been trained to mark the position of one, and only one, COVID-19 positive sample behind a cone, the dog was left free to sniff the cones before marking one cone. Once a cone was (correctly or incorrectly) marked, the trial was stopped. The data recorder indicated to the dog handler whether the dog correctly marked the cone or not; if correct, the dog handler rewarded the dog. The trial was considered a "success" if the dog correctly marked the cone with the COVID-19 positive sample, otherwise it was considered a "failure". After each trial, the dog and its handler left the room, and the data recorder placed new samples behind the cones in the line-up. The line-up in this protocol is "simultaneous" rather than "sequential" (i.e., each cone is sniffed by the dog and if the dog marks a cone, the handler asks the dog to resume the task for the remaining cones in the line-up).

The testing period lasted 21 days because most dogs could not work every day. During the training and the testing sessions, the standard environmental conditions for canine olfactory detection were observed (temperature of +18˚C and 50% humidity). No disease, symptoms or clinical abnormalities have been reported for any of the dogs involved in the study.

Both samples and cones were manipulated by the same person (the data recorder), wearing sanitary barrier protections and a pair of new surgical gloves at each trial, to avoid any olfactory contamination or interaction. All cones were cleaned with clean water after each trial, and twice daily were cleaned and disinfected with 10% aqueous acetone solution, and then dried.

Statistical analysis

Since this is a proof-of-concept study, the initial objective was to provide evidence that a trained dog can detect one COVID-19 positive sample in one olfactory cone from a line-up of three to four cones, containing either mocks or COVID-19 negative samples. It was not possible to calculate the sensitivity, specificity or false alert rates (as recommended by Johnen et al. [31]) because the line-up was simultaneous not sequential. The study outcome focused on the success rate, which was calculated by dividing the number of successful trials by the number of

trials carried out by the dog. If, for one dog, the lower bound of the 95% confidence interval (calculated by using the Clopper-Pearson's method [53]) of the estimated success rate was higher than the success rate obtained by chance alone (thereafter called "random choice proportion"), then this result would provide some evidence that this dog could actually detect COVID-19 positive samples. The dogs were initially trained to discriminate between sweat samples and mocks before being trained to discriminate between COVID-19 positive and negative samples (step 3 of the training). Therefore, the random choice proportion was calculated by subtracting the number of mocks present in the line-up, then dividing 1 by the number of COVID-19 positive or negative sweat samples in the line-up. For example, a 4-cone line-up containing one mock would produce a random choice proportion of 33% (i.e., 4–1 = 3, 1/3 = 33%). To address the impact on the success rates of the dogs being presented the same COVID-19 positive sample several times, success rates are also shown according to whether it was the first, second, or third time the sample had been presented.

Results

A total of 95 symptomatic COVID-19 positive individuals and 82 asymptomatic COVID-19 negative individuals were recruited for the study, producing 177 sweat samples for the use in the study trials. The Paris site study sample consisted of 27 symptomatic COVID-19 positive individuals and 34 asymptomatic COVID-19 negative individuals. The percentage of females was similar between the two groups (52% for COVID-19 positive and 56%, for COVID-19 negative individuals), but the mean age was higher in the COVID-19 positive group (70 years) than in the COVID-19 negative group (42 years). The Beirut site study sample consisted of 68 symptomatic COVID-19 positive individuals and 48 asymptomatic COVID-19 negative individuals. The percentage of females (43% and 46%, respectively) and the mean age (48 years and 42 years, respectively) were similar between the COVID-19 positive and COVID-19 negative groups.

Out of the 14 dogs which started training, eight dogs did not participate in testing because they were not considered ready at the time of the beginning of the testing session (which could not have been postponed). Six dogs participated in testing and their training period ranged from one to three weeks.

The characteristics of the six dogs are presented in Table 1. Five dogs were Belgian Malinois Shepherds because this is the most commonly used breed in French working dog organisations. Three dogs were explosive detection dogs (Guess, Maika, and Gun), two were colon cancer detection dogs (Bella and Jacky), and one was a search and rescue dog (Gun).

For three dogs (Oslo, Bella, and Jacky), the 4-cone line-ups contained one COVID-19 positive sample and three COVID-19 negative samples without any mocks. For one dog (Gun), most of the trials (44/47) were performed on 3-cone line-ups containing one COVID-19 positive sample and two COVID-19 negative samples without any mocks. For the last two dogs

Table 1. Characteristics of the 6 dogs participating in the study testing sessions.

	Name	Gender	Breed	Age	Organisation involved	Specialty
Paris	Guess	F	Belgian Malinois	8 years	Cynopro detection Dog	Explosives
	Maika	F	Belgian Malinois	3 years	Fire and Emerg. Dept. 77	Search and rescue
	Gun	M	Belgian Malinois	16 months	Cynopro detection Dog	Explosives
	Oslo	M	Belgian Malinois	18 months	DiagNose	Explosives
Beirut	Bella	F	Belgian Malinois	6 years	Mario-K9	Colon Cancer
	Jacky	M	Jack Russell terrier	3 years	Mario-K9	Colon Cancer

https://doi.org/10.1371/journal.pone.0243122.t001

ANEXO 9. Medicina Humana, «Universidad Privada Telesup,» Universidad Privada Telesup, 02 02 2018. [En línea]. Available: https://utelesup.edu.pe/blog-medicina/estetoscopio-el-instrumento-necesario-para-el-primer-diagnostico-en-medicina-humana/. [Último acceso: 09 01 2021].

ANEXO 10. M. Reis, «TUASAÚDE,» TUASAÚDE, 02 12 2020. [En línea]. Available: https://www.tuasaude.com/es/tipos-de-termometro/. [Último acceso: 04 01 2021].

ANEXO 11. T. Parker, «¿Qué es un oxímetro de pulso?¿De verdad necesito uno en casa?,» *The New York Times,* 29 04 2020.

¿Pueden combinarse las vacunas? El origen de la pandemia ¿Volveremos a ver a los amigos? New Desigualdad de vacunas

¿Qué es un oxímetro de pulso?¿De verdad necesito uno en casa?

Un pequeño dispositivo para la punta de los dedos puede darte información valiosa sobre tu salud durante un episodio de COVID-19 o cualquier enfermedad respiratoria.

ANEXO 12. W. Han-Ning, J. Li-Ping, X. Bin , Z. Si, Y. Lan, H. Yan-Mei, L. Dao-Guang, L. Wei, S. Xin-Nan , Z. Xiao-Xi y Z. Hai-Lu, «Characteristic patterns of normal meridian acupoint temperature,» *Journal of the Chinese Medical Association,* vol. 80, nº Issue 7, pp. 419-426, 2017.

Available online at www.sciencedirect.com

ScienceDirect

Journal of the Chinese Medical Association 80 (2017) 419–426

www.jcma-online.com

Original Article

Characteristic patterns of normal meridian acupoint temperature

Han-Ning Wei, Li-Ping Jiang, Bin Xiong, Si Zhou, Lan Yu, Yan-Mei Huang, Dao-Guang Liu, Wei Ling, Xin-Nan Song, Xiao-Xi Zhang, Hai-Lu Zhao*

Center for Systems Medicine, Guangxi Laboratory of Excellence, Faculty of Basic Medicine, Guilin Medical University, Guangxi, China

Received June 14, 2016; accepted December 9, 2016

Abstract

Background: Body temperature is an important indicator of health and illness. However, a single temperature measurement is not always reliable. Such measurements can be made using meridians, which are energy channels with acupoints being the nodes. To date, there is no published reference of meridian acupoint temperatures applicable to human health, and there is no clear digitalized indicator that could be utilized to evaluate human health by way of meridian acupoints up to now.

Methods: Our study recruited 100 healthy medical college students for the measurement of acupoint temperature. The temperatures of 135 acupoints of 14 main meridians were measured using infrared thermometers in order to provide a comprehensive body temperature reading of each study participant.

Results: The degree of the acupoint temperature consistently ranged from 34.88°C to 36.14°C. The gross thermograph was concentric, with high degree readings around the heart and low degree readings originating from the feet. The left and right body sides had significant correlation between the degrees of bilateral same name acupoint temperatures of 12 regular meridians (correlation coefficient, 0.367−0.985; $p < 0.0001$). There was also a significant correlation between the acupoint temperature for the governor vessel and the conception vessel (correlation coefficient, 0.083; $p = 0.006$).

Conclusion: These findings indicate that meridian acupoint temperature is characterized by a consistently narrow range, as well as concentricity and symmetry in body temperature degree readings in college students. Meridian acupoint temperature may be a sensitive and valuable indicator to assist in the accurate evaluation of meridian and general human health, and the significance and changes of acupoint temperature in clinical conditions warrants future exploration.

Keywords: acupoint; medical college students; meridian; skin temperature; symmetry

1. Introduction

Our previous research indicated that Chinese medicine and acupuncture demonstrated a similar efficacy for treatment of obesity as Western antiobesity drugs, but with fewer reported effects.[1] Meridian and acupoint are the unique systems recorded in *The Yellow Emperor's Internal Classic* or *Canon of Medicine*, and are considered to be energy channels with acupoints being the nodes in modern medicine.[2–4] Body temperature closely relates to energy metabolism, and it is generally understood that a quick evaluation of a person's health can be accomplished by measuring oral or axillary temperatures. However, single temperature reading is not always reliable. A patient with furunculosis may have a normal core body temperature, but the skin temperature around furunculosis may be feverish.[5] A patient with lower extremity varicose veins may have normal axillary temperature, but the feet may feel almost icy to the touch.[6] Owing to the properties

Conflicts of interest: The authors declare that they have no conflicts of interest related to the subject matter or materials discussed in this article.

* Corresponding author. Professor Hai-Lu Zhao, Center for Systems Medicine, Guangxi Laboratory of Excellence, Faculty of Basic Medicine, Guilin Medical University, 109, North 2nd Huan Cheng Road, Guilin, Guangxi 541004, China.

E-mail address: zhaohailu9@126.com (H.-L. Zhao).

http://dx.doi.org/10.1016/j.jcma.2016.12.007

of meridian and acupoint, we conjecture that skin temperature of meridian acupoint may be a good parameter to help evaluate health condition. Some studies have described some acupoint skin temperatures, but they merely focused on only one or two meridians.[4,7] There is no standard of meridian acupoint temperature and no clear digitalized indicator to evaluate health associated with meridians to date. In this study, we have summarized the characteristics of 14 main meridians acupoint temperatures and have established a meridian acupoint temperature map. In addition, meridian theory is the foundation of traditional Chinese medicine (TCM) and acupuncture. Skin temperature of meridian acupoint may also provide clearly valuable information for TCM formula modification and acupoint combination for the treatment.

2. Methods

2.1. Participants

The study processes were performed in accordance with international ethical standards and was approved by the Ethics Committee of Guilin Medical University Affiliated Hospital (approval No.: GLMC15032013HL). All participants fully understood the procedure and the purpose of this noninvasive test, and they took part in the study voluntarily. All patients provided written and signed informed consent documents before they were admitted to the university's clinical research center.

The study included 100 healthy medical college students (50 males and 50 females), aged 20.65 ± 1.53 years, with a weight range of 55.67 ± 8.33 kg. The participants met the following requirements: (1) age, between 18 years and 25 years; (2) weight, between 45 kg and 65 kg; (3) no smoking, no alcohol use, no drug use, no addiction to network; (4) vital signs of the individual including heart rate, breath rate, pulse rate, and blood pressure are normal, and the individual is proven to be healthy without illness in important organs (lung, heart, liver, and kidney) after undergoing physical examination in Guilin Medical University Affiliated Hospital; laboratory examination results (including liver function test, kidney function test, blood glucose, blood lipids, blood red cell, and blood white cell) were normal; (5) besides the requirements above, females needed to meet the requirements of duration of menstruation of 28 ± 7 days, with no uncomfortable symptoms of breast pain, diarrhea, hypogastralgia, and insomnia in the premenstrual and menstrual cycle, no pregnancy, no problem in the reproductive system proved by B ultrasonic examination, and leukorrhea routine examination, and need to avoid menstruation.

2.2. Design

The skin temperature of 135 acupoints of 14 main meridians was measured by an infrared thermometer (DT-8806H; Shenzhen Everbest Machinery Industry Co. Ltd., Shenzhen, China). Prior to use, the thermometer was validated for accuracy against a standard thermometer certified by National Bureau of Standards and accurate to 0.2°C. The 135 acupoints of 14 main meridians are shown in Table 1, and elucidated in the human body as noted in Fig. S1.

Table 1
135 acupoints of 14 main meridians in the study.

Meridian	Acupoint
Lung meridian (LU)	Zhongfu (LU1), Chize (LU5), Kongzui (LU6), Lieque (LU7), Jingqu (LU8), Taiyuan (LU9), Yuji (LU10), Shaoshang (LU11)
Large intestine meridian (LI)	Shangyang (LI1), Erjiang (LI2), Sanjiang (LI3), Hegu (LI4), Yangxi (LI5), Wenliu (LI7), Quchi (LI11), Jianyu (LI15), Yingxiang (LI20)
Stomach meridian (ST)	Chengqi (ST1), Dicang (ST4), Xiaguan (ST7), Touwei (ST8), Liangmen (ST21), Tianshu (ST25), Futu (ST32), Liangqiu (ST34), Zusanliu (ST36), Tiaokou (ST38), Xiajuxu (ST39), Jiexi (ST41), Chongyang (ST42), Xiangu (ST43), Neiting (ST44), Lidui (ST45)
Spleen meridian (SP)	Yinbai (SP1), Dadu (SP2), Taibai (SP3), Gongsun (SP4), Shangqiu (SP5), Sanyinjiao (SP6), Diji (SP8), Yinlingquan (SP9), Xuehai (SP10), Daheng (SP15), Dabao (SP21)
Heart meridian (HT)	Jiquan (HT1), Shaohai (HT3), Lingdao (HT4), Yinxi (HT6), Shenmen (HT7), Shaofu (HT8), Shaochong (HT9)
Small intestine meridian (SI)	Shaoze (SI1), Qiangu (SI2), Houxi (SI3), Wanggu (SI4), Yanggu (SI5), Zhizheng (SI7), Xiaohai (SI8), Tianzong (SI11), Tinggong (SI19)
Bladder meridian (BL)	Jiangmin (BL1), Dazhu (BL11), Feishu (BL13), Xinshu (BL15), Geshu (BL17), Ganshu (BL18), Danshu (BL19), Pishu (BL20), Weishu (BL21), Sanjiaoshu (BL22), Shenshu (BL23), Dachangshu (BL25), Xiaochangshu (BL27), Pangguangshu (BL28), Weizhong (BL40), Chengshan (BL57), Kunlun (BL60), Jinggu (BL64), Shugu (BL65), Zutonggu (BL66), Zhiyin (BL67)
Kidney meridian (KI)	Yongquan (KI1), Rangu (KI2), Taixi (KI3), Zhaohai (KI6), Fuliu (KI7), Yingu (KI10), Dahe (KI12), Huangshu (KI16)
Pericardium meridian (PC)	Quze (PC3), Ximen (PC4), Jianshi (PC5), Neiguan (PC6), Daling (PC7), Laogong (PC8), Zhongchong (PC9)
Triple energizer meridian (TE)	Guangchong (TE1), Yemen (TE2), Zhongzhu (TE3), Yangchi (TE4), Waiguang (TE5), Zhigou (TE6), Tianjing (TE10), Jianliao (TE14)
Gallbladder meridian (GB)	Fengchi (GB20), Riyue (GB24), Fengshi (GB31), Yanglingquan (GB34), Xuanzhong (GB39), Qiuxu (GB40), Zulingqi (GB41), Xiaxi (GB43), Zuqiaoyin (GB44)
Liver meridian (LR)	Dadun (LR1), Xingjian (LR2), Taichong (LR3), Zhongfeng (LR4), Ququan (LR8), Zhangmen (LR13), Qimen (LR14)
Governor vessel (GV)	Mingmen (GV4), Zhiyang (GV9), Dazhui (GV14), Fengfu (GV16), Baihui (GV20), Shangxing (GV23), Suliao (GV25), Shuigou (GV26)
Conception vessel (CV)	Zhongji (CV3), Guanyuan (CV4), Qihai (CV6), Shenque (CV8), Zhongwan (CV12), Juque (CV14), Danzhong (CV17)

Participants had their breakfast between 7:30 AM and 8:00 AM, fasted for 2 hours, and had their acupoint skin temperatures measured between 10:00 AM and 11:00 AM in the same sequence of acupoint after lying on the bed for 15 minutes in the clinic research center of Guilin Medical University Affiliated Hospital. The environmental condition of the clinic research center was controlled at a room temperature of 26 ± 0.1°C, humidity of 60 ± 10%, and barometric pressure of 1 mmHg. Every acupoint temperature was measured three times and was recorded as the mean value. The measurement was carried out from May 3 to May 14, 2013.

Data were expressed as mean ± standard deviation and analyzed using SPSS 18.0 (SPSS version 18, SPSS Inc., Chicago, IL).

3. Results

3.1. Consistency and concentricity of acupoint temperature

We measured a total of 135 acupoint skin temperatures in the study, which covered 37.4% of all classic acupoints. The ratio between measured acupoints and total acupoints of a meridian was from 20.5% to 77.8%, as shown in Table 2. The mean temperatures of 14 main meridians are shown in Table 3, with temperatures ranging from 35.50°C to 36.06°C. The mean temperature values of conception vessel and governor vessel were higher, which were higher than 36°C. The mean temperatures of lung meridian, large intestine meridian, stomach meridian, heart meridian, bladder meridian, pericardium meridian, and triple energizer meridian were around 35.85°C, whereas the mean temperatures of spleen meridian, kidney meridian, gallbladder meridian, and liver meridian were around 35.55°C.

The mean temperature of each measured acupoint is shown in Figs. 1–7. The temperatures of these acupoints were in a narrow range of 34.88–36.14°C. The average temperature of all measured acupoints was 35.76 ± 1.13°C. There were three temperature peaks: 36.14°C at right LU1 (Fig. 2), 36.12°C at right HT1 (Fig. 4), and 36.11°C at CV8 (Fig. 7). There were also three temperature valleys: 34.88°C at the right LR1 (Fig. 1), 35.10°C at the left SP1 (Fig. 3), and 35.13°C at the left BL67 (Fig. 5).

Table 2
Ratio between the measured acupoints and the total acupoints of 14 main meridians.

Meridian	No. of measured acupoint	No. of total acupoint	Percentage
LU	8	11	72.7
LI	9	20	45
ST	16	45	35.6
SP	11	21	52.4
HT	7	9	77.8
SI	9	19	47.4
BL	21	67	31.3
KI	8	27	29.6
PC	7	9	77.8
TE	8	23	34.8
GB	9	44	20.5
LR	7	14	50
GV	8	28	28.6
CV	7	24	29.2
Total	135	361	37.4

Percentage = number of measured acupoint/number of total acupoint × 100.

Table 3
Correlation and difference analysis of 14 main meridians temperatures.

Meridian	Temperature (°C)			r^a	p^b
	Left		Right		
LU	35.82 ± 0.41	—	35.86 ± 0.38	0.869	<0.001
LI	35.89 ± 0.37	—	35.91 ± 0.37	0.916	0.004
ST	35.84 ± 0.44	—	35.84 ± 0.42	0.838	0.638
SP	35.59 ± 0.66	—	35.57 ± 0.69	0.875	0.128
HT	35.83 ± 0.51	—	35.82 ± 0.48	0.925	0.989
SI	35.81 ± 0.49	—	35.81 ± 0.50	0.869	0.756
BL	35.81 ± 0.56	—	35.80 ± 0.59	0.922	0.880
KI	35.56 ± 0.79	—	35.55 ± 0.80	0.929	0.541
PC	35.94 ± 0.33	—	35.96 ± 0.28	0.833	0.136
TE	35.87 ± 0.38	—	35.87 ± 0.39	0.864	0.787
GB	35.58 ± 0.79	—	35.59 ± 0.77	0.940	0.881
LR	35.51 ± 1.11	—	35.50 ± 1.11	0.960	0.619
GV	—	36.04 ± 0.21	—	0.083	0.006
CV	—	36.06 ± 0.23	—	—	—

Data are expressed as mean ± standard deviation. Values are significantly different for $p < 0.05$.
— = no value.
[a] Correlation (r) between the temperature of the left and the right same meridian was analyzed by computing Pearson's correlation coefficient; all $p < 0.0001$. Correlation between the temperature of GV and CV was analyzed by computing Pearson's correlation coefficient; $p = 0.025$.
[b] Difference between the temperature of left and the right same meridian was analyzed by paired-samples t test; difference between temperature of GV and CV was analyzed by independent samples t test.

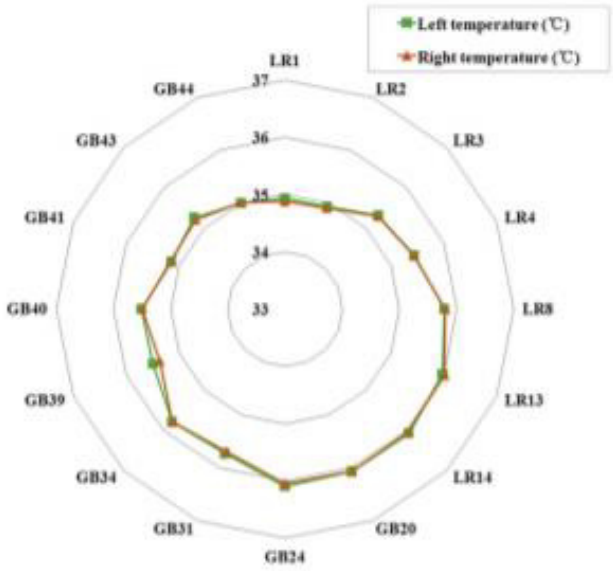

Fig. 1. Skin temperature of gallbladder meridian and liver meridian acupoint. Correlation between the temperature of the left and the right same name acupoint was analyzed by computing Pearson's correlation coefficient. The skin temperature of 16 bilateral same name acupoint showed a significant correlation with correlation coefficient from 0.367 to 0.985 and $p < 0.0001$. Difference between the temperature of left and the right same name acupoints was analyzed by paired-samples t test. Fifteen bilateral same name acupoint temperatures did not show statistical difference except GB39; $p_{GB39} = 0.003$. Values are significantly different for $p < 0.05$.

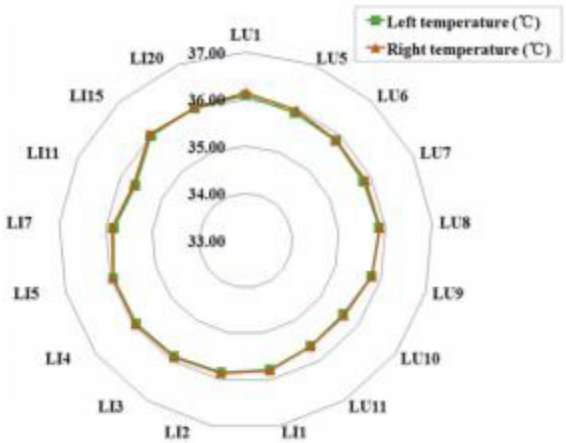

Fig. 2. Skin temperature of lung meridian and large intestine meridian acupoint. Correlation between the temperature of the left and the right same name acupoint was analyzed by computing Pearson's correlation coefficient. The skin temperature of 17 bilateral same name acupoints showed a significant correlation with correlation coefficient from 0.619 to 0.957 and $p < 0.0001$. Difference between the temperature of left and the right same name acupoint was analyzed by paired-samples t test. Fourteen bilateral same name acupoint temperatures did not show statistical difference except LU1, LU5, and LI1; $p_{LU1} = 0.036$, $p_{LU5} = 0.034$, and $p_{LI1} = 0.007$, respectively. Values are significantly different for $p < 0.05$.

Acupoint temperature was related to its position and increased centripetally. The lung meridian started from LU1, locating in the chest, to the end acupoint of LU11 beside the nail of the thumb. The acupoint temperature of it gradually decreased along the channel from 36.09°C of the left LU1 to 35.64°C of the left LU11, and from 36.14°C of the right LU1 to 35.65°C of the right LU11 (Fig. 2). The large intestine meridian started from LI1 locating in the index fingers to the

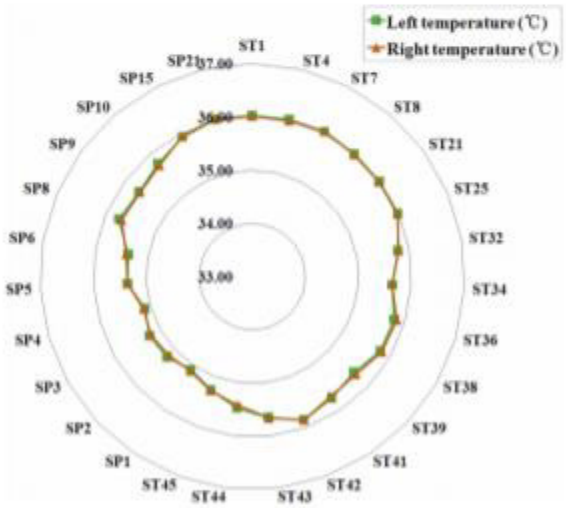

Fig. 3. Skin temperature of stomach meridian and spleen meridian acupoint. Correlation between the temperature of the left and the right same name acupoint was analyzed by computing Pearson's correlation coefficient. The skin temperature of 27 bilateral same name acupoint showed a significant correlation with correlation coefficient from 0.498 to 0.982 and $p < 0.0001$. Difference between the temperature of left and the right same name acupoint was analyzed by paired-samples t test. All 27 bilateral same name acupoint temperatures did not show statistical difference Values are significantly different for $p < 0.05$.

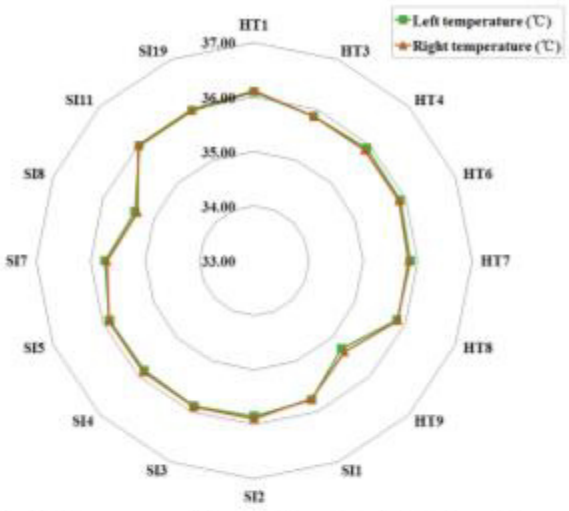

Fig. 4. Skin temperature of heart meridian and small intestine meridian acupoint. Correlation between the temperature of the left and the right same name acupoint was analyzed by computing Pearson's correlation coefficient. The skin temperature of 16 bilateral same name acupoint showed a significant correlation with correlation coefficient from 0.638 to 0.967 and $p < 0.0001$. Difference between the temperature of left and the right same name acupoint was analyzed by paired-samples t test. All 16 bilateral same name acupoint temperatures did not show statistical differences. Values are significantly different for $p < 0.05$.

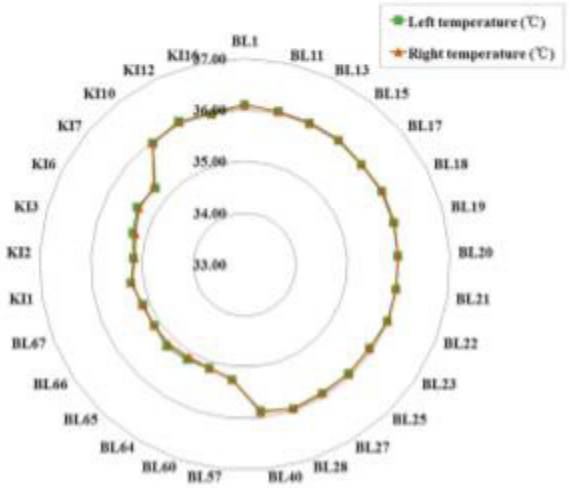

Fig. 5. Skin temperature of bladder meridian and kidney meridian acupoint. Correlation between the temperature of the left and the right same name acupoint was analyzed by computing Pearson's correlation coefficient. The skin temperature of 29 bilateral same name acupoint showed a significant correlation with correlation coefficient from 0.716 to 0.983 and $p < 0.0001$. Difference between the temperature of left and the right same name acupoint was analyzed by paired-samples t test. All 29 bilateral same name acupoint temperatures did not show statistical difference. Values are significantly different for $p < 0.05$.

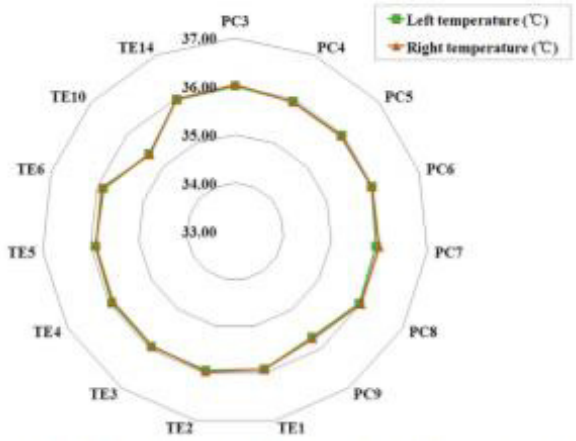

Fig. 6. Skin temperature of pericardium meridian and triple energizer meridian acupoint. Correlation between the temperature of the left and the right same name acupoint was analyzed by computing Pearson's correlation coefficient. The skin temperature of 15 bilateral same name acupoint showed a significant correlation with correlation coefficient from 0.478 to 0.923 and $p < 0.0001$. Difference between the temperature of left and the right same name acupoint was analyzed by paired-samples t test. Thirteen bilateral same name acupoint temperatures showed no statistical difference except PC7 and TE2; $p_{PC7} = 0.006$ and $p_{TE2} = 0.020$, respectively. Values are significantly different for $p < 0.05$.

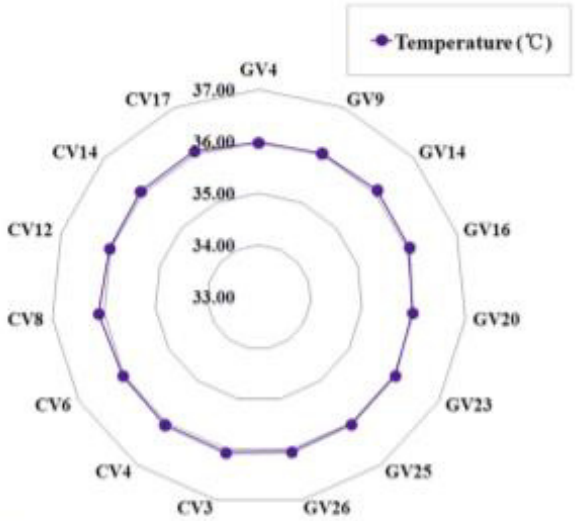

Fig. 7. Skin temperature of governor vessel and conception vessel acupoint. Correlation between the temperature of GV and CV was analyzed by computing Pearson's correlation coefficient. The skin temperature of GV and CV showed a significant correlation with correlation coefficient of 0.083 and $p = 0.006$. Difference between temperature of GV and CV was analyzed by independent samples t test with $p = 0.025$. Values are significantly different for $p < 0.05$.

end acupoint of LI20 beside the nose. The acupoint temperature of this meridian tended to gradually increase along the channel from 35.8°C of the left LI1 to 36.02°C of the left LI20, and from 35.81°C of the right LI1 to 36.02°C of the right LU20 except LI11 (Fig. 2). It was obvious that the acupoint temperature gradually declined along the channels of the stomach meridian (Fig. 3), heart meridian (Fig. 4), bladder meridian (Fig. 5), pericardium meridian (Fig. 6), and gallbladder meridian (Fig. 1), but gradually increased along the channels of the spleen meridian (Fig. 3), kidney meridian (Fig. 5), and liver meridian (Fig. 1). The acupoint temperatures of the small intestine meridian were recorded consistently at around 35.8°C, except SI8 (Fig. 4), and the acupoint temperatures of the triple energizer meridian were consistently at around 36°C except TE10 (Fig. 6). The acupoint temperatures of governor vessel and conception vessel were really consistently around 36°C (Fig. 7). We divided the acupoints into groups according to body parts, and found that temperatures of acupoints were distributed concentrically. The chest acupoint group had the highest temperature of 36.04°C, followed by, in turn, the head acupoint group of 36.03°C, belly acupoint group of 36°C, forearm acupoint group of 35.85°C, hand acupoint group of 35.82°C, thigh acupoint group of 35.73°C, shank acupoint group of 35.68°C, and feet acupoint group of 35.3°C. The temperature of the chest acupoint group was not significantly different from that of the head acupoint group, but did have a significant difference with the other groups (Table 4).

3.2. Symmetry of meridian acupoint temperature

The skin temperatures of all measured gallbladder meridian acupoints showed a significant correlation in the bilateral same name acupoints, with a correlation coefficient ranging from 0.709 to 0.957 ($p < 0.0001$), and difference analysis indicated that they did not have any difference except for GB39 (Fig. 1). The skin temperatures of all measured liver meridian acupoint showed a significant correlation in bilateral same name acupoints with a correlation coefficient from 0.367 to 0.985 ($p < 0.0001$), and difference analysis showed they did not demonstrate a significant difference (Fig. 1).

Correlation analysis and difference analysis of skin temperatures of bilateral same name acupoints of other meridians are shown in Figs. 2–6.

The skin temperature of all bilateral same name acupoints showed a significant correlation, with a correlation coefficient ranging from 0.367 to 0.985 ($p < 0.0001$) in our study. Additionally, 95% (114/120) of the bilateral acupoints

Table 4
Difference analysis of acupoint groups' temperatures in different parts of body.

Acupoint group	Temperature (°C)	p
Head	36.03 ± 0.17	0.07
Chest	36.04 ± 0.48	
Belly	36.00 ± 0.36	0.03
Forearm	35.85 ± 0.17	<0.001
Hand	35.82 ± 0.57	<0.001
Thigh	35.73 ± 0.63	<0.001
Shank	35.68 ± 0.71	<0.001
Feet	35.30 ± 0.63	<0.001

Data are expressed as mean ± standard deviation. Values are significantly different for $p < 0.05$.
Difference between temperature of each acupoint group and chest acupoint group was analyzed by independent samples t test.

ANEXO 13. M. L. Williams K, «Global warming, heat-related illnesses, and the dermatologist,» *International Journal of Women's Dermatology,* vol. l, nº 2352-6475, pp. 70-84, 2020.

International Journal of Women's Dermatology 7 (2021) 70–84

Contents lists available at ScienceDirect

International Journal of Women's Dermatology

Review

Global warming, heat-related illnesses, and the dermatologist

Mary L. Williams M.D.

Departments of Dermatology and Pediatrics, University of California San Francisco, San Francisco, CA, United States

ARTICLE INFO

Article history:
Received 23 April 2020
Received in revised form 12 August 2020
Accepted 17 August 2020

Keywords:
Anhidrosis
Drugs
Heat illness
Skin blood flow
Sweat glands
Thermoregulation

ABSTRACT

Global warming, provoked by the greenhouse effect of high levels of atmospheric gases (most notably carbon dioxide and methane), directly threatens human health and survival. Individuals vary in their capacity to tolerate episodes of extreme heat. Because skin is the organ tasked with heat dissipation, it is important for dermatologists to be versed in the physiology of cutaneous heat dissipation and cognizant of clinical settings in which the skin's thermoregulatory responses may be impaired. When the external temperature is lower than that of the skin, the skin releases internal heat through direct thermal exchange with the environment, a process that is aided by an expansion of cutaneous blood flow and eccrine sweating. Cooling through the evaporation of sweat is effective even when the external temperature exceeds that of skin. Many factors, including environmental and physiological (e.g., age and sex), and pathological (e.g., preexisting illnesses, disorders of eccrine function, and medications) considerations, affect the skin's capacity to thermoregulate. Identification of individuals at increased risk for heat-related morbidity and mortality will become increasingly important in the care of patients.

Contents

E-mail address: joan.wakefield@ucsf.edu

https://doi.org/10.1016/j.ijwd.2020.08.007
2352-6475/

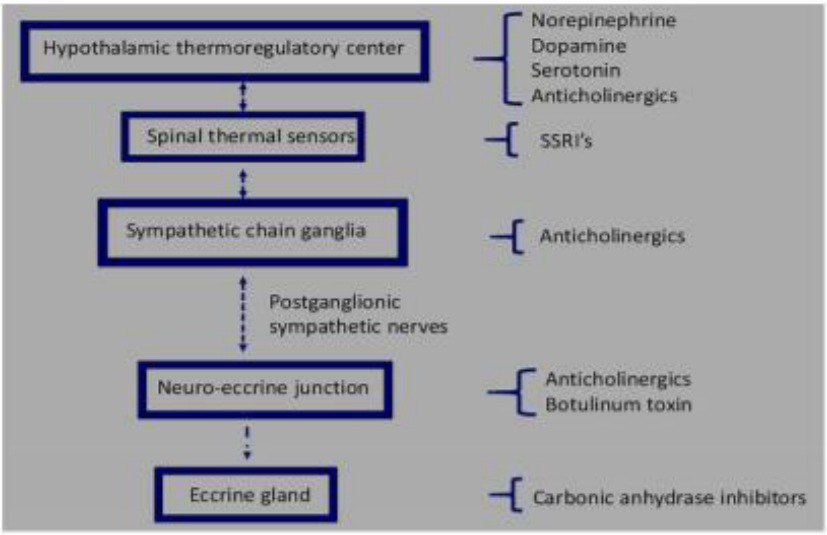

Fig. 1. Thermoregulatory pathway and sites of action by drugs that affect thermal responses.

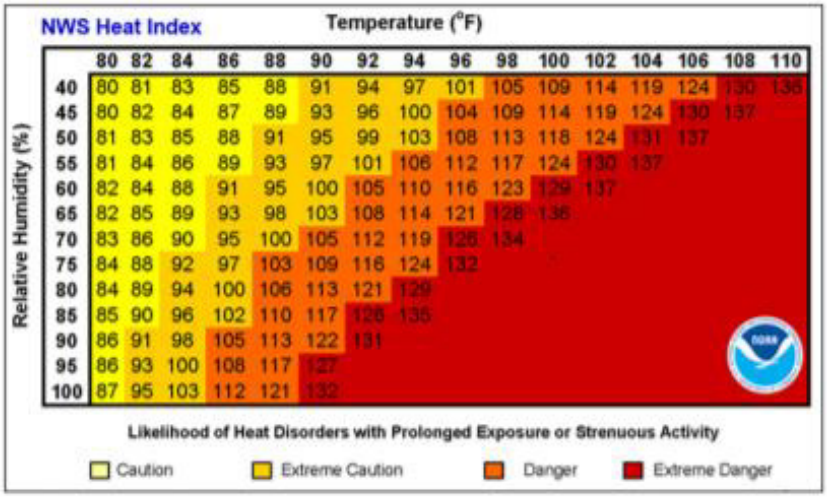

Fig. 2. Heat index as perceived temperature in relation to humidity (reproduced from: https://www.weather.gov/safety/heat-index; accessed April 2, 2020).

Physiological, developmental, and sex-related impacts on cutaneous thermoregulation

Aerobic conditioning

With aerobic conditioning, muscles become more efficient, and more metabolic energy is diverted to work with a lesser proportion lost as heat. However, even with optimal aerobic conditioning, the percentage of metabolic energy released as heat is rarely less than 70% (Taylor, 2014). In individuals who are less aerobically fit, heat occupies an even higher percentage of metabolic energy expenditures. Consequently, poor conditioning is a major risk factor for exertional HRI and contributes to the greater heat intolerance of many obese individuals.

Acclimatization

Human physiology adapts on repeated exposures to a hot environment. Thus, in temperate climates, the morbidity and mortality from HRI declines at the end of summer in comparison with the beginning of the warm season. Similarly, visitors to hot climates are more vulnerable to HRI than are residents. These differences in resilience do not seem to have a genetic or racial basis and are best explained by acclimatization (Best et al., 2019; Foster et al., 1971; Taylor, 2014). Physiological adaptations are evident after a week or two of exposure to heat stress (Tyler et al., 2016). Core temperature is lower in acclimatized individuals, allowing for greater thermal gain before exceeding tolerable levels. The basal metabolic rate also slows, resulting in less heat production at rest.

WET BULB GLOBE THERMOMETER		ACTIVITY GUIDELINES & REST BREAK GUIDELINES
Middle School	High School	
< 82	< 82	**Normal Activities:** Provide at least 3 separate rest breaks each hour with a minimum duration of 3 minutes each. Use discretion for intense or prolonged exercise.
82.1 – 83.9	82.1 – 86.9	Use discretion for intense or prolonged exercise; watch at-risk players carefully; provide separate rest breaks each hour for a minimum of 4 minutes duration each.
84.0 – 86.9	87.0 – 89.9	Maximum practice time is 2 hours each. **Football:** players are restricted to helmet, shoulder pads, and shorts during practice. If the WBGT rises to this level during practice, players may continue to workout wearing football pants without changing to shorts. **All Sports:** provide at least 4 separate rest breaks each hour with a minimum duration of 4 minutes each. **Consider delaying or rescheduling competitions.**
87.0 – 90.0	90.0 – 92.0	Maximum practice time is 1 hour. **Football:** *NO* protective equipment may be worn during practice, and there may be *NO* conditioning activities. **All Sports:** there must be 20 minutes of rest breaks distributed throughout the hour of practice. **Consider delaying or rescheduling competitions.**
> 90	> 92	***NO Outdoor Workouts:*** cancel or delay practice and competitions until a cooler WBGT is reached.

Fig. 3. State of Missouri thresholds for wet bulb globe temperature (WBGT). As constructed, the WBGT is always lower than the temperature in direct sunlight. Charts such as the one shown can be used to correlate WBGT readings with the risk for a heat-related illness (reproduced with permission from the Missouri State High School Activities Association).

Cardiovascular adaptations include expansion of the blood volume, a lower pulse rate, greater stroke volume, and increased cardiac output (Periard et al., 2015; Taylor, 2014). Cutaneous blood flow is also enhanced, with a lower onset threshold and increased sensitivity to thermal stimuli (Periard et al., 2015).

The set point for the onset of sweating is also reduced with acclimatization, permitting evaporative cooling at a lower core temperature. Sweat production becomes more copious, both as a result of central and peripheral autonomic stimulation, as well as enhanced end-organ sensitivity to acetylcholine and eccrine gland hypertrophy (Shin et al., 2016). The sodium content of sweat also declines, not only preserving sodium homeostasis but also rendering the evaporation of sweat more efficient (Buono et al., 2018). These acute adaptations take place even in humid climates where the evaporation of sweat is inhibited and the disadvantages of fluid losses through dripping sweat may predominate. Residents of hot, humid climates demonstrate many of these same physiological adaptations; however, with chronic heat stress in the setting of high humidity, sweating does indeed decrease (Taylor, 2014).

Infants and children

Infants and children are widely recognized as particularly vulnerable to overheating (Falk, 1998; Smith, 2019; Yard et al., 2010). Much of this vulnerability stems from developmental differences in thermoregulation. With a larger surface area to volume ratio, heat dissipation through convection and conduction should, in theory, be more efficient in children. However, when external temperatures exceed internal, this same physiognomy renders them more vulnerable to heat gain. A greater deposition of subcutaneous fat in most infants and young children can insulate and further retard this mechanism for heat dissipation. This greater proportion of body fat also inhibits their capacity to store heat, making them more vulnerable to a rise in core temperature with heat waves. In addition, children have a higher metabolic rate at rest and produce 10% to 15% more metabolic heat during activities (Smith, 2019). Children have a lower cardiac output at a given metabolic rate (Bytomski and Squire, 2003), yet when under thermal stress, they direct a greater proportion of their cardiac output to the skin (Smith, 2019).

A major component of the vulnerability of children to heat stress relates to age-related differences in sweat gland function. At 14 weeks of gestation, eccrine glands first appear on the palms and soles; by 28 weeks, a full complement is present over the skin surface (Mancini and Lawley, 2015). Because eccrine glands only develop during fetal life, the density of glands per unit area is approximately five-fold greater in newborns than in adults (Foster et al., 1971). Eccrine glands begin to function in newborns

ANEXO 14. Universidad de Guanajuato, Contenidos didácticos Licenciatura de Enfermeria Y Obstetricia , «Blog UGTO MX,» 15 02 2018. [En línea]. Available: https://blogs.ugto.mx/enfermeriaenlinea/unidad-didactica-5-cuidados-de-enfermeria-a-personas-con-problemas-de-termoregulacion/. [Último acceso: 17 01 2021].

1. Temperatura corporal

Es un equilibrio entre el calor producido por los tejidos (más el adquirido del ambiente) y la pérdida de calor hacia el ambiente.

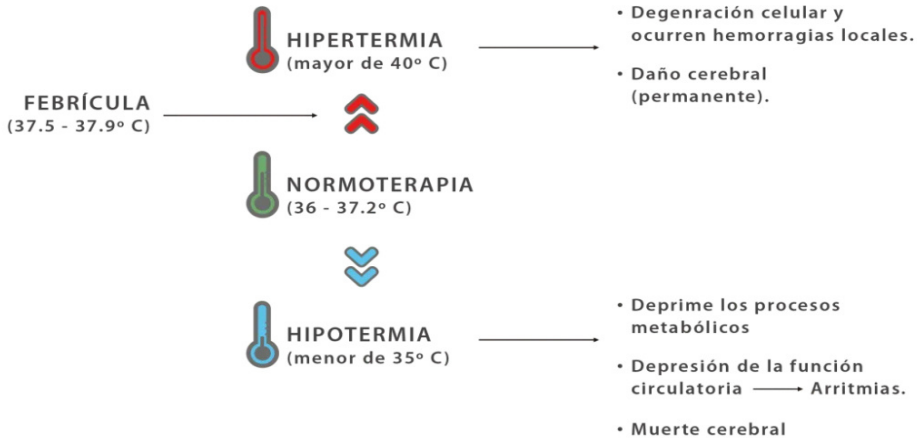

Diagrama 1. Equilibrio de calor.

La producción de calor se debe a reacciones químicas exotérmicas

- **Durante el ejercicio**, los músculos voluntarios son los que producen la mayor cantidad de calor.
- **Durante el reposo**, el hígado es el que produce la mayor cantidad de calor.
- **El metabolismo basal** aumenta (10%) por cada grado centígrado que se eleva la temperatura.

ANEXO 15. U.T.F. Alicante, «https://www.utfalicante.com/,» Unión de Trabajadores de Farmacias (U.T.F.) , 18 05 2017. [En línea]. Available: https://www.utfalicante.com/blog/tabla-de-signos-vitales-por-edad-44.html. [Último acceso: 14 01 2021].

ANEXO 16. N. Leung, «Cable News Network CNN,» A Warner Media Company, 03 01 2021. [Enlínea].Available:https://edition.cnn.com/search?size=10&q=Common%20symptoms%20of%20Covid-19&type=article. [Último acceso: 15 01 2021].

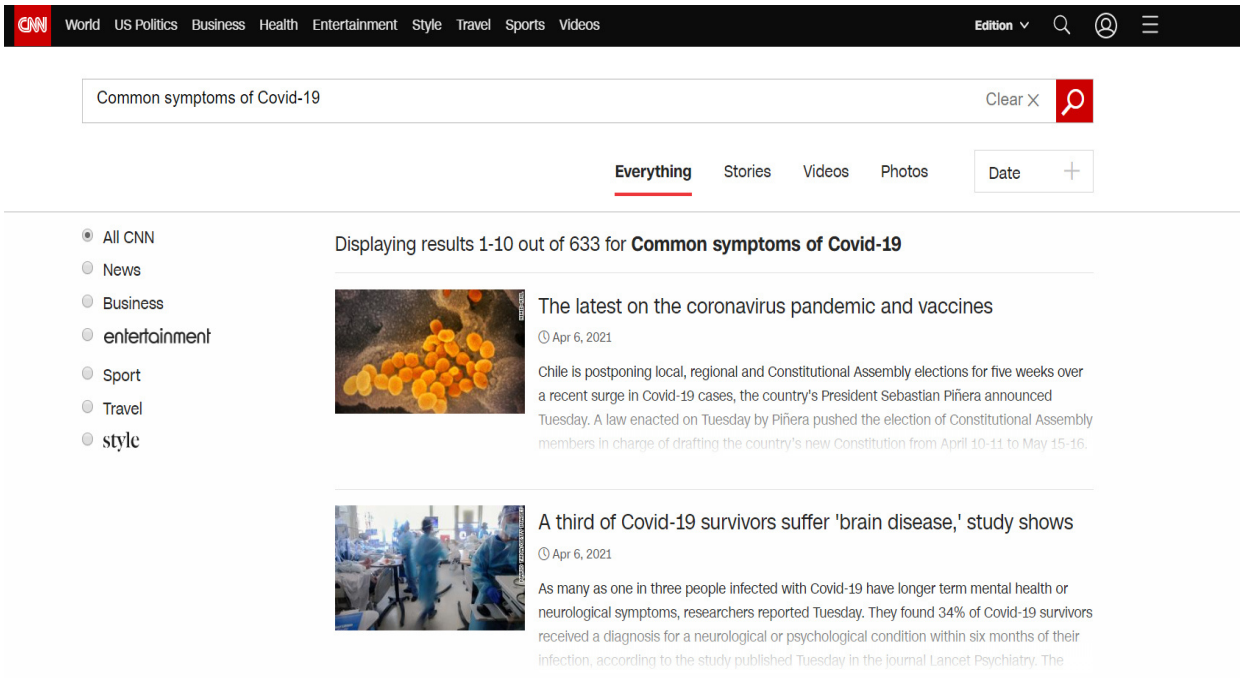

ANEXO 17. M. Cañada Soriano y R. Royo Pastor, «Termografia,» de *Termografía Infrarroja. Nivel II*, Madrid, Fundación Confemetal, 2016, pp. 1-671.

ensayados con su consiguiente deterioro e incluso inutilización.

La información que proporcionan es precisa pero no pueden ser aplicados a los productos finales, lo cual obliga a un proceso de elección de muestras representativas de la producción para sacrificarlas y obtener información significativa. La elección de muestras se basa en métodos estadísticos.

Cuando el ensayo se realiza sobre una pieza completa, será clasificado como funcional, según se ha visto anteriormente; así, si el ensayo se efectúa sobre una parte de la pieza fraccionada de su conjunto, el ensayo será destructivo.

ENSAYOS DE MATERIALES		
Mecánicos	• Dureza • Tenacidad • Resistencia • Fragilidad • Maleabilidad • Ductilidad • Fragilidad • Fatiga	• Tracción o compresión (tenacidad y resiliencia) • Cizalladura • Deformación plástica (embutición) • Dureza (Brinell, Rockwell, Vickers, Shore) • Doblado • Choque • Fatiga (flexión, torsión, flexión rotativa, etc.)
Metalográficos	Con microscopio	• Ópticos (por reflexión, por transmisión) • Electrónicos (por barrido, por transmisión)
Analíticos		
Químicos		

Tabla 1.III

1.2. TERMOGRAFÍA INFRARROJA

1.2.1. Definición

La Termografía Infrarroja (TIR) es una técnica de ensayo no destructivo (END) sin contacto que obtiene información térmica de un cuerpo a través de la captación de la radiación infrarroja que emite, mediante un dispositivo de adquisición de imágenes térmicas a distancia.

1.2.2. Historia

3.3. RADIACIÓN INFRARROJA

3.3.1. El espectro electromagnético

La transferencia de calor por conducción o convección tiene lugar en la dirección de la temperatura decreciente, es decir, de un medio a una temperatura alta hacia otro a temperatura menor. Resulta interesante que la transferencia de calor por radiación puede ocurrir entre dos cuerpos separados por un medio más frío que ambos. Por ejemplo, la radiación solar llega a la superficie de la Tierra después de pasar a través del vacío y de las capas de aire frío a grandes altitudes.

El fundamento teórico de la radiación fue establecido en 1864 por el físico James Clerk Maxwell, quien postuló que las cargas aceleradas o las corrientes eléctricas variables dan lugar a campos eléctricos y magnéticos. Estos campos que se mueven con rapidez se llaman ondas electromagnéticas o radiación electromagnética y representan la energía emitida por la materia como resultado de los cambios en las configuraciones electrónicas de los átomos o moléculas.

En 1887 Heinrich Hertz demostró de forma experimental su existencia. Las ondas electromagnéticas transportan energía y viajan a la velocidad de la luz en el vacío. Las ondas electromagnéticas se caracterizan por su frecuencia o longitud de onda. Estas propiedades en un medio se relacionan mediante:

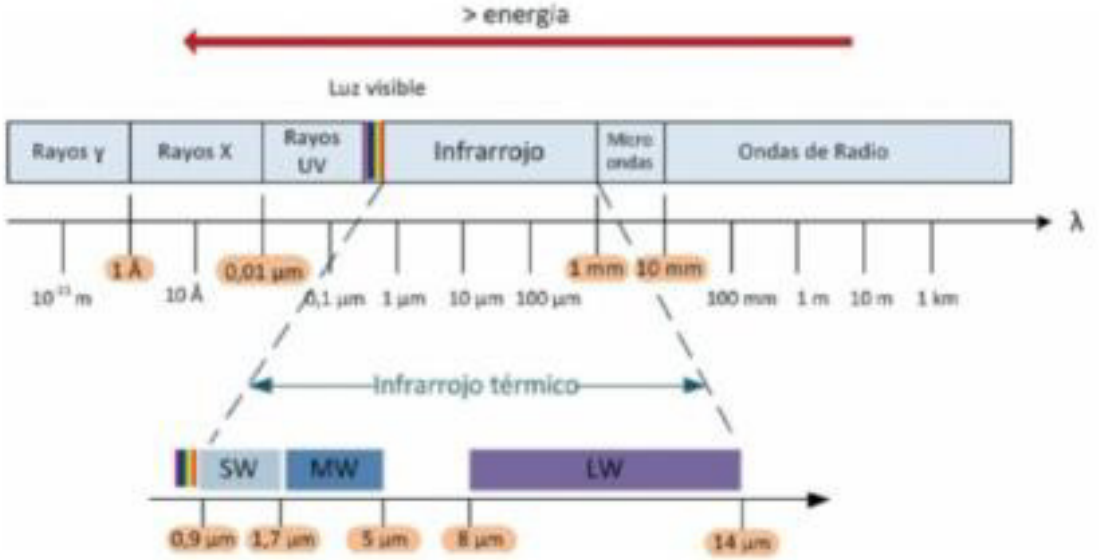

Figura 3.25. Clasificación de las ondas electromagnéticas más comunes en función de su longitud de onda

Los diferentes tipos de radiación electromagnética se producen a través de varios mecanismos.

Por ejemplo, los rayos γ son producidos por las reacciones nucleares y son los que tienen mayor frecuencia.

Los rayos X se producen por el bombardeo de metales con electrones de alta energía y son conocidos por sus aplicaciones médicas.

Las ondas microondas se producen por tipos especiales de tubos electrónicos, y las ondas de radio se producen por la excitación de algunos cristales o por el flujo de corriente alterna por conductores eléctricos.

La radiación UV es importante en el contexto del agujero de la capa de ozono ya que a menor capa de ozono en la atmósfera, mayor radiación UV del Sol en la superficie de la Tierra. Alrededor del 12% de la radiación solar se encuentra en el intervalo ultravioleta y sería devastador si llegara a alcanzar la superficie de la Tierra. La capa de ozono de la atmosfera actúa como una cubierta protectora y absorbe la mayor parte de esta radiación. Los rayos ultravioleta que permanecen en la luz solar todavía son suficientes

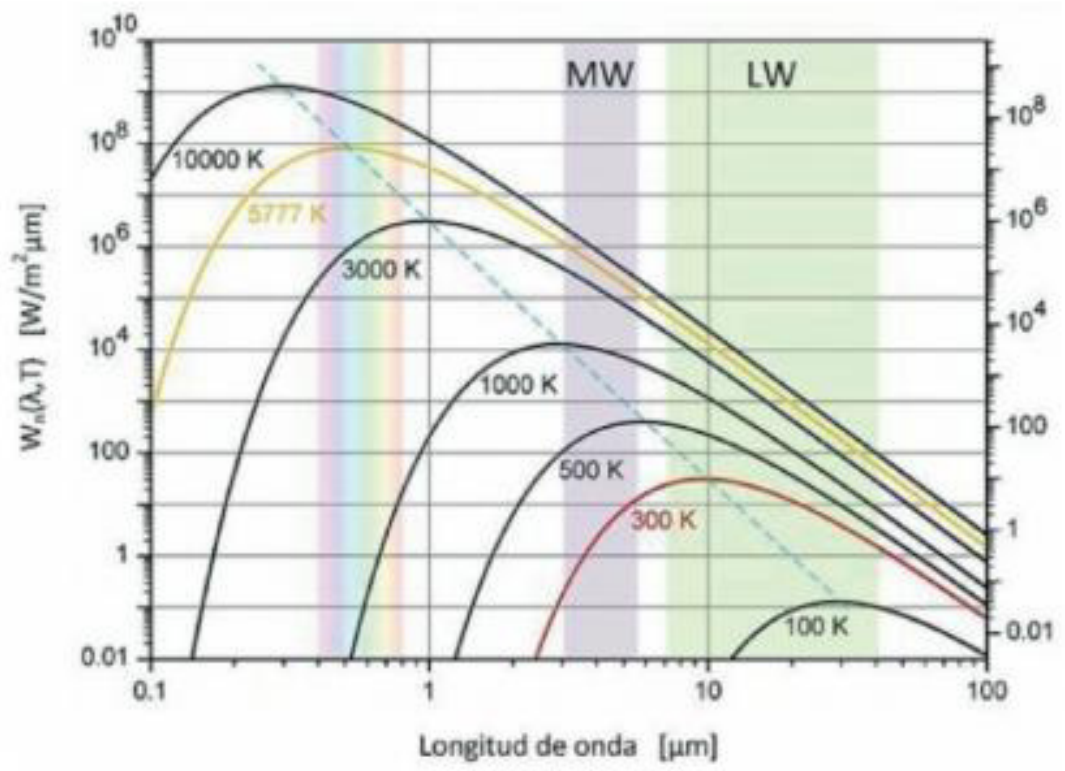

Figura 3.28. Representación de la Ley de Planck para la radiación de un cuerpo negro

En la figura 3.28 se representa la variación de la potencia de emisión espectral de un cuerpo negro con la longitud de onda para las temperaturas seleccionadas. Se muestran también los rangos de SW y LW así como el visible. Con base a esta figura, se pueden hacer varias observaciones:

1. La radiación emitida es función continua de la longitud de onda. A cualquier temperatura específica se incrementa con la longitud de onda, llega a un máximo y, a continuación, decrece al crecer la longitud de onda.
2. A cualquier longitud de onda la cantidad de radiación emitida se incrementa al aumentar la temperatura.
3. Conforme aumenta la temperatura, las curvas se desplazan a la izquierda, hacia la región de las longitudes de onda más cortas. Como consecuencia, una fracción más grande de la radiación se emite a longitudes de onda

ANEXO 18. ISO - The International Organization for Standardization, «Condition monitoring and diagnostics of machines Thermography - Part1: General Procedures,» *International Standard,* vol. 01, nº ISO 18434-1, pp. 1-32, 2008.

INTERNATIONAL STANDARD

ISO 18434-1

First edition
2008-03-01

Condition monitoring and diagnostics of machines — Thermography —

Part 1: General procedures

Surveillance et diagnostic de l'état des machines — Thermographie —
Partie 1: Procédures générales

Reference number
ISO 18434-1:2008(E)

3.17
thermogram
thermal map or image of a target where the grey tones or colour hues represent the distribution of infrared thermal radiant energy over the surface of the target

3.18
transmissivity
transmittance
τ
proportion of infrared radiant energy impinging on an object surface, for any given spectral interval, that is transmitted through the object

NOTE 1 $\tau = 1 - \varepsilon - \rho$

where

τ is transmissivity;

ε is emissivity;

ρ is reflectivity.

NOTE 2 For a black body, $\tau = 0$. Transmissivity is that fraction of incident radiation transmitted by matter.

3.19
working distance
distance from the target to the instrument, usually to the primary optic

4 Thermography techniques

There are several recognized IRT techniques in use throughout industry. *Comparative thermography* is the most common technique and it is normally used to provide the best available data in lieu of ideal, or absolute, thermal measurements. When encountering changing machinery operating conditions, the ability to perform rough emissivity estimates, and the ability to differentiate emissivity differences on machinery equipment, provides useful information for the condition monitoring and diagnostics of the machine under the less-than-ideal circumstances frequently encountered in the field. The confidence level of the information obtained depends on the IRT equipment used, the training and experience of the thermographer, and the detection method applied.

Non-contact thermometry using infrared thermal cameras is used when it is essential to know as precisely as possible the true temperature of a target. However, this technique is not normally used for condition monitoring and diagnostics.

Comparative thermography is normally used as part of a condition-monitoring process when such a process is implemented in accordance with ISO 17359. IRT can also be used as a primary or secondary technique for diagnosis and prognosis when these processes are carried out in accordance with ISO 13379 and ISO 13381-1 respectively.

5 Comparative thermography

5.1 Types of comparative thermography

Comparative thermography can be either *quantitative* or *qualitative*. The *quantitative* technique requires the determination of a temperature value to distinguish the severity of a component's condition. This value is determined by comparing the target's temperature to that of similar service equipment or baseline data. For high emissivity surfaces both temperature, T, and temperature difference, ΔT, values are typically reliable provided good measurement techniques are followed. T and ΔT values of low emissivity surfaces are often

unreliable due to surface and environmental variations. In addition, many applications also require assigning values to observed thermal patterns for the purposes of analysis, trending, designating severity levels and assigning priorities.

However, there are many applications where quantitative data are not required to monitor the condition of machinery, or to diagnose a problem and recommend the appropriate corrective action. In these cases, *qualitative* techniques may be more than adequate.

5.2 Comparative quantitative thermography

The comparative quantitative thermography method is an accepted and effective method for evaluating the condition of a machine or component by determining approximate temperatures. It is very difficult to determine precisely the actual temperatures of a component using IRT in the field. This is due to a certain extent to the physics of IRT which must take into consideration the multiple parameters that enable a true absolute temperature measurement. These IRT considerations are: emissivity, reflectivity and transmissivity. As a result, estimates of these IRT considerations can be readily made to obtain a component's approximate temperature, which, in most cases, is more than sufficient to determine the severity of an adverse condition.

An example of comparative quantitative thermography would be that, if two or more machines are operating in the same environment and under the same load conditions, and one is experiencing an elevated temperature, this is usually an indication that a deteriorating condition may exist. However, the determination of the temperature difference would then assist in establishing the severity of the condition. In this example, a 5 °C differential would be considered minor, whereas a 100 °C differential may be considered to be critical. Also, knowing the approximate value of the elevated temperature would provide an indication that the temperature limit of a component may be approaching published values. Therefore, while qualitative measurements can also detect deficiencies, it is the quantitative measurements that have the capability of determining severity.

Since it is not always practical to determine the exact temperature, or even emissivities, of each machine surface, the alternative use of comparative thermography becomes more practical. Comparative measurement, unlike qualitative measurement, identifies a thermal deficiency by comparing the temperatures obtained using a consistent emissivity value, $\varepsilon_{default}$, for those surfaces of similar emissivity, i.e. across the surface of a single machine or between the surfaces of similar machines. The temperature *differential* between two or more identical or similar surfaces is measured numerically. Assuming that the environmental conditions and surface properties for both components are similar, the differential temperature for the given piece of equipment is recorded as being the amount above the normal operating temperature of the similar equipment.

The comparative measurement technique uses quick emissivity estimates, reflected apparent temperature and component distance measurements. The emissivity factors of the materials are obtained through experience.

It is possible to check the emissivities of the most commonly encountered materials in a plant to assign default values that can then be used when inspecting components with these materials.

Each plant must develop its own set of default values, as similar components in different plants may have different environments (such as cleanliness), or the equipment may have different surface finishes, and these varying conditions will result in different default values. Once emissivities, distances, and reflected apparent temperatures are estimated, these values are entered into the IRT camera to indicate a temperature value for each component. This type of measurement is effective when surveying many components. It is quick and it provides useful information for determining the severity of a component's condition.

5.3 Comparative qualitative thermography

Comparative qualitative measurement compares the thermal pattern or profile of one component to that of an identical or similar component under the same or similar operating conditions. When searching for differing thermal patterns or profiles, an anomaly is identified by the intensity variations between any two or more similar objects, without assigning temperature values to the patterns. This technique is quick and easy to apply, and it does not require any adjustments to the infrared instrument to compensate for atmospheric or

environmental conditions, or surface emissivities. Although the result of this type of measurement can identify a deficiency, it does not provide a level of severity.

This IRT technique is used throughout most industries. It is very effective in identifying hot bearings or other abnormally hot machine components, hot spots in electrical equipment, undesirable hot electrical connections, leaking or blocked fluid heat exchange equipment and components (tubes), and fluid leaks from pressure vessels, pipes and valves.

6 Non-contact thermometry using infrared thermography cameras

The determination of the corrected temperature of a target using IRT can be difficult because of the many technical and environmental factors involved. As a result, absolute IRT measurements are done only if very precise temperature values, or small temperature differentials, are critical to a process. These determinations are normally attempted only under extremely controlled conditions. This type of measurement using IRT cameras is not normally used for condition monitoring.

7 Baseline measurements

For both comparative and absolute techniques, it is strongly recommended that baseline measurements be taken of critical plant equipment for diagnostic and prognostic reference. This is very important when making later IRT surveys of machines or components and comparing them with previous thermograms of the same machines operating under the same load and environmental conditions. This condition monitoring procedure is useful for identifying developing problems early, thus preventing major maintenance operations or catastrophic failures. Some examples of baseline measurements are contained in Annex C.

8 Safety

Prior to the commencement of work, minimum safety rules and guidelines shall be established in accordance with applicable local or national standards and regulations and particularly where hazardous environments may exist. An example of minimum safety rules and guidelines is contained in Annex B.

9 Calibration

Thermographers shall have IRT cameras calibrated to original equipment manufacturers' guidelines, or established industry practice. Documented calibration checks should be carried out using a traceable black-body reference in accordance with manufacturer's recommendations, client specification or any applicable industry standard. Quick calibration checks are recommended to be performed prior to each inspection or survey.

NOTE A quick check can be made, for example, by using the human face tear duct, boiling water or a melting ice cube, using the correct emissivities under ideal conditions.

10 Data collection

Data collection shall be carried out in accordance with the following.

a) Infrared inspections should be performed when environmental and physical conditions such as solar, wind, surface and atmospheric conditions and heat transfer are favourable to gathering accurate data.

b) The operating and environmental conditions under which data are acquired should be repeatable and consistent with normal conditions.

c) The thermographer shall ensure that all emissivity and reflected apparent temperature determinations are carried out in accordance with Annex A.

Annex A
(normative)

Field measurements of reflected apparent temperature and emissivity

A.1 How to measure reflected apparent temperature

A.1.1 Equipment requirements

In order to measure target reflected apparent temperature the following equipment is required:

a) a calibrated quantitative IRT camera that allows the thermographer to input reflected apparent temperature, T_{refl}, and emissivity, ε, values;

b) an infrared reflector such as a crumpled and re-flattened piece of aluminium foil placed shiny side up on a piece of cardboard.

A.1.2 Reflector method

The procedure for determining the reflected apparent temperature, T_{refl}, using the reflector method shall be as follows.

a) Set the IRT camera's emissivity control to 1,00 and distance to 0.

b) Place the IRT camera at the desired location and distance from the target to be measured. Aim and focus the IRT camera on the target.

c) Place the reflector in the field-of-view of the IRT camera. The reflector shall be placed in front of, and in the same plane as, the target surface (see Figure A.1). Maintain a safe working distance from any energised or potentially dangerous targets.

d) Without moving the camera, measure the apparent surface temperature of the reflector with the camera. Note this temperature, which is the reflected apparent temperature, T_{refl}, of the target.

e) For greater accuracy, repeat procedures b) to d) a minimum of three times and average the temperatures.

f) Compensate for the reflected apparent temperature by entering the averaged reflected apparent temperature in the IRT camera under the T_{refl} input (sometimes referred to as "TAM", "amb. temp.", "reflected apparent temperature" or "background temperature").

Key

1 IRT camera
2 reflected heat source
3 reflector parallel to target
4 target

Figure A.1 — Reflector method

A.1.3 Direct method

The procedure for determining the reflected apparent temperature, T_{refl}, using the direct method shall be as follows.

a) Set the IRT camera's emissivity control to 1,00.

b) Place the IRT camera at the desired location and distance from the target. Estimate the angle of reflection, α, and the angle of incidence, β, when viewing the target with the camera from this location (see Figure A.2).

c) Position the IRT camera so that it is at the angle of reflection from the target, α, and view the sources reflected by the target (see Figure A.3).

d) Measure the average apparent temperature of these sources with the camera. Use any camera features available (such as area averaging) that average these reflected apparent temperatures. Note this temperature, which is the reflected apparent temperature, T_{refl}, of the target.

e) For greater accuracy, repeat procedures b) to d) a minimum of three times and average the temperatures.

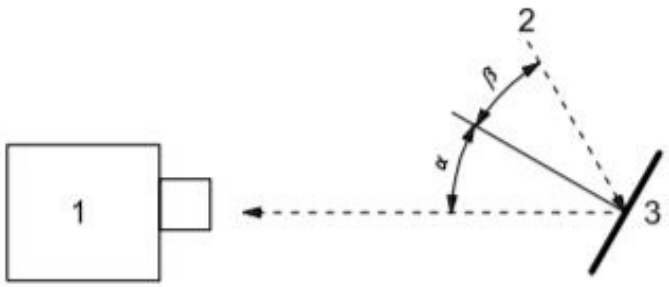

Key

1 IRT camera
2 reflected heat source
3 target

α angle of reflection
β angle of incidence
$\alpha = \beta$

Figure A.2 — Direct method step b)

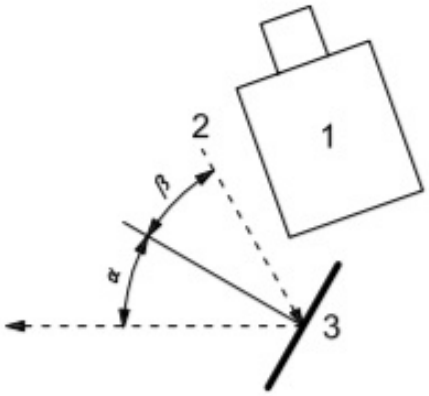

Key

1 IRT camera
2 reflected heat source
3 target

α angle of reflection
β angle of incidence
$\alpha = \beta$

Figure A.3 — Direct method step c)

Compensation for the reflected apparent temperature can be made by entering the averaged reflected apparent temperature in the IRT camera under the T_{refl} input (sometimes referred to as "TAM", "amb. temp.", "reflected apparent temperature", or "background temperature").

Thermographers can test for the significance of reflected apparent temperatures by shielding the target from various angles and observing any visual or temperature changes shown in the thermal image. Errors caused by hot or cold sources of reflected radiation can also be reduced by shielding the target from these sources.

Reflections produced by a point source (such as the sun) can often be avoided by moving the camera position and angle relative to the target. It should also be remembered that reflected apparent temperatures can be lower than ambient temperatures.

Thermographers should also be aware that the direct method usually does not include the heat from the thermographer's body as a source of reflected radiation, which, in some cases, can create a significant error.

A.2 How to measure the emissivity of a target

A.2.1 Equipment requirements

In order to measure target emissivity the following equipment is required:

a) a calibrated quantitative IRT camera that allows the thermographer to input reflected apparent temperature, T_{refl}, and emissivity, ε, values; and

b) a natural or induced means of heating or cooling the target at least 20 °C above or below the reflected apparent temperature such that the target temperature is stable and close to the temperature of the target(s) to be measured; and

c) a calibrated contact, non-contact, or mirrored thermometer; or

d) a surface-modifying material such as paint or tape with a known high emissivity in the waveband of the IRT camera being used and at a temperature close to that of the target.

ANEXO 19. H. Maldonado, R. Bayareh, I. A. Torres, A. Vera, J. Gutiéttez y L. Lejia, «Automatic detection of risk zones in diabetic foot soles by processingthermographic images taken in an uncontrolled environment,» *Infrared Physics & Technology,* vol. 105, nº 103187, pp. 1-21, 2020.

Infrared Physics and Technology 105 (2020) 103187

Contents lists available at ScienceDirect

Infrared Physics & Technology

journal homepage: www.elsevier.com/locate/infrared

Automatic detection of risk zones in diabetic foot soles by processing thermographic images taken in an uncontrolled environment

H. Maldonado[a,*], R. Bayareh[a], I.A. Torres[a], A. Vera[a,*], J. Gutiérrez[b], L. Leija[a,*]

[a] Department of Electrical Engineering/Bioelectronics, CINVESTAV-IPN, Mexico City, Mexico
[b] Instituto Nacional de Rehabilitación, Mexico City, Mexico

ARTICLE INFO

Keywords:
Diabetic foot risk detection
Thermographic images processing
Deep-learning
Transfer learning
Thermography

ABSTRACT

Diabetes mellitus has become a global healthcare issue with incidence levels growing exponentially each year. Diabetic foot is one of the complications related with the ailment, and if it is not attended in time, it can progressively deteriorate to a condition that necessitates foot amputation. This study aimed to establish a non-invasive monitoring system for diabetic foot. This proposed system detects and classifies temperature differences in foot sole zones as ulcerous if > 2.2 °C and necrotic if < -2.2 °C, by processing thermographic images of foot soles. This is achieved without homogeneous background or room temperature control. There are reports of systems that are designed to work under controlled environments; however, their performance declines or falters altogether under uncontrolled, home environments.

The system proposed in this paper combines step-by-step and end-to-end algorithms that compensate for the limitations in data and, at the same time, enhance performance. It uses deep-learning techniques to segment visible-spectrum images using a retrained Mask R-CNN model, which is adjusted with 141 images to segment foot soles. These results are used over the temperature matrix in order to isolate the foot sole temperatures. The visualisation and classification methods use step-by-step algorithms with comparisons of homologous foot sole regions, convolutions with a two-dimensional (2D) Gaussian function, filters that process and compare areas of 1.5 cm^2 over each foot sole, and a thermal threshold to differentiate ulcerous from necrotic zones.

The results illustrated a detection accuracy of 90% for ulcers and 88% for necrosis, while the labelled areas had an error of 7.05% and 10%, respectively. These results demonstrated that the system is capable of successfully detecting and visualising the specific temperature differences over samples under an uncontrolled environment.

1. Introduction

Diabetes mellitus (DM) is a known global healthcare concern with incidence levels that grow exponentially each year. Statistics released by international organisations such as the International Diabetes Federation (IDF) or the World Health Organization indicate a global DM population of 425 million [1]. The origin of this pathology can be either autoimmune pancreas destruction, low or null insulin production (type I), or insulin production reduction alongside the body's failure to seize insulin (type II) [2].

By comparing the IDF atlas from 2000 [3] to 2017 [1], it can be estimated that the global diabetic population increased over 300% between 1994 and 2017. DM leads to body deterioration, which originates complications such as blindness, cardiac illness, nervous system damage, ulcers, and lower-limb amputations [1]. Studies estimate that between 27% and 75.5% of DM patients will have to undergo a lower-limb amputation, which translates into approximately 700 amputations out of 100,000 patients each year [4]. Every ulcer and amputation results in high monetary costs, alongside a reduction in the quality of life. In order to prevent these situations, international healthcare organisations (IHOs) concentrate on the prevention of diabetic foot (DF) complications by educating the patients as stated by Dorresteijn [5] and by promoting prevention campaigns as proposed by Meaney [6]. For prevention, IHOs advise feet evaluations with healthcare professionals at least once a year, and, through education, they encourage patients to perform daily inspections of their feet so they can identify risk factors [7]. Örneholm [8] states that a patient's proactivity to addressing these risk factors can help reduce the rate of ulcer complications by effectively expediting professional treatment, which is essential for a better prognosis. According to Pemayun [9] and Edo [10], most of the

* Corresponding authors.
E-mail addresses: hmaldonado@cinvestav.mx (H. Maldonado), arvera@cinvestav.mx (A. Vera), lleija@cinvestav.mx (L. Leija).

https://doi.org/10.1016/j.infrared.2020.103187
Received 15 October 2019; Received in revised form 4 January 2020; Accepted 6 January 2020
Available online 10 January 2020

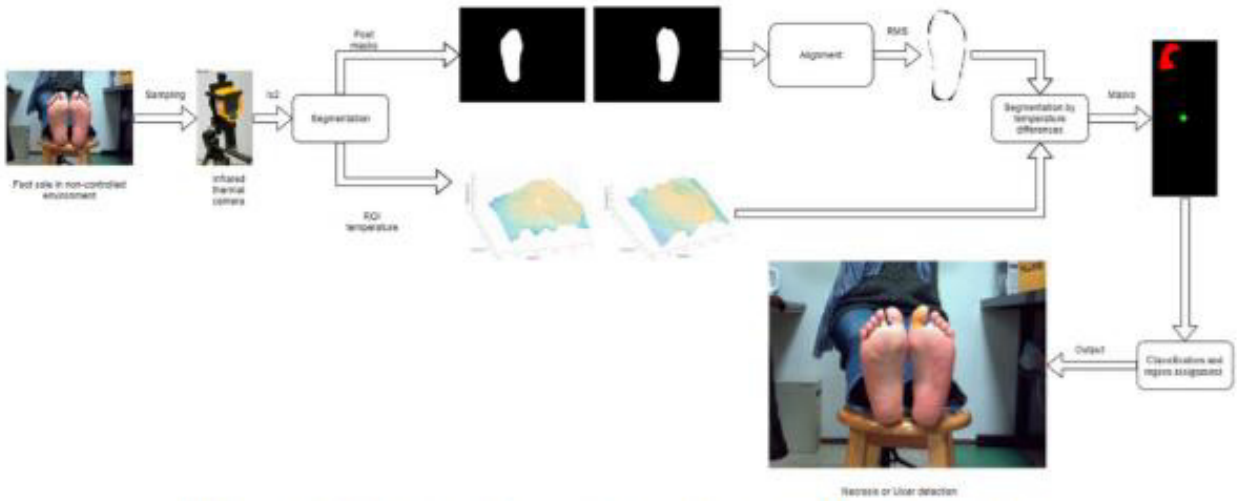

Fig. 1. Graphic diagram depicting each processing step required by the proposed system's overall application.

Fig. 2. Infrared thermal camera FLUKE TI32.

Table 2
TI32 infrared thermal camera characteristics and specifications.

Specifications	Metrics	
	Range	Units
Temperature Measurement Range	−20 to +600	°C
Accuracy	± 2	°C
Thermal Sensitivity (NETD)	≤ 0.05	°C
Infrared Spectral Band	8.0 – 14	μm
Minimum Focus Distance	46	Cm
Resolution of Visual Spectrum Camera	480 × 640	Pixel
Resolution of infrared thermographic camera	240 × 320	Pixel

verify and measure the efficiency of our method for diverse environments. Fig. 4 shows the IRT images which correspond to Fig. 3 samples and the background effect in IRT. Table 3 shows the sample distribution for each background in DB1. When building DB1, images were taken at different moments, reducing the number of volunteers in each background.

The second database (DB2) was built for VS image segmentation using the deep-learning algorithm Mask R-CNN and for transfer learning using the method reported by Abdulla [37]. The training of the Mask R-CNN only required VS images in the RGB colour space and JPG format. The IRT matrix was not necessary for Mask R-CNN, and thus, camera TI32 was not needed to build DB2.

DB2 contained a total of 141 images from 47 new volunteers, which translates into three images per volunteer. There was no restriction on the age, gender, or current state of health of the volunteers in order to ensure sample variation in foot size and morphology. However, there was only one exclusion criteria: foot soles with amputations or lacerations that could drastically change the foot morphology.

Volunteers who accepted to participate were informed about the database, study aims, and the identity confidentiality policy; they were also informed that DB2 was not going to be distributed in any way. Fig. 5 shows some samples of DB2 taken after obtaining consent from the volunteers. The samples show that the environments and backgrounds were not controlled.

The volunteers took the pictures with their smartphone's application of preference and sent the digital file to an electronic reservoir specifically open for this project. Personnel from the research team were not allowed to participate in sample taking; and in this way, it was guaranteed that the conditions for the sample taking were not under control and that they were taken by non-specialised users. The only criteria for image inclusion was to ensure that the images showed complete feet soles and that three picture samples were taken per volunteer: one with both feet soles and one each for the individual foot soles. Fig. 5 shows two of the three samples taken from two volunteers. A specific image background or structure was not required. As a result, the 141 samples had varied image backgrounds with resolutions between 394 × 1280 and 2304 × 4096 pixels.

2.4. Database processing

2.4.1. DB1 processing

DB1 files were in IS2 FLUKE TI32 camera format. The IS2 data stored the IRT camera information, room temperature registered by the user, VS image, the matrix of measured temperatures, and the material emissivity. The data of significance from the IS2 files were the VS image and the temperatures measured. A modified version of the algorithm Readis2 from Beauducel [38] was used to extract, process, and store the

Fig. 3. Backgrounds used for building DB1: (A) support structure of ABS material, (B) modified support structure without lateral borders, (C) Black homogeneous background, and (D) non-homogeneous background. The depicted sample images are for the same volunteer.

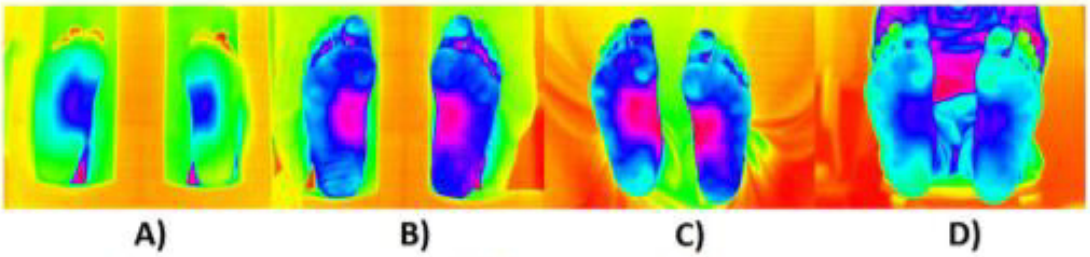

Fig. 4. IRT images that correspond respectively to Fig. 3 samples. The depicted sample images are for the same volunteer.

Table 3
DB1 sample distribution for each background from Fig. 3.

Backgrounds	Number of samples	Number of Volunteers sampled in each background	Number of samples per volunteer
structure made of ABS material	32	16 of 16	2 samples per volunteer
modified support structure without lateral borders	42	14 of 16	3 samples per volunteer
non-homogeneous background	26	10 of 16	5 volunteers – 3 samples
		+	5 volunteers – 2 samples
		one that only participated in this set	1 volunteer – 1 sample
black homogeneous background	8	4 of 16	2 samples per volunteer

files. The pictures in Fig. 4 are an RGB representation of the temperatures measured; therefore, they were not considered essential for saving.

2.4.2. Processing database to be used by mask R-CNN

The Mask R-CNN algorithm was applied to 141 images from DB2 for training and on 24 VS images from DB1 for testing. The images from DB1, taken with the FLUKE TI32, had a lower resolution than those from DB2; therefore, DB1 was used to measure how the accuracy of the system was affected by the low resolution of the images. Each photo for Mask R-CNN was segmented and labelled with the respective class using the free software VGG image annotator (VIA) [39,40] from the Visual Geometry Group of the Department of Engineering Science, University of Oxford. Fig. 6 shows the manual segmentation and annotation using VIA; here, the Mask R-CNN training algorithm was used to generate the necessary binary masks.

2.4.3. Temperature changes by 2D Gaussian distributions

Temperature changes added to the IRT matrix in order to simulate a zone with temperature differences showed a 2D Gaussian distribution according to the following equation reported by Talbi [41]:

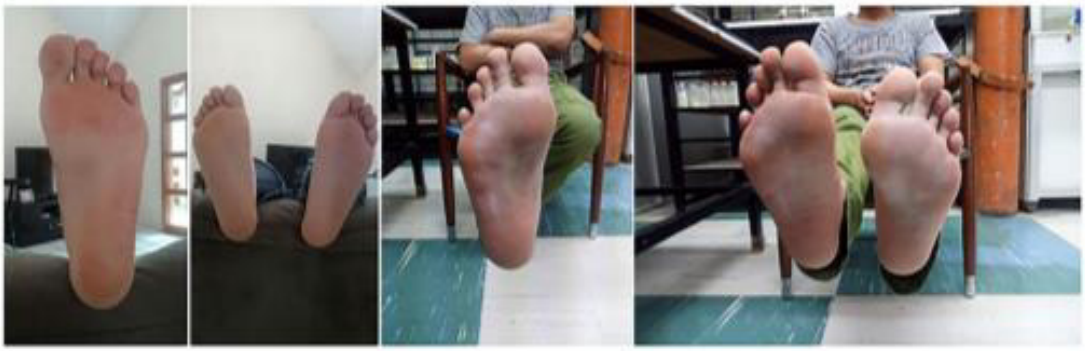

Fig. 5. Samples from DB2 that demonstrate the different sample taking environments in non-homogeneous backgrounds.

ANEXO 20. International Union of Railways - UIC, «UIC.org RAILsiliencia,» 07 2020. [Enlínea].Available:https://uic.org/IMG/pdf/uic_covid_taskforce_thermal_cameras_espanol.pdf. [Último acceso: 18 01 2021].

UIC COVID-19 TASK FORCE

RAILsiliencia

De la utilización de cámaras térmicas para la medición de temperatura en las personas para combatir el Covid-19

Estado del arte - **Julio 2020**

INTERNATIONAL UNION OF RAILWAYS

GRUPO DE TRABAJO UIC COVID-19

Ante el brote de la enfermedad por coronavirus, la UIC estableció un grupo de trabajo que combina miembros de la UIC, expertos y otros actores relevantes como: AAR, AFRA, Unión Africana, ALAF, AllRail, ANPTrilhos, APTA, CER, CIT, EIM, EPF, ERFA, ETF, ETOA, IATA, OTIF, UITP y UNECE, para encontrar formas de dar respuestas a esta crisis, adaptadas al sector ferroviario.

El objetivo principal del grupo de trabajo UIC Covid-19 es proporcionar un espacio de confianza para que nuestros miembros y otras asociaciones compartan información sobre esta crisis. Dado que se trata de una crisis mundial sin precedentes, poder unirnos y beneficiarnos de las experiencias de los demás ha sido clave en la lucha por proteger vidas asegurando un mínimo de nuestro servicio esencial: el transporte.

Dado que ésta sigue siendo una crisis global, necesita una respuesta global, y UIC se encuentra en una posición única para crear un espacio donde la comunidad ferroviaria mundial pueda reunirse y cooperar. En las reuniones del grupo de trabajo, ferrocarriles de Asia, África, Europa, Oriente Medio, Oceanía y las Américas, se benefician del conocimiento y la experiencia de los demás.

Responder a esta crisis desde el sector ferroviario obliga a navegar en un entorno cambiante, con un enfoque ágil y cotidiano, en el presente y también en el corto y mediano plazo.

Entre marzo y julio de 2020, se han publicado cinco guías de la UIC para los actores del sector ferroviario y se han puesto a disposición en línea en: https:// uic.org/covid-19.

Toda la información compartida está disponible al unirse al grupo de trabajo y registrarse en la extranet de UIC en el espacio de trabajo del Grupo de trabajo Covid-19 https:// extranet.uic.org/index.php

La información se comparte de manera constante entre los miembros. La información multimedia relevante está disponible en el Centro Multimedia de la UIC https://mediacenter.uic.org.fr.

El grupo de trabajo de UIC Covid-19 también ha creado un grupo LinkedIn donde se comparten artículos de periódicos relevantes y seminarios web. https://www.linkedin.com/ groups/13846065/

5

ANEXO 21. E. O. Peña Rodríguez y L. Y. Neita Duarte, «Temperatura Y Calor,» de *Principios Básicos de la Termografia Infrarroja y su Utilización como técnica para mantenimiento predictivo*, Floridablanca, Universidad Pontificia Bolivariana - Facultad de IngenierÍa Electrónica, 2011, pp. 56-221.

PRINCIPIOS BÁSICOS DE LA TERMOGRAFÍA INFRARROJA Y SU UTILIZACIÓN COMO TÉCNICA PARA MANTENIMIENTO PREDICTIVO

LIDIA YANETH NEITA DUARTE
ELKIN OMAR PEÑA RODRÍGUEZ

UNIVERSIDAD PONTIFICIA BOLIVARIANA
FACULTAD DE INGENIERÍA ELECTRÓNICA
FLORIDABLANCA
2011

En 1879 Stefan concluye a partir de experimentos que la energía total irradiada por un cuerpo negro es función directa de la cuarta potencia de su temperatura absoluta. En 1884 Boltzmann llegó a la misma conclusión. Esto es conocido como la Ley de Stefan-Boltzmann:

$$W = \sigma T^4 \quad (5)$$

Donde,

W Potencia emisiva superficial

σ Constante de Stefan-Boltzmann (5,67 x10^{-8} W/cm^2K^4)

T Temperatura

Otra ley de la radiación es la ley de Wien que es conocida como la Ley de desplazamiento; fue formulada por Wilhelm Wien en 1884 de forma empírica. Esta ley establece la relación entre la temperatura y la longitud de onda donde ocurre la máxima emisión de energía:

$$\lambda_{max} = \frac{2.898}{T}(\mu m) \quad (6)$$

Donde,

λ Longitud de onda

T temperatura

Las consecuencias de la ley de Wien es que cuanta mayor sea la temperatura de un cuerpo negro menor es la longitud de onda en la cual emite.

En la Figura 17 se muestra una gráfica de Longitud de Onda Vs Energía Radiada por un objeto a diferentes temperaturas, con una mayor temperatura el pico de energía ocurre en una la longitud de onda más corta, por el contrario a bajas temperaturas el pico de energía se produce en una longitud de onda larga.

Figura 17. Longitud de onda Vs Energía Radiada

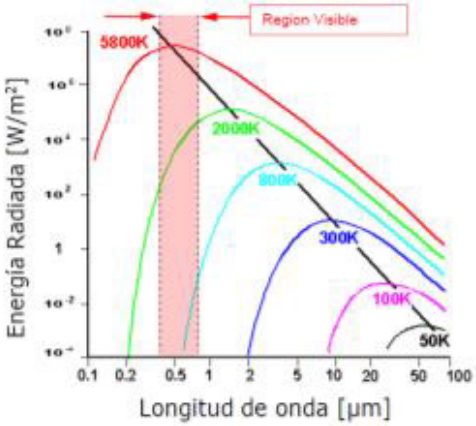

Fuente: tomado de [15].

En 1900 Max Planck anunció otra ley de la radiación denominada la Ley de Planck que establece la distribución de la potencia radiada por un cuerpo negro a lo largo del espectro.

$$W = \frac{2\pi hc^2}{\lambda^5\left(e^{\left(hc/\sigma\lambda T\right)}-1\right)} \quad (7)$$

Donde,

W Potencia emisiva superficial

λ Longitud de onda

T Temperatura

h Constante de Planck $6{,}626\times10^{-34}$ J.s

c Velocidad de la luz en el vacío $2{,}997\times10^{8}$ m/s

σ Constante de Stefan-Boltzmann

Para varias temperaturas se produce una familia de curvas, cuanto más alta es la temperatura menor es la longitud de onda para la cual W es máxima.

2.4.2.1 Radiación incidente. "La radiación incidente es toda la radiación que llega a un cuerpo procedente de su entorno" [12] (ver Figura 18). Para una misma longitud de onda λ se tiene que el balance de la radiación incidente de un cuerpo es dado por la ecuación 9 y contribuyen tres procesos que dependen de la habilidad de los cuerpos de:

- Absorber, llamada absortividad α
- Reflejar, llamada Refletividad ρ
- Transmitir, llamada Transmisividad τ

La suma de los tres procesos es siempre uno (ver ecuación 8)

$$\alpha + \rho + \tau = 1 \quad (8)$$

Figura 18. Balance de la radiación incidente de un cuerpo

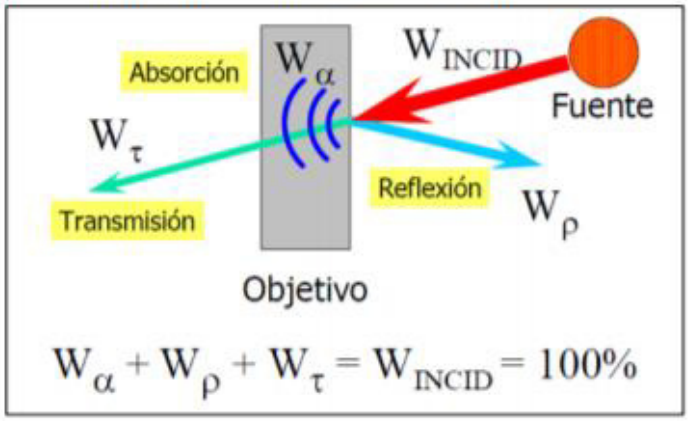

Fuente: tomado de [12].

Cuando la radiación incidente (W_{INCID}) alcanza la superficie de un cuerpo corren tres cosas, parte la radiación será absorbida y el cuerpo la retiene, esta se conoce como Radiación Absorbida ($W\alpha$) en la Figura 18. La segunda llamada

AEXO 22. I. Mártil, «Público,» 27 05 2016. [En línea]. Available: https://blogs.publico.es/ignacio-martil/2016/05/27/la-invisible-y-muy-real-radiacion-infrarroja/. [Último acceso: 23 05 2021].

Ignacio Mártil

Catedrático de Electrónica de la Universidad Complutense de Madrid y miembro de la Real Sociedad Española de Física

Imagen visible (izquierda) e infrarroja (centro) de la cabeza de un perro. La escala de la derecha identifica los colores de la imagen con la temperatura a la que se encuentra cada zona

Sí, es lo que parece, la cabeza de un perro tomada con una cámara que capta la radiación infrarroja que emite. Se aprecia que las tonalidades de colores son diferentes en cada parte de la cabeza, indicando los cambios de temperatura que hay de unas a otras. Pero, ¿qué es la radiación infrarroja? ¿Para qué sirve y en qué se emplea? En este artículo lo explico con cierto detalle

Longitud de onda (µm)

Densidad espectral de energía radiada por cuerpos situados a diferentes temperaturas, expresada en grados Kelvin. La línea roja (300 K) corresponde a un cuerpo situado a la temperatura ambiente. Ambos ejes están en escala logarítmica.

El espectro IR abarca un rango amplio de longitudes de onda, que se clasifican tradicionalmente en tres zonas, aunque los intervalos de cada una pueden variar según el esquema de clasificación que se siga. La tabla los recoge, junto con los semiconductores que detectan cada una de ellas:

Denominación	Margen de longitud de onda (µm)	Semiconductor y rango de detección (µm)
IR Cercano	0.7–3	Si (0.7-1); InGaAs, PbSe (1-3)
IR Medio	3–50	InSb (3-5); HgCdTe (8-14); Si:As (15-30)
IR Lejano	50–1000	Detectores térmicos

Clasificación de las bandas IR de acuerdo al estándar ISO 20473, que especifica la división de la radiación óptica en bandas espectrales.

ANEXO 23. J. M. Ruiz Echeverri y J. M. Meza Arenas, Fundamentos para una metodología para el diagnóstico cuantitativo de la función lagrimal humana utilizando termografía Infra-Roja., Pereira: Universidad Tecnológica de Pereira - Departamento de Física, grupo de Electrofisiología, 2018.

FUNDAMENTOS PARA UNA METODOLOGÍA PARA EL DIAGNÓSTICO CUANTITATIVO DE LA FUNCIÓN LAGRIMAL HUMANA UTILIZANDO TERMOGRAFÍA INFRA-ROJA.

JULIÁN MAURICIO RUIZ ECHEVERRI

JUAN MATEO MEZA ARENAS

TRABAJO DE GRADO PRESENTADO COMO REQUISITO PARCIAL PARA OPTAR AL TÍTULO DE INGENIERO FÍSICO

DIRECTOR

LUIS ENRIQUE LLAMOSA RINCÓN

MSC. EN FÍSICA

UNIVERSIDAD TECNOLÓGICA DE PEREIRA

GRUPO DE ELECTROFISIOLOGÍA

FACULTAD DE INGENIERÍAS - DEPARTAMENTO DE FÍSICA

PEREIRA 2018

2. MARCO TEÓRICO.

2.1 Termografía infrarroja

La Termografía Infrarroja es una técnica que permite, a distancia y sin contacto, medir y visualizar temperaturas de superficies con precisión, siendo esto posible gracias a que todos los cuerpos emiten radiación infrarroja y esta energía irradiada es proporcional a la temperatura superficial. Como lo expresan Sanz, et al. (2008), la cámara infrarroja recibe y cuantifica dichas radiaciones térmicas emitidas y reflejadas por los diferentes materiales y las transforma en imágenes digitales. Además, De Grado (1998) afirma que los cuerpos emiten esta radiación debido a la vibración y rotación propia de los átomos y moléculas que componen un material. Expone De Grado (1998), que la historia de la Termografía Infrarroja se remonta a los años de 1800, cuando Sir William Herschel, astrónomo alemán, en momentos que buscaba un filtro óptimo para su telescopio, observó que ciertos cristales coloreados dejaban pasar más calor solar que otros; midió entonces los diferentes haces de colores en que se descompone la luz solar al atravesar un prisma de Newton, y encontró que la temperatura iba creciendo desde el violeta hasta el rojo, pero que la mayor temperatura se registraba en una zona oscura, fuera del haz visible, más allá del color rojo, conocida hoy en día como la radiación infrarroja, llamada en sus inicios "calor oscuro", en el espectro electromagnético, la región de la radiación infrarroja está comprendida aproximadamente entre los 0,7 µm y 1.0 µm., de longitud de onda[9].

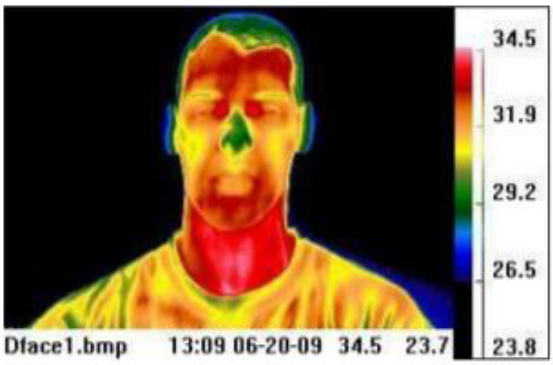

Figura1.Imagen termográfica
Fuente. http://www.thermology.com

MATERIALES Y MÉTODOS

ANEXO 24. R. Hernández Sampieri, «Metodología de la investigación Sexta edición,» de *Metodología de la investigación Sexta edición*, Mexico, McGRAW-HILL Interamericana Editores, S.A. DE C.V., 2014, p. 634.

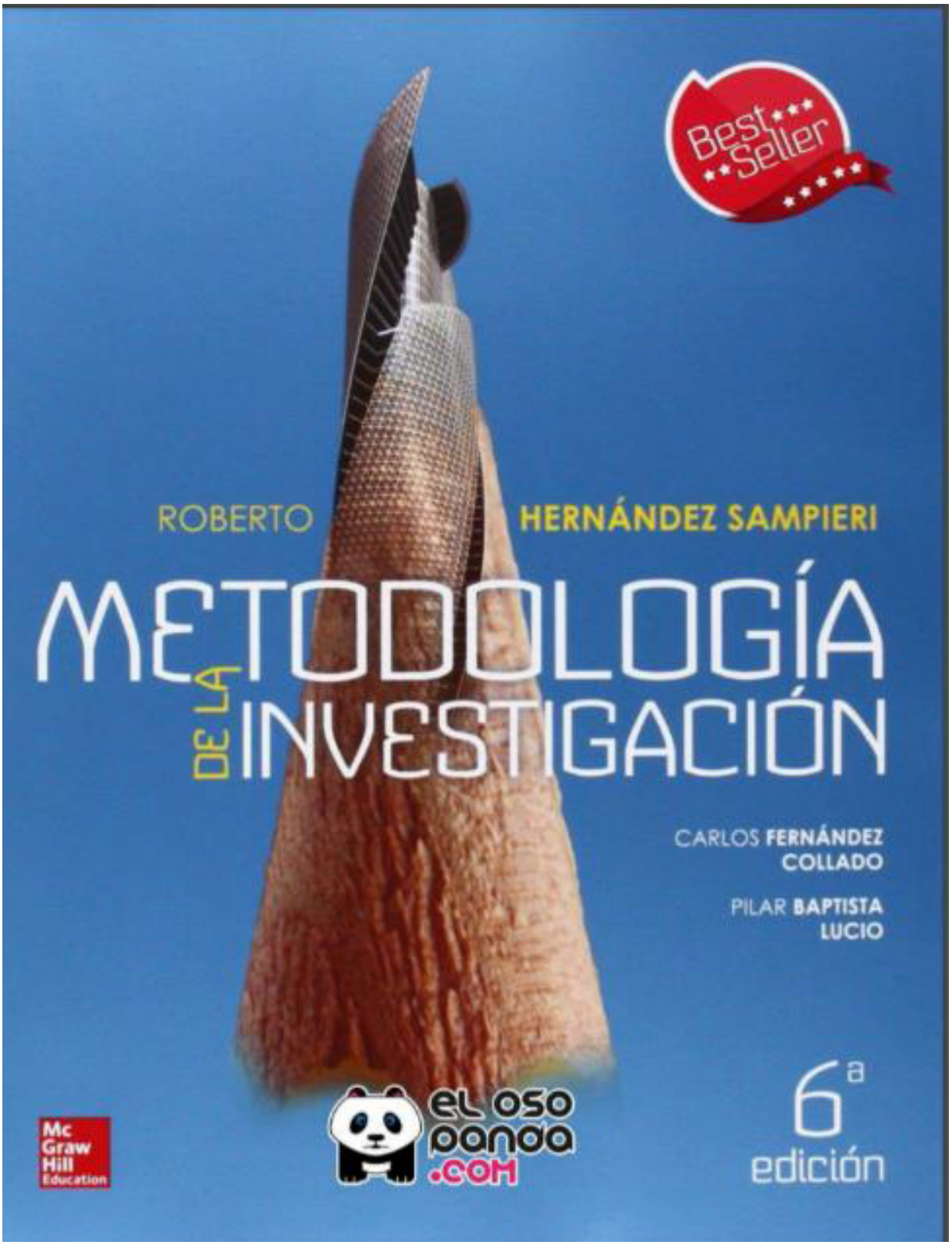

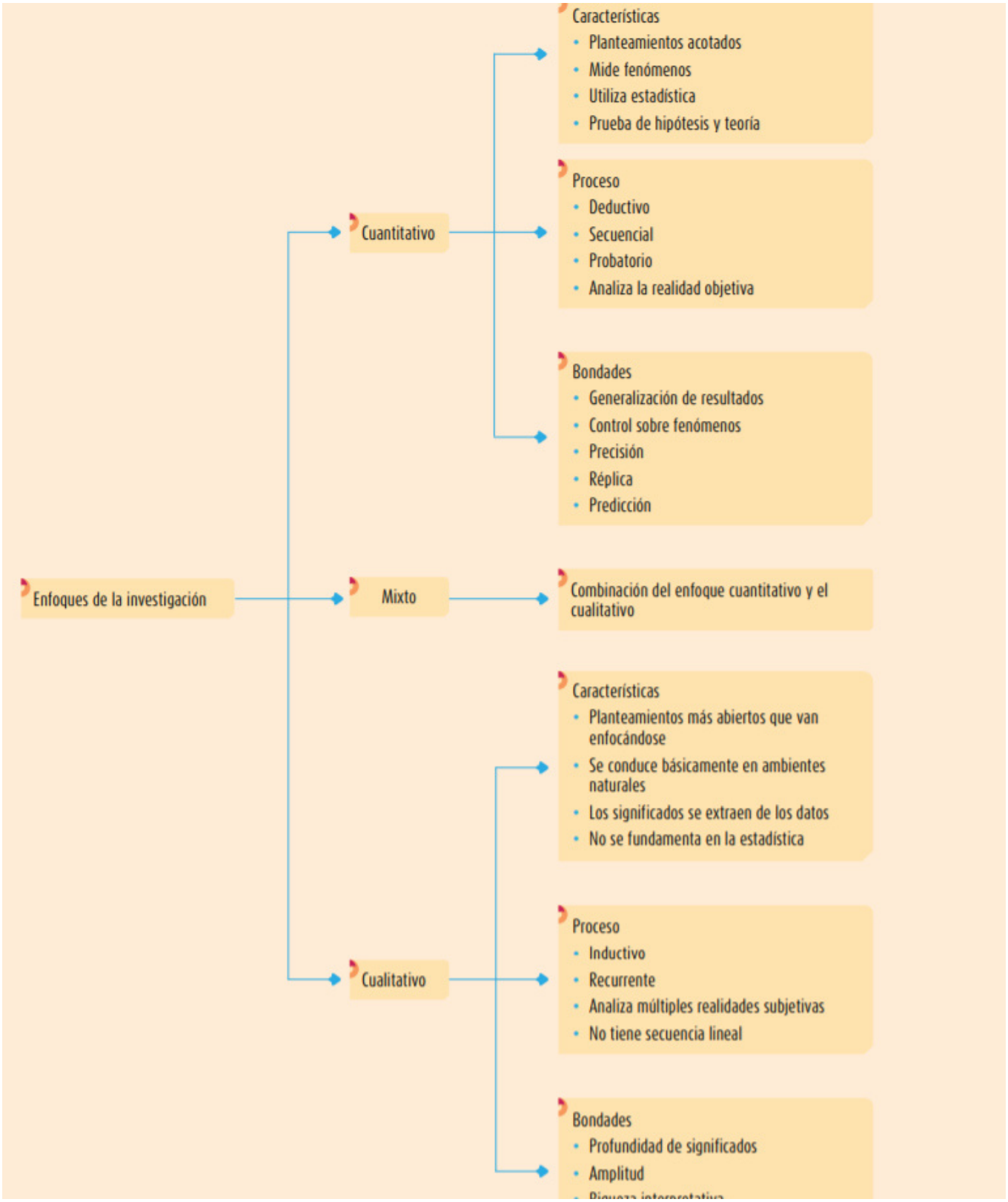
Enfoques de la investigación
Cuantitativo
Características
Planteamientos acotados
Mide fenómenos
Utiliza estadística
Prueba de hipótesis y teoría
Proceso
Deductivo
Secuencial
Probatorio
Analiza la realidad objetiva
Bondades
Generalización de resultados
Control sobre fenómenos
Precisión
Réplica
Predicción
Mixto
Combinación del enfoque cuantitativo y el cualitativo
Cualitativo
Características
Planteamientos más abiertos que van enfocándose
Se conduce básicamente en ambientes naturales
Los significados se extraen de los datos
No se fundamenta en la estadística
Proceso
Inductivo
Recurrente
Analiza múltiples realidades subjetivas
No tiene secuencia lineal
Bondades
Profundidad de significados
Amplitud

¿Cómo se define la investigación?

La **investigación** es un conjunto de procesos sistemáticos, críticos y empíricos que se aplican al estudio de un fenómeno o problema.

¿Qué enfoques se han presentado en la investigación?

1

A lo largo de la historia de la ciencia han surgido diversas corrientes de pensamiento (como el empirismo, el materialismo dialéctico, el positivismo, la fenomenología, el estructuralismo) y diversos marcos interpretativos, como el realismo y el constructivismo, que han abierto diferentes rutas en la búsqueda del conocimiento. No se profundizará por ahora en ellas; su revisión, aunque breve, se incluye en el centro de recursos en línea, en: http://www.mhhe.com/he/fumi6e de esta edición.[1] Sin embargo, y debido a las diferentes premisas que las sustentan, desde el siglo pasado tales corrientes se "polarizaron" en dos aproximaciones principales de la investigación: el enfoque cuantitativo y el enfoque cualitativo.[2]

Centro de recursos en línea

Ambos enfoques emplean procesos cuidadosos, metódicos y empíricos en su esfuerzo para generar conocimiento, por lo que la definición previa de investigación se aplica a los dos por igual. En términos generales, estos métodos utilizan cinco estrategias similares y relacionadas entre sí (Grinnell, 1997):

1. Llevan a cabo la observación y evaluación de fenómenos.
2. Establecen suposiciones o ideas como consecuencia de la observación y evaluación realizadas.
3. Demuestran el grado en que las suposiciones o ideas tienen fundamento.
4. Revisan tales suposiciones o ideas sobre la base de las pruebas o del análisis.
5. Proponen nuevas observaciones y evaluaciones para esclarecer, modificar y fundamentar las suposiciones e ideas o incluso para generar otras.

Sin embargo, aunque las aproximaciones cuantitativa y cualitativa comparten esas estrategias generales, cada una tiene sus propias características.

¿Qué características posee el enfoque cuantitativo de investigación?

2

El enfoque cuantitativo (que representa, como dijimos, un conjunto de procesos) es secuencial y probatorio. Cada etapa precede a la siguiente y no podemos "brincar" o eludir pasos.[3] El orden es riguroso, aunque desde luego, podemos redefinir alguna fase. Parte de una idea que va acotándose y, una vez delimitada, se derivan objetivos y preguntas de investigación, se revisa la literatura y se construye un marco o una perspectiva teórica. De las preguntas se establecen hipótesis y determinan variables; se traza un plan para probarlas (diseño); se miden las variables en un determinado contexto; se analizan las mediciones obtenidas utilizando métodos estadísticos, y se extrae una serie de conclusiones

Enfoque cuantitativo Utiliza la recolección de datos para probar hipótesis con base en la medición numérica y el análisis estadístico, con el fin establecer pautas de comportamiento y probar teorías.

Centro de recursos en línea

[1] En el centro de recursos en línea: http://www.mhhe.com/he/fernite, el lector encontrará un capítulo sobre los antecedentes de las aproximaciones cuantitativa y cualitativa (véase el primer capítulo de los adicionales: "Historia de los enfoques cuantitativo, cualitativo y mixto").

[2] El significado original del término "cuantitativo" (del latín *quantus*) se remite a conteos numéricos y métodos matemáticos, mientras que la palabra "cualitativa" (del latín *qualitas*) hace referencia a la naturaleza, carácter y propiedades de los fenómenos (Teglas, 2010), y aunque en el centro de recursos en línea se profundiza más en este tema, por ahora basta decir que el enfoque cuantitativo en las ciencias sociales se origina fundamentalmente en la obra de Auguste Comte (1798-1857) y Emile Durkheim (1858-1917). Ellos propusieron que el estudio de los fenómenos sociales requiere ser "científico", es decir, susceptible a la aplicación del mismo método que se utilizaba con éxito en las ciencias naturales. Tales autores sostenían que todas las "cosas" o fenómenos que estudiaban las ciencias eran medibles. A esta corriente se le llama positivismo.

El enfoque cualitativo tiene su origen en otro pionero de las ciencias sociales: Max Weber (1864-1920), quien introdujo el término *verstehen* (en alemán, "entender"), reconociendo que además de la descripción y medición de variables sociales, deben considerarse los significados subjetivos y la comprensión del contexto en el que ocurre el fenómeno. Weber propuso un método híbrido, con herramientas como los tipos ideales, en el que los estudios no sean únicamente de variables macrosociales, sino de instancias individuales.

[3] Por ejemplo, no podemos definir y seleccionar la muestra si aún no hemos establecido las hipótesis. Tampoco es posible recolectar o analizar datos si previamente no hemos desarrollado el diseño o no hemos definido la muestra.

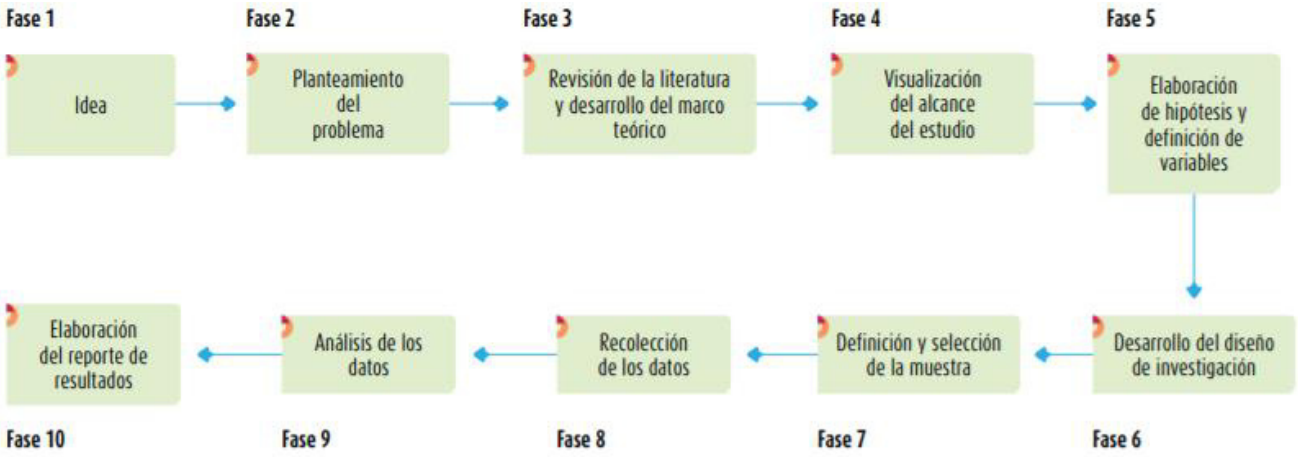

El enfoque cuantitativo tiene las siguientes características: 3

1. Refleja la necesidad de medir y estimar magnitudes de los fenómenos o problemas de investigación: ¿cada cuánto ocurren y con qué magnitud?
2. El investigador o investigadora *plantea un problema de estudio delimitado y concreto* sobre el fenómeno, aunque en evolución. Sus preguntas de investigación versan sobre cuestiones específicas.
3. Una vez planteado el problema de estudio, el investigador o investigadora considera lo que se ha investigado anteriormente (la *revisión de la literatura*) y construye un *marco teórico* (la teoría que habrá de guiar su estudio), del cual deriva una o varias *hipótesis* (cuestiones que va a examinar si son ciertas o no) y las somete a prueba mediante el empleo de los diseños de investigación apropiados. Si los resultados corroboran las hipótesis o son congruentes con éstas, se aporta evidencia a su favor. Si se refutan, se descartan en busca de mejores explicaciones y nuevas hipótesis. Al apoyar las hipótesis se genera confianza en la teoría que las sustenta. Si *no* es así, se rechazan las hipótesis y, eventualmente, la teoría.
4. Así, las hipótesis (por ahora denominémoslas "creencias") se generan antes de recolectar y analizar los datos.
5. La *recolección de los datos* se fundamenta en la medición (se miden las variables o conceptos contenidos en las hipótesis). Esta recolección se lleva a cabo al utilizar procedimientos estandarizados y aceptados por una comunidad científica. Para que una investigación sea creíble y aceptada por otros investigadores, debe demostrarse que se siguieron tales procedimientos. Como en este enfoque se pretende *medir*, los fenómenos estudiados deben poder observarse o *referirse* al "mundo real".
6. Debido a que los datos son producto de mediciones, se representan mediante números (cantidades) y se deben *analizar* con *métodos estadísticos*.
7. En el proceso se trata de tener el mayor control para lograr que otras posibles explicaciones, distintas o "rivales" a la propuesta del estudio (hipótesis), se desechen y se excluya la incertidumbre y minimice el error. Es por esto que se confía en la experimentación o en las pruebas de causalidad.
8. Los análisis cuantitativos se interpretan a la luz de las predicciones iniciales (hipótesis) y de estudios previos (teoría). La interpretación constituye una explicación de cómo los resultados encajan en el conocimiento existente (Creswell, 2013a).

Figura 1.2 Relación entre la teoría, la investigación y la realidad en el enfoque cuantitativo.

¿Qué características posee el enfoque cualitativo de investigación?

2

El enfoque cualitativo[5] también se guía por áreas o temas significativos de investigación. Sin embargo, en lugar de que la claridad sobre las preguntas de investigación e hipótesis preceda a la recolección y el análisis de los datos (como en la mayoría de los estudios cuantitativos), los *estudios cualitativos* pueden desarrollar preguntas e hipótesis antes, durante o después de la recolección y el análisis de los datos. Con frecuencia, estas actividades sirven, primero, para descubrir cuáles son las preguntas de investigación más importantes; y después, para perfeccionarlas y responderlas. La acción indagatoria se mueve de manera dinámica en ambos sentidos: entre los hechos y su interpretación, y resulta un proceso más bien "circular" en el que la secuencia no siempre es la misma, pues varía con cada estudio. A continuación intentamos representarlo en la figura 1.3, pero cabe señalar que es simplemente eso, un intento, porque su complejidad y flexibilidad son mayores. Este proceso se despliega en la parte 3 del libro.

Enfoque cualitativo Utiliza la recolección y análisis de los datos para afinar las preguntas de investigación o revelar nuevas interrogantes en el proceso de interpretación.

Figura 1.3 Proceso cualitativo.

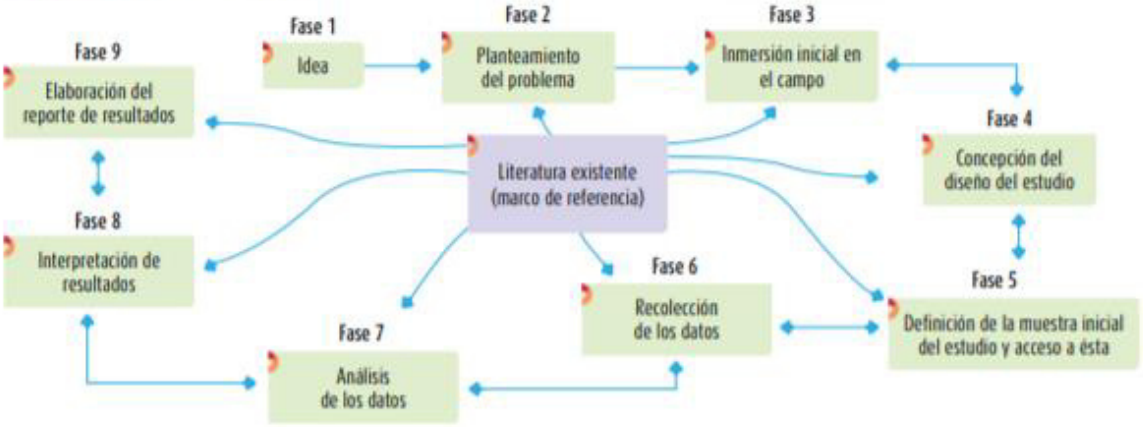

[5] Este enfoque también se conoce como investigación naturalista, fenomenológica, interpretativa o etnográfica, y es una especie de "paraguas" en el cual se incluye una variedad de concepciones, visiones, técnicas y estudios no cuantitativos. Según Sparkes y Smith (2014) y Savin-Baden y Major (2013), existen diversos marcos interpretativos, como el interaccionismo, la etnometodología, el constructivismo, el feminismo, la fenomenología, la psicología de los constructos personales, la teoría crítica, etc., que se incluyen en este "paraguas para efectuar estudios".

ANEXO 25. A. Mariño Mur, Caracterización Térmica de un conjunto de edificaciones del Pirineo Oscense Mediante Termografia Infrarroja, Valéncia: Universidad Politécnica de Valéncia, Escuela Técnica Superior Ingeniería de Edificación, 2012.

CARACTERIZACIÓN TÉRMICA

DE UN CONJUNTO DE EDIFICACIONES

DEL PIRINEO OSCENSE

MEDIANTE TERMOGRAFÍA INFRARROJA

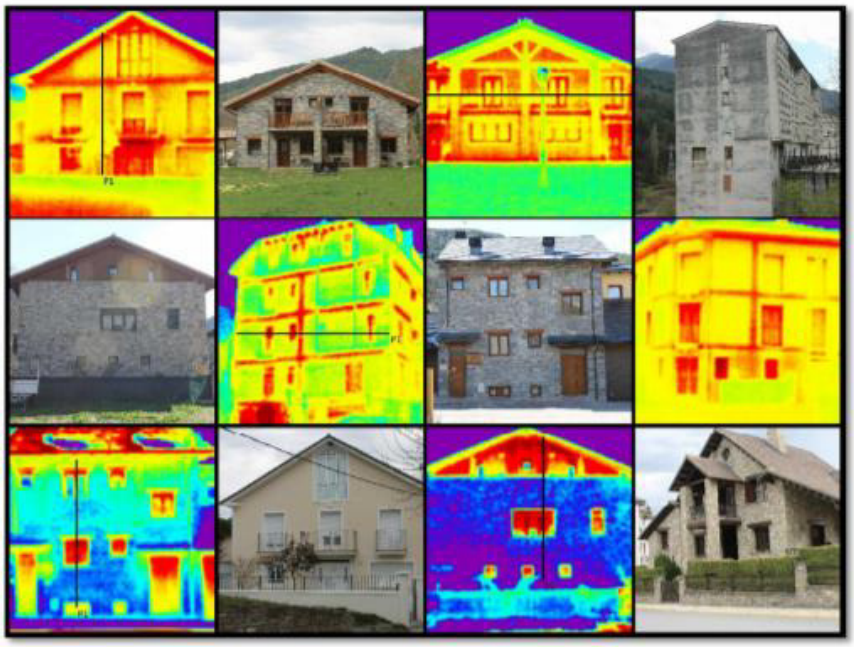

ALEJANDRO MARIÑO MUR

Tutores

ANDREA SALANDIN - ISABEL TORT AUSINA

CURSO 2011/2012

ESCUELA TÉCNICA SUPERIOR INGENIERÍA DE EDIFICACIÓN

UNIVERSITAT POLITÈCNICA DE VALÈNCIA

T18

fue posible al crear un detector no refrigerado, denominándose microbolómetro, este detector no refrigerado también hizo a estas cámaras más económicas y menos susceptibles de averías. Fue a partir del uso del microbolómetro cuando se extendió el uso de las cámaras termográficas a campos más comerciales, como pueden ser el industrial, automovilístico, marítimo, aeronáutico o el de la edificación.

1.3 PRINCIPIOS FISICOS Y APLICACIONES

Todos los materiales tienen la capacidad de absorber radiación infrarroja aumentando su temperatura; asimismo todos los materiales con una temperatura superior al cero absoluto emiten energía infrarroja. La termografía es una técnica que aprovecha la radiación emitida por la superficie de un cuerpo como variable termométrica. Esta radiación es proporcional a la cuarta potencia de la temperatura superficial del objeto (Ley de Stefan-Boltzmann):

$$W = \mu \cdot A \cdot T^4 \ (\mathrm{W/m^2})$$

Donde W es la energía radiante de un cuerpo, μ es la emisividad (valor entre 0 y 1), A es la constante de Stefan Boltzmann ($5{,}7 \cdot 10^{-8}$ $\mathrm{W \cdot m^{-2} \cdot K^{-4}}$) y T es la temperatura absoluta del objeto. [2]

A pesar de ser función de λ, T y el ángulo de incidencia, en la práctica se puede considerar la emisividad como una constante propia de cada material. Por tanto, si se conoce la emisividad del objeto que vamos a inspeccionar, la medida de la radiación nos dará un valor de temperatura.

La termografía es un método de medición pasivo, sin contacto. La imagen termográfica muestra la distribución de temperatura en la superficie de un objeto, por lo que no se debe utilizar una cámara termográfica para "mirar" el interior o a través de los objetos.

La radiación registrada por la cámara termográfica consiste en la radiación de onda larga, **emitida, reflejada y trasmitida** que surge de los objetos presentes en el campo de visión de la cámara.

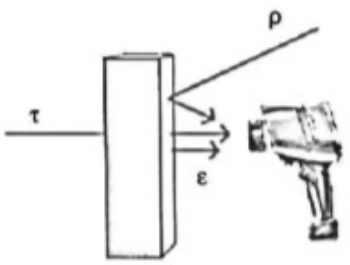

Figura 2. Emisión, reflexión y transmisión

A continuación se explican las diferentes formas en las que nos podemos encontrar estas radiaciones de onda.

ANEXO 26. R. Pascual Arribas, «Captura y procesamiento de imágenes de una cámara térmica,» de *Captura y procesamiento de imágenes de una cámara térmica*, Madrid, Universidad Politécnica de Madrid - Escuela Técnica Superior de Ingenieros Informáticos., 2016, pp. 13-19.

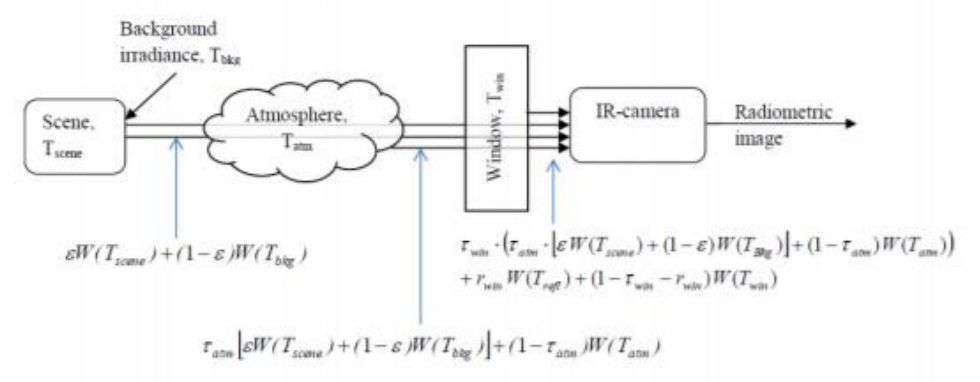

$$S = \tau_{win} \cdot \left(\tau_{atm} \cdot \left[\varepsilon W(T_{scene}) + (1-\varepsilon) W(T_{Bkg})\right] + (1-\tau_{atm}) W(T_{atm})\right) + r_{win} W(T_{refl}) + (1-\tau_{win} - r_{win}) W(T_{win})$$

Notation	Description
S	Value of the 14-bit digital video in counts
ε	Emissivity of the scene.
τ_{win}	Transmission coefficient of the window
T_{win}	Window temperature
r_{win}	Window reflection
T_{refl}	Temperature reflected in the window
τ_{atm}	Transmission coefficient of the atmosphere between the scene and the camera
T_{atm}	Atmospheric temperature
T_{bkg}	Background temperature (reflected by the scene)
T_{scene}	Scene temperature
$W(T)$	Radiated flux (in units of counts) as function of the temperature of the radiating object. The conversion from temperature to flux can be done using the camera command GET_FLUX_FROM_TEMP (function code 0xB6)

Ilustración 1. Modelo de compensación de temperatura

La cámara incorpora mecanismos de corrección de la transmisión de energía por parte de la atmósfera, eliminando el flujo radiométrico que ésta emite y compensando su coeficiente de transmisión. Lo mismo sucede con la óptica de la cámara (Window), sólo que en este caso también se aplica una corrección para compensar la reflexión de la temperatura. Los coeficientes de este modelo vienen calibrados de fábrica y sólo se pueden modificar en cámaras con radiometría avanzada.

Como se ha mencionado anteriormente, la cámara de la que se dispone no tiene habilitadas las funcionalidades de radiometría avanzada, que permitirían obtener valores de temperatura de forma sencilla a partir de una imagen ya capturada. Según el documento [6] apartado 6.3, la temperatura de un píxel de una imagen capturada se puede obtener de la siguiente manera:

$$T_{pix} = Res \cdot S$$

La cámara debe conectarse a un puerto USB. En el caso de Ubuntu (14.04) no es necesario instalar ningún controlador, y aparece como dispositivo en /dev/ttyUSB0. Para poder enviar y recibir mensajes a través del puerto serie es necesario asignarle los permisos correspondientes de lectura y escritura mediante el comando *chmod* en Ubuntu cada vez que se conecte la cámara, o hacer al usuario miembro del grupo *dialout* para tener esos permisos activos siempre. Las funciones de la API reciben como argumento el descriptor de fichero del puerto serie abierto, por lo que antes de llamar a cualquiera de ellas habrá que llamar *setSerial(<path_puerto>, <baudios>),* que abre el puerto serie en modo de lectura y escritura. Se debe definir el nombre del puerto serie al que se conecta la cámara en la variable de entorno CAMERA_PORT. A continuación se muestra el puerto correspondiente a la máquina de desarrollo:

```
export CAMERA_PORT=/dev/ttyUSB0
```

El código hace uso de tres librerías dinámicas:

- LibPNG: para la creación de imágenes en formato PNG
- LibGSL y LibGSLcblas: GNU Scientific Library. Para el algoritmo de mínimos cuadrados

Para instalarlas en Ubuntu se usa la herramienta de gestión de paquetes apt-get:

```
sudo apt-get install libpng-dev
sudo apt-get install libgsl0-dev
```

4.6.2 Configuración de la aplicación

En este apartado se van a detallar los pasos a seguir para configurar la aplicación en la máquina cliente, así como calibrar la cámara para capturar imágenes y temperaturas correctamente. Se va a mostrar un programa de ejemplo que hace uso de la API. El código completo del ejemplo se encuentra en el fichero main.c.

Para la calibración del brillo y contraste para imágenes con información de temperatura se debe utilizar el siguiente fragmento de código:

```
(...)
int brightness, contrast, res;
contrast = 20;//adjust depending on scene
res=set_AGC_params(fd, buf, &rec_MSG,
                   contrast, AUTO_BRIGHT);
```

De este modo el brillo se ajusta automáticamente según la escena en ese instante (AUTO_BRIGHT). No sucede lo mismo con el contraste, debido a que el ajuste automático según el ancho del histograma está bloqueado en esta cámara. El usuario

ANEXO 27. FLIR Systems, Inc., «Apliter Termografia,» 11 04 2019. [En línea]. Available: https://apliter.com/wp-content/uploads/2019/09/FLIR-FLIR-ONE-PRO-C%C3%A1mara-termogr%C3%A1fica-para-smartphone-Ficha-t%C3%A9cnica.pdf. [Último acceso: 29 01 2021].

Language:
Modified: 2019-04-11
Formatted: 2019-04-11

Website

http://www.flir.com

Customer support

http://support.flir.com

Disclaimer

Specifications subject to change without further notice. Camera models and accessories subject to regional market considerations. License procedures may apply. Products described herein may be subject to US Export Regulations. Please refer to exportquestions@flir.com with any questions.

Key features
VividIR Image Processing • The most advanced image resolution enhancement detects the thermal details you need to find the problems fast. • FLIR MSX embosses visible edges from the 1440 × 1080 HD camera onto the thermal imagery to create a sharper, easier to understand image. OneFit Connector • Adjust the length of the connector up to an additional 4 mm to fit your phone's protective case.

Imaging and optical data	
NETD	70 mK
Field of view	55° × 43°
Minimum focus distance	• Thermal: 0.15 m (0.49 ft.) • MSX: 0.3 m (0.98 ft.)
Spatial resolution (IFOV)	6.5 mrad/pixel
F-number	1.1
Image frequency	8.7 Hz
Focus	Focus free

Detector data	
Focal Plane Array	Uncooled microbolometer
Spectral range	8–14 µm
Detector pitch	12 µm
IR sensor size	160 × 120

Measurement	
Object temperature range	–20°C to +400°C (–4°F to +752°F)
Accuracy	±3°C (±5.4°F) or 5%, typical percent of the difference between ambient and scene temperature. Applicable 60 s after start-up when the unit is within +15 °C to +35°C (+59°F to +95° F) and the scene is within +5°C to +120°C (+41°F to +248°F)

P/N: 435-0011-03

#435-0011-03; r. 56720;

Set-up	
Set-up commands	Local adaptation of units, language, date, and time formats
Languages	Czech, Danish, Dutch, English, Estonian, Finnish, French, German, Greek, Hungarian, Italian, Japanese, Korean, Norwegian, Polish, Portuguese, Russian, Simpl. Chinese, Spanish, Swedish, Trad. Chinese, Turkish. Dependent on the language set in the mobile phone.

Lamp	
Lamp	Uses the flashlight of the mobile phone.

Storage of images	
Storage of images	Yes, in the gallery of the mobile phone.
Image file format	• Standard JPEG • 16-bit measurement data included
Video file format	MPEG-4 (MP4)

Digital camera	
Digital camera	1440 × 1080 pixels
Digital camera, focus	Fixed focus 15 cm – infinity

Data communication interfaces	
USB, connector type	Micro USB
USB, standard	USB 2.0

Power system	
Battery type	Rechargeable Li-ion polymer battery
Battery voltage	3.7 V
Battery operating time	1 h
Charging system	Female USB-C (5V / 1A)
Charging time	40 min.
Power management	Automatic shut-down

Environmental data	
Operating temperature range	0°C to +35°C (+32°F to +95°F) Battery charging 0°C to +30°C (+32°F to +86°F)
Storage temperature range	–20°C to +60°C (–4°F to +140°F)
Drop	1.8 m (5.9 ft)

Compliance	
Battery regulations	UL 1642, EN 62133 ED2
EMC	• EN 61000-6-3 • EN 61000-6-1 • FCC 47 CFR Part 15 Class B
Magnetic fields	EN 61000-4-8
RoHS	RoHs 2011/65/EC
WEEE	WEEE 2012/19/EC

FLIR ONE PRO, Android Micro-USB

P/N: 435-0011-03

#435-0011-03; r. 56720;

App	
Auto orientation	Yes
Image adjustment (alignment calibration)	Yes
VividIR	Yes
Capture modes	• Video • Photo • Time lapse
Image presentation modes	• Infrared image • Visual image • MSX • Gallery
Measurement analysis	Adjustable spots and areas of interest; • 3 spots • 3 rectangular areas (max.) • 3 circular areas (max.) Resolution 0.1°C / 0.1°F
Emissivity correction	Yes; • matte • semi-matte • semi-glossy • glossy
Measurements correction	• Emissivity • Reflected apparent temperature +22°C (+72° F)
Color palettes	• Iron • Rainbow • Rainbow HC • Gray • Arctic • Lava • Wheel • Hottest • Coldest
Camera software update	Yes
Battery indicator	0-100%

Physical data	
Weight (incl. Battery)	36.5 g (1.3 oz)
Size (L × W × H)	68 × 34 × 14 mm (2.7 × 1.3 × 0.6 in.)
Housing material	• PC and ABS, partially covered with TPE • Aluminum
Color	Black and gray

ANEXO 28. Seek Thermal© , «Thermal.com,» 2020. [En línea]. Available: https://www.thermal.com/uploads/1/0/1/3/101388544/compactpro-sellsheet-usav1.pdf. [Último acceso: 15 02 2021].

CompactPRO

AFFORDABLE, HIGH-PERFORMANCE THERMAL IMAGING FOR YOUR SMARTPHONE.

KEY CAMERA SPECS

- 320 x 240 Thermal Sensor
- 32° Field of View
- -40 to 626F Temperature Range
- 6 inches to 1,800 feet Distance
- Works Day & Night
- Waterproof Carrying Case

Seek thermal

thermal.com

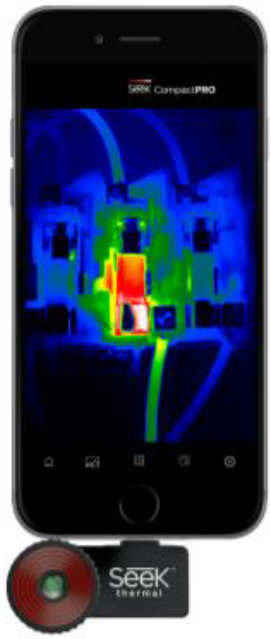

CompactPRO is our most advanced thermal imaging camera designed for your smartphone. Made for iPhone® and Android™ top models, this highly-portable thermal imaging camera features a large, 320x240 thermal sensor with high sensitivity and a wide, 32-degree field of view. Offering adjustable thermal span, level, and emissivity settings, the CompactPRO delivers unprecedented high-resolution thermal imaging and software capabilities available at this price.

Designed and Manufactured in Santa Barbara, California with Global Components.

Product Name:	Seek CompactPRO
Product Type:	Thermal Imaging Camera Made for Smartphones
Seek CompactPRO Made for iPhone:	UPC: 855753005617 Part Number: LQ-AAAX
Seek CompactPRO Made for Android:	UPC: 855753005631 Part Number: UQ-AAAX
Export Regulations	Subject to US EAR Export Regulations.

Single Unit	
Included in the box:	• Seek CompactPRO • Waterproof Carrying Case
Device Dimensions (H x W x D)	1 x 1.75 x 1 inches
Device Weight:	.5 ounces
Box Dimensions (H x W x D)	7 x 3.75 x 1.75 inches
Box Weight:	8.3 ounces

KEY FEATURES

320 x 240 High-Resolution Thermal Sensor
76,800 temperature pixels for maximum image clarity and sensitivity

Adjustable Emissivity
Calibrate for reflective surfaces when accuracy is critical

Wide, 32-Degree Field of View
Easily scan a large area to identify potential hazards in seconds

Focusable Lens for Quick Identification
Aim and focus from 6 inches to 1,800 feet for the sharpest image

Utilizes the Power and Display of Your Smartphone
Intuitive, free mobile app available on Google Play and iTunes App Store

Waterproof Case that Protects
Comes with its own waterproof case to withstand the elements

BENEFITS & USES

Connect-and-Detect Convenience
Pocket-sized, highly portable, and easy to use

See More Thermal Detail Where You Need it Most
Level and span controls let you isolate and capture the details that matter

Accurately Inspect Mechanical and Electrical Equipment
Diagnose and assess the problem source quickly

Safely Monitor Hazardous Environments
Evaluate potentially dangerous situations from a safe distance

Time of Day Won't Slow You Down
Safely examine any job site in daylight or total darkness

Easily Document and Share
Record images and video of industrial inspections for accurate documentation

TECHNICAL SUMMARY

SPECIFICATIONS	DESCRIPTION
Thermal Sensor	320 x 240 (76,800 pixels)
Detection Distance	6 inches to 1,800 feet
Field of View	32 Degree FOV
Temperature Range	-40°F to 626°F
Frame Rate	< 9 Hz
Focus	Adjustable Focus
Lens Material	Chalcogenide
Microbolometer	Vanadium Oxide
Thermal Sensitivity	< 70 mK
Spectral Range	7.5 - 14 Microns
User Interface	Free Seek Thermal Mobile App
Temp. Display Scale	Fahrenheit, Celsius, or Kelvin
Color Palettes	9 Options
Storage Media	Stores Directly to Smartphone
Battery	Low power provided by smartphone (280 mW)
Phone Compatibility	Top iPhone® and Android™ models

For support and user guides
visit **support.thermal.com**

MOBILE APP

The free Seek Thermal app allows you to customize your experience, record images and videos directly to your smartphone, and easily share them. Product registration required through app at first-time set up.

Download on the App Store

GET IT ON Google play

USER INTERFACE

PHOTO & VIDEO

Capture and share thermal photos and videos

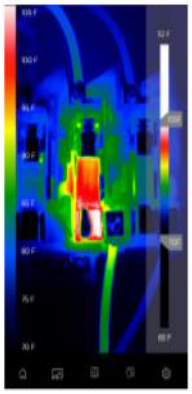

SPAN & LEVEL

Isolate and capture the thermal details that matter

EMISSIVITY

Calibrate for reflective surfaces when accuracy is critical

THERMAL APPLICATIONS

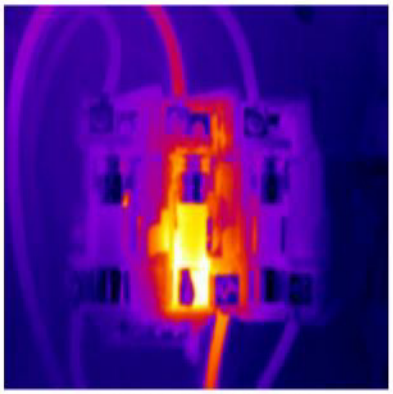

ELECTRICAL INSPECTION

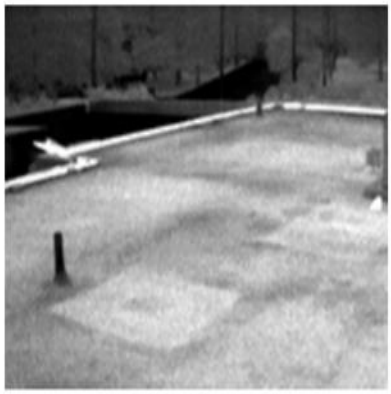

ROOF INSPECTION

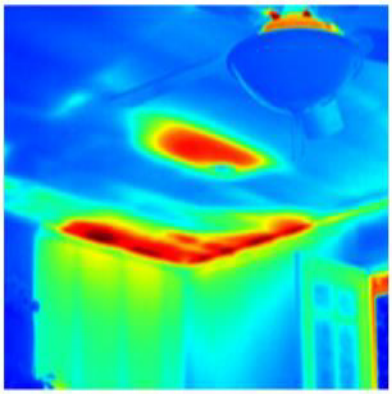

INSULATION & HVAC INSPECTION

ANEXO 29. Fluke Corporation©, «Fluke.com,» 2021. [En línea]. Available: https://www.fluke.com/es-ec/producto/camaras-termicas/tis60plus. [Último acceso: 15 02 2021].

Especificaciones: Cámara termográfica Fluke TiS60+

Principales características	
Resolución espacial (IFOV)	1,86 mrad, D:S (relación de distancia al objetivo) 532:1
Resolución de infrarrojos	320 x 240 (76.800 píxeles)
Campo de visión	34,1 °H x 25,6 °V
Sistema de enfoque	Fijo
Distancia focal mínima	46 cm (18")
Pantalla de alta resistencia	LCD de 320 x 240 y 3,5" (panorámica de 8,9 cm)
Diseño ergonómico	Diseñada para su uso con una sola mano

Medida de temperatura	
Rango de temperatura (no calibrada por debajo de -10 °C)	-20 °C a 400 °C (-4 °F a 752 °F)
Precisión	± 2 °C o 2% (a 25 °C nominales, la mayor de ambas)
Sensibilidad térmica (NETD)	≤ 0,045 °C a una temp. del objetivo de 30 °C (45 mK)
Corrección de emisividad en pantalla	Sí (valor y tabla)
Compensación de temperatura reflejada en el fondo de la pantalla	Sí
Corrección de transmitancia en pantalla	No

ANEXO 30. AsIAP, «Asociación de Informáticos del Uruguay,» 2003. [En línea]. Available: http://www.asiap.org/AsIAP/index.php/raee/300-articulos/3004-que-es-el-rohs-y-por-que-es-importante. [Último acceso: 01 02 2021].

Qué es el RoHS y por qué es importante

RoHS es una sigla que proviene del Inglés y significa: "Restriction of Hazardous Substances".

El RoHS es una directiva que adopto la Comunidad Europea en febrero de 2003 (2002/95/CE) y está orientada a reducir el uso de algunas sustancias peligrosas en aparatos eléctricos y electrónicos. Recientemente ha sido sustituida por la DIRECTIVA 2011/65/UE que abarca la anterior pero se extiende a otros productos además de los eléctricos y electrónicos.

Muchas veces se menciona como "libre de plomo", pero esta directiva restringe el uso de las siguientes seis sustancias a los niveles definidos:

1. Plomo (Pb) : <1000 ppm
2. De mercurio (Hg) : <100 ppm
3. Cadmio (Cd) : <100 ppm
4. El cromo hexavalente: (Cr VI) <1000 ppm
5. Los bifenilos polibromados (PBB): <1000 ppm
6. Los éteres difenil polibromados (PBDE) : <1000 ppm

Características y daños de estos productos:

ANEXO 31. Nativ Or , «CEO 360 Compliance,» [En línea]. Available: https://contact.telit.com/hubfs/Events/IoT%20Roadshow/2019/Minneapolis/Minneapolis%20Presentations/Telit_Technical_Workshop_2019_FCC_and_CE_Wireless_Certification_Nativ_Or.pdf. [Último acceso: 01 02 2021].

FCC & CE – Wireless Certification

REGULATORY TESTING FROM START TO CERTIFICATE

360compliance.co

EMC | Radio | Safety | Sustainability | Market Access | Cyber

360Compliance provides value delivered help you **SHORTEN TTM** with the most **COST EFFECTIVE** solutions while minimizing your risks

PRICES - FIXED COSTS FROM START TO CERTIFICATE

- Time Frame - the Faster TTM turnaround
- Full project management with almost no effort from your side
- Technical Support - Pretesting and debugging
- Testing & Certification - CE, FCC, UL-STD and more
- Global Market Access - Covering ~ 195 countries

3

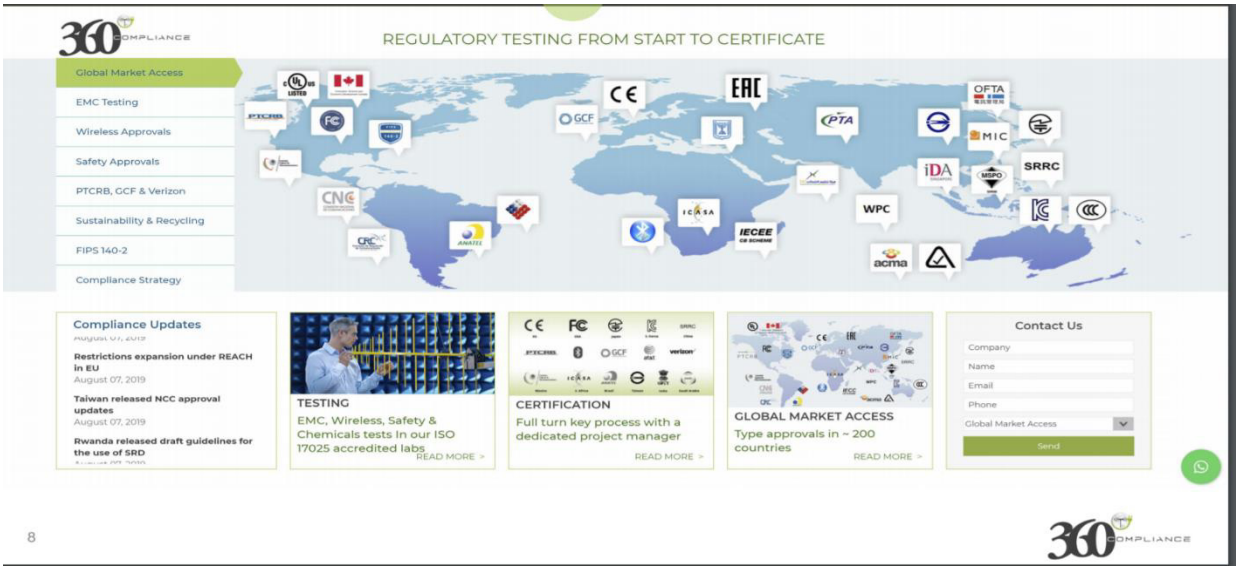

8

ANEXO 32. Diario Oficial de la Unión Europea, «Directiva 2014/30/UE del Parlamento Europeo y del Consejo,» *Diario Oficial de la Unión Europea,* vol. 30, nº L 96/79, pp. 1-28, 2014.

DIRECTIVA 2014/30/UE DEL PARLAMENTO EUROPEO Y DEL CONSEJO

de 26 de febrero de 2014

sobre la armonización de las legislaciones de los Estados miembros en materia de compatibilidad electromagnética (refundición)

(Texto pertinente a efectos del EEE)

EL PARLAMENTO EUROPEO Y EL CONSEJO DE LA UNIÓN EUROPEA,

Visto el Tratado de Funcionamiento de la Unión Europea y, en particular, su artículo 114,

Vista la propuesta de la Comisión Europea,

Previa transmisión del proyecto de acto legislativo a los Parlamentos nacionales,

Visto el dictamen del Comité Económico y Social Europeo [1],

De conformidad con el procedimiento legislativo ordinario [2],

Considerando lo siguiente:

(1) La Directiva 2004/108/CE del Parlamento Europeo y del Consejo, de 15 de diciembre de 2004, relativa a la aproximación de las legislaciones de los Estados miembros en materia de compatibilidad electromagnética y por la que se deroga la Directiva 89/336/CEE [3] debe modificarse en una serie de aspectos. En aras de una mayor claridad, conviene proceder a la refundición de dicha Directiva.

(2) El Reglamento (CE) nº 765/2008 del Parlamento Europeo y del Consejo, de 9 de julio de 2008, por el que se establecen los requisitos de acreditación y vigilancia del mercado relativos a la comercialización de los productos [4], regula la acreditación de los organismos de evaluación de la conformidad, adopta un marco para la vigilancia del mercado de los productos y para los controles de los productos procedentes de terceros países y establece los principios generales del marcado CE.

(3) La Decisión nº 768/2008/CE del Parlamento Europeo y del Consejo, de 9 de julio de 2008, sobre un marco común para la comercialización de los productos [5], establece principios comunes y disposiciones de referencia aplicables a toda la legislación sectorial con el fin de establecer una base coherente para la elaboración, revisión o refundición de dicha legislación. Conviene adaptar la Directiva 2004/108/CE a dicha Decisión.

(4) Los Estados miembros deben ser responsables de garantizar que las radiocomunicaciones, incluidas la recepción por radio y los servicios de radioaficionados operados de conformidad con la normativa sobre radiotransmisiones de la Unión Internacional de Telecomunicaciones (UIT), las redes de suministro eléctrico y las redes de telecomunicaciones, así como los equipos conectados a los mismos, estén protegidas de las perturbaciones electromagnéticas.

(5) Las disposiciones de Derecho nacional de protección frente a las perturbaciones electromagnéticas necesitan armonizarse para garantizar la libre circulación de aparatos eléctricos y electrónicos sin reducir los niveles justificados de protección en los Estados miembros.

(6) La presente Directiva se aplica a aquellos productos que constituyan una novedad en el mercado de la Unión en el momento de introducirse en el mismo, es decir, que o bien se trata de productos nuevos fabricados por un fabricante establecido en la Unión, o bien son productos, nuevos o de segunda mano, importados de un tercer país.

(7) La presente Directiva debe aplicarse a toda forma de suministro, incluida la venta a distancia.

(8) Entre los equipos a los que se aplica la presente Directiva deben figurar tanto los aparatos como las instalaciones fijas. No obstante, deben formularse disposiciones distintas para cada grupo, dado que los aparatos como tales pueden circular libremente dentro de la Unión, mientras que las instalaciones fijas se instalan para un uso permanente y en un sitio predefinido como conjuntos de distintos tipos de aparatos y, cuando procede, de otros dispositivos. La composición y función de estas instalaciones corresponde en la mayoría de los casos a las necesidades particulares de sus operadores.

(9) Cuando la presente Directiva regule aparatos, debe aplicarse a aparatos acabados e introducidos en el mercado de la Unión. Ciertos componentes o subconjuntos deben, bajo determinadas condiciones, considerarse aparatos si están a disposición del usuario final.

(10) La presente Directiva no debe aplicarse a los equipos radioeléctricos y los equipos terminales de telecomunicación dado que estos ya están regulados por la Directiva

[1] DO C 181 de 21.6.2012, p. 105.
[2] Posición del Parlamento Europeo de 5 de febrero de 2014 (no publicada aún en el Diario Oficial) y Decisión del Consejo de 20 de febrero de 2014.
[3] DO L 390 de 31.12.2004, p. 24.
[4] DO L 218 de 13.8.2008, p. 30.
[5] DO L 218 de 13.8.2008, p. 82.

ANEXO 33. EPSMA, «PFC Harmonic Current Emissions – Guide to EN61000-3-2:2014,» *European Power Supplies Manufacturers' Association ,* vol. 2, nº 3-2, pp. 1-19, 2018.

norma española

UNE-EN 61000-6-1

Junio 2007

TÍTULO

Compatibilidad electromagnética (CEM)

Parte 6-1: Normas genéricas

Inmunidad en entornos residenciales, comerciales y de industria ligera

(IEC 61000-6-1:2005)

Electromagnetic compatibility (EMC). Part 6-1: Generic standards. Immunity for residential, commercial and light-industrial environments. (IEC 61000-6-1:2005).

Compatibilité électromagnétique (CEM). Partie 6-1: Normes génériques. Immunité pour les environnements résidentiels, commerciaux et de l'industrie légère. (CEI 61000-6-1:2005).

CORRESPONDENCIA

Esta norma es la versión oficial, en español, de la Norma Europea EN 61000-6-1:2007, que a su vez adopta la Norma Internacional IEC 61000-6-1:2005.

OBSERVACIONES

Esta norma anulará y sustituirá a la Norma UNE-EN 61000-6-1:2002 antes de 2009-12-01.

ANTECEDENTES

Esta norma ha sido elaborada por el comité técnico AEN/CTN 208 *Compatibilidad Electromagnética* cuya Secretaría desempeña UNESA.

Editada e impresa por AENOR
Depósito legal: M 28399:2007

LAS OBSERVACIONES A ESTE DOCUMENTO HAN DE DIRIGIRSE A:
AENOR Asociación Española de Normalización y Certificación
C Génova, 6
28004 MADRID-España
Teléfono 91 432 60 00
Fax 91 310 40 32

21 Páginas
Grupo 15

Compatibilidad electromagnética (CEM)
Parte 6-1: Normas genéricas
Inmunidad en entornos residenciales, comerciales y de industria ligera

1 OBJETO Y CAMPO DE APLICACIÓN

Esta parte de la Norma IEC 61000 sobre los requisitos de inmunidad en materia de compatibilidad electromagnética se aplica a los aparatos eléctricos y electrónicos destinados a ser utilizados en los entornos residenciales, comerciales y de la industria ligera, según se describe más adelante. Esta norma cubre los requisitos de inmunidad en la gama de frecuencias de 0 Hz a 400 GHz. No es necesario realizar ensayos a frecuencias para las cuales no se especifiquen requisitos.

Esta norma genérica de inmunidad en materia de compatibilidad electromagnética (CEM) se aplica en ausencia de una norma de inmunidad CEM específica aplicable a un producto o a una familia de productos.

Esta norma se aplica a los aparatos destinados a ser conectados directamente a la red pública de alimentación de baja tensión o a una fuente específica de corriente continua destinada a servir de interfaz entre el aparato y la red pública de alimentación de baja tensión. Esta norma se aplica igualmente a los aparatos alimentados por pilas o baterías o por un sistema de distribución no público de baja tensión, pero no industrial, cuando estos aparatos se destinan para su utilización en los emplazamientos descritos a continuación.

Los entornos cubiertos por esta norma son los lugares residenciales, los locales comerciales y de la industria ligera, tanto interiores como exteriores. La lista siguiente, aunque no es exhaustiva, da una indicación de los sitios que se incluyen:

- propiedades residenciales, por ejemplo casas, apartamentos;
- lugares de venta al por menor, por ejemplo tiendas, supermercados;
- centros de negocios, por ejemplo oficinas, bancos;
- locales de espectáculos públicos, por ejemplo cines, bares, clubes de baile;
- lugares al exterior, por ejemplo estaciones de servicio, aparcamientos, centros de diversión y deportivos;
- locales de la industria ligera, por ejemplo talleres, laboratorios, centros de servicios.

Los lugares que se caracterizan por recibir directamente el suministro en baja tensión de la red pública se consideran como residenciales, comerciales y de la industria ligera.

El objetivo de esta norma es definir los requisitos de los ensayos de inmunidad a las perturbaciones continuas y transitorias, conducidas y radiadas, incluidas las descargas electrostáticas, para los aparatos definidos en el campo de aplicación.

Los requisitos de inmunidad han sido seleccionados para asegurar un nivel adecuado de inmunidad para los aparatos utilizados en lugares residenciales, comerciales y de la industria ligera. Sin embargo, estos niveles no cubren los casos extremos que puedan aparecer en cualquier lugar, pero con muy baja probabilidad de ocurrir. En esta norma no se incluyen, por motivos de ensayo, todos los tipos de perturbaciones, sino únicamente aquellos considerados como relevantes para los aparatos cubiertos por la norma. Estos requisitos de ensayo representan los requisitos esenciales de compatibilidad electromagnética concernientes a la inmunidad.

NOTA 1 En la Norma IEC 61000-4-1 se da información sobre otros tipos de perturbaciones.

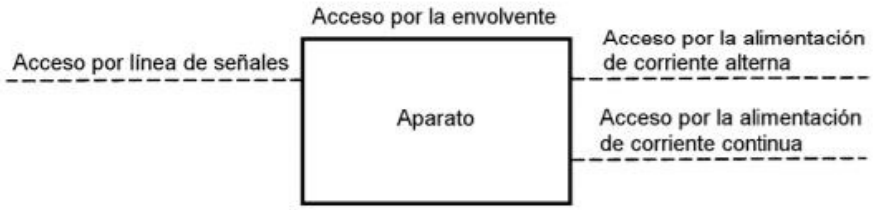

Figura 1 – Ejemplos de accesos

3.2 acceso por la envolvente:
Frontera física del aparato a través de la cual los campos electromagnéticos pueden radiarse o con la que pueden chocar.

3.3 acceso por los cables:
Punto en el que un conductor o un cable esta conectado al aparato.

NOTA Como ejemplos están los accesos de señales y de potencia.

3.4 acceso de señales:
Acceso por el que un conductor o un cable que transporta información para transmisión de datos está conectado al aparato.

NOTA Como ejemplos están las líneas de entrada y salida analógicas y de control; buses de datos; redes de comunicaciones, etc.

3.5 acceso de potencia:
Punto por el que un conductor o un cable, que transporta la energía eléctrica primaria necesaria para el funcionamiento del aparato o de un aparato auxiliar, está conectado al aparato.

3.6 redes públicas de alimentación:
Líneas eléctricas a las que tienen acceso cualquier categoría de consumidores, siendo regidas por un organismo que asegura el suministro y/o la distribución de la energía eléctrica.

3.7 líneas de gran longitud:
Líneas conectadas a un acceso de señales, que en el interior de un edificio tienen una longitud superior a 30 m, o que salen del edificio (incluyendo las líneas de las instalaciones exteriores).

3.8 baja tensión:
Tensión eléctrica de un valor inferior a un límite adoptado por convención.

(véase el VEI 151-15-03)

4 CRITERIOS DE APTITUD PARA LA FUNCIÓN

La variedad y diversidad de los aparatos definidos en el campo de aplicación de esta norma hace imposible la definición de criterios precisos para la evaluación de los resultados de los ensayos de inmunidad.

Si, como resultado de la aplicación de los ensayos definidos en esta norma, el aparato llega a ser peligroso o inseguro, se debe considerar que el aparato no ha superado el ensayo.

Una descripción funcional y una definición de los criterios de aptitud para la función, durante o como consecuencia de los ensayos de CEM, deben ser proporcionados por el fabricante y anotados en el informe del ensayo basado en los siguientes criterios para cada ensayo como se especifica en las tablas 1 a 4.

ANEXO 34. IEC, «Electromagnetic compatibility (EMC) Limits – Limitation of voltage changes, voltage fluctuations and flicker in public low-voltage supply systems, for equipment with rated current ≤ 16 A per phase and not subject to conditional connection,» *International Electrotechnical Commission,* vol. 3, nº 3-3, pp. 1-24, 2013.

IEC 61000-3-3

Edition 3.2 2021-03
CONSOLIDATED VERSION

INTERNATIONAL STANDARD

Electromagnetic compatibility (EMC) –
Part 3-3: Limits – Limitation of voltage changes, voltage fluctuations and flicker in public low-voltage supply systems, for equipment with rated current ≤ 16 A per phase and not subject to conditional connection

INTERNATIONAL
ELECTROTECHNICAL
COMMISSION

ICS 33.100.10

ISBN 978-2-8322-9622-6

INTERNATIONAL ELECTROTECHNICAL COMMISSION

ELECTROMAGNETIC COMPATIBILITY (EMC) –

Part 3-3: Limits – Limitation of voltage changes, voltage fluctuations and flicker in public low-voltage supply systems, for equipment with rated current ≤ 16 A per phase and not subject to conditional connection

FOREWORD

1) The International Electrotechnical Commission (IEC) is a worldwide organization for standardization comprising all national electrotechnical committees (IEC National Committees). The object of IEC is to promote international co-operation on all questions concerning standardization in the electrical and electronic fields. To this end and in addition to other activities, IEC publishes International Standards, Technical Specifications, Technical Reports, Publicly Available Specifications (PAS) and Guides (hereafter referred to as "IEC Publication(s)"). Their preparation is entrusted to technical committees; any IEC National Committee interested in the subject dealt with may participate in this preparatory work. International, governmental and non-governmental organizations liaising with the IEC also participate in this preparation. IEC collaborates closely with the International Organization for Standardization (ISO) in accordance with conditions determined by agreement between the two organizations.
2) The formal decisions or agreements of IEC on technical matters express, as nearly as possible, an international consensus of opinion on the relevant subjects since each technical committee has representation from all interested IEC National Committees.
3) IEC Publications have the form of recommendations for international use and are accepted by IEC National Committees in that sense. While all reasonable efforts are made to ensure that the technical content of IEC Publications is accurate, IEC cannot be held responsible for the way in which they are used or for any misinterpretation by any end user.
4) In order to promote international uniformity, IEC National Committees undertake to apply IEC Publications transparently to the maximum extent possible in their national and regional publications. Any divergence between any IEC Publication and the corresponding national or regional publication shall be clearly indicated in the latter.
5) IEC itself does not provide any attestation of conformity. Independent certification bodies provide conformity assessment services and, in some areas, access to IEC marks of conformity. IEC is not responsible for any services carried out by independent certification bodies.
6) All users should ensure that they have the latest edition of this publication.
7) No liability shall attach to IEC or its directors, employees, servants or agents including individual experts and members of its technical committees and IEC National Committees for any personal injury, property damage or other damage of any nature whatsoever, whether direct or indirect, or for costs (including legal fees) and expenses arising out of the publication, use of, or reliance upon, this IEC Publication or any other IEC Publications.
8) Attention is drawn to the Normative references cited in this publication. Use of the referenced publications is indispensable for the correct application of this publication.
9) Attention is drawn to the possibility that some of the elements of this IEC Publication may be the subject of patent rights. IEC shall not be held responsible for identifying any or all such patent rights.

This consolidated version of the official IEC Standard and its amendments has been prepared for user convenience.

IEC 61000-3-3 edition 3.2 contains the third edition (2013-05) [documents 77A/809/FDIS and 77A/816/RVD], its amendment 1 (2017-05) [documents 77A/952/FDIS and 77A/960/RVD] and its amendment 2 (2021-03) [documents 77A/1075/CDV and 77A/1093/RVC].

In this Redline version, a vertical line in the margin shows where the technical content is modified by amendments 1 and 2. Additions are in green text, deletions are in strikethrough red text. A separate Final version with all changes accepted is available in this publication.

ANEXO 35. ETSI, «Electromagnetic compatibility and Radio spectrum Matters (ERM); Impact of CENELEC EN 55032 on ETSI EMC Standards,» *European Telecommunications Standards Institute,* vol. 1.1.1, nº 1, pp. 1-12, 2015.

4 ETSI EMC deliverables

4.1 Harmonised EMC standards

ETSI currently produces and maintains the following harmonised EMC standards; ETSI EN 300 386 [i.4], ETSI EN 301 489 [i.5] series and ETSI EN 301 843 [i.6] series. At the present time all of these reference CENELEC EN 55022 [i.2] for their emission limits and/or methods or measurements.

4.2 Other EMC Standards

4.2.1 ETSI Standard ETSI ES 201 468

ETSI ERM WG EMC also produces and maintains ETSI ES 201 468 [i.7].

ETSI ES 201 468 [i.7] clause 8 references ETSI EN 300 386 [i.4] for all of its emission requirements, therefore any changes made to ETSI EN 300 386 [i.4] would automatically be carried though to the present document without requiring any work to be done on ETSI ES 201 468 [i.7].

It is therefore deemed that no action is required on ETSI ES 201 468 [i.7] as a result of the publication of CENELEC EN 55032 [i.1].

4.2.2 European Norm ETSI EN 300 127

ETSI EN 300 127 [i.15] Radiated emission testing of physically large telecommunication systems. Although this is an EN it is not a harmonised standard. This standard references CENELEC EN 55022 [i.2] for both limits and methods of measurement,

4.3 Other ETSI deliverables relating to EMC

4.3.1 Summary

ETSI has also published and maintains five guidance documents dealing with various aspects of EMC. These are; ETSI EG 202 414 [i.8], ETSI TR 103 088 [i.9], ETSI TR 101 651 [i.10], ETSI TR 102 552 [i.11] and ETSI TR 102 070-1 [i.14].

4.3.2 ETSI Guide ETSI EG 202 414

ETSI EG 202 414 [i.8] provides information on the demonstration of conformity for after market Electric/electronic Sub-Assemblies (ESAs) to the motor vehicle EMC Directive 2004/104/EC [i.17].

Having carefully studied the present document it is clear that it makes no reference to CENELEC EN 55022 [i.2] and is therefore not impacted by the publication of CENELEC EN 55032 [i.1].

4.3.3 Technical Report ETSI TR 103 088

ETSI TR 103 088 [i.9] is a guidance document that is designed to help the user apply the ETSI EN 301 489 [i.5] series by providing detail upon the changes between the different editions within the ETSI EN 301 489 [i.5] series and information as to the coverage of each part within the series.

Although the technical report does not specify any limits, it does highlight changes between different versions of the individual parts of the ETSI EN 301 489 [i.5] series and as a consequence could require updating once all of the changes to these parts have been completed.

4.3.4 Technical Report ETSI TR 101 651

ETSI TR 101 651 [i.10] provides information on the electromagnetic environmental conditions encountered where telecommunications equipment is installed and is a compilation of data concerning electromagnetic environmental conditions.

Having carefully studied the present document it is clear that it makes no reference to CENELEC EN 55022 [i.2] and is therefore not impacted by the publication of CENELEC EN 55032 [i.1].

4.3.5 Technical Report ETSI TR 102 552

ETSI TR 102 552 [i.11] is a code of practice relating to the standardization of the measurement of emissions, data collection and reporting of results for powerline systems.

Having carefully studied the present document it is clear that it makes no reference to CENELEC EN 55022 [i.2] and is therefore not impacted by the publication of EN 55032 [i.1].

4.3.6 Technical Report ETSI TR 102 070-1

ETSI TR 102 070-1 [i.14] is a guide on the assessment of EMC in combined radio/non-radio product and multi-radio products. CENELEC EN 55022 [i.2] is quoted in an annex of the present document to show the range of standards used for different product families to detail their emission limits.

It should be noted that the conclusions and recommendations from the present document were incorporated into annex C of ETSI EN 301 489-1 [i.5].

5 Comparison between CENELEC EN 55032 and CENELEC EN 55022

5.1 Introduction

For the purposes of the present document, comparisons are between CENELEC EN 55032 [i.1]: and CENELEC EN 55022:2010 [i.2]

5.2 Radiated Emissions

5.2.1 Limits

Table 1 shows the radiated emissions limits from CENELEC EN 55022 [i.2] and CENELEC EN 55032 [i.1].

Table 1: Comparison of radiated emission limits

		80 - 230 MHz	230 - 1 000 MHz	1 - 3 GHz	3 - 6 GHz
EN55022	Class A	40 dBµV/m	47 dBµV/m	76 dBµV/m	80 dBµV/m
	Class B	30 dBµV/m	37 dBµV/m	70 dBµV/m	74 dBµV/m
EN55032	Class A	40 dBµV/m	47 dBµV/m	76 dBµV/m	80 dBµV/m
	Class B	30 dBµV/m	37 dBµV/m	70 dBµV/m	74 dBµV/m
		10 m measurement distance, quasi peak values		3 m measurement distance, peak values	

From the table above it can be seen that the radiated emission limits in CENELEC EN 55032 [i.1] are identical to those contained within CENELEC EN 55022 [i.2].

5.2.2 Measurement Methods

Although the table above quotes limits for a 10 m measurements distance for both CENELEC EN 55022 [i.2] and CENELEC EN 55032 [i.1], there is also the option of conducting these tests at a 3 m measurement distance when using CENELEC EN 55032 [i.1]. Where this is used the limits are 10 dB higher for both class A and class B. It should be remembered that this option was not available under CENELEC EN 55022 [i.1] and as a result it is not possible to provide a comparison between the two standards when using this measurement distance.

5.2.3 Conclusion

The information shown in clauses 5.1.1 and 5.1.2 shows that a piece of equipment meeting the requirements of CENELEC EN 55022 [i.2] for radiated emissions has a high probability of satisfying the requirements of CENELEC EN 55032 [i.1] for radiated emissions.

5.3 Conducted Emissions

5.3.1 Limits

Table 2 shows the conducted emission limits from CENELEC EN 55022 [i.2] and CENELEC EN 55032 [i.1].

Table 2: Comparison of conducted emission limits

		AC Mains			Signal and Control lines	
		150 - 500 KHz	0,5 - 5 MHz	5 - 30 MHz	150 - 500 KHz	0,5 - 30 MHz
CENELEC EN 55022 [i.2]	Class A	79 dBµV	73 dBµV	73 dBµV	97-87 dBµV	87 dBµV
	Class B	66-56 dBµV	56 dBµV	60 dBµV	84-74 dBµV	74 dBµV
CENELEC EN 55032 [i.1]	Class A	79 dBµV	73 dBµV	73 dBµV	97-87 dBµV	87 dBµV
	Class B	66-56 dBµV	56 dBµV	60 dBµV	84-74 dBµV	74 dBµV
NOTE: All values are quasi - peak values.						

From table 2 it can be seen that the conducted emission limits in CENELEC EN 55032 [i.1] are identical to those contained within CENELEC EN 55022 [i.2].

5.3.2 Measurement Methods

Although the two standards are constructed in a very different manner, close examination does not reveal any significant differences in the test methods used for conducted measurements on the types of ports seen on equipment subject to ETSI standards.

5.4 Class A versus Class B

CENELEC EN 55022 [i.2] contains definitions for class A and class B equipment, reproduced below:

4.1 Class B ITE

Class B ITE is a category of apparatus which satisfies the class B ITE disturbance limits.
Class B ITE is intended primarily for use in the domestic environment and may include:
- *equipment with no fixed place of use; for example, portable equipment powered by built-in batteries;*
- *telecommunication terminal equipment powered by a telecommunication network;*
- *personal computers and auxiliary connected equipment.*

NOTE The domestic environment is an environment where the use of broadcast radio and television receivers may be expected within a distance of 10 m of the apparatus concerned.

4.2 Class A ITE

Class A ITE is a category of all other ITE which satisfies the class A ITE limits but not the class B ITE limits. The following warning shall be included in the instructions for use:

WARNING: This is a class A product. In a domestic environment this product may cause radio interference in which case the user may be required to take adequate measures.

Whilst CENELEC EN 55032 [i.1] retains the concept of class A and class B equipment, the wording used (reproduced below) has changed substantially:

4 Classification of equipment

This standard defines Class A equipment and Class B equipment associated with two types of end-use environment.

Class A equipment is equipment which meets the requirements given in Table A.2, Table A.3,Table A.8, and Table A.10, using the limitations defined in Table A.1 and Table A.7.

Class B equipment is equipment which meets the requirements given in Table A.4, Table A.5,Table A.6, Table A.9, Table A.11 and Table A.12, using the limitations defined in Table A.1 and Table A.7.

The Class B requirements for equipment are intended to offer adequate protection to broadcast services within the residential environment.

ANEXO 36. ISL , «International Standards Laboratory,» 02 08 2017. [En línea]. Available: https://www.winstar.com.tw/uploads/files/f5c8e0a6d0e2e68dcf6f8347d1845011.pdf. [Último acceso: 01 02 2021].

ISL International Standards Laboratory http://www.isl.com.tw

Certificate

Issue Date: August 2, 2017
Ref. Report No. ISL-17LE479CE

Product Name	:	Display Module
Model(s)	:	Display Module
Brand	:	WINSTAR
Applicant	:	WINSTAR DISPLAY CO., LTD.
Address	:	Central Taiwan Science Park 5F., No. 31, Keya Rd., Daya Dist., Taichung City 428, Taiwan

We, **International Standards Laboratory**, hereby certify that:

The device bearing the trade name and model specified above has been shown to comply with the applicable technical standards as indicated in the measurement report and was tested in accordance with the measurement procedures specified in European Council Directive- EMC Directive 2014/30/EU. The device was passed the test performed according to :

CE

Standards:

EN 55032:2012+AC:2013, CISPR 32:2012
AS/NZS CISPR 32:2013
EN 55032:2015+AC:2016, CISPR 32: 2015+COR1:2016
AS/NZS CISPR 32:2015
EN 61000-3-2:2014 and IEC 61000-3-2:2014
EN 61000-3-3: 2013 and IEC 61000-3-3: 2013
EN 55024: 2010+A1:2015 and CISPR 24: 2010+A1:2015
EN 61000-4-2: 2009 and IEC 61000-4-2: 2008
EN 61000-4-3: 2006+A1: 2008 +A2: 2010 and
IEC 61000-4-3:2006+A1: 2007+A2: 2010
EN 61000-4-4:2012 and IEC 61000-4-4:2012
EN 61000-4-5: 2014 and IEC 61000-4-5: 2014
EN 61000-4-6:2014+AC:2015 and IEC 61000-4-6:2013
EN 61000-4-8: 2010 and IEC 61000-4-8: 2009
EN 61000-4-11: 2004 and IEC 61000-4-11: 2004

I attest to the accuracy of data and all measurements reported herein were performed by me or were made under my supervision and are correct to the best of my knowledge and belief. I assume full responsibility for the completeness of these measurements and vouch for the qualifications of all persons taking them.

International Standards Laboratory

Bert Chen / Director

☐ **Hsi-Chih LAB**:
No. 65, Gu Dai Keng Street, Hsi-Chih Dist.,
New Taipei City 221, Taiwan
Tel: 886-2-2646-2550; Fax: 886-2-2646-4641

☒ **Lung-Tan LAB**:
No. 120, Lane 180, Hsin Ho Rd., Lung-Tan Dist.,
Tao Yuan City 325, Taiwan
Tel: 886-3-407-1718; Fax: 886-3-407-1738

TAF Nemko ELA113A

TAF Nemko ELA1138

Declaration of Conformity

Name of Responsible Party:	WINSTAR DISPLAY CO., LTD.
Address of Manufacturer:	Central Taiwan Science Park 5F., No. 31, Keya Rd., Daya Dist., Taichung City 428, Taiwan
Declares that product:	Display Module
Model:	Display Module
Brand:	WINSTAR
Assembled by:	Same as above
Address:	Same as above

Conforms to the EMC Directive 2014/30/EU as attested by conformity with the following harmonized standards:

EN 55032:2012+AC:2013, CISPR 32:2012: Electromagnetic compatibility of multimedia equipment - Emission requirements
AS/NZS CISPR 32:2013: Electromagnetic compatibility of multimedia equipment- Emission requirements
EN 55032:2015+AC:2016, CISPR 32: 2015+COR1:2016: Electromagnetic compatibility of multimedia equipment - Emission requirements.
AS/NZS CISPR 32:2015: Electromagnetic compatibility of multimedia equipment- Emission requirements

Performed Item	Test Performed	Deviation	Result
Conducted emissions from the AC mains power ports	Yes	No	PASS
Telecommunication Port Conducted Emissions (asymmetric mode)	Yes	No	PASS
Radiated emissions at frequencies below 1 GHz	Yes	No	PASS
Radiated emissions at frequencies above 1 GHz	Yes	No	PASS
Radiated emissions from FM receivers	N/A	N/A	N/A
Voltage Disturbance Emissions at Antenna Terminals	N/A	N/A	N/A
Differential voltage emissions	N/A	N/A	N/A
Outdoor units of home satellite receiving systems	N/A	N/A	N/A

<to be continued>

EN 55024:2010+A1:2015 and CISPR 24:2010+A1:2015: Information technology equipment-Immunity characteristics - Limits and methods of measurement.

Standard	Description	Results	Criteria
EN 61000-4-2:2009 IEC 61000-4-2:2008	Electrostatic Discharge	Pass	B
EN 61000-4-3:2006+A1:2008 +A2:2010 IEC 61000-4-3:2006+A1:2007+A2:2010	Radio-Frequency, Electromagnetic Field	Pass	A
EN 61000-4-4:2012 IEC 61000-4-4:2012	Electrical Fast Transient/Burst	Pass	B
EN 61000-4-5:2014 IEC 61000-4-5:2014	Surge	Pass	B
EN 61000-4-6:2014+AC:2015 IEC 61000-4-6:2013	Conductive Disturbance	Pass	A
EN 61000-4-8:2010 IEC 61000-4-8:2009	Power Frequency Magnetic Field	Pass	A
EN 61000-4-11:2004 IEC 61000-4-11:2004	Voltage Dips / Short Interruption and Voltage Variation		
	>95% in 0.5 period	Pass	B
	30% in 25 period	Pass	C
	>95% in 250 period	Pass	C

Standard	Description	Results
EN 61000-3-2:2014 IEC 61000-3-2:2014	Limits for harmonics current emissions	Pass
EN 61000-3-3:2013 IEC 61000-3-3:2013	Limits for voltage fluctuations and flicker in low-voltage supply systems.	Pass

We, WINSTAR DISPLAY CO., LTD., hereby declare that the equipment bearing the trade name and model number specified above was tested conforming to the applicable Rules under the most accurate measurement standards possible, and that all the necessary steps have been taken and are in force to assure that production units of the same equipment will continue to comply with the requirements.

WINSTAR DISPLAY CO., LTD.
Date: August 2, 2017

RESULTADOS Y DISCUSIÓN

ANEXO 36. LYFTRACK©, «https://lyftrack.com/,» LYFTRACK©, 2020. [En línea]. Available: https://lyftrack.com/. [Último acceso: 21 03 2021]. Elemento a comparar con relacion al dispositivo termografico, mediante entrada visual.

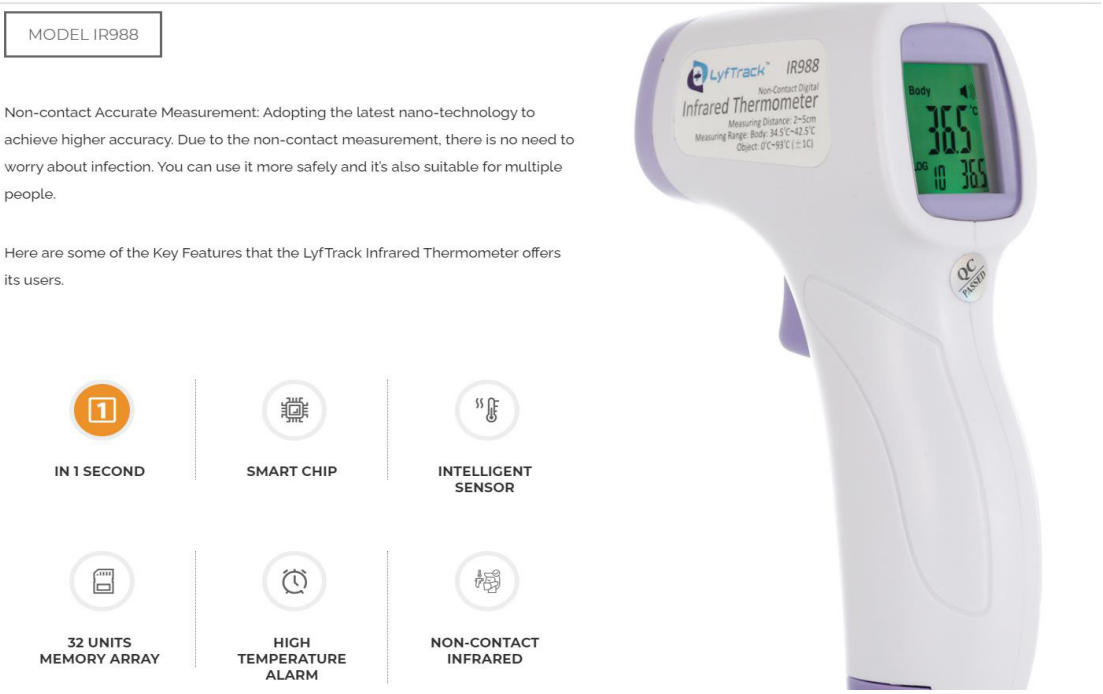

ANEXO 37. MATLAB Resource FLIR, «Face-Detection-and-Tracking-Sample-Code.zip,» FLIR,14022016[Enlínea].Available:https://flir.app.box.com/s/o1t1safir7o2soqj2vnv4vy7e1qnmz9a. [Último acceso: 03 03 2021]. Software para recopilacion de datos.

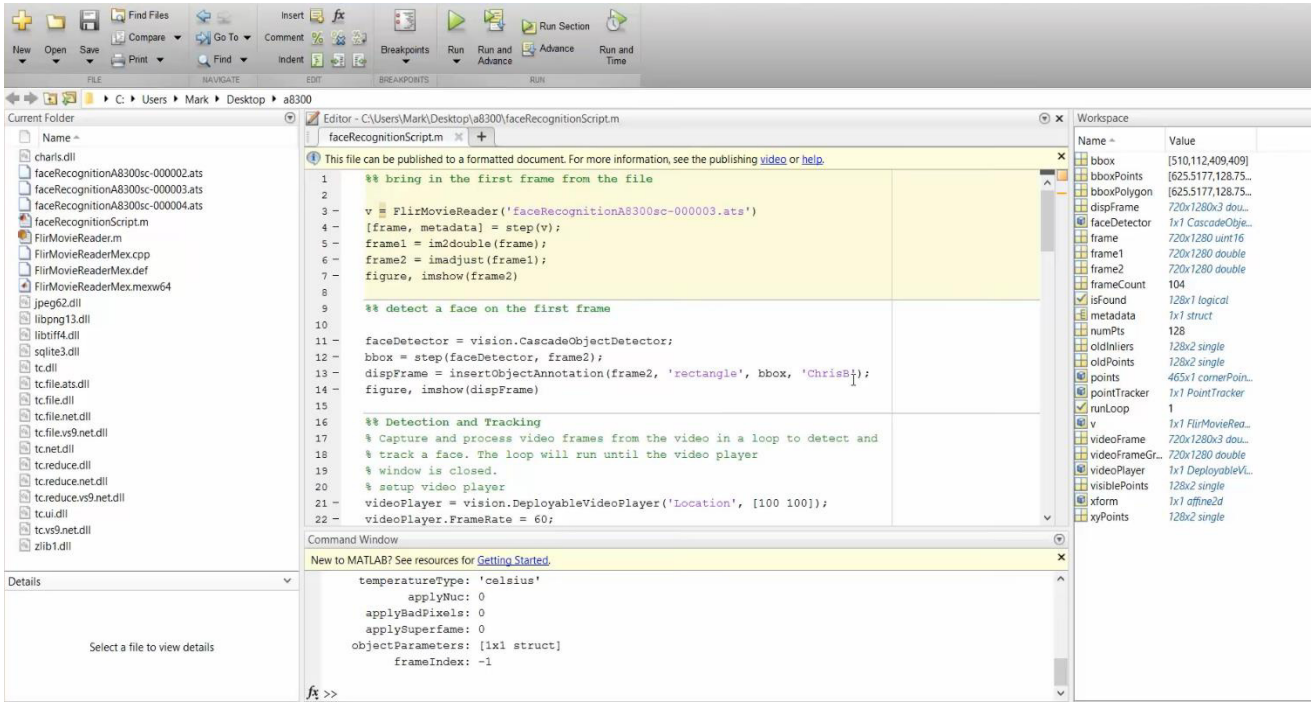

ANEXO 38. Tabulación y análisis de datos de datos primera etapa.

CAMARA TERMOGRÁFICA UIDE (GRUPO DE 2)

N° Periodos de medición	Hora	Rango de medida (m)	Puntos de medición	Lugar de medición de temperatura	Temperatura en °C Persona 1	Temperatura en °C Persona 2	Distancia entre participantes (m)
1	19:16:00	0,5 m	1	Cara	30,6	25,02	0,1
	19:16:00	1 m	1	Cuerpo	28,4	29	0,3
	19:16:00	1,5 m	1	Cuerpo	27,3	27,7	0,3
	19:16:00	2 m	1	Cuerpo	27,4	24,4	0,3
2	20:46:00	0,5 m	1	Cara	30,4	31,7	0,1
	20:46:00	1 m	1	Cuerpo	28,5	27,6	0,3
	20:46:00	1,5 m	1	Cuerpo	26,7	24,4	0,3
	20:46:00	2 m	1	Cuerpo	25,4	23,5	0,3
3	18:26:00	0,5 m	1	Cara	34,7	28,5	0,1
	18:26:00	1 m	1	Cuerpo	28,8	25,4	0,3
	18:26:00	1,5 m	1	Cuerpo	26,1	24,2	0,3
	18:26:00	2 m	1	Cuerpo	24,4	22,2	0,3

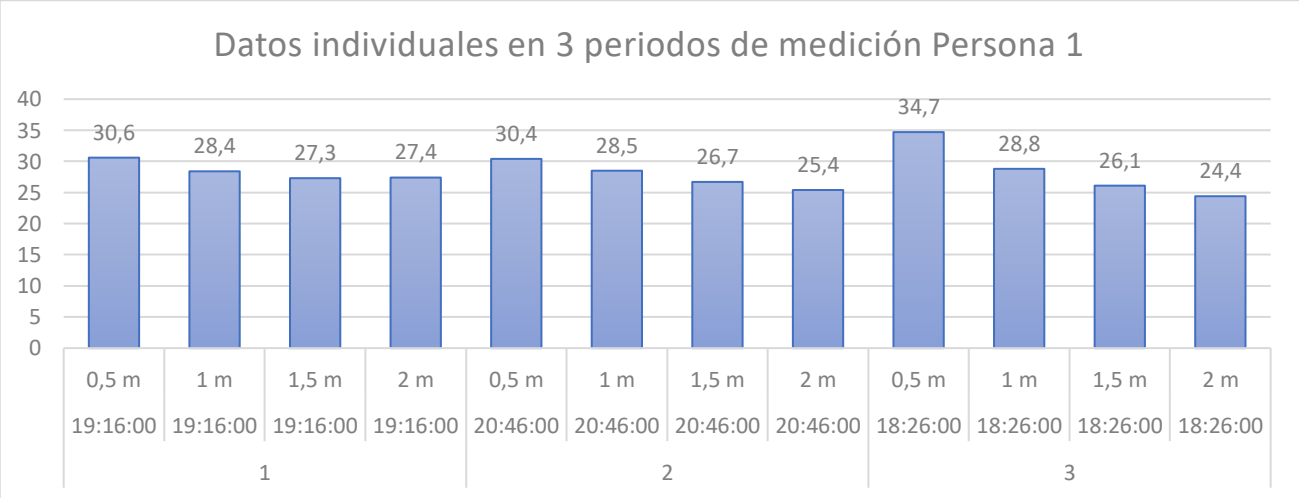

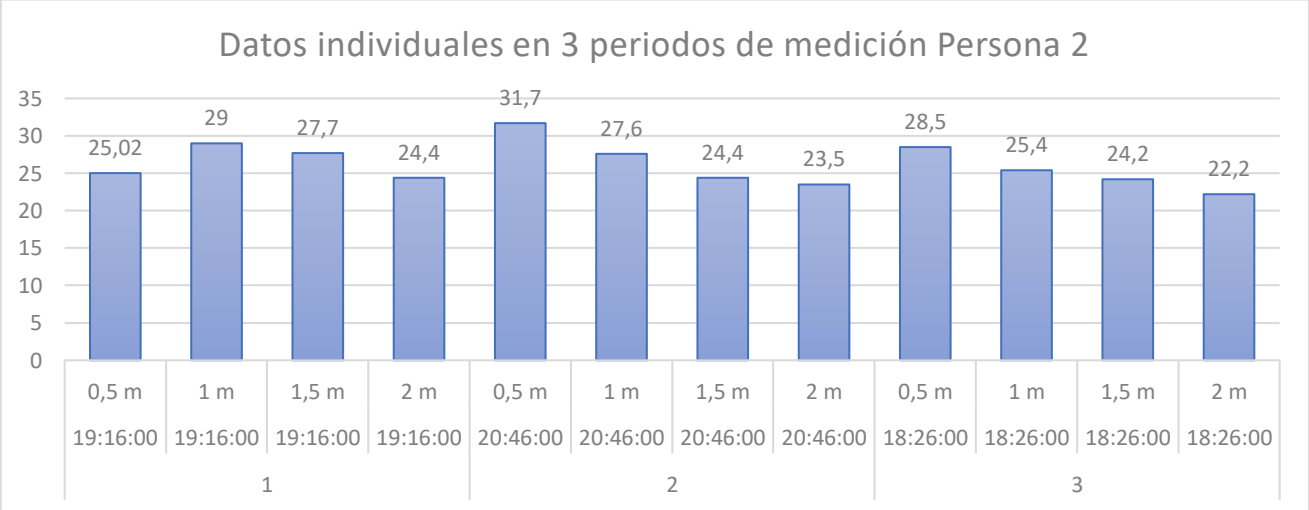

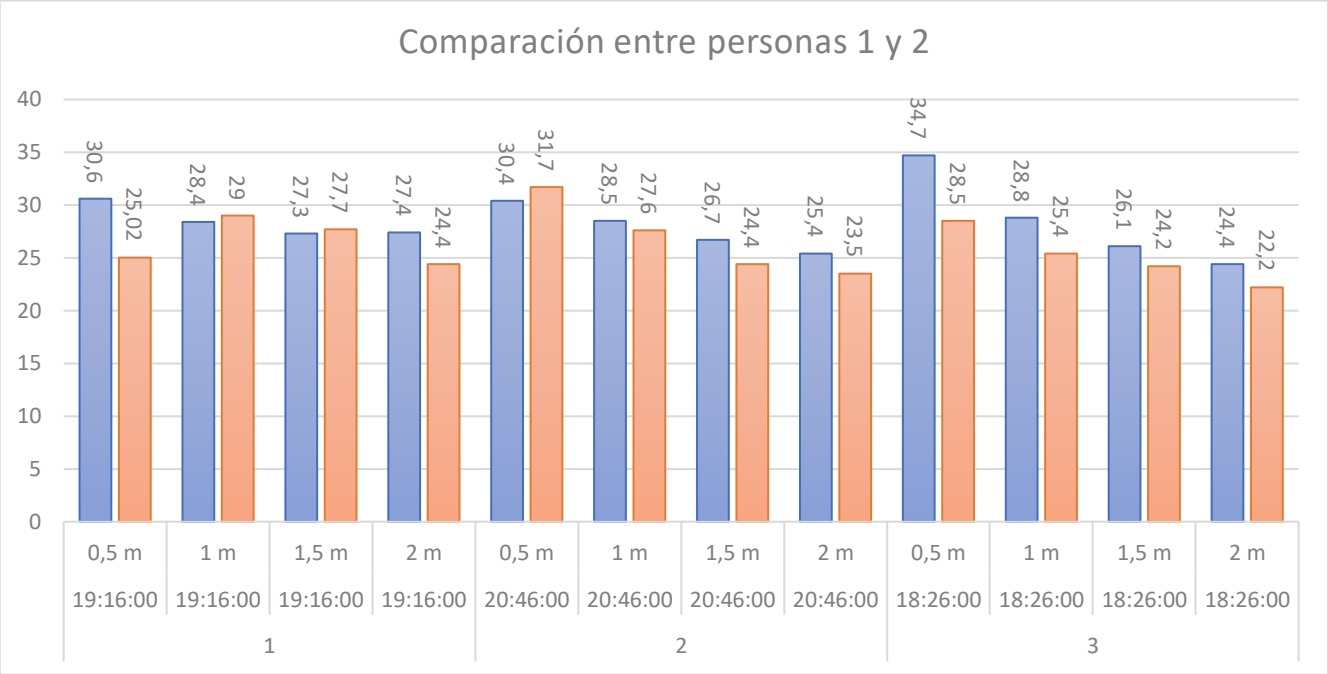

Etiquetas de fila	Promedio de Temperatura en C° Persona 1	Promedio de Temperatura en C° Persona 2
0,5 m	31,9	28,4
1 m	28,6	27,3
1,5 m	26,7	25,4
2 m	25,7	23,4
Total, general	**28,2**	**26,1**

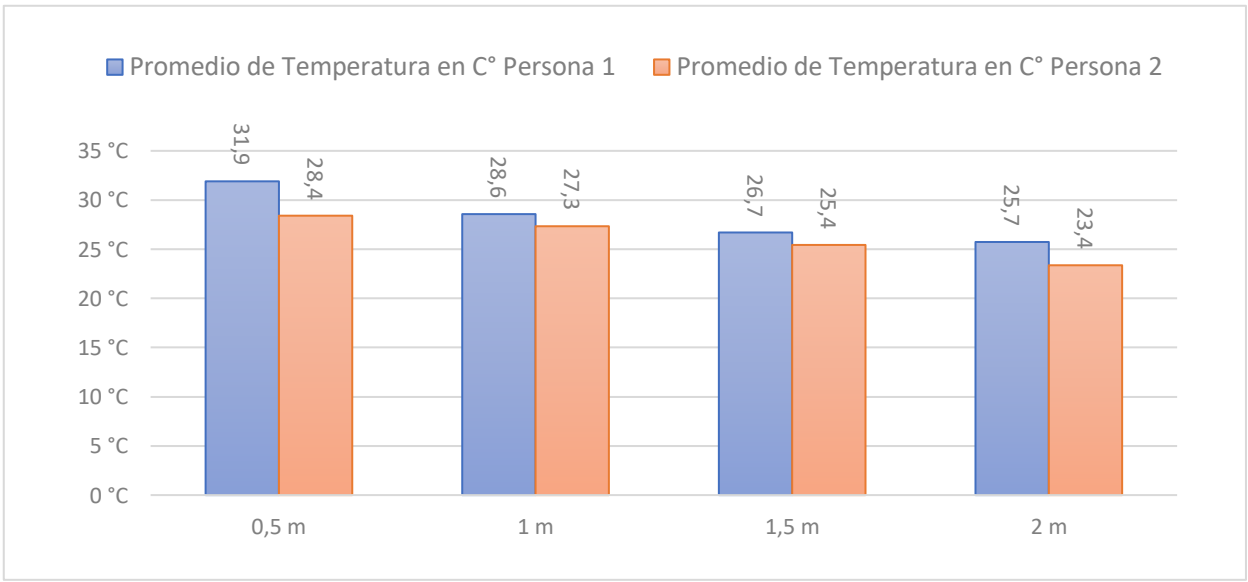

ANEXO 39. Tabulación y análisis de datos de datos segunda etapa.

CAMARA TERMOGRÁFICA UIDE							
Sujeto	Hora	Temperatura ambiente °C	Sensación térmica °C	Rango de medida (cm)	Puntos de medición	Lugar de medición de temperatura	Temperatura en °C
1	7:00:00	8 °C	6 °C	3 cm	1	Frente	33,1
1	7:01:00	8 °C	6 °C	5 cm	1	Frente	34,3
1	7:02:00	8 °C	6 °C	7 cm	1	Frente	34
1	7:03:00	8 °C	6 °C	9 cm	1	Frente	33,9
1	7:04:00	8 °C	6 °C	11 cm	1	Frente	35,9
1	7:05:00	8 °C	6 °C	13 cm	1	Frente	36
1	7:06:00	8 °C	6 °C	15 cm	1	Frente	36,2
1	7:07:00	8 °C	6 °C	17 cm	1	Frente	35,6
1	7:08:00	8 °C	6 °C	19 cm	1	Frente	35,7
1	7:09:00	8 °C	6 °C	21 cm	1	Frente	35,8
1	7:10:00	8 °C	6 °C	23 cm	1	Frente	36,3
1	7:11:00	8 °C	6 °C	25 cm	1	Frente	36,1
1	7:12:00	8 °C	6 °C	27 cm	1	Frente	35,8
1	12:06:00	18 °C	18 °C	3 cm	1	Frente	35,4
1	12:07:00	18 °C	18 °C	5 cm	1	Frente	35,7
1	12:08:00	18 °C	18 °C	7 cm	1	Frente	36,2
1	12:09:00	18 °C	18 °C	9 cm	1	Frente	35,1
1	12:10:00	18 °C	18 °C	11 cm	1	Frente	35,9
1	12:11:00	18 °C	18 °C	13 cm	1	Frente	36,2
1	12:12:00	18 °C	18 °C	15 cm	1	Frente	36,2
1	12:12:00	18 °C	18 °C	17 cm	1	Frente	36,2
1	12:13:00	18 °C	18 °C	19 cm	1	Frente	36,3
1	12:14:00	18 °C	18 °C	21 cm	1	Frente	36
1	12:15:00	18 °C	18 °C	23 cm	1	Frente	36,3
1	12:16:00	18 °C	18 °C	25 cm	1	Frente	36,2
1	12:16:00	18 °C	18 °C	27 cm	1	Frente	36,2
1	18:00:00	16 °C	14 °C	3 cm	1	Frente	32,6
1	18:07:00	16 °C	14 °C	5 cm	1	Frente	34,4
1	18:08:00	16 °C	14 °C	7 cm	1	Frente	34,3
1	18:09:00	16 °C	14 °C	9 cm	1	Frente	35
1	18:10:00	16 °C	14 °C	11 cm	1	Frente	36,2
1	18:11:00	16 °C	14 °C	13 cm	1	Frente	36,1
1	18:12:00	16 °C	14 °C	15 cm	1	Frente	36,3
1	18:13:00	16 °C	14 °C	17 cm	1	Frente	36
1	18:14:00	16 °C	14 °C	19 cm	1	Frente	36
1	18:15:00	16 °C	14 °C	21 cm	1	Frente	36,2
1	18:16:00	16 °C	14 °C	23 cm	1	Frente	36,2
1	18:17:00	16 °C	14 °C	25 cm	1	Frente	36,1
1	18:19:00	16 °C	14 °C	27 cm	1	Frente	36
2	7:30:00	8 °C	6 °C	3 cm	1	Frente	33,1
2	7:31:00	8 °C	6 °C	5 cm	1	Frente	34,9

2	7:32:00	8 °C	6 °C	7 cm	1	Frente	35,4
2	7:33:00	8 °C	6 °C	9 cm	1	Frente	35,1
2	7:34:00	8 °C	6 °C	11 cm	1	Frente	36,2
2	7:35:00	8 °C	6 °C	13 cm	1	Frente	36,2
2	7:36:00	8 °C	6 °C	15 cm	1	Frente	36
2	7:38:00	8 °C	6 °C	17 cm	1	Frente	36,1
2	7:39:00	8 °C	6 °C	19 cm	1	Frente	36,2
2	7:40:00	8 °C	6 °C	21 cm	1	Frente	36,3
2	7:42:00	8 °C	6 °C	23 cm	1	Frente	36,8
2	7:43:00	8 °C	6 °C	25 cm	1	Frente	36,3
2	7:45:00	8 °C	6 °C	27 cm	1	Frente	36,1
2	12:30:00	19 °C	19 °C	3 cm	1	Frente	32,5
2	12:31:00	19 °C	19 °C	5 cm	1	Frente	34
2	12:31:00	19 °C	19 °C	7 cm	1	Frente	34,1
2	12:33:00	19 °C	19 °C	9 cm	1	Frente	34,5
2	12:34:00	19 °C	19 °C	11 cm	1	Frente	34,9
2	12:34:00	19 °C	19 °C	13 cm	1	Frente	35,7
2	12:35:00	19 °C	19 °C	15 cm	1	Frente	35,2
2	12:36:00	19 °C	19 °C	17 cm	1	Frente	34,9
2	12:36:00	19 °C	19 °C	19 cm	1	Frente	35
2	12:37:00	19 °C	19 °C	21 cm	1	Frente	35,3
2	12:38:00	19 °C	19 °C	23 cm	1	Frente	35,4
2	12:39:00	19 °C	19 °C	25 cm	1	Frente	35,7
2	12:43:00	19 °C	19 °C	27 cm	1	Frente	35
2	19:55:00	11 °C	9 °C	3 cm	1	Frente	33,4
2	19:56:00	11 °C	9 °C	5 cm	1	Frente	35,6
2	19:57:00	11 °C	9 °C	7 cm	1	Frente	35,5
2	19:58:00	11 °C	9 °C	9 cm	1	Frente	35,3
2	19:59:00	11 °C	9 °C	11 cm	1	Frente	36,2
2	20:00:00	11 °C	9 °C	13 cm	1	Frente	36,2
2	20:01:00	11 °C	9 °C	15 cm	1	Frente	36
2	20:02:00	11 °C	9 °C	17 cm	1	Frente	36,1
2	20:03:00	11 °C	9 °C	19 cm	1	Frente	36,2
2	20:04:00	11 °C	9 °C	21 cm	1	Frente	36,3
2	20:05:00	11 °C	9 °C	23 cm	1	Frente	36,2
2	20:06:00	11 °C	9 °C	25 cm	1	Frente	35,8
2	20:07:00	11 °C	9 °C	27 cm	1	Frente	35,8
3	8:00:00	8 °C	6 °C	3 cm	1	Frente	35,7
3	8:01:00	8 °C	6 °C	5 cm	1	Frente	36,2
3	8:02:00	8 °C	6 °C	7 cm	1	Frente	35,1
3	8:03:00	8 °C	6 °C	9 cm	1	Frente	35,9
3	8:04:00	8 °C	6 °C	11 cm	1	Frente	35
3	8:05:00	8 °C	6 °C	13 cm	1	Frente	36,2
3	8:06:00	8 °C	6 °C	15 cm	1	Frente	36,1
3	8:07:00	8 °C	6 °C	17 cm	1	Frente	36,3
3	8:08:00	8 °C	6 °C	19 cm	1	Frente	36,2
3	8:09:00	8 °C	6 °C	21 cm	1	Frente	36,3
3	8:10:00	8 °C	6 °C	23 cm	1	Frente	36

3	8:11:00	8 °C	6 °C	25 cm	1	Frente	36,3
3	8:12:00	8 °C	6 °C	27 cm	1	Frente	36,2
3	12:53:00	19 °C	19 °C	3 cm	1	Frente	33,1
3	12:54:00	19 °C	19 °C	5 cm	1	Frente	34,9
3	12:55:00	19 °C	19 °C	7 cm	1	Frente	35,4
3	12:55:00	19 °C	19 °C	9 cm	1	Frente	35,1
3	12:56:00	19 °C	19 °C	11 cm	1	Frente	36,3
3	12:57:00	19 °C	19 °C	13 cm	1	Frente	36,1
3	12:58:00	19 °C	19 °C	15 cm	1	Frente	35,4
3	12:59:00	19 °C	19 °C	17 cm	1	Frente	36,2
3	13:00:00	19 °C	19 °C	19 cm	1	Frente	36,4
3	13:01:00	19 °C	19 °C	21 cm	1	Frente	36,2
3	13:02:00	19 °C	19 °C	23 cm	1	Frente	36
3	13:03:00	19 °C	19 °C	25 cm	1	Frente	35,8
3	13:04:00	19 °C	19 °C	27 cm	1	Frente	36,5
3	18:49:00	13 °C	12 °C	3 cm	1	Frente	33,5
3	18:50:00	13 °C	12 °C	5 cm	1	Frente	35,6
3	18:51:00	13 °C	12 °C	7 cm	1	Frente	36,4
3	18:52:00	13 °C	12 °C	9 cm	1	Frente	36
3	18:53:00	13 °C	12 °C	11 cm	1	Frente	36,4
3	18:54:00	13 °C	12 °C	13 cm	1	Frente	35,8
3	18:55:00	13 °C	12 °C	15 cm	1	Frente	36,3
3	18:56:00	13 °C	12 °C	17 cm	1	Frente	36
3	18:57:00	13 °C	12 °C	19 cm	1	Frente	36,2
3	18:58:00	13 °C	12 °C	21 cm	1	Frente	35,9
3	18:59:00	13 °C	12 °C	23 cm	1	Frente	36,8
3	19:00:00	13 °C	12 °C	25 cm	1	Frente	36,3
3	19:01:00	13 °C	12 °C	27 cm	1	Frente	36,1

PISTOLA TÉRMICA							
N° Participantes	Hora	Temperatura ambiente °C	Sensación térmica °C	Rango de medida (cm)	Puntos de medición	Lugar de medición de temperatura	Temperatura en °C
1	7:00:00	8 °C	6 °C	3 cm	1	Frente	36,3
1	7:01:00	8 °C	6 °C	5 cm	1	Frente	36,2
1	7:02:00	8 °C	6 °C	7 cm	1	Frente	36
1	7:03:00	8 °C	6 °C	9 cm	1	Frente	35,6
1	7:04:00	8 °C	6 °C	11 cm	1	Frente	35
1	7:05:00	8 °C	6 °C	13 cm	1	Frente	34,5
1	7:06:00	8 °C	6 °C	15 cm	1	Frente	34,1
1	7:07:00	8 °C	6 °C	17 cm	1	Frente	33,1
1	7:08:00	8 °C	6 °C	19 cm	1	Frente	32,5
1	7:09:00	8 °C	6 °C	21 cm	1	Frente	32,2
1	7:10:00	8 °C	6 °C	23 cm	1	Frente	31,6
1	7:11:00	8 °C	6 °C	25 cm	1	Frente	0

1	7:12:00	8 °C	6 °C	27 cm	1	Frente	0
1	12:06:00	18 °C	18 °C	3 cm	1	Frente	36,2
1	12:07:00	18 °C	18 °C	5 cm	1	Frente	36,2
1	12:08:00	18 °C	18 °C	7 cm	1	Frente	36,2
1	12:09:00	18 °C	18 °C	9 cm	1	Frente	35,8
1	12:10:00	18 °C	18 °C	11 cm	1	Frente	35,6
1	12:11:00	18 °C	18 °C	13 cm	1	Frente	34,7
1	12:12:00	18 °C	18 °C	15 cm	1	Frente	34,4
1	12:12:00	18 °C	18 °C	17 cm	1	Frente	33,2
1	12:13:00	18 °C	18 °C	19 cm	1	Frente	32,9
1	12:14:00	18 °C	18 °C	21 cm	1	Frente	32,8
1	12:15:00	18 °C	18 °C	23 cm	1	Frente	32
1	12:16:00	18 °C	18 °C	25 cm	1	Frente	0
1	12:16:00	18 °C	18 °C	27 cm	1	Frente	0
1	18:00:00	16 °C	14 °C	3 cm	1	Frente	36,4
1	18:07:00	16 °C	14 °C	5 cm	1	Frente	36,3
1	18:08:00	16 °C	14 °C	7 cm	1	Frente	36,2
1	18:09:00	16 °C	14 °C	9 cm	1	Frente	36,2
1	18:10:00	16 °C	14 °C	11 cm	1	Frente	36
1	18:11:00	16 °C	14 °C	13 cm	1	Frente	36
1	18:12:00	16 °C	14 °C	15 cm	1	Frente	35,6
1	18:13:00	16 °C	14 °C	17 cm	1	Frente	35,1
1	18:14:00	16 °C	14 °C	19 cm	1	Frente	34,6
1	18:15:00	16 °C	14 °C	21 cm	1	Frente	34
1	18:16:00	16 °C	14 °C	23 cm	1	Frente	33,6
1	18:17:00	16 °C	14 °C	25 cm	1	Frente	33,4
1	18:19:00	16 °C	14 °C	27 cm	1	Frente	32,9
2	7:30:00	8 °C	6 °C	3 cm	1	Frente	36,2
2	7:31:00	8 °C	6 °C	5 cm	1	Frente	36,1
2	7:32:00	8 °C	6 °C	7 cm	1	Frente	36,1
2	7:33:00	8 °C	6 °C	9 cm	1	Frente	35,9
2	7:34:00	8 °C	6 °C	11 cm	1	Frente	35,9
2	7:35:00	8 °C	6 °C	13 cm	1	Frente	35,7
2	7:36:00	8 °C	6 °C	15 cm	1	Frente	35
2	7:38:00	8 °C	6 °C	17 cm	1	Frente	34,8
2	7:39:00	8 °C	6 °C	19 cm	1	Frente	34,2
2	7:40:00	8 °C	6 °C	21 cm	1	Frente	33,8
2	7:42:00	8 °C	6 °C	23 cm	1	Frente	33,3
2	7:43:00	8 °C	6 °C	25 cm	1	Frente	32,7
2	7:45:00	8 °C	6 °C	27 cm	1	Frente	32,3
2	12:30:00	19 °C	19 °C	3 cm	1	Frente	36,4
2	12:31:00	19 °C	19 °C	5 cm	1	Frente	36,4
2	12:31:00	19 °C	19 °C	7 cm	1	Frente	36,2
2	12:33:00	19 °C	19 °C	9 cm	1	Frente	36
2	12:34:00	19 °C	19 °C	11 cm	1	Frente	35,5
2	12:34:00	19 °C	19 °C	13 cm	1	Frente	35,1
2	12:35:00	19 °C	19 °C	15 cm	1	Frente	35
2	12:36:00	19 °C	19 °C	17 cm	1	Frente	34,6

2	12:36:00	19 °C	19 °C	19 cm	1	Frente	32,8
2	12:37:00	19 °C	19 °C	21 cm	1	Frente	32,6
2	12:38:00	19 °C	19 °C	23 cm	1	Frente	32,1
2	12:39:00	19 °C	19 °C	25 cm	1	Frente	0
2	12:43:00	19 °C	19 °C	27 cm	1	Frente	0
2	19:55:00	11 °C	9 °C	3 cm	1	Frente	36,5
2	19:56:00	11 °C	9 °C	5 cm	1	Frente	36,4
2	19:57:00	11 °C	9 °C	7 cm	1	Frente	36,2
2	19:58:00	11 °C	9 °C	9 cm	1	Frente	36,2
2	19:59:00	11 °C	9 °C	11 cm	1	Frente	36,1
2	20:00:00	11 °C	9 °C	13 cm	1	Frente	36
2	20:01:00	11 °C	9 °C	15 cm	1	Frente	35,7
2	20:02:00	11 °C	9 °C	17 cm	1	Frente	35,6
2	20:03:00	11 °C	9 °C	19 cm	1	Frente	35,5
2	20:04:00	11 °C	9 °C	21 cm	1	Frente	34,7
2	20:05:00	11 °C	9 °C	23 cm	1	Frente	34,1
2	20:06:00	11 °C	9 °C	25 cm	1	Frente	33,8
2	20:07:00	11 °C	9 °C	27 cm	1	Frente	33
3	8:00:00	8 °C	6 °C	3 cm	1	Frente	36,4
3	8:01:00	8 °C	6 °C	5 cm	1	Frente	36,3
3	8:02:00	8 °C	6 °C	7 cm	1	Frente	36,2
3	8:03:00	8 °C	6 °C	9 cm	1	Frente	36,1
3	8:04:00	8 °C	6 °C	11 cm	1	Frente	36
3	8:05:00	8 °C	6 °C	13 cm	1	Frente	35,9
3	8:06:00	8 °C	6 °C	15 cm	1	Frente	35,7
3	8:07:00	8 °C	6 °C	17 cm	1	Frente	35,4
3	8:08:00	8 °C	6 °C	19 cm	1	Frente	35,2
3	8:09:00	8 °C	6 °C	21 cm	1	Frente	34,6
3	8:10:00	8 °C	6 °C	23 cm	1	Frente	34,3
3	8:11:00	8 °C	6 °C	25 cm	1	Frente	33,6
3	8:12:00	8 °C	6 °C	27 cm	1	Frente	32,9
3	12:53:00	19 °C	19 °C	3 cm	1	Frente	36,5
3	12:54:00	19 °C	19 °C	5 cm	1	Frente	36,4
3	12:55:00	19 °C	19 °C	7 cm	1	Frente	36,3
3	12:55:00	19 °C	19 °C	9 cm	1	Frente	36,3
3	12:56:00	19 °C	19 °C	11 cm	1	Frente	36,1
3	12:57:00	19 °C	19 °C	13 cm	1	Frente	35,8
3	12:58:00	19 °C	19 °C	15 cm	1	Frente	35,2
3	12:59:00	19 °C	19 °C	17 cm	1	Frente	34,4
3	13:00:00	19 °C	19 °C	19 cm	1	Frente	33,6
3	13:01:00	19 °C	19 °C	21 cm	1	Frente	32,6
3	13:02:00	19 °C	19 °C	23 cm	1	Frente	33
3	13:03:00	19 °C	19 °C	25 cm	1	Frente	0
3	13:04:00	19 °C	19 °C	27 cm	1	Frente	0
3	18:49:00	13 °C	12 °C	3 cm	1	Frente	36,5
3	18:50:00	13 °C	12 °C	5 cm	1	Frente	36,5
3	18:51:00	13 °C	12 °C	7 cm	1	Frente	36,4
3	18:52:00	13 °C	12 °C	9 cm	1	Frente	36,3

3	18:53:00	13 °C	12 °C	11 cm	1	Frente	36
3	18:54:00	13 °C	12 °C	13 cm	1	Frente	35,8
3	18:55:00	13 °C	12 °C	15 cm	1	Frente	35,6
3	18:56:00	13 °C	12 °C	17 cm	1	Frente	35,2
3	18:57:00	13 °C	12 °C	19 cm	1	Frente	34,4
3	18:58:00	13 °C	12 °C	21 cm	1	Frente	33,8
3	18:59:00	13 °C	12 °C	23 cm	1	Frente	33,2
3	19:00:00	13 °C	12 °C	25 cm	1	Frente	33
3	19:01:00	13 °C	12 °C	27 cm	1	Frente	32,4

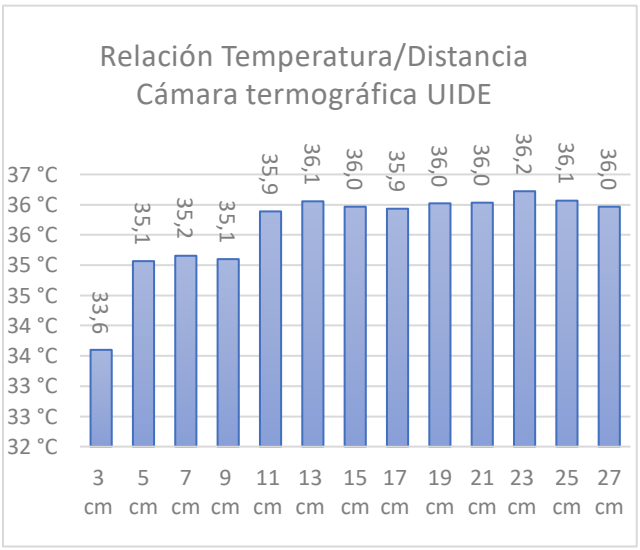

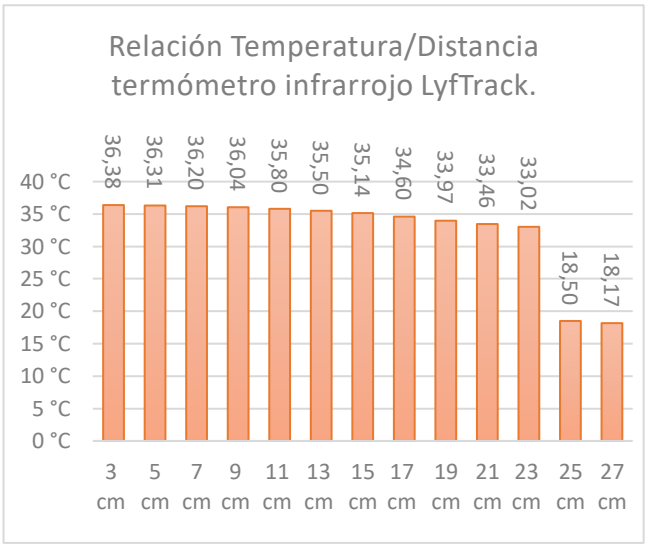

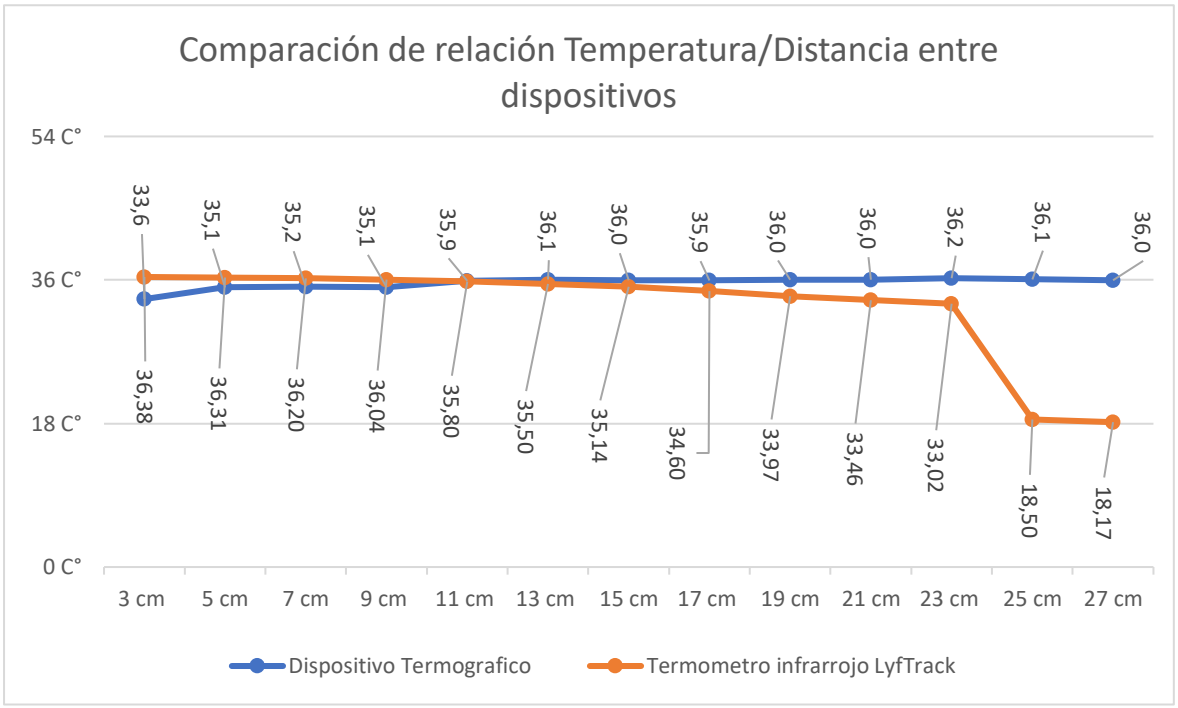

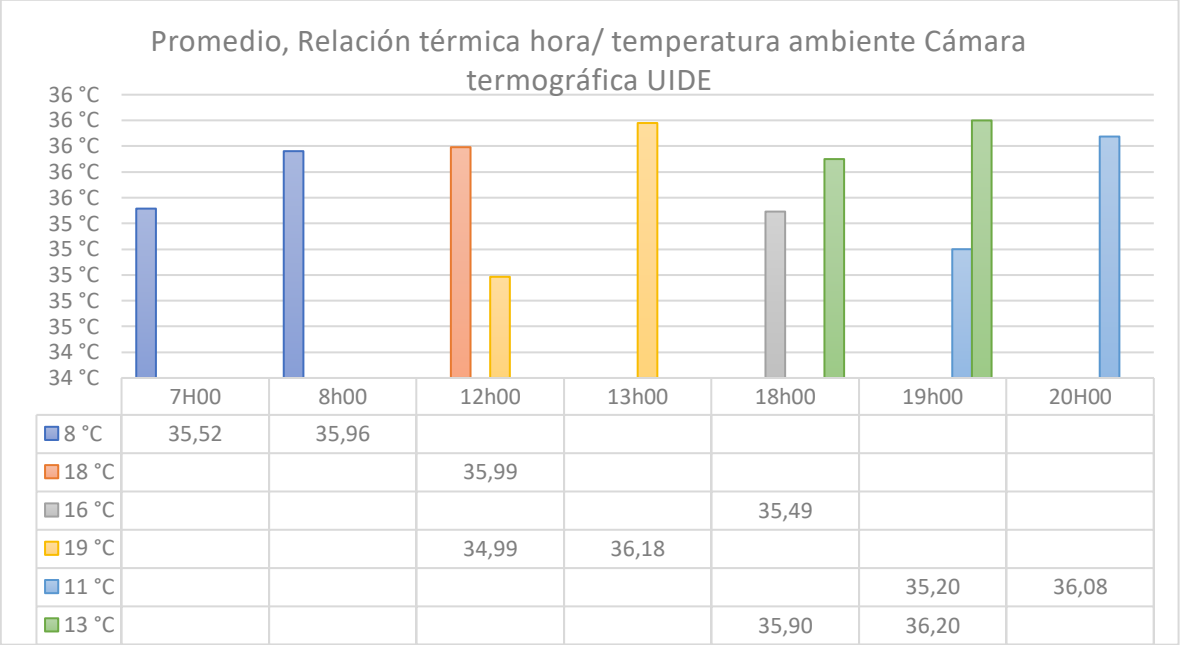

Promedio de Temperatura en C° Etiquetas de fila	Etiquetas de columna 8 °C	18 °C	16 °C	19 °C	11 °C	13 °C	Total, general
7H00	**35,52**						**35,52**
8h00	**35,96**						**35,96**
12h00		**35,99**		**34,99**			**35,37**
13h00				**36,18**			**36,18**
18h00			**35,49**			**35,90**	**35,68**
19h00					**35,20**	**36,20**	**35,49**
20H00					**36,08**		**36,08**
Total general	**35,66**	**35,99**	**35,49**	**35,22**	**35,74**	**35,95**	**35,62**

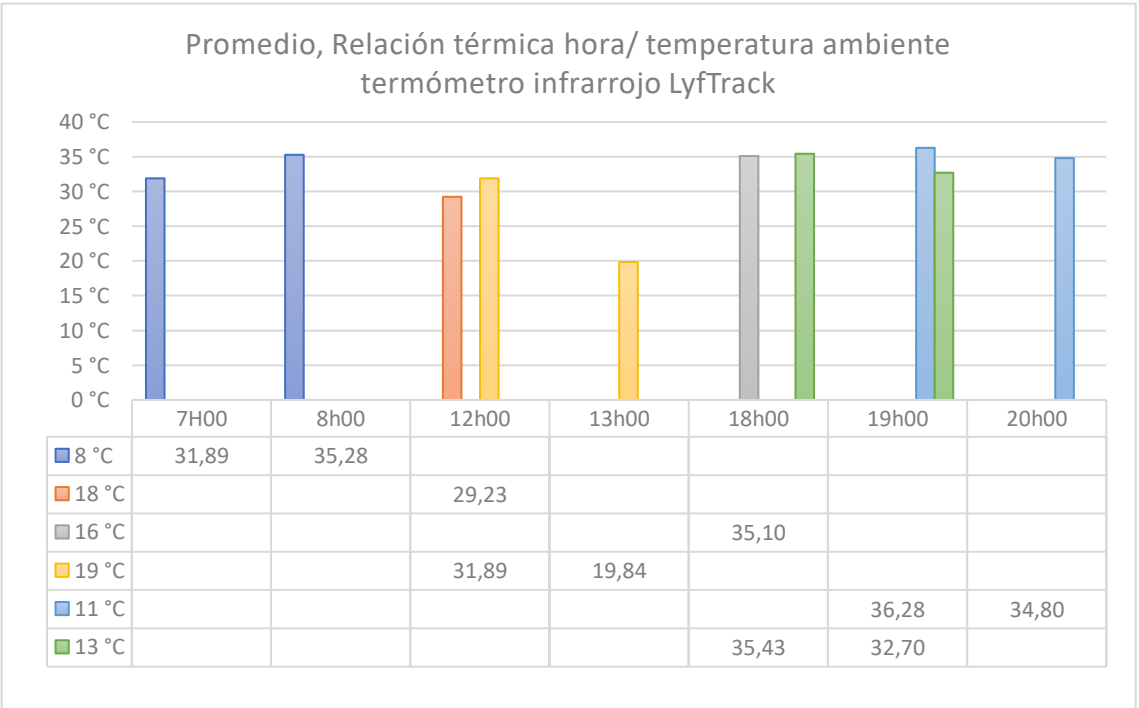

Promedio de Temperatura en C°	Etiquetas de columna						
Etiquetas de fila	8 °C	18 °C	16 °C	19 °C	11 °C	13 °C	Total, general
7H00	31,89						31,89
8h00	35,28						35,28
12h00		29,23		31,89			30,87
13h00				19,84			19,84
18h00			35,10			35,43	35,25
19h00					36,28	32,70	35,26
20h00					34,80		34,80
Total, general	33,02	29,23	35,10	29,57	35,37	35,01	32,55

ANEXO 40. Tabulación y análisis de datos de datos tercera etapa.

CAMARA TERMOGRÁFICA UIDE						
Sujeto	Hora	Rango de medida (m)	Puntos de medición	Lugar de medición de temperatura	Temperatura en °C	Distancia entre participantes
1	19:00:00	0,5	3	Frente, nariz y cuello	36,3	0
1	19:00:00	1	3	Frente, torso	35,1	0
1	19:00:00	1,5	1	Cara	34,5	0
1	19:00:00	2	1	Medio cuerpo	33,1	0
2	19:19:00	0,5	3	Frente, nariz y cuello	36,4	0
2	19:19:00	1	3	Frente, torso	35	0
2	19:19:00	1,5	1	Cara	34,2	0
2	19:19:00	2	1	Medio cuerpo	33,5	0
3	19:31:00	0,5	3	Frente, nariz y cuello	36,5	0
3	19:31:00	1	3	Frente, torso	35,2	0
3	19:31:00	1,5	1	Cara	35,1	0
3	19:31:00	2	1	Medio cuerpo	33,9	0
4	19:41:00	0,5	3	Frente, nariz y cuello	36,4	0
4	19:41:00	1	3	Frente, torso	35,3	0
4	19:41:00	1,5	1	Cara	34,1	0
4	19:41:00	2	1	Medio cuerpo	33	0
5	20:31:00	0,5	3	Frente, nariz y cuello	36,6	0
5	20:31:00	1	3	Frente, torso	35,5	0
5	20:31:00	1,5	1	Cara	33,9	0
5	20:31:00	2	1	Medio cuerpo	31,1	0
6	20:21:00	0,5	3	Frente, nariz y cuello	36	0
6	20:21:00	1	3	Frente, torso	35,1	0
6	20:21:00	1,5	1	Cara	34,8	0
6	20:21:00	2	1	Medio cuerpo	33,4	0
7	18:10:00	0,5	3	Frente, nariz y cuello	35,7	0
7	18:10:00	1	3	Frente, torso	33,4	0

7	18:10:00	1,5	1	Cara	33	0
7	18:10:00	2	1	Medio cuerpo	31,2	0
8	18:22:00	0,5	3	Frente, nariz y cuello	36,3	0
8	18:22:00	1	3	Frente, torso	34,5	0
8	18:22:00	1,5	1	Cara	34	0
8	18:22:00	2	1	Medio cuerpo	33,3	0
9	18:27:00	0,5	3	Frente, nariz y cuello	36,6	0
9	18:27:00	1	3	Frente, torso	35,9	0
9	18:27:00	1,5	1	Cara	34,7	0
9	18:27:00	2	1	Medio cuerpo	33,2	0
10	15:48:00	0,5	3	Frente, nariz y cuello	36	0
10	15:48:00	1	3	Frente, torso	34,8	0
10	15:48:00	1,5	1	Cara	34,8	0
10	15:48:00	2	1	Medio cuerpo	34	0
11	15:56:00	0,5	3	Frente, nariz y cuello	36,9	0
11	15:56:00	1	3	Frente, torso	34,8	0
11	15:56:00	1,5	1	Cara	34,8	0
11	15:56:00	2	1	Medio cuerpo	34	0
12	15:59:00	0,5	3	Frente, nariz y cuello	36,5	0
12	15:59:00	1	3	Frente, torso	34,7	0
12	15:59:00	1,5	1	Cara	34,2	0
12	15:59:00	2	1	Medio cuerpo	33,5	0
13	16:04:00	0,5	3	Frente, nariz y cuello	36,4	0
13	16:04:00	1	3	Frente, torso	35,6	0
13	16:04:00	1,5	1	Cara	34,3	0
13	16:04:00	2	1	Medio cuerpo	33,8	0
14	16:17:00	0,5	3	Frente, nariz y cuello	36,2	0
14	16:17:00	1	3	Frente, torso	35,5	0
14	16:17:00	1,5	1	Cara	34,9	0
14	16:17:00	2	1	Medio cuerpo	34,6	0

PISTOLA TÉRMICA						
N° Participantes	Hora	Rango de medida (m)	Puntos de medición	Lugar de medición de temperatura	Temperatura en °C	Distancia entre participantes
1	19:00:00	0,03	1	frente	36,3	0
2	19:17:00	0,03	1	frente	36,4	0
3	19:31:00	0,03	1	frente	36,5	0
4	19:41:00	0,03	1	frente	36,4	0
5	20:30:00	0,03	1	frente	36,5	0
6	20:39:00	0,03	1	frente	36,3	0
7	18:11:00	0,03	1	frente	36,3	0
8	18:22:00	0,03	1	frente	36,5	0
9	18:34:00	0,03	1	frente	36,6	0
10	15:48:00	0,03	1	frente	36,6	0

11	15:56:00	0,03	1	frente	36,6	0
12	15:59:00	0,03	1	frente	36,4	0
13	16:04:00	0,03	1	frente	36,5	0
14	16:17:00	0,03	1	frente	36,6	0

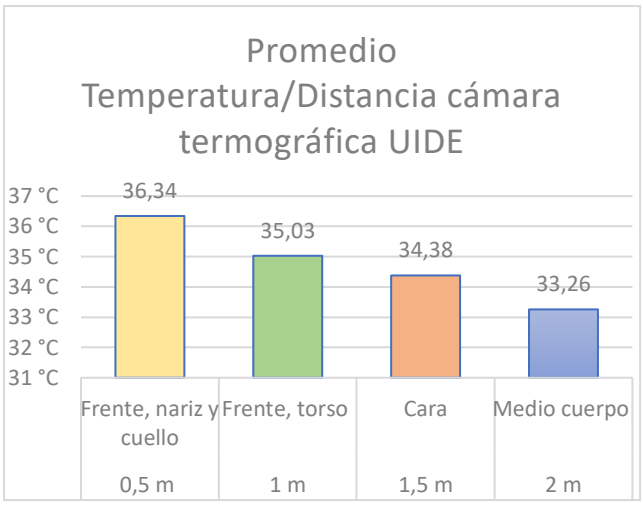

Etiquetas de fila	Promedio de Temperatura en °C
0,5 m	**36,34**
Frente, nariz y cuello	36,34
1 m	**35,03**
Frente, torso	35,03
1,5 m	**34,38**
Cara	34,38
2 m	**33,26**
Medio cuerpo	33,26
Total, general	**34,75**

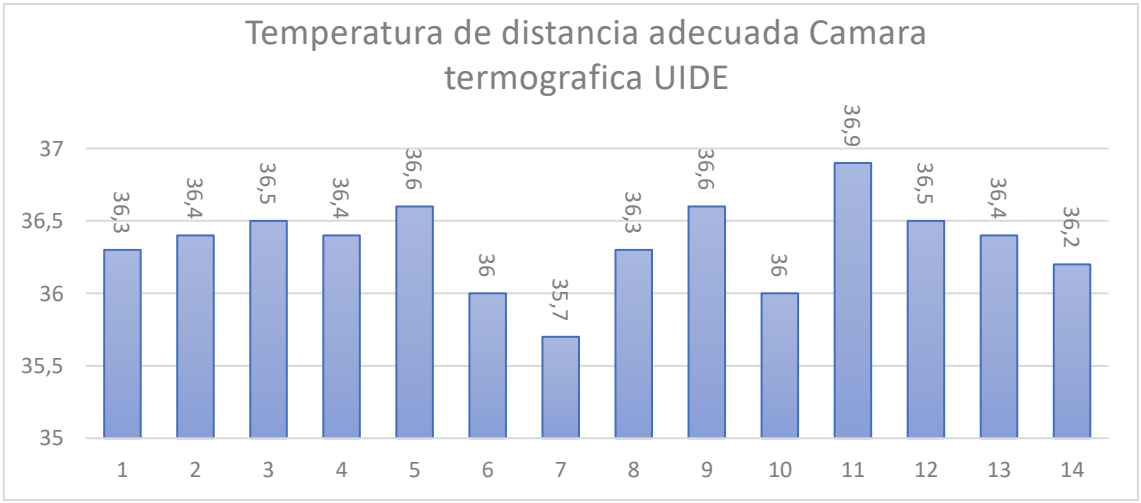

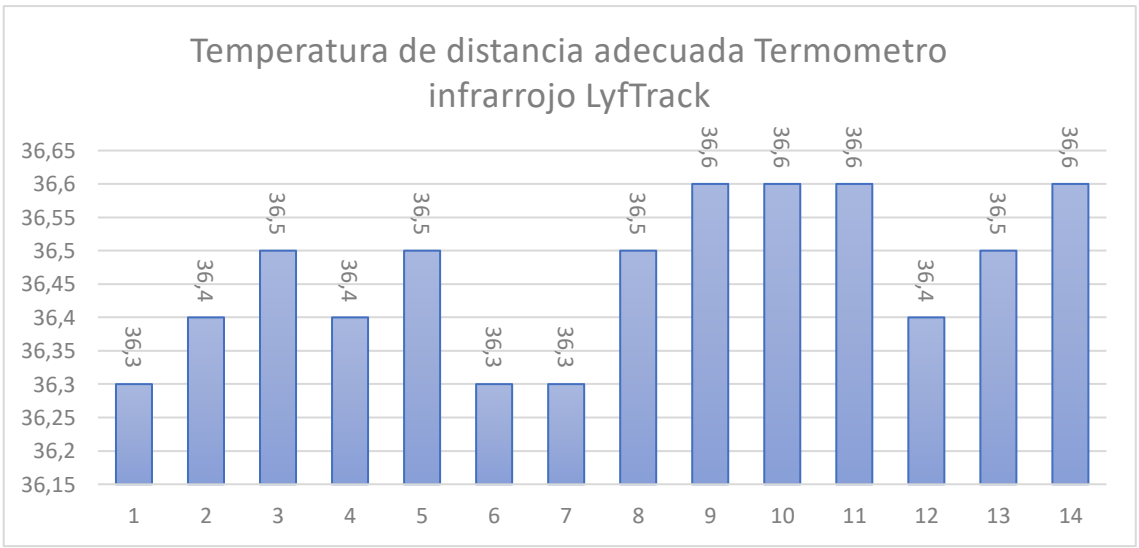

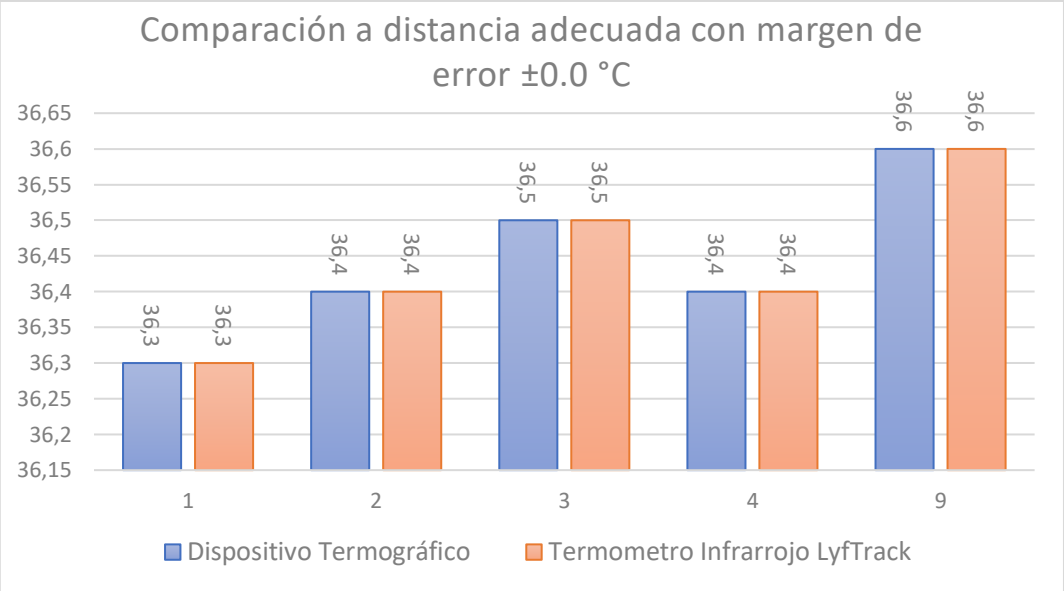
Comparación a distancia adecuada con margen de error ±0.0 °C
36,65
36,6
36,55
36,5
36,45
36,4
36,35
36,3
36,25
36,2
36,15
36,3
36,3
36,4
36,4
36,5
36,5
36,4
36,4
36,6
36,6
1
2
3
4
9
Dispositivo Termográfico
Termometro Infrarrojo LyfTrack

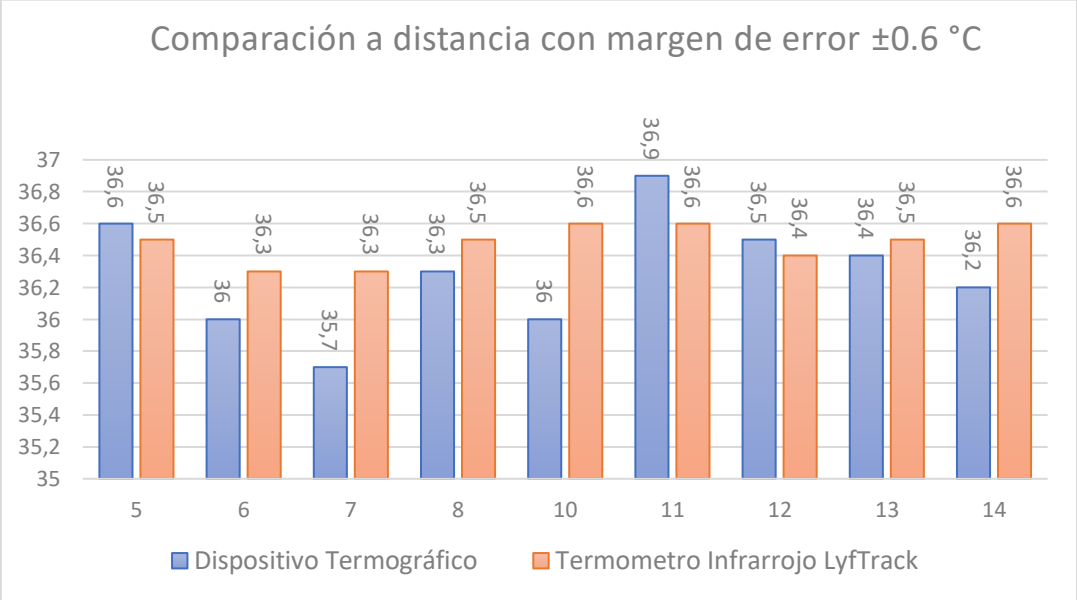
Comparación a distancia con margen de error ±0.6 °C
37
36,8
36,6
36,4
36,2
36
35,8
35,6
35,4
35,2
35
36,6
36,5
36
36,3
35,7
36,3
36,3
36,5
36
36,6
36,9
36,6
36,5
36,4
36,4
36,5
36,2
36,6
5
6
7
8
10
11
12
13
14
Dispositivo Termográfico
Termometro Infrarrojo LyfTrack

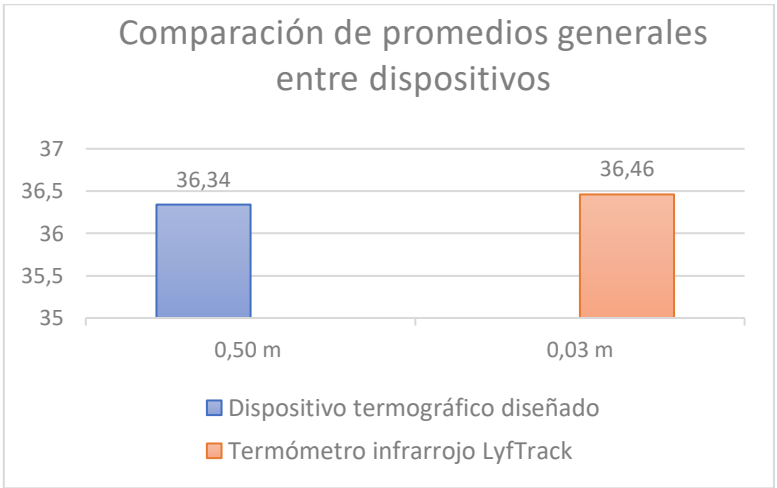
Comparación de promedios generales entre dispositivos
37
36,5
36
35,5
35
36,34
36,46
0,50 m
0,03 m
Dispositivo termográfico diseñado
Termómetro infrarrojo LyfTrack

MANUAL DE USUARIO CÁMARA TERMOGRÁFICA UIDE

Para poder hacer uso de la cámara termográfica, es importante disponer de un teléfono o dispositivo con sistema operativo Android, esto con el fin de poder descargar la aplicación detallada previamente que se encuentra en PlayStore. También es importante que el dispositivo o celular cuente con una entrada de tipo Micro USB tipo C para poder enlazar la cámara y así ver en la pantalla de nuestro dispositivo externo todo lo que nuestra cámara está procesando.

1. Conectar la cámara al dispositivo Android mediante la entrada USB Micro C.

2. Entrar a la aplicación mencionada en el artículo.

3. Encender la cámara termográfica aplastando en su botón que se encuentra en la parte inferior, mantener pulsado el botón hasta que la luz roja empiece a titilar de color verde.

4. Verificar que la cámara se encuentre debidamente conectada al celular o dispositivo para evitar un fallo en la interfaz.

5. Seleccionar el punto que se desea realizar una medición termográfica. Para obtener una lectura más precisa, se recomienda situar el objeto a ser medido a una distancia de 0,5m.

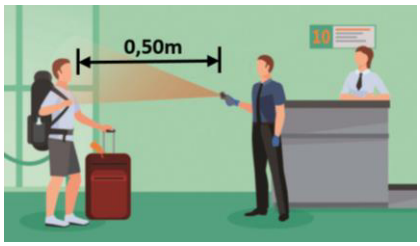

Si se desea realizar la medición de más de un solo objeto o persona, el dispositivo cuenta con la opción de realizar hasta un máximo de 3 puntos fijos a medir.
Para acceder a esta opción se debe aplastar en el botón que se encuentra en la parte superior central dentro de la aplicación. Se puede identificar el símbolo ya que tiene forma circular con líneas a sus lados, al hacer “clic” podemos agregar los puntos de medición necesarios.

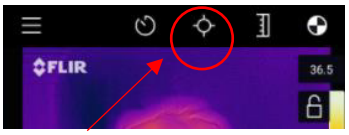

6. Debido a que siempre existen factores presentes en el ambiente que pueden hacer que la medición varíe o no sea exacta, la aplicación presenta un botón de “Calibrar” con el que se lograra obtener una medición más acercada a la realidad, este botón y encuentra en la esquina superior derecha de la pantalla.

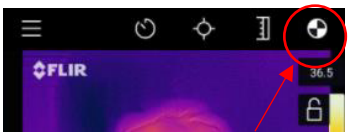

Debido a que la cámara termográfica es un instrumento distinto del dispositivo de control, tenemos una batería, que con su carga al 100%, nos da una duración de 1 hora y para cargarlo o realizar una conexión continua a una fuente externa, el dispositivo ésta cuenta con un cable y un cargador que permitirán cargarla para seguirla utilizando.

ANEXO FOTOGRÁFICO

DISPOSITIVO Y CARCASA

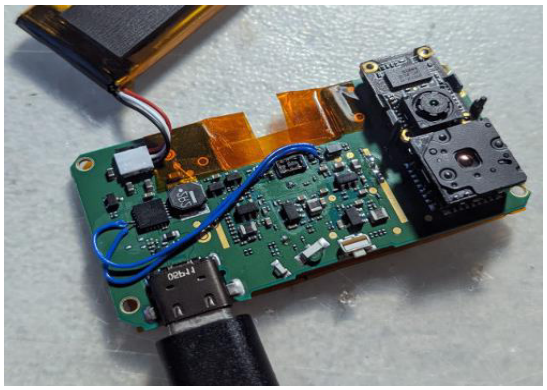

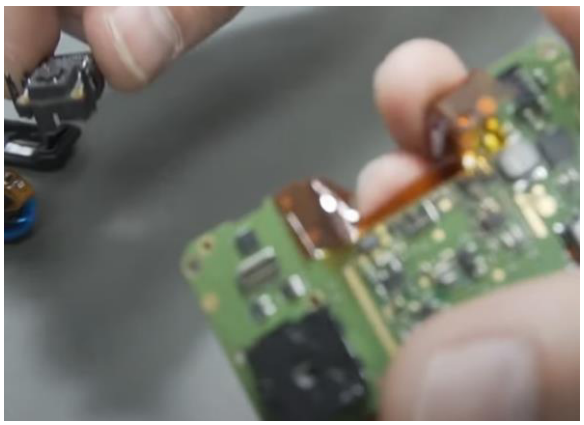

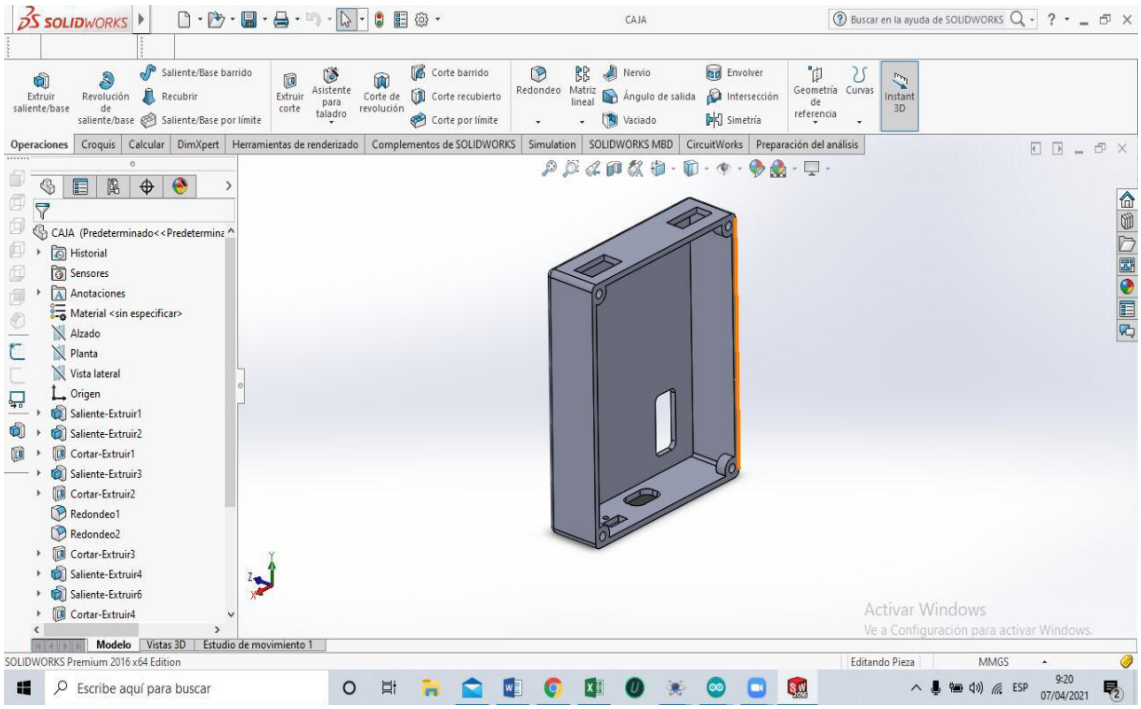

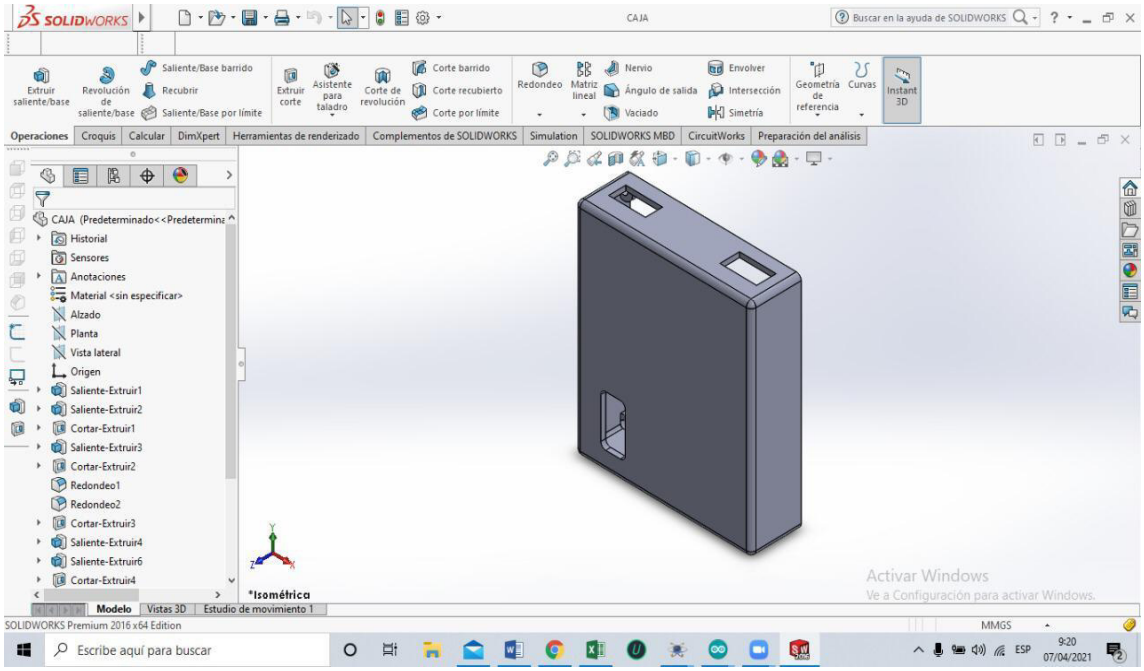
SOLIDWORKS
CAJA
Buscar en la ayuda de SOLIDWORKS
Extruir saliente/base
Revolución de saliente/base
Saliente/Base barrido
Recubrir
Saliente/Base por límite
Extruir corte
Asistente para taladro
Corte de revolución
Corte barrido
Corte recubierto
Corte por límite
Redondeo
Matriz lineal
Nervio
Ángulo de salida
Vaciado
Envolver
Intersección
Simetría
Geometría de referencia
Curvas
Instant 3D
Operaciones
Croquis
Calcular
DimXpert
Herramientas de renderizado
Complementos de SOLIDWORKS
Simulation
SOLIDWORKS MBD
CircuitWorks
Preparación del análisis
CAJA (Predeterminado<<Predetermina
Historial
Sensores
Anotaciones
Material <sin especificar>
Alzado
Planta
Vista lateral
Origen
Saliente-Extruir1
Saliente-Extruir2
Cortar-Extruir1
Saliente-Extruir3
Cortar-Extruir2
Redondeo1
Redondeo2
Cortar-Extruir3
Saliente-Extruir4
Saliente-Extruir6
Cortar-Extruir4
*Isométrica
Activar Windows
Ve a Configuración para activar Windows.
Modelo
Vistas 3D
Estudio de movimiento 1
SOLIDWORKS Premium 2016 x64 Edition
MMGS
Escribe aquí para buscar
ESP
9:20
07/04/2021

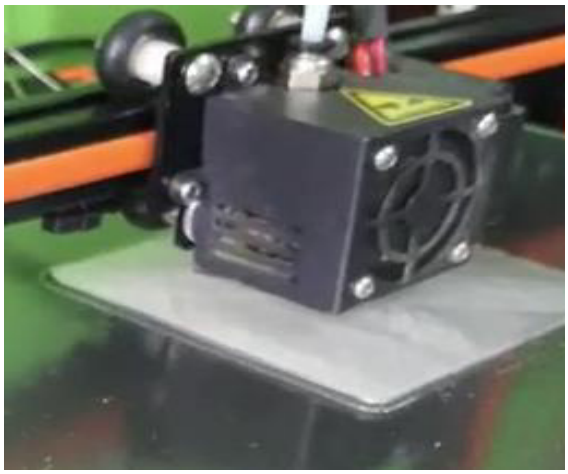

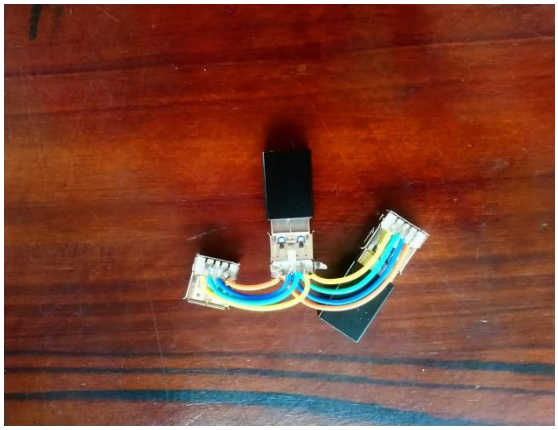

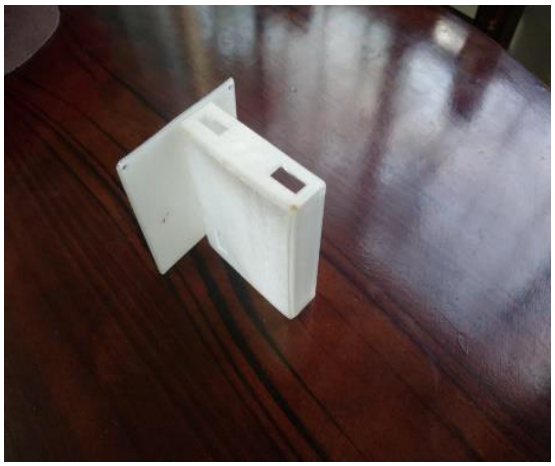


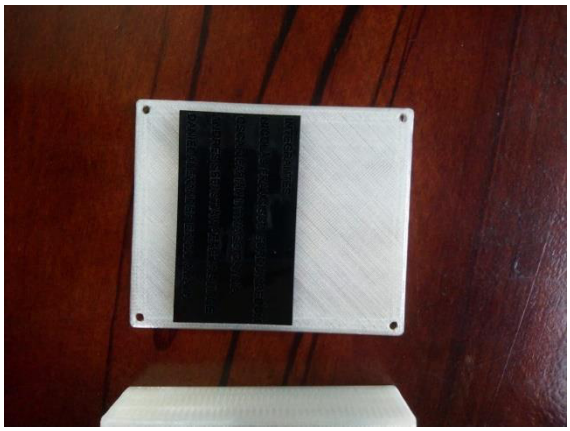

FOTOGRAFÍAS DE MEDICIONES REALIZADAS

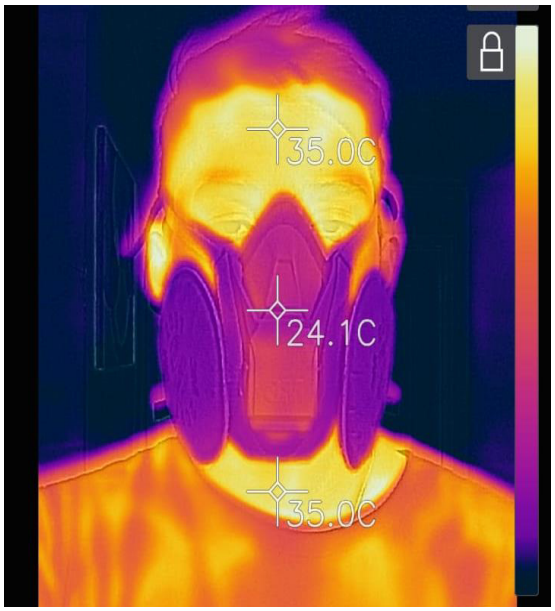

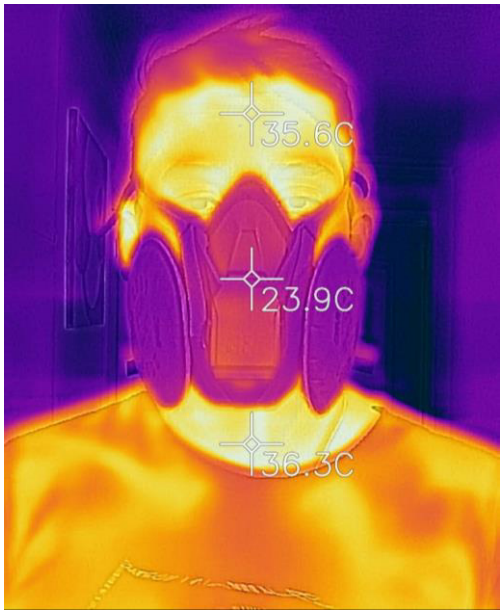
35.6C
23.9C
36.3C

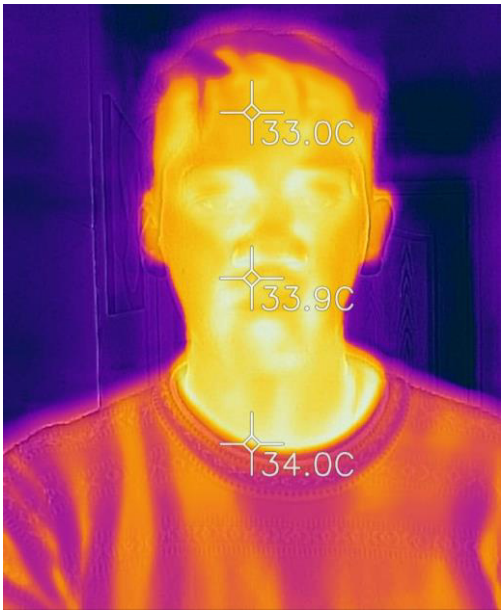
33.0C
33.9C
34.0C

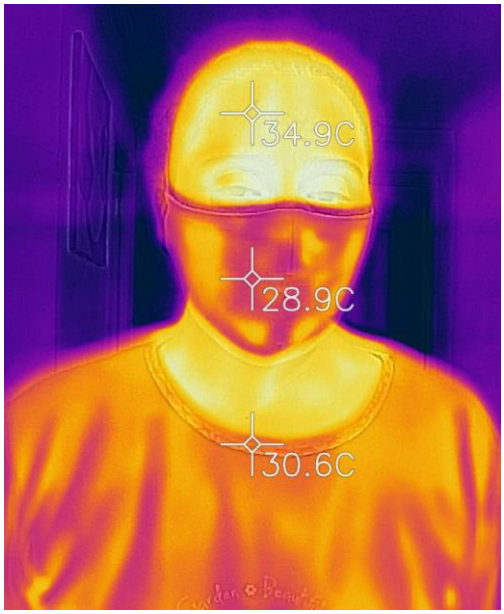
34.9C
28.9C
30.6C

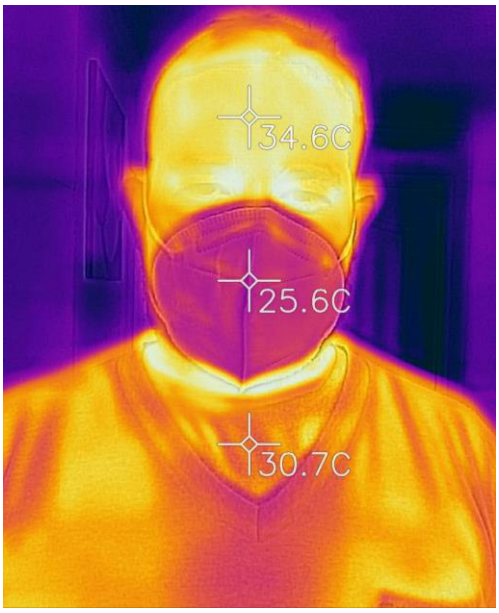
34.6C
25.6C
30.7C

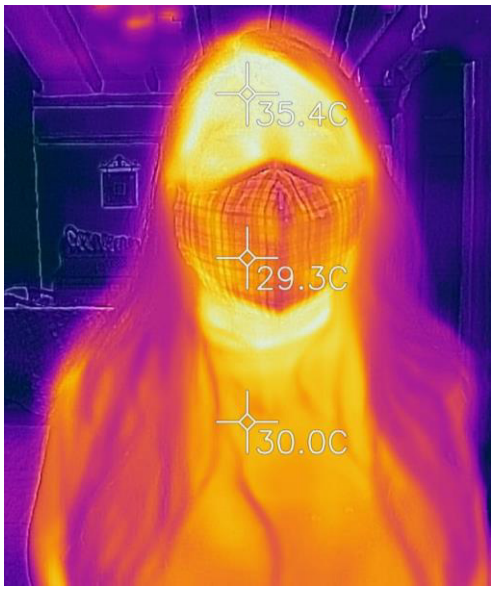
35.4C
29.3C
30.0C


34.5C
27.0C
35.8C


31.4C
30.3C
35.4C
28.6C
26.1C
36.2C
26.4C
32.0C
35.1C
30.8C
30.7C
35.6C
32.8C
34.6C
34.9C
30.5C
34.0C

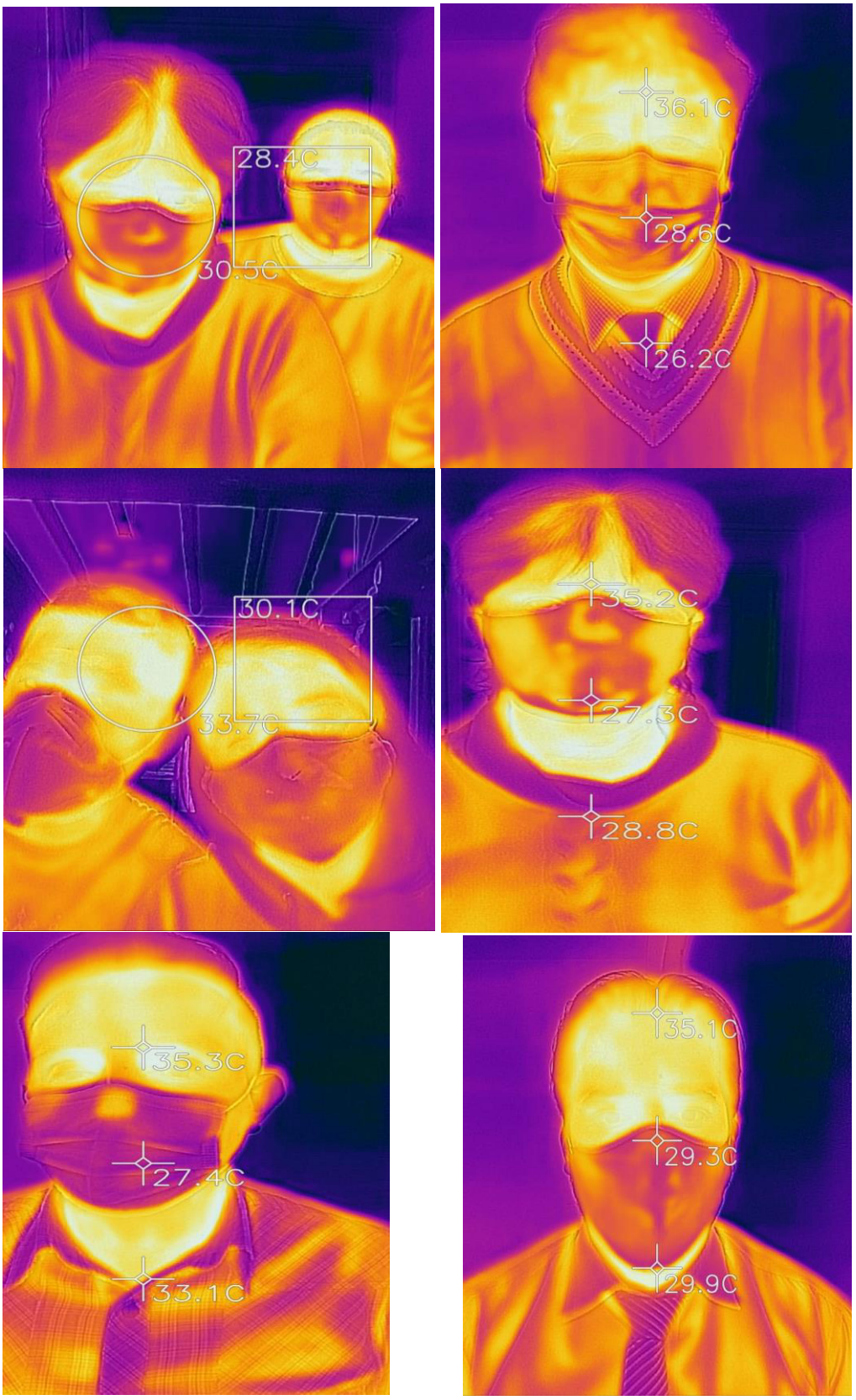
28.4C
30.5C
36.1C
28.6C
26.2C
30.1C
33.7C
35.2C
27.3C
28.8C
35.3C
27.4C
33.1C
35.1C
29.3C
29.9C